Norwegian University
of Life Sciences

Master's Thesis 2020 30 Credits
Faculty of Science and Technology

Experimental Assessment of a Steel Dissipating System

Mathilde Birch-Aune Marthinsen
Structural Engineering and Architecture

Abstract

Older RC frame structures are often not designed considering seismic action, and their failure when subjected to strong earthquakes causes great human and economic losses. Most existing retrofitting solutions are costly, time consuming and irreversible. An innovative energy dissipating system adding CLT panels and friction dampers to the structures was proposed. Four friction dampers of slightly different design were experimentally investigated, focusing on the friction connecting in the dampers.

In chapter one, a short introduction to an ongoing research project in which this thesis is a part of is given, as well as the specific aspects studied in this thesis. The dampers consisted of two separate profiles, where one had a side with elongated holes, connected by two bolts creating a friction surface.

In chapter two, some basic theory concerning earthquake engineering and how friction dampers affect the outcome of vibrations are presented. Also, theory directly related to the aspects studied in the thesis concerning the preload, slip friction joint, shim layers, cyclic test methods, and sensitivity of a sensor are explained.

In chapter three, relevant results from an analytical and numerical investigation of the dampers done by a previous master student are summarized.

In chapter four, information about the specimens used, the set-up and all the tests performed is given. One monotonic and several cyclic tests were described. The aim of the tests was to find the optimal preload to reach a certain slip load, and to study how the different designs behaved.

In chapter five, the results from the experiments are given and discussed. It was discovered that the preload needed to be much lower than specified by the standard. Scraping of steel by the washers in the bolting assembly was a problem. This was successfully solved by adding an additional steel plate to the friction connection in addition to two shim layers. Also, a twisting effect due to the bending moment in one profile and the eccentricity due to asymmetrical arrangement of the bolts was discovered. The twisting resulted in the measuring of both the friction and the resistance of the elongated holes.

In chapter six, a summary of all the tests is given, including both the protocols and results.

In chapter seven, the main findings of this thesis are summarized, and conclusions are drawn.

In chapter eight, modifications are suggested for future testing of the dampers.

Sammendrag

Eldre rammekonstruksjoner av betong er ofte ikke konstruert med hensyn på seismikk aktivitet, noe som har store konsekvenser får bade menneskeliv og økonomi når de blir utsatt for skade grunnet sterke jordskjelv. Eksisterende løsninger ved bruk av ettermontering er dyre, tidskrevende, og irreversible. Det foreslås et innovativt energispredningsystem ved bruk av KL-tre panel og friksjonsdempere. Fire ulike friksjonsdempere med litt ulike design ble testet med fokus på friksjonsforbindelsen i demperne.

I kapittel én, gis en kort introduksjon til prosjektet denne oppgaven er del av, og spesifikt det oppgaven dreier seg om. Demperne besto av to separate profiler, hvor den ene hadde avlange hull, satt sammen av to bolter og dannet dermed en friksjonsflate.

I kapittel to, presenteres grunnleggende teori om jordskjelv og hvordan friksjonsdempere påvirker vibrasjoner. Det presenteres også teori om temaer direkte relater ting oppgaven: Forspenning, glippfriksjonsforbindelse, bruk av ekstra lag, syklisk test metoder, og sensitiviteten til en sensor.

I kapittel tre, oppsummeres relevante resultater fra en tidligere masteroppgave som omhandler en analytisk og numerisk investigering av demperne.

I kapittel fire, gis informasjon om prøvene brukt, oppsettet, og alle testene som ble utført. Én monoton og flere sykliske tester ble beskrevet. Målet med testene var å finne den optimale forspenningen for å nå den optimale glippkraften, og å undersøke hvordan de ulike designene oppførte seg.

I kapittel fem, gis og diskuteres resultatene av forsøkene. Det ble oppdaget at forspenningen måtte være mye lavere enn spesifisert av standarden. At skivene brukt med boltene skrapte opp stålet ble oppdaget. Dette ble løst ved å introdusere en ekstra stålplate på utsiden av friksjonsforbindelsen i tillegg til to innvendige tynne plater. En vridningseffekt grunnet momentet i den ene profilen og eksentrisitet grunnet plasseringen av boltene ble også oppdaget. Vridningen resulterte i at motstanden til de avlange hullene ble malt i tillegg til friksjonskraften.

I kapittel seks, gis en oppsummering av alle testene som inkluderer bade protokollene og resultatene.

I kapittel syv, oppsummeres de viktigste funnene og konklusjoner trekkes.

I kapittel åtte, foreslås endringer til videre testing av demperne.

Preface

In the spring of 2020, Magnus Rød Hatletveit preformed an analytical and numerical investigation of the friction dampers in this thesis for his master thesis, supervised by Francesco Boggian and Roberto Tomasi. In June of 2020, the planning of an experimental investigated was started. It was decided which prototypes to produce and test, and Francesco Boggian design the set-up in collaboration with Roberto Tomasi and Øyvind Hansen. I joined the project full-time in September of 2020, when the more specific planning and preparing of the experiments were started. The experiments were finally carried out in November of 2020 by me and Francesco Boggian in collaboration.

I want to thank my supervisors Roberto Tomasi and Francesco Boggian for following up all the way. Especially Francesco for great teamwork. It was nice to have someone to discuss the work with along the way, making the work less lonely.

Also, I want to thank Øyvind Hansen for building the set-up and always finding solutions to all out mechanical problems. And for doing so surprisingly quickly!

I also want to thank Dag Pascal Pasca for helping with reading the data from our sensors into the computer correctly.

Lastly, I want to thank Sverre Horn for giving me the love and support I needed through the work of this project. And, for taking care of our young daughter, enabling me to write my master thesis.

Ås, December 2020

Mathilde Birch-Aune Marthinsen

Table of Contents

1 Introduction

Traditionally, buildings have been designed only considering gravity loads (Tardo et al., 2020). Today, buildings in seismic zones are designed to withstand earthquake activity by allowing plastic deformations. It ensures public safety, but the damage after a major earthquake can end in costly repairs.

This project was part of an ongoing research project named e-SAFE (energy and Seismic AFfordable rEnovation solutions) based in Italy concerning renovation of existing multistory buildings with reinforced concrete (RC) frame structures using cross laminated timber (CLT) panels to improve seismic behavior. e-SAFE aims to investigate affordable, innovative, and combinable integrated retrofitting inventions. (Tardo et al., 2020)

Steel friction dampers were proposed and designed to connect the CLT panels to the existing RC frame, as seen in Figure 1-1. In the case of moderate ground motion, the connections are designed to be rigid, and be activated in the case of strong ground motion. When activated, some movement is allowed, as shown in the figure, dissipating some of the input energy. This reduces the damage of structural and non-structural parts. (Tardo et al., 2020)

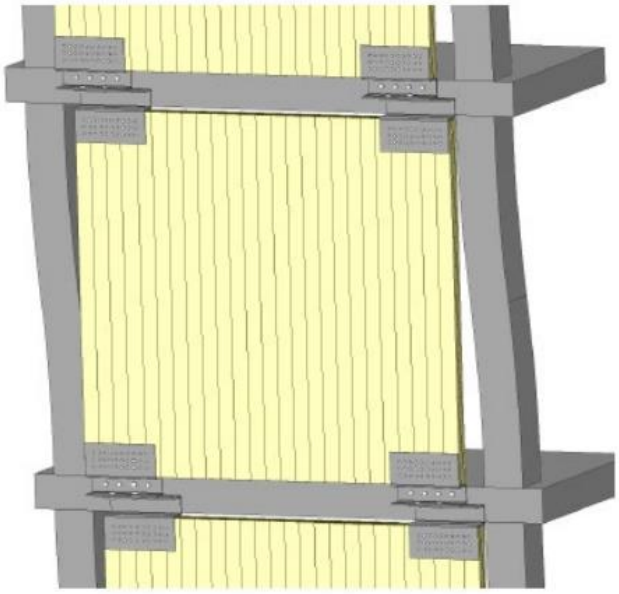

Figure 1-1: CLT panels connected to the RC frame using friction dampers under seismic loads. (Tardo et al., 2020)

A total of four friction dampers of slightly different design using S235 grade steel were proposed by Tardo et al. (2020), shown in Figure 1-2 a), Figure 1-3 a), Figure 1-4 a), and Figure 1-5 a), with the names listed in Table 1-1.

Table 1-1: Name configurations for the prototypes.

Prototype	Description of name
STD	Standard
STD-1H	Standard with 1 hole
STD-R	Standard with reinforcement
ALT	Alterative design

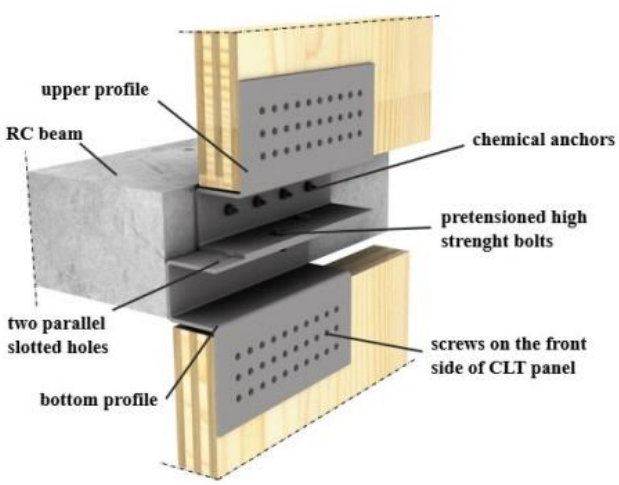

a) Model. (Tardo et al., 2020)

b) Reality.

Figure 1-2: Prototype STD.

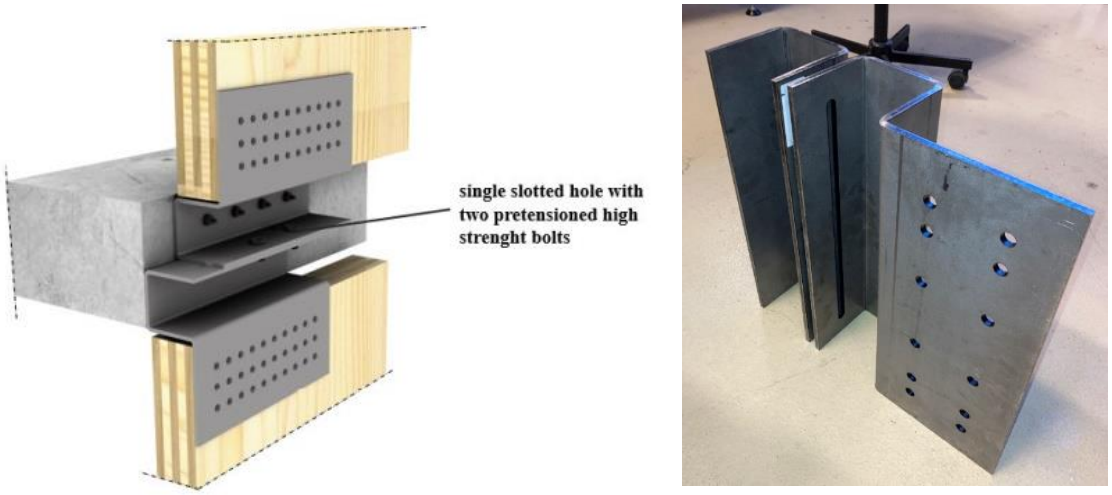

a) Model. (Tardo et al., 2020) *b) Reality.*

Figure 1-3: Prototype STD-1H.

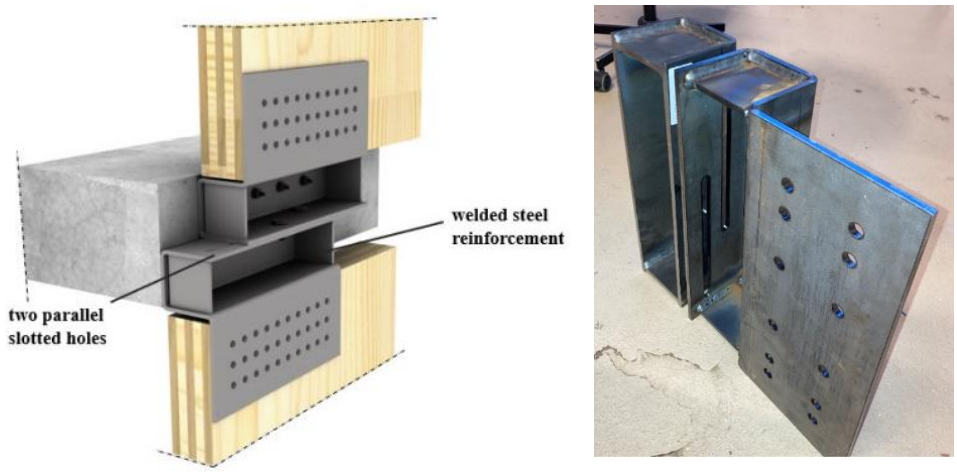

a) Model. (Tardo et al., 2020) *b) Reality.*

Figure 1-4: Prototype STD-R.

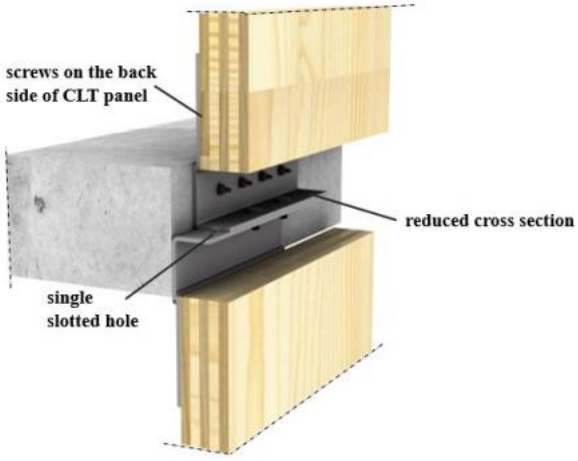

a) Model. (Tardo et al., 2020)

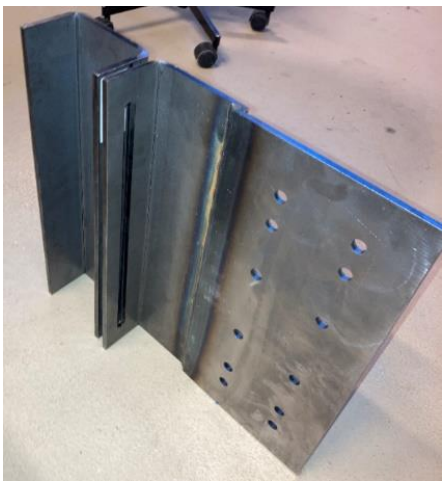

b) Reality.

Figure 1-5: Prototype ALT.

An analytical and numerical investigation of prototypes STD, STD-R and ALT was performed by Hatletveit (2020), studying all aspects of the dampers and considering both gravity loads and seismic loads. In this thesis an experimental investigation was performed to study the friction behavior and only considering the seismic loads. For both investigations, the slip friction resistance of the connector was aimed to be at a value of 30 kN, chosen according to similar test campaigns (Tardo et al., 2020).

To isolate the friction behavior of the dampers, modifications were done to the designs of the prototypes as seen in Figure 1-2 b),Figure 1-3 b), Figure 1-4 b), and Figure 1-5 b). The bottom profile was connected to a rigid steel frame. The upper profile was connected to a moving steel column simulating the movement of the RC beam, the part connected to the top CLT panel removed.

This thesis studies the performance of the four proposed prototypes in activation mode under seismic load. The goal was to obtain slip friction resistance of 30 kN in the friction connections. To do so, an Instron press machine was used to conduct preliminary experiments on the prototypes. The tests were preliminary as they were the very first tests done, and what to expect was very uncertain.

2 Theory

2.1 Earthquake engineering

Earthquakes are the cause of around 10.000 deaths each year, in addition to causing great economical losses of billions of dollars (Elnashai & Sarno, 2008). They are caused by movement in the tectonic plates causing the ground to vibrate. The earthquakes occur between the plates. This in addition to some plates being more active than others is the reason why some places in the world experience stronger and/or more frequent earthquakes.

Several earthquakes usually occur within a short time in the same area. These earthquakes are divided into foreshocks, mainshock and aftershocks, creating a sequence of earthquakes. The foreshocks occur before the main shock, while the aftershocks occur after the main shock. All are smaller than the mainshock in magnitude. The mainshock can be the initial shock, meaning an earthquake sequence does not need to have foreshocks. The different earthquakes occurring in the sequence can first be surely classified after the sequence has finished. An earthquake initially classified as the mainshock during the sequence, can be reclassified as a foreshock when a larger earthquake occurs. (Roberson, 2020)

The main goals of considering earthquakes when designing a construction, is to prevent the loss of lives and reduce the costs of damage. EN 1998-1 (CEN, 2004) gives two requirements for structures in seismic regions:

1. No collapse requirement
   Shall withstand an earthquake with reference probability of exceedance in 50 years without local or global failure.
2. Damage limitation requirement
   Shall withstand an earthquake with reference probability of exceedance in 10 years with limited damage.

Requirement 1 allows for plastic deformations in the structure, meaning the need for repairs after a major earthquake is existent. The reference probability can be set by the individual country, but the recommended value set by the standard is 10%.

Figure 2-1 shows the peak ground acceleration (PGA) required to be designed for by requirement 1 in Europe, with a reference probability of 10% as recommended by the standard. The PGA is the maximum acceleration at ground level during an earthquake and is the base for estimating future earthquakes. Seen from the figure, the countries Italy, Greece, Turkey, Romania, Slovenia and Iceland are especially at risk for experiencing strong earthquakes.

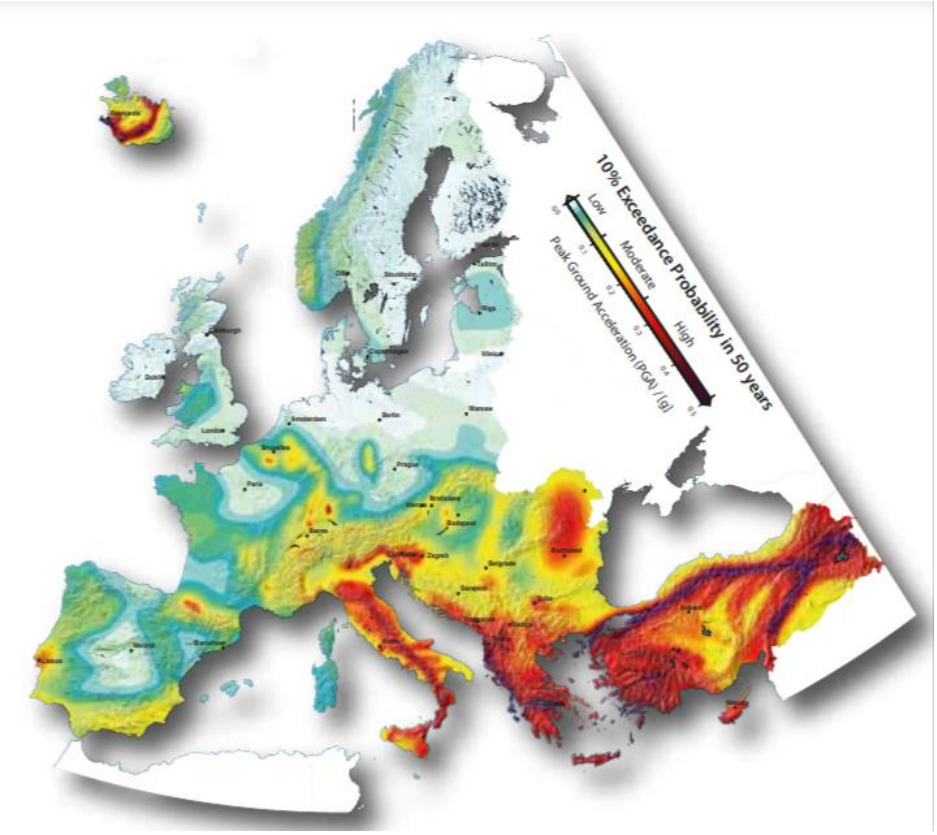

Figure 2-1: European Seismic Hazard Map displays the Peak Ground Acceleration (PGA) with a probability of being reached or exceeded within 50 years in Europe with a return period of 475 years. (Giardini et al., 2013)

EN 1998-1 (CEN, 2004) has a method for estimating the design lateral force at a specific floor in a structure due to earthquake. The standard uses a simplified response spectrum, seen in Figure 2-2. A response spectrum is a plot of the peak responses (in this case the acceleration) of many single degree of freedom systems with varying natural frequencies and thereby periods. The x-axis in the figure shows the periods, and the y-axis shows the elastic response divided by the design ground acceleration. A structure's natural period (T) is dependent on its mass and its stiffness, which depends on its height. A tall building will be less stiff and therefore have a higher natural period (T). Seen from Figure 2-2, this means tall buildings are less affected by the acceleration of the ground than short buildings. The natural period (T) can calculated using the stiffness and mass, or be estimated from EN 1998-1 (CEN, 2004).

The response in Figure 2-2 is also dependent on the ground type. EN 1998-1 (CEN, 2004) gives loose ground types a low response and opposite.

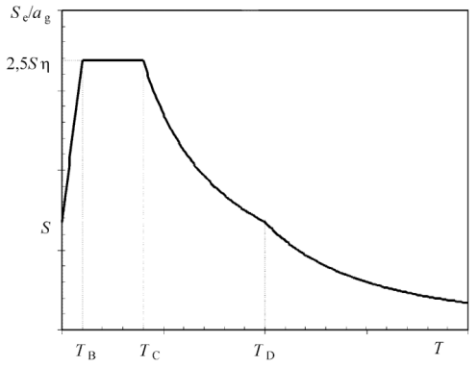

Figure 2-2: Shape of a simplified response spectrum from EN 1998-1 (CEN, 2004).

The base shear and horizontal force at a given height of a structure is given by EN 1998-1 (CEN, 2004):

$$F_b = S_d(T)m\lambda \qquad \textit{Eq. 2-1}$$

F_b base shear

$S_d(T)$ response at period T

m total mass of the structure

λ correction factor

$$F_i = F_b \frac{z_i m_i}{\sum z_j m_j} \qquad \textit{Eq. 2-2}$$

F_i horizontal force at given height

z_i height at the given mass m_i

m_i mass at the given floor of a building

z_j all heights for all masses m_j

m_j masses at all floors of a building

This method described from the standard EN 1998-1 (CEN, 2004) is appliable for elastic analysis. In EN 1998-1 3.2.2.5(8) it is specified that this method is not sufficient for the design of systems of base-isolation or energy-dissipation. For systems of this kind, the response spectrum must be more extensively investigated.

2.2 Friction damping

In modeling a physical system, there are three main types of damping models used: viscous, coulomb, and solid. Viscous damping describes a body moving through a fluid at a moderate speed. It is convenient to use mathematically and is therefore the most used model. Coulomb damping, also called friction damping, describes the dissipation of energy between two dry surfaces. Solid damping, also called structural damping, describes the dissipation of internal energy within the materials in the structure. (Schmitz & Smith, 2012)

A friction force always acts in the opposite direction of the moving body, as represented in Figure 2-3. The friction force, F_f, is dependent on a friction coefficient for the material of the friction surfaces, and the normal force acting on the body at the friction surface:

$$F_f = \mu N \qquad \textit{Eq. 2-3}$$

F_f	friction force
μ	friction coefficient
N	normal force

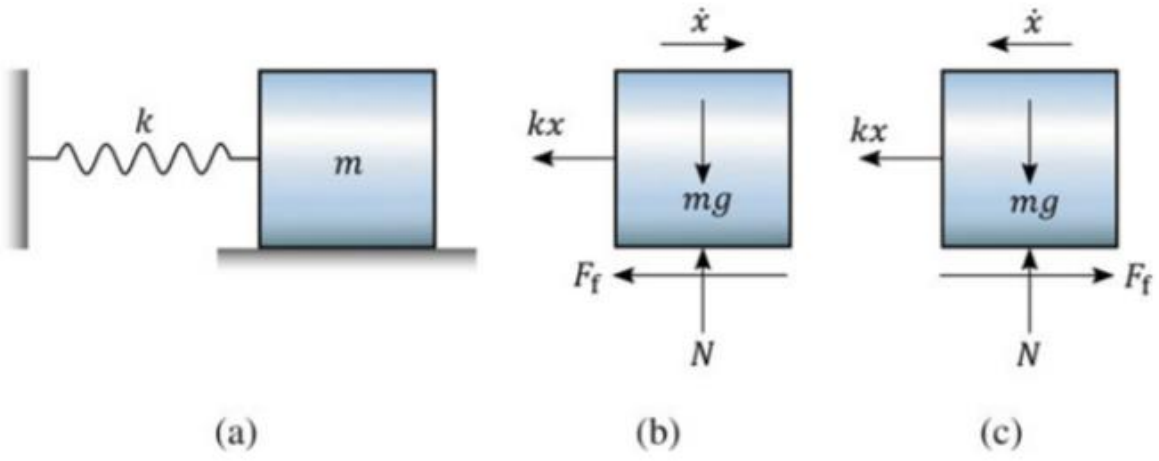

Figure 2-3: Free body diagram, coulomb damping. (Shabana et al., 2019)

The friction coefficient for metal on metal, range between 0.12 and 0.45 (Shabana et al., 2019).

The equation of motion for free vibration for the free body diagram in Figure 2-3 becomes,

$$m\ddot{x} + kx = \mp F_f \qquad \textit{Eq. 2-4}$$

m mass of the body

x displacement of the body

k stiffness

considering the friction force can act in both directions. Solving the equation, it is found that the displacement can be described as,

$$x(t) = \left(x_0 - 3\frac{F_f}{k}\right)\cos \omega t - \frac{F_f}{k} \qquad \textit{Eq. 2-5}$$

t time

x_0 initial displacement

ω natural frequency

when the body is moving to the right. At the end of the first cycle the time equals the period of the natural oscillation; $t = 2\pi/\omega$. The displacement then becomes

$$x\left(\frac{2\pi}{\omega}\right) = x_0 - \frac{4F_f}{k} \qquad \textit{Eq. 2-6}$$

which shows there is a decrease in the amplitude of displacement of $4F_f/k$ after one cycle. This amount of decrease is actually constant between every cycle, meaning the function follows the form of linear decay, as shown in Figure 2-4. (Shabana et al., 2019)

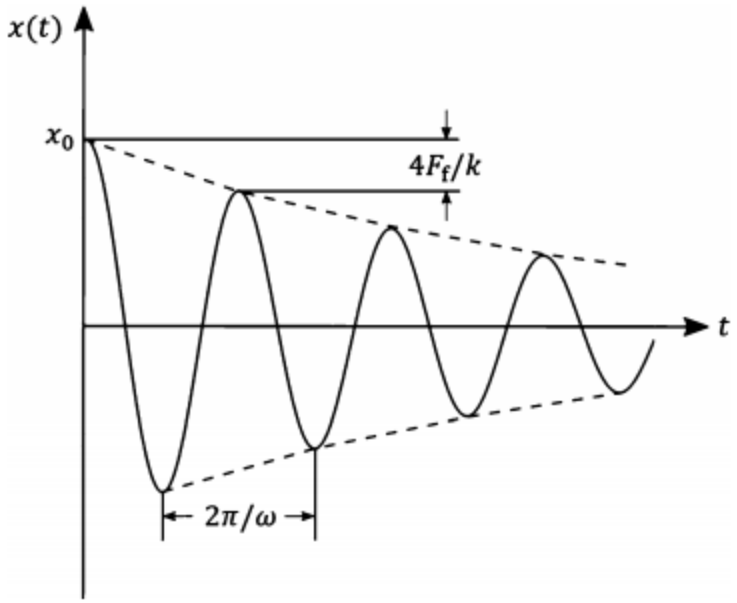

Figure 2-4: Effect of Coulomb damping (Shabana et al., 2019).

2.3 Preloaded bolts

In a preloaded bolt, a torque is applied to the bolt to obtain a tension force in its shank. This induces a compression force on the plies held together by the bolt. By Newton's laws, this compressive force is equal to the preload force in the shank of the bolt. Everything is therefore in equilibrium, as can be seen in Figure 2-5. (NSC2, 2005)

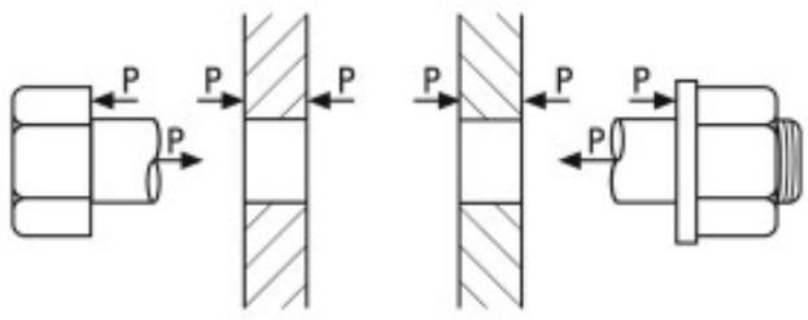

Figure 2-5: Free body diagram - equilibrium of a preloaded bolt (NSC2, 2005).

When no specific preload is specified, the nominal minimum preload is given by EN 1090-2:2018 (CEN, 2018a) and EN 1993-1-8:2005 (CEN, 2005):

$$P_{min} = 0.7 * f_{ub} A_s \quad \text{Eq. 2-7}$$

P_{min} nominal minimum bolt preload

f_{ub} nominal ultimate strength of the bolt given in EN 1993-1-8 (CEN, 2005)

A_s stress area of the bolt.

Understanding Eq. 2-7, the nominal minimum preload is 70% of the bolt's capacity in tension.

The necessary torque to be applied to obtain a certain preload, can be calculated from Eq. 2-8. The torque coefficient (k_m) is dependent on the geometry of the thread of the bolt, and the friction coefficient of the thread and the collar. Its value is individual for each set of bolts produced, and therefore must be given by the producer. (Euler, 2002)

$$M_r = k_m d P \quad \text{Eq. 2-8}$$

M_r bolt installation torque

k_m torque coefficient

d bolt nominal shank diameter.

For bolting assemblies (bolt together with necessary nuts and washers) to be preloaded by applying a preloading method given in EN 1090-2 (CEN, 2018a), the assemblies are divided into two classes. The classes expresses their ability to be tightened by the different methods, as presented by Vescovini Group (2018). The classes depend on the delivery and the torque coefficient (k_m):

Class K1 - The bolts, nuts and washers are delivered in the same package. 0,10≤ k_m≤ 0,16.

Class K2 - The bolts, nuts and washers are delivered in separate packages. 0,10≤ k_m≤ 0,23.

For both classes, the assemblies must be delivered as a set supplied by the same manufacturer. If not, the torque coefficient (k_m) given by the manufacturer(s) will not be valid.

EN 1090-2 (CEN, 2018a) specifies two methods for tightening a preload-bolt using a torque wrench. Both methods apply the torque in two steps:

1. The torque method

This method shall only be used for bolting assemblies in class K2.

Step 1: All bolts in the connection shall be tightened to a value of $0{,}75 * M_r$.

Step 2: All bolts in the connection shall be tightened to a value of $1{,}10 * M_r$.

2. The combined method

This method can be used for bolting assemblies in both class K1 and K2. Bolting assemblies in class K1 shall use a value of $k_m = 0{,}125$.

Step 1: All bolts in the connection shall be tightened to a value of $0{,}75 * M_r$.

Step 2: All bolts in the connection shall be turned by an angle given in table 21 in EN 1090-2 (CEN, 2018a).

2.4 Slip Friction Joints

A slip friction joint uses friction to withstand forces until the applied force exceeds the friction force of the connector, at which point some movement in the joint is allowed. The idea is that the connection does not take harm in the event of large forces being applied, by allowing movement when a regular connection would deform or break. Preloaded bolts holding two or more plies together is used to increase the friction in the surface(s) between the plies. It is anyways important to know what the normal force between the plies are to predict the friction force in the friction surface(s).

There are two types of friction connections: Symmetric and asymmetric, as illustrated in Figure 2-6. External loads are applied to the middle plate, with a force equal to the slip friction load for the friction surface. In the case of an asymmetric connection, all the external load is as well applied to one of the outside plates, leaving the second to be dragged along by the bolts. This causes complex stresses in the bolts. Still, the asymmetric connections have shown to perform well, only having a chipping effect during the beginning of movement after the plates change direction before stabilizing at a constant force. In the symmetric connection, the slip load is divided equally between the two outside plates. A symmetric slip friction connection produces a perfectly rectangular force-displacement curve. (Loo et al., 2014)

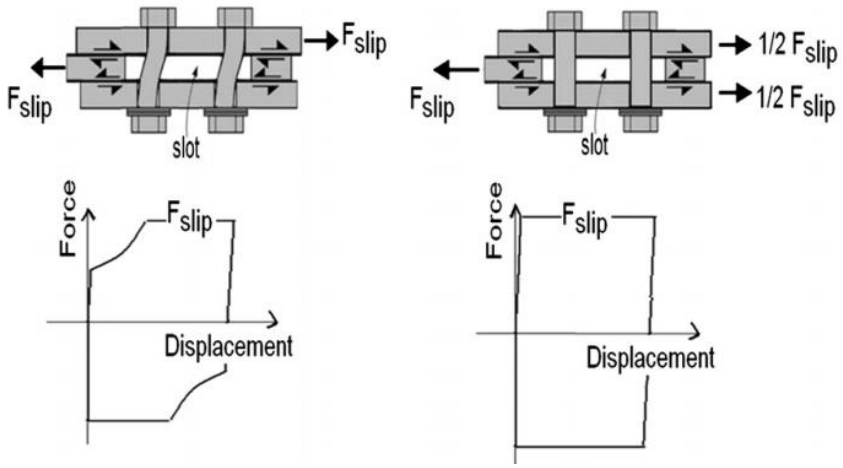

a) Asymmetric *b) Symmetric*

Figure 2-6: Two slip friction connections and their typical force-displacement curves.(Loo et al., 2014)

The slip resistance of a slip friction joint can be derived from Eq. 2-3 in chapter 2.2. Realizing that the preload force is the same as the normal force between the plies, and also taking into account that there can be more than one friction surface in a slip friction joint, the slip resistance is

$$F_{s,R} = mn\mu P \qquad \textit{Eq. 2-9}$$

$F_{s,R}$ slip resistance

m number of bolts

n number of friction surfaces

μ friction coefficient. Can be found experimentally or an assumed value from Table 2-1 from table 17 in EN 1090-2 (CEN, 2018a) can be used.

P preload in bolt.

Table 2-1: Friction coefficients according to EN 1090-2 (CEN, 2018a).

Table 17 — Classifications that may be assumed for friction surfaces

Surface treatment	Class [a]	Slip factor μ [b]
Surfaces blasted with shot or grit with loose rust removed, not pitted.	A	0,50
Surfaces hot dip galvanized to EN ISO 1461 and flash (sweep) blasted [c] and with alkali-zinc silicate paint with a nominal thickness of 60 μm [d].	B	0,40
Surfaces blasted with shot or grit: a) coated with alkali-zinc silicate paint with a nominal thickness of 60 μm [d]; b) thermally sprayed with aluminium or zinc or a combination of both to a nominal thickness not exceeding 80 μm.	B	0,40
Surfaces hot dip galvanized to EN ISO 1461 and flash (sweep) blasted (or equivalent abrasion method) [c]	C	0,35
Surfaces cleaned by wire-brushing or flame cleaning, with loose rust removed	C	0,30
Surfaces as rolled	D	0,20

[a] Classes as given in G.6.

[b] The potential loss of preloading force from its initial value is considered in these slip factor values.

[c] Unless alternative equivalent abrasion process capability can be demonstrated, flash (sweep) blasting of hot dip galvanized surfaces shall be carried out according to the procedures and conditions set out in EN 15773. After flash (sweep) blasting the appearance of a matt surface indicates that a soft surface layer of un-alloyed zinc has been removed.

[d] Dry thickness to be within 40 μm to 80 μm range.

2.5 Use of shim layers in slip friction joints

A shim layer is an additional layer placed on the friction surface of a friction connection. The friction in the connection can be manipulated by using thin shim layers of a different material than the connection in general.

Golondrino et al. (2012) studied the effects of shim layers of brass, aluminum, steel and bisalloy in a steel slip friction connection. Brass and aluminum were categorized as materials of low hardness (70-100 BH), steel and bisalloy 80 were of medium hardness (100-300 BH), and bisalloy 400 and bisalloy 500 were of high hardness (300-500 BH). The first two showed to be moderately unstable, the second two very unstable, and the third two stable, as seen in Figure 2-7. Stable refers to the force-displacement graphs being perfectly rectangular, while unstable assumes an irregular shape. It was assumed that the instability was caused by wear particles produced during sliding interfering with the properties of the

friction surfaces. The materials of medium hardness were assumed to produce the most wear particles, the low hardness materials some, and the high hardness materials close to none.

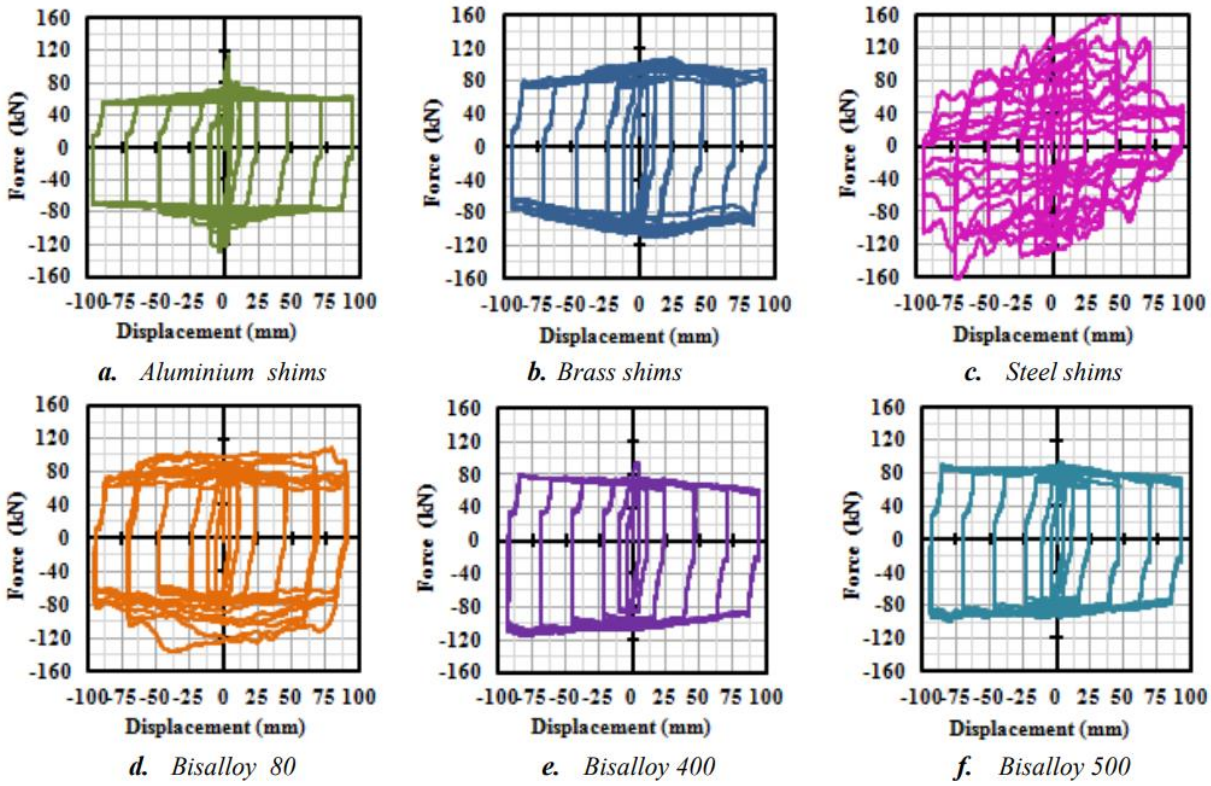

Figure 2-7: Load-displacement curves using shim layers of different materials (Golondrino et al., 2012).

2.6 Cyclic test method

Cyclic testing is when a test is performed several times, instead of only completing one cycle. In civil engineering, this can mean applying a load on a test object in one direction, and then the other, several times. The magnitude of the load does not have to be the same for each cycle.

It is common to perform a cyclic test using a displacement control method, such as in Figure 2-8. In such a protocol, each cycle runs until it has reached a given displacement. The time it takes, is dependent on the chosen rate of slip, which according to ISO16670 (2003) should be between 0.1 mm/s and 10 mm/s. According to another standard, EN 12512 CEN (2001), this rate should be between 0.02 mm/s and 0.2 mm/s. Both standards are meant for mechanical fasteners in timber structures.

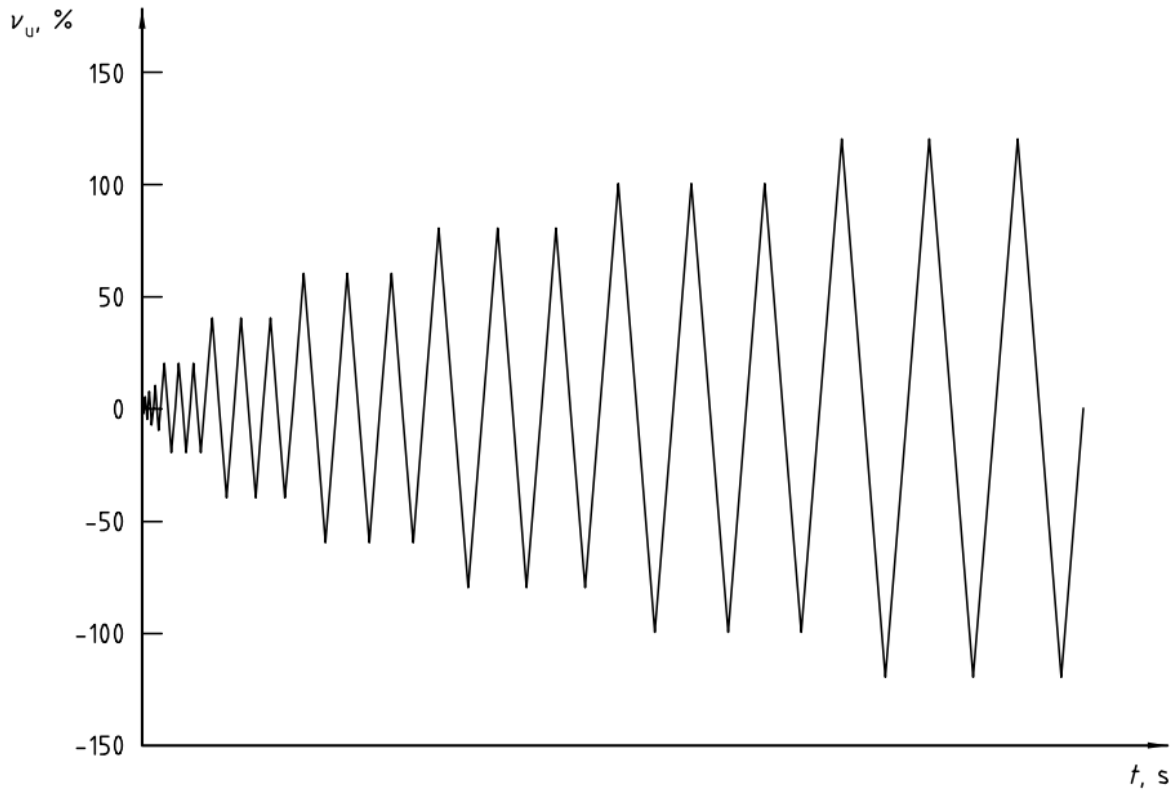

Figure 2-8: Standard cyclic displacement schedule from ISO16670 (ISO, 2003). v_u is the percentage of the maximum displacement.

Figure 2-8 specifically shows a schedule standardized by ISO16670 (2003). In this standardization, all amplitudes of displacement are calculated as a percentage of the maximum displacement, as seen on the y-axis in the figure. The cycles with the smaller displacements are only run once, while the rest are run three times each. The magnitude of the amplitudes should increase for every new and different cycle through the test.

Figure 2-9 shows another standardized cyclic displacement schedule, by EN 12512 CEN (2001). In this model, the displacements are calculated from the yielding displacement instead of the maximum, but a percentage is used here as well.

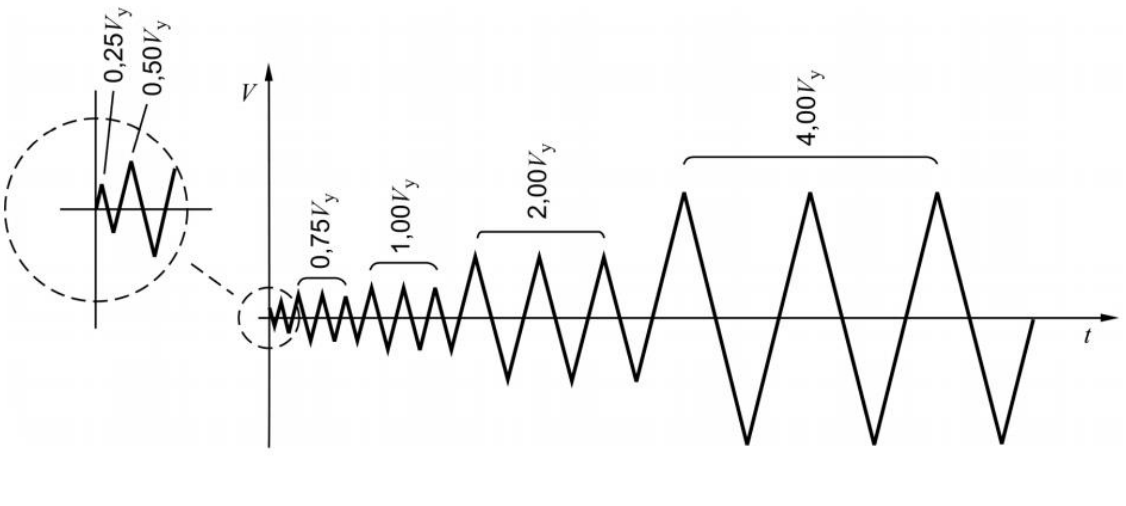

Figure 2-9: Standard cyclic displacement schedule from EN 12512 (CEN, 2001). V_y is the yield slip (displacement).

To produce reliable mechanical properties, a minimum of 6 replicates should be used. The test machinery must be able to continuously record the load applied and displacement of the joint with an accuracy of ± 1% or better. The set up should be in such a way that the inclusion of member deformation should be minimized. (ISO, 2003)

Both ISO16670 (2003) and EN 12512 (CEN, 2001) are meant to use for timber. There is however a standard that is specified for steel and also gives a method to use for new devices that have not been tested before. In short, EN 15129 (CEN, 2018b) specifies that the device shall be tested in full-scale but not installed in the structure. Only one specimen needs to be tested if the results are reasonable and can be assumed correct for the new device. Cycles of amplitudes 25% and 50% of the maximum displacement shall be repeated 5 times each, then a cycle of amplitude 100% of the maximum displacement shall be repeated 10 times.

2.7 Sensitivity of a sensor

Sensors are used to measure physical values for different purposes. They are connected to a computer and their usual output is in volt. To translate this output into a meaningful physical value, the sensitivity is needed.

In short, the sensitivity describes the relationship between the output in volt and the physical value. A sensor would have both a range in volt, and a range in some physical value. Each value in volt correspond to a specific physical value. In this way, a graph representing the relationship can be made, where the slope at each point will be the sensitivity. Most common is for this relationship to be linear.

For this case, the sensitivity is the same at every point and can simply be calculated by dividing the maximum physical value by the maximum value in volt. The sensitivity is given in units “physical unit”/V.

3 Analytical and numerical investigation of the connections

In July of 2020, Magnus Rød Hatletveit completed the master thesis *Mechanical assessment of a steel dissipating system for RC buildings retrofitting with CLT panels*. Hatletveit's thesis is a part of the same project as this thesis. It is an analytical investigation of the connections STD, STD-R and ALT, in addition to a few more. In an unpublished conference paper *Mechanical Characterization of Energy Dissipation Devices In Retrofit Solution of Reinforced Concrete Frames Coupled With Solid Wood Panels* (Tardo et al., 2020) the so far progress in this project is presented, also including the results from Hatletveit (2020).

In this chapter, relevant findings directly from Hatletveit (2020) and as presented in Tardo et al. (2020) are summarized.

There was one major difference between the work by Hatletveit (2020) and this thesis. In Hatletveit (2020) the connections were analyzed taking into account the horizontal force acting on the friction surfaces, as well as vertical forces acting on the connections, as seen in Figure 3-1. In this thesis the friction part of the connection is isolated, and therefore only the horizontal force acting on the friction part of the connection is considered.

A preload of 22 kN was used by Hatletveit (2020) for the friction connection in all prototypes.

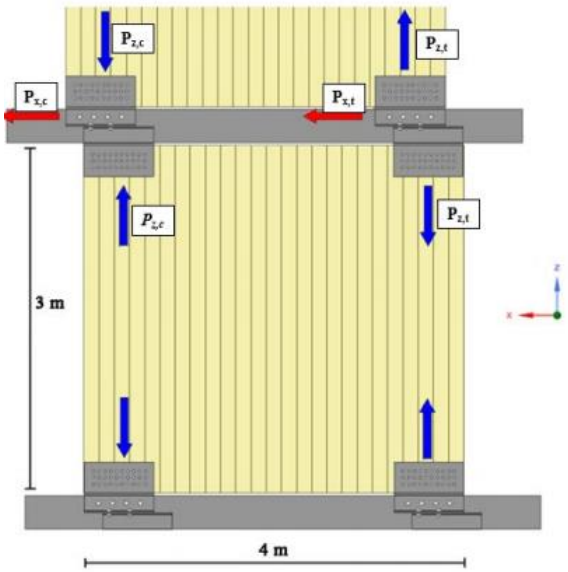

Figure 3-1: Representation of forces in the system applied to the connections. (Tardo et al., 2020) (Image used courtesy of ANSYS, Inc.)

3.1 Standard prototype STD

The upper profile of the STD prototype shown in Figure 3-2 a) experienced a stress 2,8 times the characteristic yield capacity of steel S235 at the bottom right corner shown as max in the figure. The second most critical stress was observed in the upper bend of the bottom profile in Figure 3-2 b) with a stress of 2,0 times the yield capacity of steel S235. This last stress was thought to be a result of a moment about the x-axis due to high eccentricities caused by the vertical load in the friction connection, in addition to a high moment $M_{y,c}$ resulting in a torsion effect. (Tardo et al., 2020)

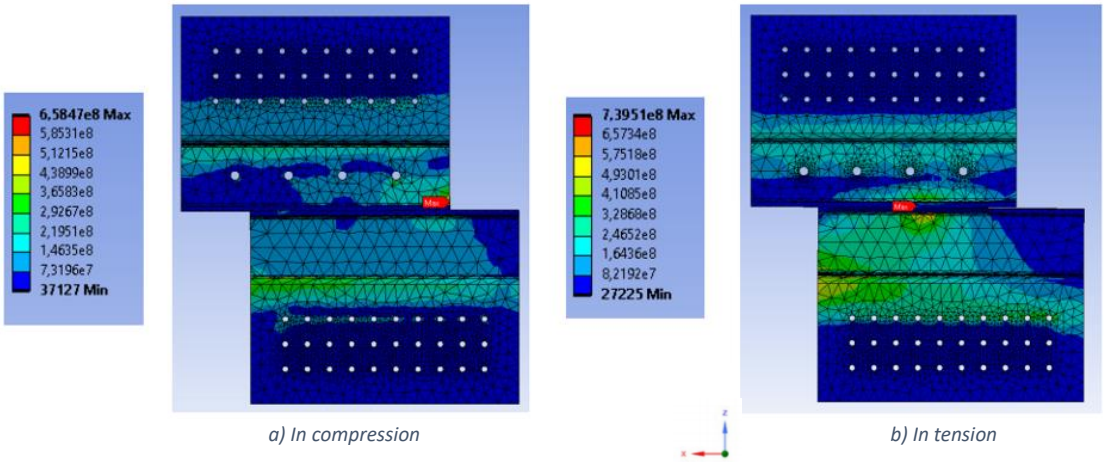

a) In compression *b) In tension*

Figure 3-2: Equivalent von-Mises stresses on the STD prototype [N/m²]. (Tardo et al., 2020) (Images used courtesy of ANSYS, Inc.)

The case of the moment $M_{x,c}$ was not relevant in this thesis since this was assumed to be caused by the vertical loads as described above not being present in the work of this thesis. Seen in Figure 3-2 there are in both cases a) and b) large stresses along the bottom and outwards most bend of the bottom profile.

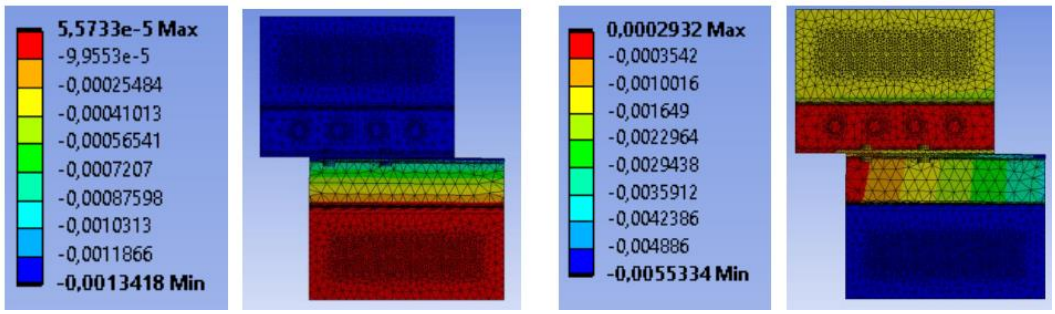

a) Along x-axis in tension [m]. *b) Along z-axis in tenson [m].*

Figure 3-3: Deformations in prototype STD in tension. (Hatletveit, 2020) (Images used curtesy of ANSYS, Inc.)

Figure 3-3 shows the deformations in the profiles. Image b) indicates a small rotation of the U-shape of the bottom profile, while image a) shows an insignificant deformation of the bolted plate of the bottom profile along the x-axis.

3.2 Standard prototype with reinforcement STD-R

The stresses at the bends of both profiles were observed to be smaller than in prototype STD, as seen in Figure 3-4. This was a result of the reinforcement making the profiles stiffer at the bends. (Tardo et al., 2020)

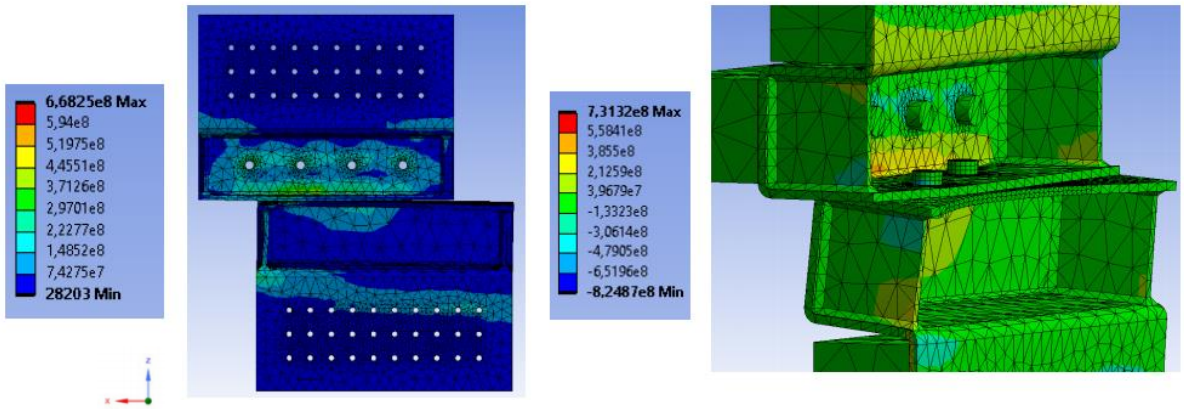

a) Equivalent von Mises stresses [N/m²] *b) Equivalent stresses along the z-axis [N/m²]*

Figure 3-4: Highlighted results of prototype STD-R. (Tardo et al., 2020) (Images used courtesy of ANSYS, Inc.)

Deformations of the bottom profile, seen in Figure 3-5 a), indicated a rotation of the of the U-shape of the reinforced bottom profile about the y-axis. However, the displacements were small, at max 1,7 mm along the z-axis, so the rotation was also small. Image b) show small displacements along the x-axis.

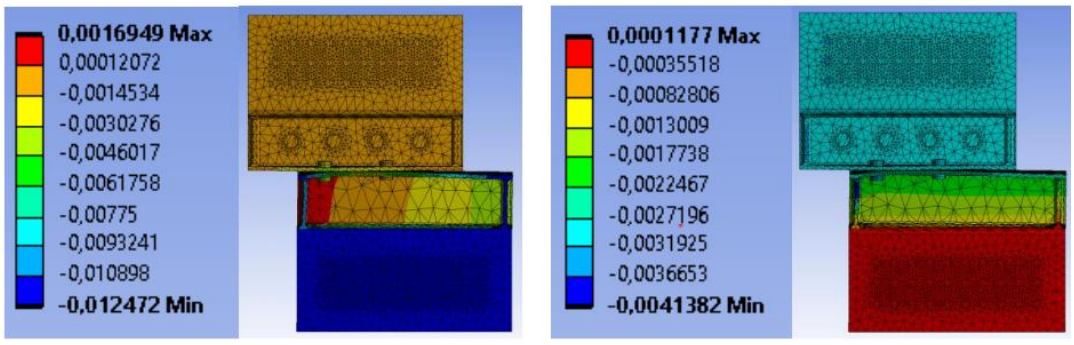

a) Along z-axis in tension [m]. *b) Along x-axis in tenson [m].*

Figure 3-5: Deformations in prototype STD-R in tension. (Hatletveit, 2020) (Images used curtesy of ANSYS, Inc.)

3.3 Alternative prototype ALT

In the prototype ALT proposed by Hatletveit (2020) as a result of the behavior of prototypes STD and STD-R, the stresses were observed to be much lower than for the two previous prototypes. This indicated that the plates in the profiles are much more rigid in the ALT prototype. (Tardo et al., 2020)

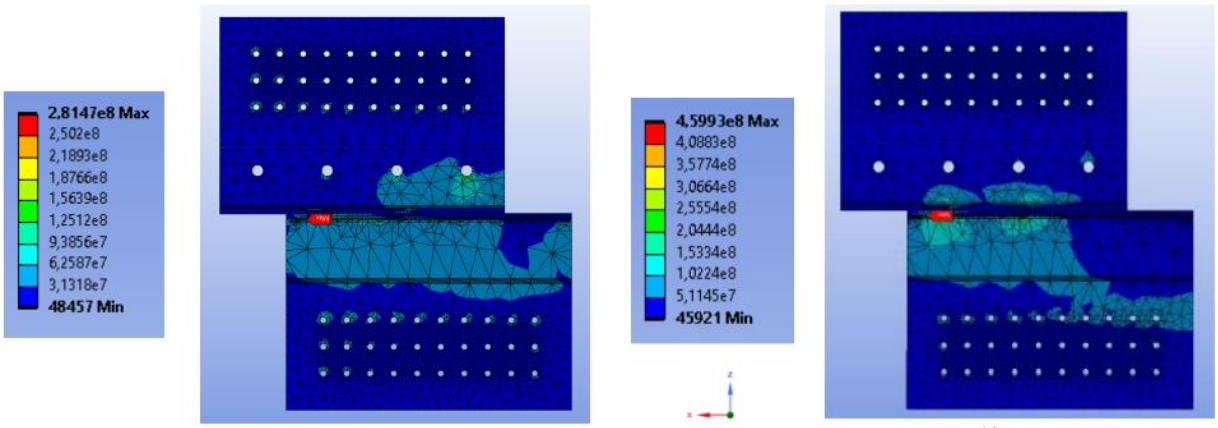

a) In compression *b) In tension*

Figure 3-6: Equivalent von-Mises stresses on the prototype ALT [N/m²]. (Tardo et al., 2020) (Images used courtesy of ANSYS, Inc.)

Figure 3-7 shows the deformations in the ALT prototype. Image b) shows a very small rotation of the U-shaped part of the bottom profile. The deformation along the x-axis is very small as well.

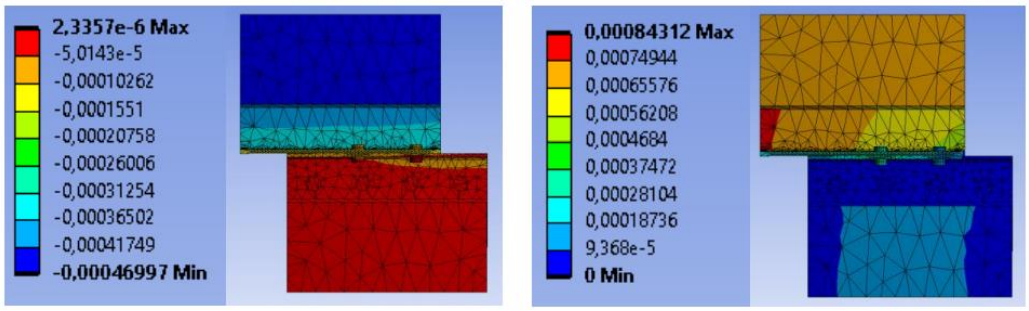

a) Along x-axis in tension [m]. *b) Along z-axis in tenson [m].*

Figure 3-7: Deformations in prototype STD-R in tension. (Hatletveit, 2020) (Images used curtesy of ANSYS, Inc.)

4 Material and method

4.1 Specimen

Three sets of each prototype, shown in Figure 4-1, were ordered from Italy. However, the producer sent several more as seen in Table 4-1. This allowed for the elimination of specimens with major or minor imperfections.

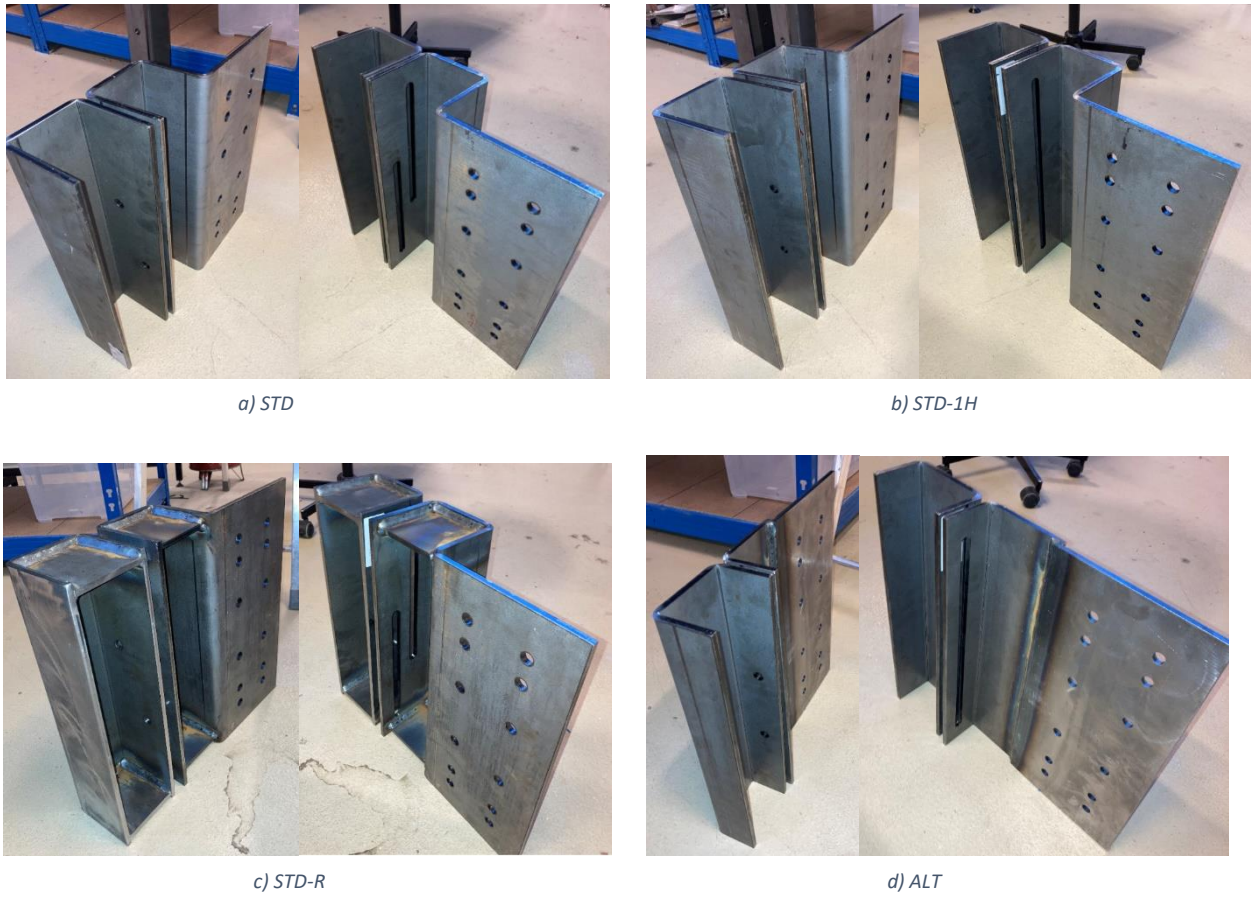

a) STD *b) STD-1H*

c) STD-R *d) ALT*

Figure 4-1: All prototypes viewed from two angles. Left profile is the upper profile, right profile is the bottom profile.

Table 4-1: Number of received specimen.

Prototype	Description of name	Bottom profile	Upper profile
STD	Standard	6	4
STD-1H	Standard with 1 hole	4	5
STD-R	Standard with reinforcement	4	3
ALT	Alterative design	3	6

All dimensions, including the angles of the corners, of the received specimen were measured and checked against the drawings of the prototypes. The angles varied in a range of 89 to 91 degrees, which was not very different from 90 and therefore accepted. Also, the angles tended to differ within the length of one specimen, with a difference of maximum one degree. The left “leg” of the U-shaped part of the bottom profiles was consistently lower than of the drawing, and therefore also shorter than the right “leg”, illustrated in Figure 4-2. Small imperfections like these made it important to be able to adjust the specimen in all directions on the set up to connect the friction connection correctly. All holes were the correct size for all specimens. The total lengths were also always as in the drawings. All the measurements can be found in appendix A, along with technical drawings of all the prototypes.

Figure 4-2: Illustration of differing lengths in the bottom profiles.

When the faulted specimens had been eliminated and upper and bottom profiles had been matched together, there ended up being 3-4 sets of each prototype as seen in Table 4-2. The individual sets were denoted _1, _2 and _3. Originally, all prototypes were going to be tested three times each with the same protocol using a total of three specimens each and were therefore given these names. The fourth set was then seen as an extra and denoted _test, meant for being used for preliminary testing since they could be wasted. This ended up not being the case, however the names were kept. Not all sets in Table 4-2 ended up being used.

Table 4-2: Overview of available specimen.

Prototype	Description of name	Number of sets	Denotations
STD	Standard	4	_1, _2, _3, _test
STD-1H	Standard with 1 hole	4	_1, _2, _3, _test
STD-R	Standard with reinforcement	3	_1, _2, _3
ALT	Alterative design	3	_1, _2, _3

4.2 Set-up

Figure 4-3 shows the set-up built to hold the specimen. It consisted of a frame used to hold the bottom profile, and a T-shape element connected to the moving beam of the Instron press, used to hold and move the upper profile up and down.

The set-up was designed to be as stiff as possible, so the friction connection was isolated such that the set-up would not affect the results of the test. In this way the only thing being tested would be the friction connection. To be sure this was true, the rotation of the right column (the column which experiences most forces) was measured by measuring the displacement at the top and bottom of the column.

In addition to the two LDT-sensors, a wire sensor was placed at the base between the columns to measure the displacement of the upper profile. See chapter 4.3 for more information about the sensors, and chapter 4.4 for mor information about the data extracted.

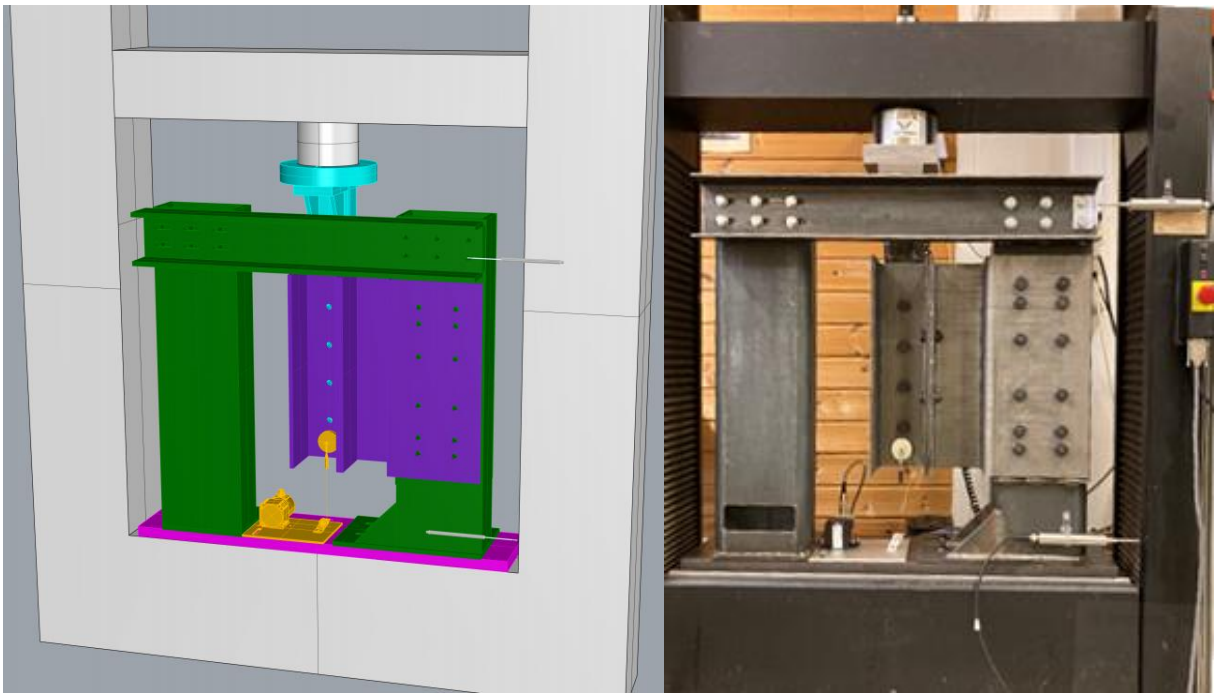

a) Model *b) Reality*

Figure 4-3: Set-up mounted on the Instron press.

Figure 4-4 shows all the connections in the set-up and Table 4-3 gives a description of each one. The bolts used in connection H, G and F were most important to be exact and there is therefore more information given for these bolts.

The connections were made so that the set-up had the possibility to move in all directions, to account for imperfections in the specimen and making sure it was always possible to mount the specimen correctly. Elongated holes in connection B and D allowed movement of the frame in the x-direction, and elongated holes in connection E allowed movement of the upper profile in the y-direction. The press

already allowed rotation of the load cell so that the upper profile could rotate about the z-axis, and the movement of the press in z-direction allowed the upper profile to move in this direction. Washers are used at all connections.

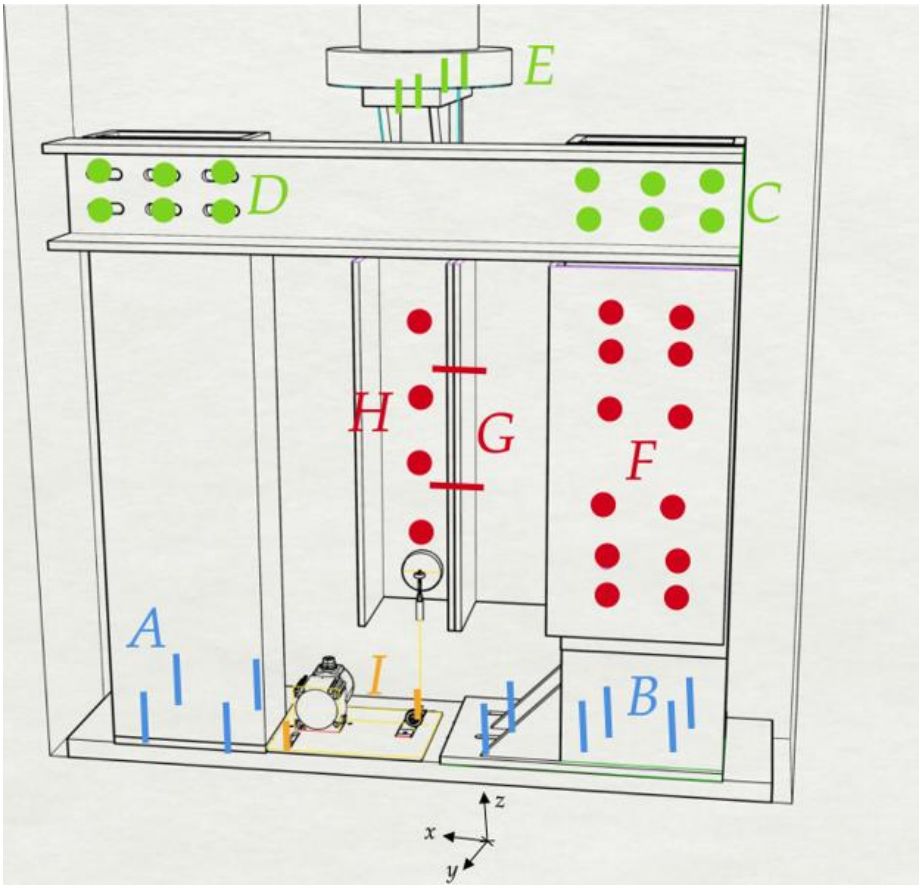

Figure 4-4: Connections in the set-up.

Table 4-3: Description of the connections in the set-up.

Connection	Connecting	Holes	Bolts/Screws	Specifications
A	Left column of frame to the base plate.	Round M11. Threaded at base plate.	4 x M10. Length uncertain. Quality uncertain.	Tightened once.
B	Right column of frame to the base plate.	Elongated M11 at the column, round M10 at the base plate. Threaded at base plate.	6 x M10. Length uncertain. Quality uncertain.	Loosened and tightened before each test.

C	Beam of the frame to the right column of the frame.	Round M12. Threaded at column.	6 x M12 8.8. Length uncertain.	Tightened once.
D	Beam of the frame to the left column of the frame.	Elongated M13 at the beam, round M12 at the column. Threaded at column.	6 x M12 8.8. Length uncertain.	Loosened and tightened before each test.
E	T-shape and the load cell by using a plate connected to the load cell.	Elongated M13 at the T-shape, round Ø12 at the plate. Threaded at plate.	4 x M12 8.8. Length uncertain.	Loosened and tightened before each test.
F	Bottom profile to the right column of the frame.	Round M15. Threaded at column.	12 x M14x50 10.9 (x2). Fully threaded. Hexagon head.	Bolts are screwed into the column once from the inside. Nuts on the outside are preloaded for each change of specimen. An identical configuration was on the back side of the column as well meant for connecting prototype ALT as it was a bit different.
G	Upper and bottom profile.	Elongated M15 at the bottom profile, round M15 at the upper profile. The placement of the holes differs between the prototypes.	2 x M14x40 or M14x50 10.9 Partly threaded. Hexagon head.	Bolts are changed and preloaded before each test. Inserted from the upper profile, nuts used to connect on the other side.
H	Upper profile to the T-shape.	Round M15.	4 x M14x50 10.9. Partly threaded. Hexagon head.	Bolts are preloaded for each change of specimen. Inserted from the T-shape, nuts used to connect on the other side.
I	Steel plate with wire sensor to the base plate.	Elongated M8 at the steel plate, round M8 at the base plate. Threaded at the base plate. Total of 4 holes, allowing to move the sensor far back for the connection of	2 x M8. Quality uncertain. Length uncertain.	Bolts adjusted when needed to.

		prototype ALT as it was a bit different.		

Connections A and C were tightened when the set-up was mounted and did not need to be loosened or tightened for the purpose of mounting a specimen. The rest of the connections were tightened or preloaded in a certain way when mounting a new specimen, aiming to connect the friction connection (G) as perfectly as possible:

1) Connections B, D and E were fastened, but left loose enough to perform further adjustments.
2) Connections F and H were fastened, but not tightened or preloaded.
3) The friction surfaces in connection G were aligned as perfectly as possible, and then preloaded to a certain value specified for the test to be performed.
4) Connection E was tightened.
5) Connections F and H were preloaded with a torque of 110 Nm. ($0{,}75M_r$ for preload of $P_{min} = 80{,}5\ kN$, step 1 calculated in chapter 4.5.1.)
6) Connection H was preloaded with a torque of 160 Nm. ($1{,}10M_r$ for preload of $P_{min} = 80{,}5\ kN$, step 2 calculated in chapter 4.5.1.)
7) Connections B and D were tightened.
8) A magnet was mounted as shown in the pictures, making sure the wire was as straight as possible. The wire was then drawn through the pulley and onto the hook of the magnet. Connection I was lastly adjusted if needed.

A certain preload of connections F and H was used to be sure they were stiff enough to not slip during the test. If the preload of these connections were enough, was checked in the very first test presented in chapter 4.5.1. By applying the same preload every time, it is assured that the connections are not damaged in any test and are able to support the specimen being tested. Connection F was preloaded at a lower value than H because it consisted of many more bolts and assumed to be much stiffer, not needing an as high preload.

When a new specimen was mounted, the load from the Instron press was always calibrated to zero to account for the weight of the upper specimen before tightening or preloading any of the connections as explained in the steps above. After everything was tightened or preloaded, the displacement of the beam of the press was adjusted using a “fine position” function, which changes the position of the beam only slightly. This was done to release the tension caused by the tightening and preloading so the load would start at an initial value as close to zero as possible. The displacements of the Instron press, wire and two LDT-sensors were then set to zero before starting the test.

4.3 Sensors

Three sensors in total were attached to the set-up and specimen: two LDT-sensors, and one wire sensor. All sensors measure displacement.

The LDT-sensors in Figure 4-5 were used to measure the rotation of the right column in the set-up by placing one sensor at the top and one at the bottom and measuring the displacement at each point. They had a measuring range of 50 mm. The sensors were fastened using two clips to make the sensors stay as horizontal as possible. Sensor b) was attached to the side of the press, using a plate attached to the bolts in the beam to extend the width of column so that the sensor could make contact. Senor a) was attached to the column, making contact with a hard part of the side of the press.

a) Sensor at the bottom of the right column *b) Sensor at the top of the right column*

Figure 4-5: LDT-sensors.

The wire sensor in Figure 4-6 was used to measure the displacement of the upper profile at its base. This was to see if the displacement at the top (input displacement from Instron) differed from the bottom. The measuring range of the wire sensor was 500 mm. The wire from the sensor was dragged out, under the pulley, and fastened at a hook on the magnet seen in the picture.

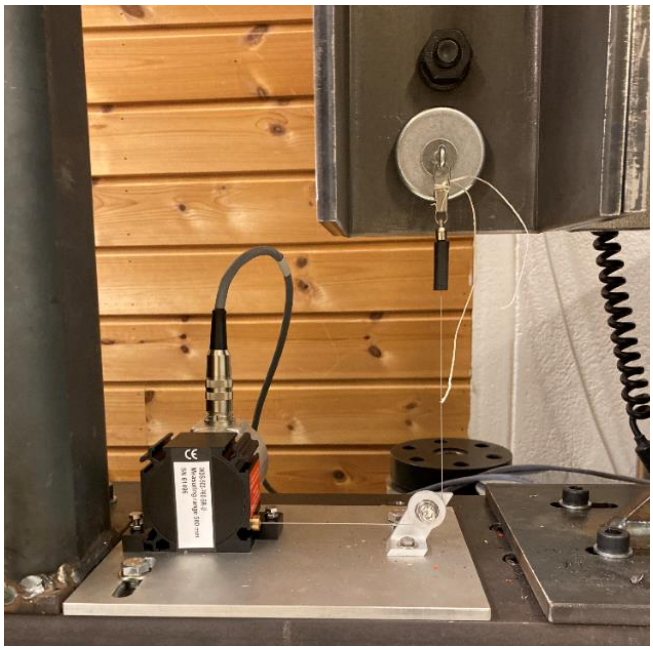

Figure 4-6: Wire sensor.

When mounting the wire sensor, it was most important to keep the horizontal part of the wire completely straight and in line with the x-axis in Figure 4-4. Therefore, the sensor and pulley were fastened permanently to a plate, so it only had to be accounted for once. The second most important was that the vertical part of the wire was straight and in line with the z-axis in Figure 4-4. These two things were specified by the producer for the sensor to work as expected.

4.4 Software

Instron Bluehill was used to create and run the protocols for all test, while Catman was mainly used for logging the data obtained. The data logged by Catman was

- the displacement from the wire sensor connected to the bottom of the top profile
- the load from the load cell from Instron
- the displacement from the LDT-sensor at the top of the right column
- the displacement from the LDT-sensor at the bottom of the right column
- and the displacement from Instron that would be the same as the input for the protocols.

All data was not logged by Catman from the beginning. The sensors were not ready to set up when the first tests were carried out. Also, the displacement from Instron was not logged correctly from the beginning, as it took some time to understand how to read it correctly into Catman.

Logging the displacement and load from Instron using Instron Bluehill was also tried for the first tests but showed not to be promising.

Detailed information about the software can be found in appendix B.

4.5 Tests

The tests were performed in the order they are presented. All preliminary tests, except the initial, are a result of the previous test. The goal of the tests was to figure out what preload to use and treatment to be done to the friction surfaces in order to obtain a slip friction load close to 30 kN, in addition to seeing how the different prototypes performed.

Bolts M14x40 and M14x50 were used for the friction connections. The k_m given by the manufacturer was 0,129.

In the investigation of the preload, the starting-out value was chosen as the nominal minimum preload given by Eq. 2-7:

$$P_{min} = 0{,}7 * f_{ub} * A_S = 80{,}5\ kN$$

Where,

$f_{ub} = 1000\ MPa$ for 10.9 bolts

$A_S = 115\ mm^2$ for M14 bolts.

This preload was used as a base in the investigation of the preload, since it was discovered that this preload was too large. All preloads in the tests are given as a percentage of P_{min}.

It was chosen to use the torque method for tightening the preloaded bolts in the friction connection as presented in chapter 2.3, even though the bolt assembly used was categorized as class K1. This was because this method was found to be the simplest to apply. It was also argued that the only reason for the bolting assembly being categorized as K1 might have been to make delivery easier, but that hopefully it could have qualified as class K2.

A simple test was performed at the end of all tests in chapters 4.5.3 and 4.5.4 to see if any of the preload was lost by attempting to preload the bolts in the friction connection to the initial value using a torque wrench. If it was possible to turn the torque wrench, some unknown value of preload had been lost during the test.

Several tests were often done to the same specimen when it looked to be intact after the previous test. The connection is meant to be intact after experiencing an earthquake and should therefore be able to experience several earthquakes and their foreshocks and aftershocks without being harmed to the extent that it would no longer work. If this were not true, it would have been discovered by the testing of one specimen several times.

The bolts in the friction connection were changed before every test. All other bolts used in the set-up were reused as they did not seem to show any damage (see chapter 5.3).

The displacement schedules used did not follow any of the standards presented in chapter 2.6, though they were based on ISO16670 (ISO, 2003) and EN 15129 (CEN, 2018b). This was because these were preliminary tests at an early stage, and the results of the initial test did not show promising results. It was therefore chosen to use lower displacements and the protocols were created to study the areas of interest more closely. The maximum displacement for the specimen was set to ±100 mm.

50 kN was set as an “end of test” criterion in the cyclic protocols created in Instron Bluehill, as this was the maximum load the used load cell could apply in cyclic testing. If the force reached this value during a test, then the test stopped automatically. The maximum value for a monotonic compression test was 100 kN.

It was expected that the load-displacement graphs produced from the cyclic tests would be perfect rectangles with a chipping effect due to the asymmetry of the connection. The slip friction load should be constant when the specimen is moving and change to a slip friction load of the same magnitude but with the opposite sign when the specimen changes direction.

4.5.1 Monotonic compression test (prototype STD)

The goal of this test was to investigate what the actual slip load would be when applying a preload according to the standards, as explained in chapter 2.3 and 2.4. Also, the test was to check that the tightening methods for the column and the T-shape were sufficient. It was chosen to use specimen STD_test which was one of the extras and therefore disposable in case something went wrong.

Bolts M14x40 were used with a preload of 100%P_{min} for the G connection. The torque to apply was calculated by Eq. 2-8:

$$M_r = k_m * d * P = 145\ Nm$$

It was chosen to not perform any treatment on the friction surfaces. The theoretical slip load was calculated by Eq. 2-9:

$$F_{s,R} = m * n * \mu * P = 32{,}2\ kN$$

Where,

$m = 2$	two bolts
$n = 1$	one friction surface
$\mu = 0{,}2$	the theoretical value for steel surfaces with no treatment
$P = 80{,}5\ kN$	100%P_{min}.

Table 4-4 summarizes the values applied to the friction connection. For the friction coefficient (μ) it was chosen to do no treatment to the friction surfaces because this was the easiest treatment, and therefore seen as a good starting point. The value of the friction coefficient (μ) was uncertain, so a standardized value from EN 1090-2 (CEN, 2018a) was chosen. The preload value (P) was chosen after the standards to have a starting point. Also, the friction coefficient (μ) and preload value (P) chosen produced a theoretical slip load close to 30 kN, which was the wanted value. As seen in the beginning of chapter 4.5, these were the two factors that were to be adjusted to obtain the wanted slip load.

A high speed of 4 mm/s was used to run the test, as it would be realistic for an earthquake to work at a high speed. The profile was to move 100 mm down from its initial position. All sensors had not yet been set up, so only the load and displacement data were logged using Instron Bluehill, in addition to also logging the load and displacement measured by Instron using Catman to see if Catman was working as expected. It was, however, not figured out how to give the right analog displacement output from Instron to use in Catman, but the values produced were still logged in hope of finding a method for converting the values to the correct ones afterwards.

Table 4-4: Overview of the monotonic compression test.

Specimen used	STD_test
Bolts	M14x40
Preload 100%P_{min}	80.5 kN
Applied torque	145 Nm
Torque application step 1 (0,75*Mr)	110 Nm
Torque application step 2	160 Nm
Treatment of friction surface	none
Theoretical friction coefficient	0,2
Theoretical slip load	32,2 kN
Maximum displacement	100 mm
Speed	4 mm/s

The procedure for tightening and preloading the connections as described in chapter 4.2 was not yet developed. For this test, step 3) occurred after step 6).

4.5.2 Loose tests (prototype STD)

The goal of this test was to check that the bolts were moving along the elongated holes as expected, to be sure that the unexpected results of the previous test was not due to imperfections in the specimen, set-up or load application causing the bolts to alter their direction of movement. The test was done twice, the second time connecting all the sensors. The sensors were before this not ready to be connected, so when they were it was decided to do a simple test to check that everything was working as expected with the Catman software logging all data from the sensors. The analog displacement output from Instron was still not working.

A new specimen, STD_1, was used, as STD_test was damaged beyond reuse by the previous test.

The bolts in the friction connection were left completely loose, so the forces acting on the system from the friction connection should be close to nothing.

First, one cycle of 50 mm was run, and then a cycle of 100 mm. The speed was reduced to 0.5 mm/s to be able to stop the test before the specimen taking damage in the case something went wrong. Figure 4-7 shows the displacement schedule for the tests.

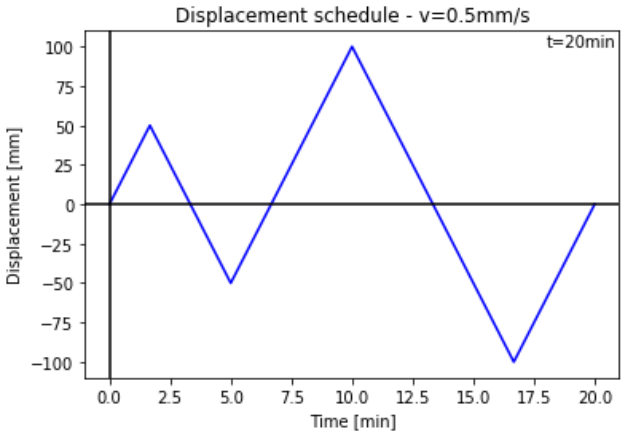

Figure 4-7: Displacement schedule for loose tests.

The tests are summarized in Table 4-5:

Table 4-5: Overview of the loose tests.

	Test A	Test B
Specimen used	STD_1	
Preload (% of P_{min} = 80,5 kN)	0% = 0 kN	
Cycles	1 x 50 mm 1 x 100 mm	
Speed	0,5 mm/s	
Data logged	Displacement and load form Instron using Instron Bluehill.	Data from all sensors using Catman. (Analog displacement output from Instron not working.)

4.5.3 30%P_{min} cyclic tests (prototype STD)

Specimen STD_1 was intact after the previous tests and was therefore reused for the three tests in this section.

As a result of the test in section 4.5.1, the preload was now decreased to a much smaller value of $30\%P_{min}$ to see if the specimen performed better and if the load came closer to the wanted value of 30 kN.

Bolts M14x40 were used. The torque to apply was calculated by Eq. 2-8:

$M_r = k_m * d * P = 43{,}6\ Nm$

It was chosen to still not do any treatment to the friction surfaces, as this would increase the friction coefficient and thereby the slip load which was the opposite of what was necessary. The theoretical slip load was calculated by Eq. 2-9:

$F_{s,R} = m * n * \mu * P = 19{,}4\ kN$

Where,

$m = 2$	two bolts
$n = 2$	two friction surfaces, realizing that the washers together with the bottom profile were acting as a friction surface
$\mu = 0{,}2$	the theoretical value for steel surfaces with no treatment
$P = 24{,}2\ kN$	30%P_{min}.

First, it was decided to start slowly performing a test A with a small maximum displacement of 30 mm. A quite simple protocol was used, starting at one cycle of a displacement of 5 mm, then 3 cycles for each new maximum displacement starting at 10 mm and increasing by 10 for all the rest. If that went well, it was decided to extend the protocol to a maximum of 50 mm and perform a test B. A third test C identical to test B was performed, as the results of test B were surprising. The one difference between test B and C was that test B was set up and preloaded two days before performing the test, while for test C the test was performed right away. The test A was also performed right away. The protocols are visualized in Figure 4-8.

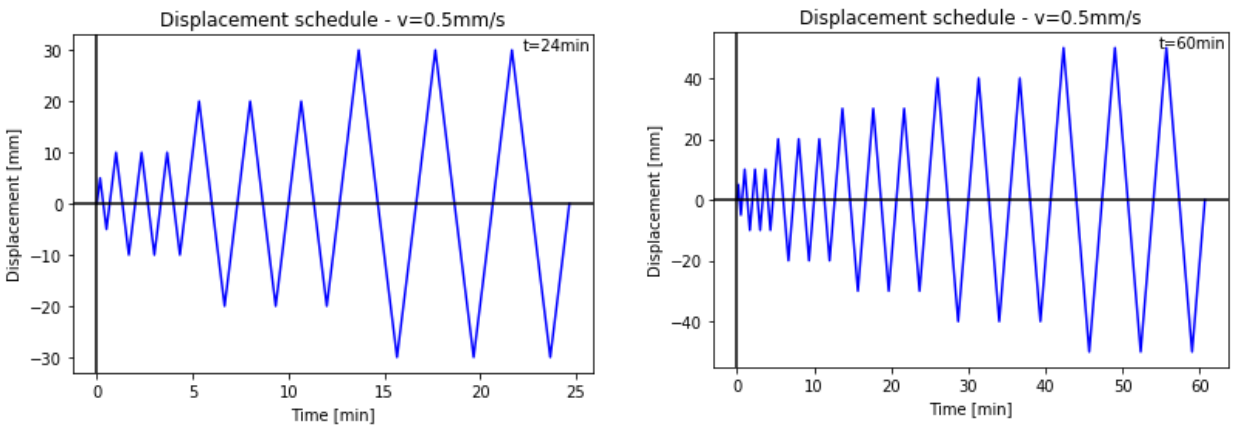

a) Test A

b) Test B and C

Figure 4-8: Displacement schedules for 30%P_{min} tests.

A slow speed of 0,5 mm/s was used to have better control over the tests, being able to stop it if something went wrong or in case the connection needed time to adjust to move correctly. It was in general decided to use this slow speed until something seemed to work well, meaning the friction connection working as a friction connection, giving a somewhat correct slip load, and weaknesses in the specimen not affecting the friction connection.

The tests are summarized in Table 4-6:

Table 4-6: Overview of the 30%P_{min} tests.

	Test A	Test B	Test C
Specimen used	STD_1		
Preload (% of P_{min} = 80,5 kN)	30% = 24,2 kN		
Applied torque (Mr)	43,6 Nm		
Torque application step 1 (0,75Mr)	32,7 Nm		
Torque application step 2 (1,10Mr)	48 Nm		
Cycles	1 x 5 mm 3 x 10 mm 3 x 20 mm 3 x 30 mm	1 x 5 mm 3 x 10 mm 3 x 20 mm 3 x 30 mm 3 x 40 mm 3 x 50 mm	
Speed	0,5 mm/s		
Treatment of friction surface	None		
Theoretical friction coefficient	0,2		
Theoretical slip friction load	19,4 kN		

4.5.4 Cyclic tests using aluminum shim layers (all prototypes)

At this point, a new type of configuration of the friction connection was designed and tested, as described in chapter 2.5 and shown in Figure 4-9. A steel plate of 8 mm thickness was introduced on the outside of the friction surface on the side of the bottom profile. This plate would replace the washers as a friction surface, hopefully resolving a problem of steel from the bottom profile being scraped off by the washers as will be seen in the results in chapter 5. Thin aluminum plates of 2 mm thickness were added in between as shim layers. Aluminum was specifically chosen because it could easily be obtained and because it was used in the research presented in chapter 2.5.

Bolts M14x50 were used for these tests, as the bolts would require a larger length due to the added plates.

Figure 4-9: Friction connection with an extra steel plate and aluminum shim layers.

At this point the standard prototype STD had thoroughly been tested, and problems related to the friction connection were attempted to be resolved by the new configuration used for the tests in this section. For these tests it was therefore decided to perform at least one test for each prototype. A maximum of four tests could have been performed for each prototype. To move on to the next test, the previous had to be seen as a success. The four possible tests were as follows:

Test A - Preload of $30\%P_{min}$ with displacement schedule a) in Figure 4-10 with a speed of 0,5 mm/s.

Test B - Preload estimated from results of test A to reach a slip load of 30 kN derived from Eq. 2-9:

$F_{s,R} = mn\mu P$ becomes
$F_{s,R} = CP$ when $C = mn\mu$ is a constant. *Eq. 4-1*
The value of the constant C can be calculated from the results of test A:
$C = \frac{F_{s,R,A}}{P_A}$. *Eq. 4-2*
The preload for test B is then
$P_B = \frac{30\ kN}{C}$. *Eq. 4-3*

Using displacement schedule a) in Figure 4-10 with a speed of 0,5 mm/s.

Test C - Same preload as in test B but using displacement schedule b) in Figure 4-10 with a speed of 2,0 mm/s.

Test D - Same preload as in test B and C, but using displacement schedule c) in Figure 4-10 which goes all the way to 100 mm, with a speed of 2,0 mm/s.

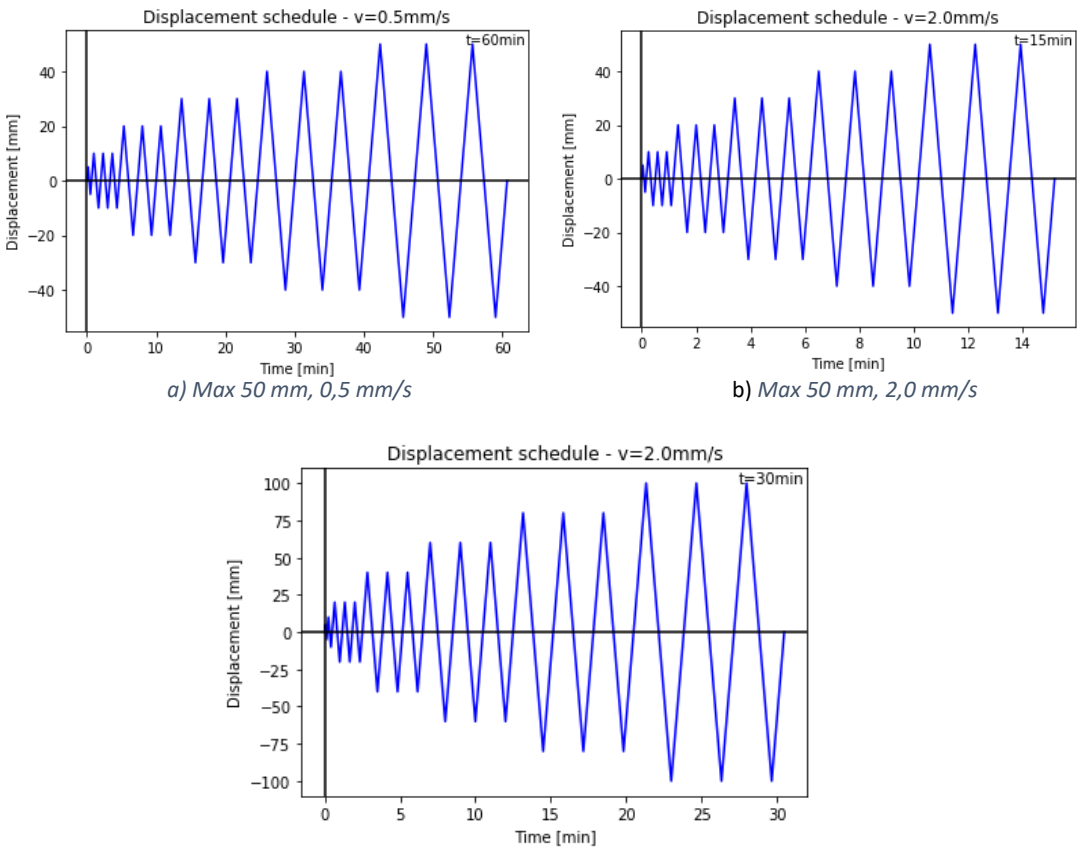

a) Max 50 mm, 0,5 mm/s

b) *Max 50 mm, 2,0 mm/s*

c) Max 100 mm, 2,0 mm/s

Figure 4-10: Displacement schedules for cyclic tests using aluminum shim layers.

For all tests A using $30\%P_{min}$, the torque applied and theoretical slip load is the same as calculated in chapter 5.6. Two prototypes made it to test B, and the preloads, torques to apply and theoretical slip loads were calculated as follows using Eq. 4-2, Eq. 4-3 and Eq. 2-8:

STD-1H_1:

$$C = \frac{F_{s,R,A}}{P_A} = 0{,}662$$

Where,

$F_{s,R,A} = 15\ kN$ from chapter 5.6

$P_A = 24{,}1\ kN.$

$$P_B = \frac{30\ kN}{C} = 45{,}3\ kN$$

$$\frac{45{,}3}{80{,}5} = 56\% P_{min}$$

$$M_r = k_m * d * P = 81{,}8\ Nm$$

ALT_1:

$$C = \frac{F_{s,R,A}}{P_A} = 0{,}830$$

Where,

$F_{s,R,A} = 20\ kN$ from chapter 5.6

$P_A = 24{,}1\ kN.$

$$P_B = \frac{30\ kN}{C} = 36{,}1\ kN$$

$$\frac{36{,}1}{80{,}5} = 45\% P_{min}$$

$$M_r = k_m * d * P = 65{,}2\ Nm$$

The tests are summarized in Table 4-7:

Table 4-7: Overview of cyclic tests using aluminum shim layers.

Prototype	STD	STD-1H		STD-R	ALT			
	Test A	Test A	Test B	Test A	Test A	Test B	Test C	Test D
Specimen used	STD_2	STD-1H_1		STD-R_1	ALT_1			
Preload (% of P_{min} = 80,5 kN)	30% = 24,2 kN	30% = 24,2 kN	56% = 45,3 kN	30% = 24,2 kN	30% = 24,2 kN	45% = 36,1 kN		
Applied torque (Mr)	43,6 Nm	43,6 Nm	81,8 Nm	43,6 Nm	43,6 Nm	65,2 Nm		
Torque application step 1 (0,75Mr)	32,7 Nm	32,7 Nm	61,4 Nm	32,7 Nm	32,7 Nm	48,9 Nm		
Torque application step 2 (1,10Mr)	48 Nm	48 Nm	90,0 Nm	48 Nm	48 Nm	71,7 Nm		
Cycles	1 x 5 mm 3 x 10 mm 3 x 20 mm 3 x 30 mm 3 x 40 mm 3 x 50 mm							1 x 5 mm 1 x 10 mm 3 x 20 mm 3 x 40 mm 3 x 60 mm 3 x 80 mm 3 x 100 mm
Speed	0,5 mm/s						2 mm/s	
Treatment of friction surface	none							
Theoretical friction coefficient	0,2							
Theoretical/ estimated slip friction load	19,4 kN	19,4 kN	30 kN	19,4 kN	19,4 kN	30 kN		

For the mounting procedure described in chapter 4.2, one exception was done. For the test using prototype STD-R, step 4) was done before step 3) due to space issues caused by the reinforcement.

5 Results and discussion

All graphs, also those not presented in here, are found in appendix C.

For many of the tests, some preload was lost. The standard specifies a minimum preload value of 70% of the bolt tensile capacity, as presented in chapter 2.3. Only the initial test uses a preload of this value, while all others are using a much lower value. Though the reason is unknown, the standard must have a reason for specifying a minimum value, and it should not be surprising that ignoring this might cause problems. Using other preload values than allowed might be one reason for loosing preload in the tests, and the preload in general being unpredictable.

5.1 Set-up

The displacements in mm of the column measured by the LDT-sensors for most of the tests were small, resulting in a small rotation in radians as well. Figure 5-1 shows the graph created from the data form test B of the $30\%P_{min}$ tests with specimen STD_1 as an example. Here, the maximum displacement of the top of the column including the sliding of the bottom was as high as 1,5 mm. This was the maximum value measured for any of the test. For several tests the maximum stayed as small as 0,4 mm.

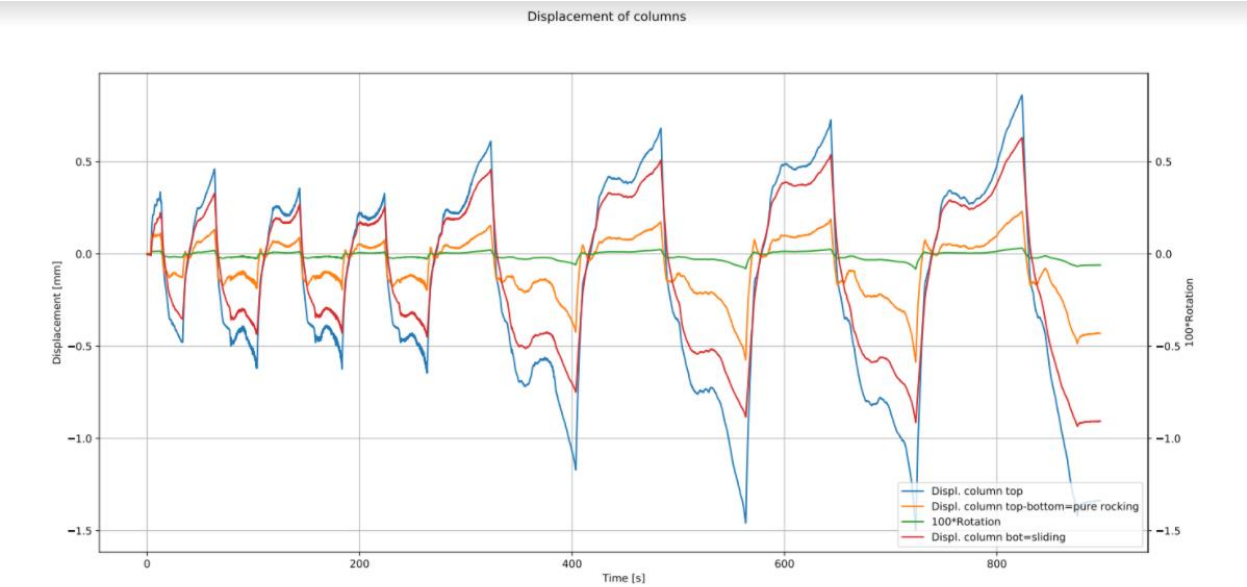

Figure 5-1: Displacement and rotation of the right column i the set-up for test B of the $30\%P_{min}$ tests (specimen STD_1).

It is seen in the figure that the displacements and rotations appear in cycles, which is in accordance with the protocols of the tests. The bending moment acting on the column increases as the displacement of the protocols increases, which is seen as an increased displacement and rotation of the column.

5.2 Displacement from Instron vs. wire sensor

The difference between the displacement measured by the Instron press at the top of the upper profile and the wire sensor at the bottom of the upper profile were plotted in a graph for all test where both measurements were logged. Figure 5-2 shows the curve plotted for test B of the $30\%P_{min}$ tests with specimen STD_1 as an example. The difference usually stayed at a maximum of 0,75 mm for all the tests, sometimes going as high as 1,5 mm.

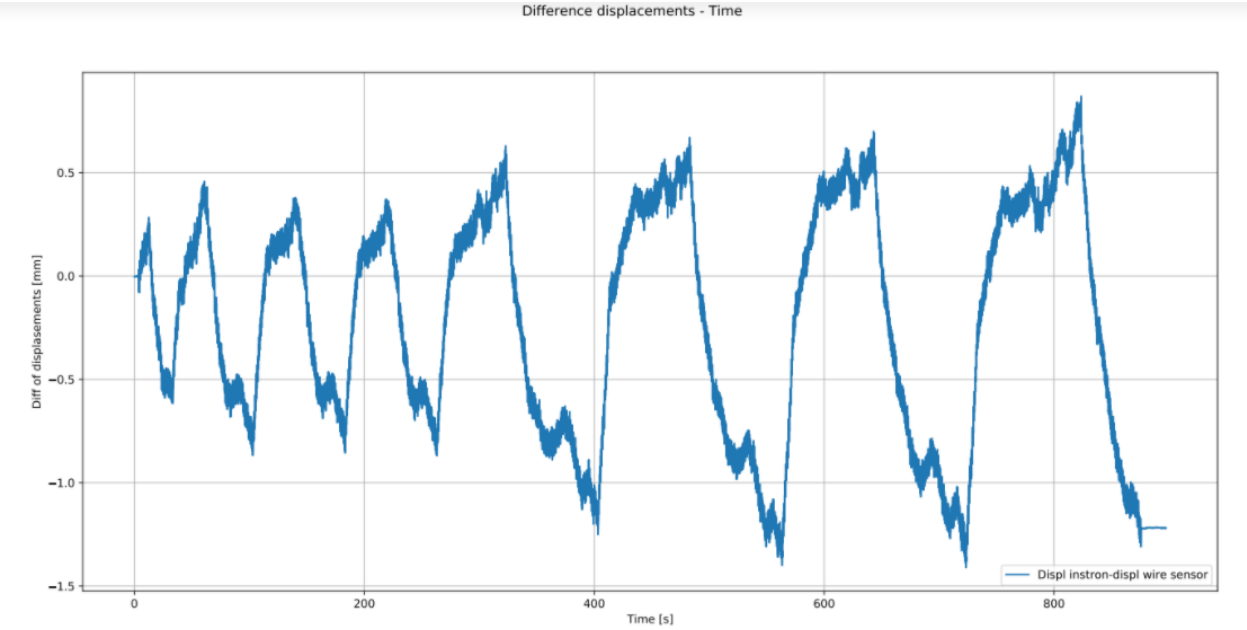

Figure 5-2: Difference between displacements measured by the wire sensor and Instron press for test B of the $30\%P_{min}$ tests (specimen STD_1).

It was observed during testing, that the wire on the wire sensor did not stay straight during testing but changed angle as the specimen moved. This indicated that there was some rotation in the T-element which explains the difference in displacements. This rotation was however not measured.

The load-displacement curves created using the two different displacements looked very much alike, the only difference being the wire sensor not quite reaching the maximum displacements. It was therefore chosen to only show force-displacement curves created using one of the displacements. The displacement from the wire sensor was chosen.

5.3 Monotonic compression test (prototype STD)

The connections of the upper profile to the T-element, and the bottom profile to the column did not look to be affected by the test. The connections kept the profiles in place as expected, and no damage was done to the bolting assemblies.

Large deformations in the bottom profile were instantly observed. At 90,24 mm the deformations were so large, it was decided to stop the test.

a)

b)

c)

d)

Figure 5-3: Twisting seen in specimen STD_test after the monotonic compression test.

Figure 5-3 shows the deformations in the profiles after the monotonic compression test was stopped. The lateral force applied to the friction connection created a bending moment as visualized in Figure 5-4. As seen in the figure, the bending moment will create forces in the positive x-direction at the top of the rightmost surface of the U-shape of the bottom profile (DC), and forces in the negative x-direction at the bottom (GH). These forces caused the plate CDGH to deform plasticly in the positive x-direction at point C and in the negative x-direction at point G, as seen in Figure 5-3 a). Points D and H did not deform because they are held in place by the rigid connection in plate HDIJ. This caused the biggest stresses in the steel profile to be in the line HD as this was the resisting part of the plate CDGH.

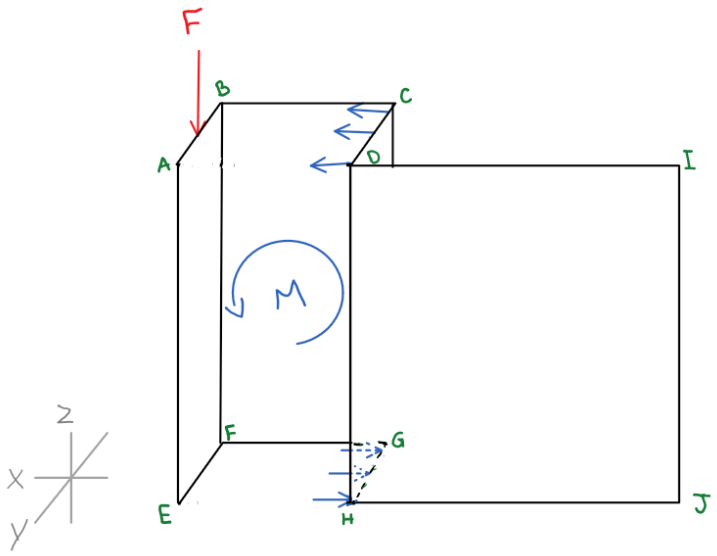

Figure 5-4: Demonstration of the bending moment in the bottom profile due to the friction force applied to the bottom profile.

The deformations described also caused a twisting effect in the plate ABEF. When the force was applied as shown in Figure 5-4, the plate started to twist in the direction A-E-F-B, as seen in Figure 5-3 b) and c). After the initial twist of the steel plate, the twist was most likely worsened by the eccentricities caused by the distance between the bolts in the friction connection in the y-direction. The force would probably no longer go through the center of the plate, thus the force would not be transferred to the bolts with an equal magnitude, as shown in Figure 5-5. This created a moment about the center of the plate, amplifying the twist. This again effects the plate CDGH by transferring more force and causing even bigger deformations.

In total, the deformations are seen as torsional deformation of the U-shape of the bottom profile, as seen in Figure 5-3 d). The upper profile did not have any visible deformations.

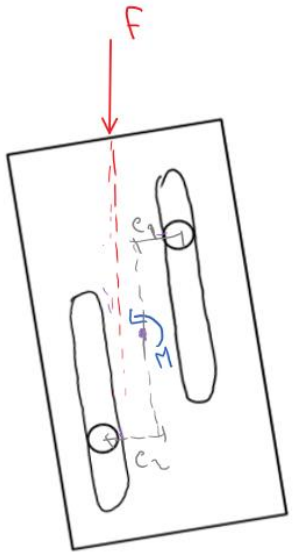

Figure 5-5: Effect of eccentricities on the twisting effect.

a) *b)*

Figure 5-6: M14x40 bolts in the friction connection of STD_test after performing the monotonic compression test.

During the test, the washers of the bolts on the inside of the bottom profile easily scraped off the steel material on the profile as shown in Figure 5-6. This was due to the washers and the outside of the elongated holes acting as a friction surface that was not accounted for. The washers having a small area, applied a concentrated stress onto the steel plate. The washers and bolts were of a much higher

hardness than the steel profile and could therefore easily scape off the material of the plate. The washers did though suffer deformations. This effect could have been reduced by using washers with a larger area, distributing the preload over a larger area and reducing the magnitude of the stress applied to the steel plate.

Figure 5-7 shows the force-displacement curve obtained from the test. Instron Bluehill failed to record any data, but the load was logged by Catman and the timestamp from Catman was used to calculate the displacements related to the forces. (A method for translating the analog displacements from Instron press that were read into Catman in the wrong way, was not possible at this stage.)

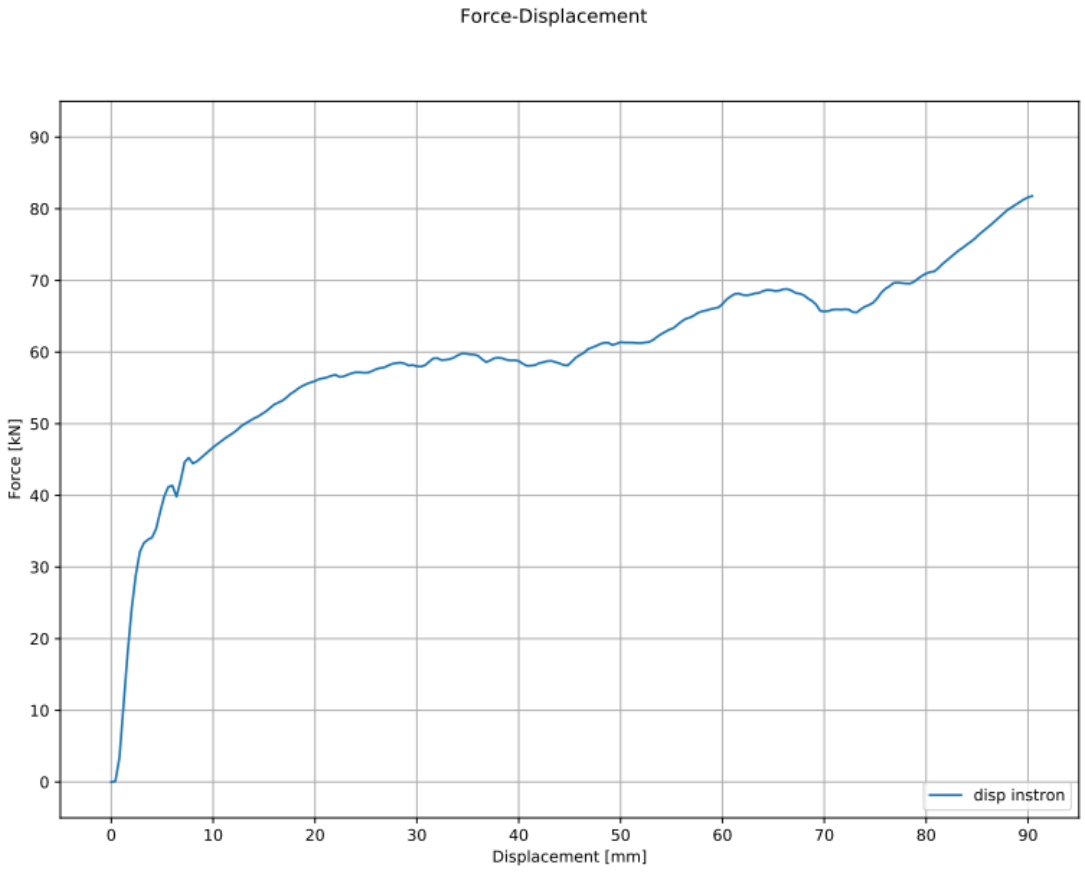

Figure 5-7: Force-displacement graph produced from the monotonic compression test.

Seen from the graph, the connection looked to start slipping at a load of about 35 kN, but slowly increasing with the displacement until stabilizing at about 60 kN for a while. Later, the force started to increase again, ending at a load of about 82 kN.

The stabilized value was most likely to be the slip friction load, as a slip friction load is expected to be stable at slip. Realizing that there were two friction surfaces in the connection, and not the assumed one, it was not surprising that this value was about twice of that calculated.

Due to the twisting effect of the friction connection, the bolts were pushing against the sides of the elongated holes. It was therefore not only the friction affecting the force in Figure 5-7, but a combination of the friction between the surfaces of the profiles, the friction between the bolts and sides of the elongated holes, and the resistance of the elongated holes where the bolts pushed against the sides. The twisting increased at larger displacement, resulting in the last mentioned phenomenon having a large effect and causing another increase in force at the end of the test. This can be seen by the deformations of the elongated hole in Figure 5-6 b). The profiles were not designed to withstand this load at the sides of the elongated holes, so this deformation was not surprising.

5.4 Loose tests (prototype STD)

Both test A and B went as expected. The bolts were moving along the elongated holes without any problems. This means the results of the previous test were not due to imperfections in the specimen, set-up or load application.

All sensors worked as expected, and their outputs were read into Catman without problems.

5.5 30%P_{min} cyclic tests (prototype STD)

For these tests, both twisting and scraping of steel on the sides of the elongated holes were observed as well. The scraping however only occurred during test A. For tests B and C, the washers simply seemed to be sliding on the path created by test A. A lot of noise was observed in the initial cycles of test A, assumably due to the scraping of the steel. The scraping did not continue in the cycles with larger displacements. As seen in Figure 5-8, the marks created by the scraping only extended approximately 20 mm from the initial position.

For test A the bottom bolt was completely loose after the test finished, meaning all preload was lost during the test, while it was possible to preload the upper bolt to the initial value using a torque wrench. Less, but a significant amount of preload was therefore lost in the upper bolt. A significant amount of preload was also lost in both bolts in test C. It was first assumed that the preload being lost was the reason for the scraping only to be present for the initial cycles, but in test B the preload was intact after the test so this could not have been the case. After completing test B, there was also a theory that the scraping of the holes caused the loss of preload and that that was the reason for not losing any preload in test B. Running test C, this turned out not to be the case since preload was again lost. The preload only being intact for test B, was more likely due to the preload being left for two days before running the test. In any case, the preload showed to be very unpredictable.

Figure 5-8: Detail of the specimen after test A.

The twisting effect was much larger in the beginning of test A and C than later, while in test B it was large during the whole test. This corresponds with the preload in the systems at all times, as more preload would transfer more loads into the system creating higher bending moments. In addition, the eccentricities caused by the arrangement of the bolts causing more twist and bending moment. The reader is referred to chapter 5.3 for details on how this worked.

In test A, Figure 5-9 a), there was an increase in the force for the initial cycles, but then the force dropped for every cycle, at last almost stabilizing at approximately 14 kN. The same increases and drops were observed in the curves in Figure 5-9 c) form test C, though there was a lot of noise in the graph. The reason for the noise could be because the specimen was already tested twice, meaning there could have been some particles scraped off the steel making the path of the friction connection less smooth. Test C also at some point suddenly goes off the path of the curve and reaches the maximum value of 50 kN. This sudden and rapid increase in force was likely due to the friction connection surprisingly experiencing a higher twist, resulting in the bolt pushing more against the sides of the elongated holes resulting in the resistance of the elongated holes being measured.

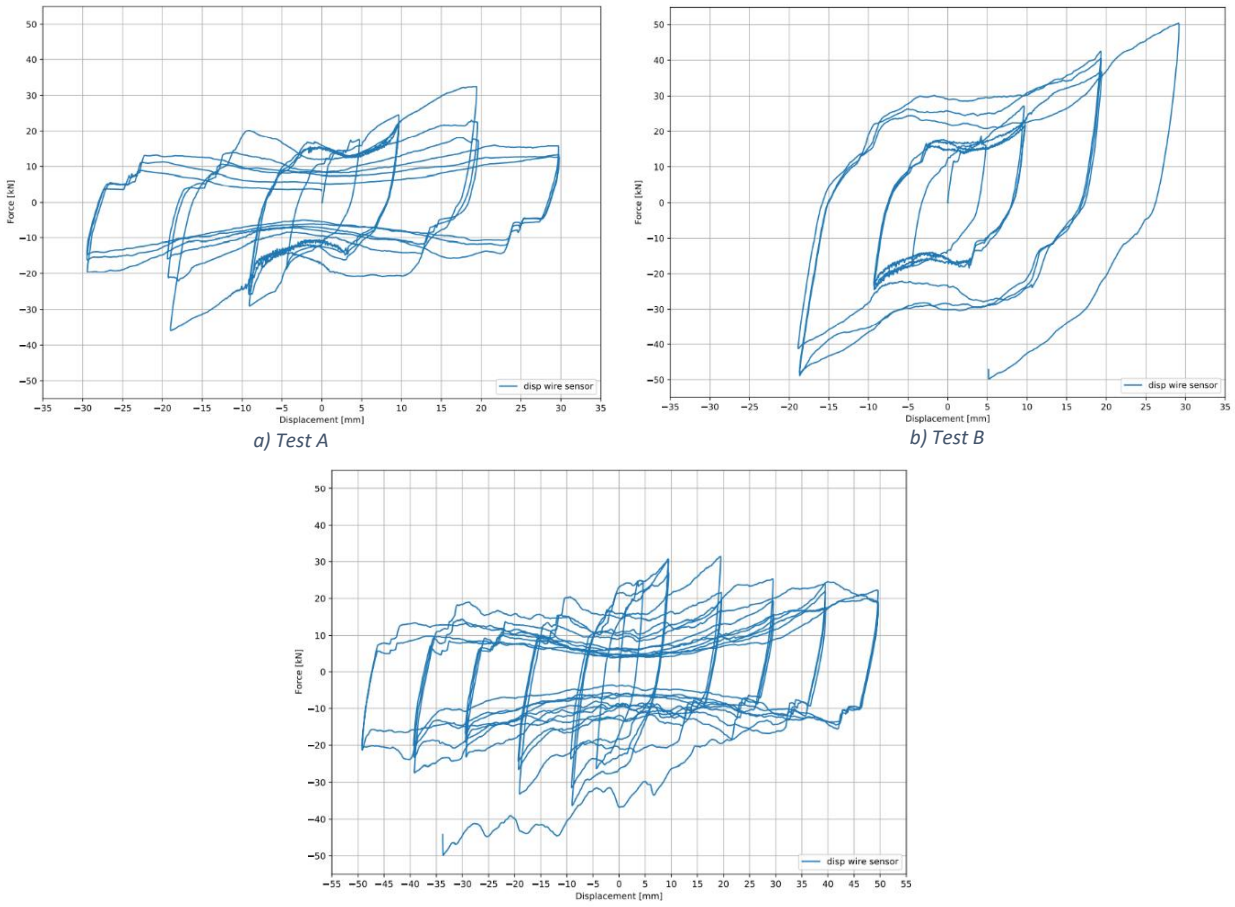

a) Test A

b) Test B

f) Test C

Figure 5-9: Force-displacement curves for the $30\%P_{min}$ tests.

In test B, Figure 5-9 b), where the preload was kept intact, the load kept increasing throughout the test. The higher preload being present throughout the test, meant a large bending moment, and especially a larger twisting effect due to the eccentricities caused by the arrangement of the bolts. The twisting increased for each load step, resulting in bolts pushing harder against the sides of the elongated holes for each increase in maximum displacement, resulting in the maximum force increasing every time. The force increasing with an increasing displacement during every cycle as well, indicates the continued twisting during the movement of the specimen. Test B also stopped when reaching a force of 50 kN.

With some imagination curves in Figure 5-9 and Figure 5-10 were seen as rectangles, but far from perfect rectangles as expected. Looking closer, the force always increased with an increasing displacement, as noted for test B this shows that the specimen was twisting during the test. This shows clearly that the force always was a combination of the slip friction load and the bolts pushing against the edges of the elongated holes. Eliminating the moment occurring in the bottom profile by making the profile more moment resistant and reducing the eccentricities by changing the bolts so they are

symmetric about the axis parallel to the length of the profile, would reduce or even remove this twisting and the curves would likely be closer to perfect squares.

Figure 5-10: Force-displacement curves for tests A, B and C for the $30\%P_{min}$ tests plotted together.

From Figure 5-10 it can be seen that all the tests created almost the same curve in the initial cycles with small maximum displacements, while for the rest of the tests only test A and C looked the same. Test B experienced higher loads than test A and C. This was due to the test B being the only one keeping its preload intact. The test A and C being so much similar also indicated that their loss of preload followed a somewhat similar development.

No plastic deformations were observed on the specimen by eye.

5.6 Cyclic tests using aluminum shim layers (all prototypes)

The problem of the washers scraping off steel material from the plate of the bottom profile was no longer existent. The extra steel plate worked as expected, substituting the washers in acting as a friction surface.

The aluminum plates in the friction connection experienced some wear during testing, as seen in Figure 5-11. Specimen STD_2 is used as an example in the figure, but the friction surfaces for all the specimens looked somewhat the same. Some material was scraped off the aluminum plates, concentrated along where the elongated holes would have been. The friction surface on the steel profiles did not suffer this same scraping since steel is harder than aluminum. It was assumed that it was better for the aluminum to be slightly worn out than the steel profiles, as it would be much easier and cheaper to change the aluminum plates in the case of an earthquake producing this damage to the connection.

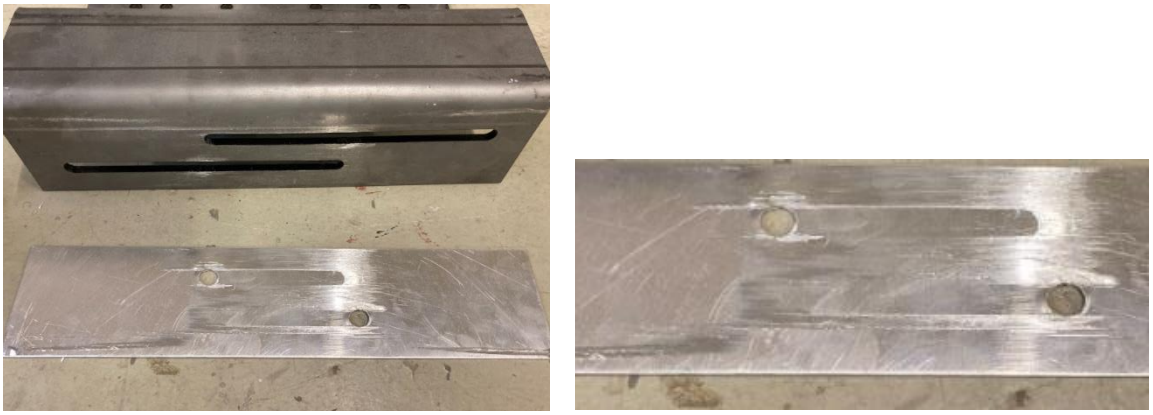

a) Bottom profile and aluminum plate *b) Worn part of aluminum plate*

Figure 5-11: Detail showing the surfaces of one friction connection after testing of STD_2.

5.6.1 Prototype STD

The test stopped during the first cycle of 20 mm as it reached the maximum force of 50 kN, as seen in Figure 5-12. The same issues of twisting previously presented and discussed, was present also this time testing the prototype STD. Because of this it was decided that no more tests would be done on this specimen, since the friction connection would not work properly without increasing the moment resistance of the bottom profile and reducing the increase of twisting due to the arrangement of the bolts.

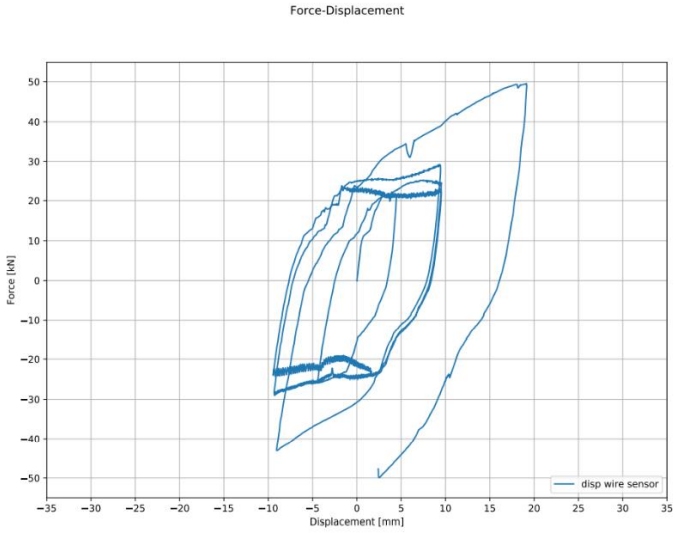

Figure 5-12: Force-displacement curves for prototype STD test A for the cyclic tests using aluminum shim layers.

No preload was lost, likely due to the test not lasting for very long.

No plastic deformations were observed on the specimen by eye.

5.6.2 Prototype STD-1H

Test A of $30\%P_{min}$ preload went unexpectedly well. The test completed all its cycles, and the force-displacement curve in Figure 5-13 a) was close to looking like perfect rectangles. A peak in the force in the initial cycles corresponded with the use of aluminum shim layers, as seen in Figure 2-7 b) presented in chapter 2.5 showing a force-displacement curve also using aluminum shim layers in a steel slip friction connection.

The shape of the curves indicates that the alterative arrangement of the bolts being aligned along the length of the profiles, reduced the increase in twisting, and was effective to isolate the slip friction force as the only force. Much less twisting was also observed, substantiating this assumption.

After the initial cycles, the force did however decrease a small amount for every cycle. After the initial peak in the force, it stabilizes at approximately 15 kN, and slowly decreases for every cycle, ending at a force of about 10 kN. This indicated that some preload was lost during the test, which was verified after the test using the torque wrench to successfully tighten the bolts to the initial preload.

The value of 15 kN was assumed to be the slip load for the initial preload and used to calculate the preload for test B.

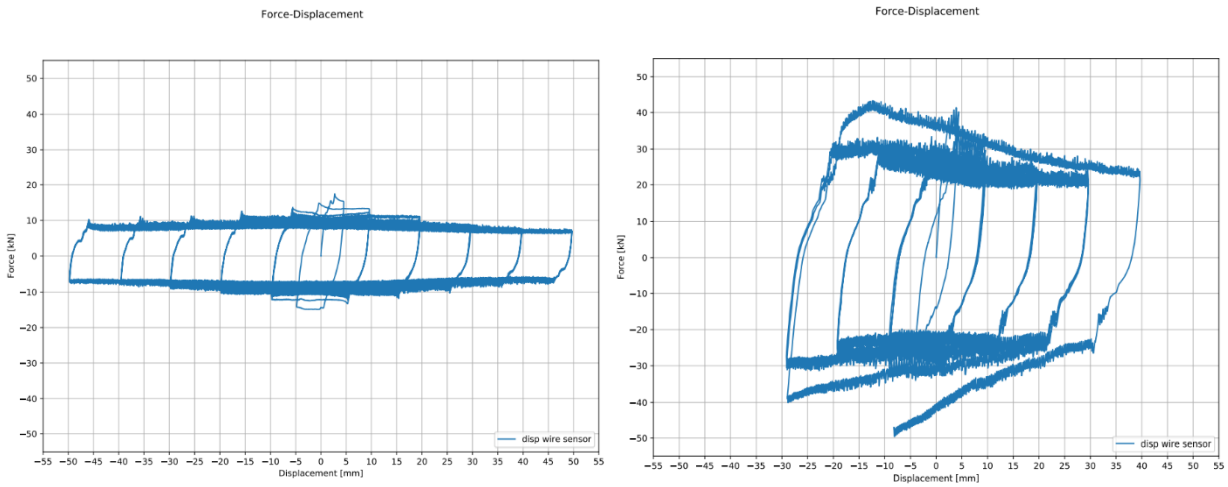

a) Test A *b) Test B*

Figure 5-13: Force-displacement curves for prototype STD-1H for the cyclic tests using aluminum shim layers.

The force-displacement curve of test B, in Figure 5-14 b), were not perfect rectangles. More twisting deformations of the bottom profile than in test A was observed, though still less compared to prototype STD. This means that the increased preload produced a slip friction force creating a higher bending moment in the bottom profile that the bottom profile was not able to withstand. For this reason, it was decided not to perform any more test on the STD-1H prototype.

Test B stopped before completing the protocol, as the load reached the maximum value of 50 kN. The preload was intact after the test.

No plastic deformations were observed on any of the specimens by eye.

5.6.3 Prototype STD-R

Seen in Figure 5-14, this test stopped due to reaching the maximum value of 50 kN very early in the protocol.

Much more twisting was observed for this test, than for all tests done on prototype STD. The reinforcement made the U-shape of the bottom profile much stiffer. Instead of much of the deformation happening in the plate CDGH alone, the whole rectangular block of the U-shape was moving as one rigid body, increasing the twisting caused by the initial bending moment due to the slip friction force. This, in

addition to the configuration of the bolts being unsymmetric about the z-axis causing the unwanted eccentricities, created a large twisting effect. Because of this, it was decided not to perform any more tests on this prototype.

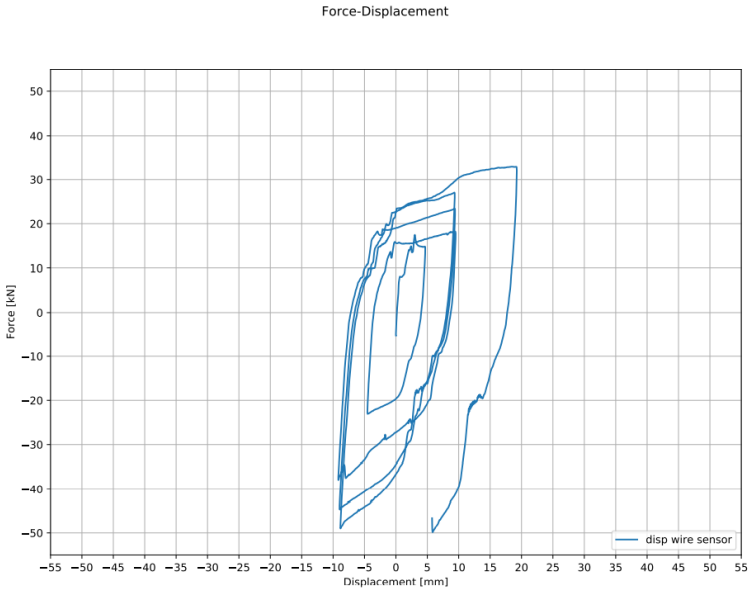

Figure 5-14: Force-displacement curves for prototype STD-R test A for the cyclic tests using aluminum shim layers.

The curve in Figure 5-14 did not start at a load of exactly zero. This was because it was neglected to fine adjust the displacement before starting the test to release the force caused by the preloading and tightening of all bolts in the connection and set-up. Besides the curve starting at a lower load, this did not affect the results in the graph.

No preload was lost during the test, likely due to the test not last for very long.

No plastic deformations were observed on the specimen by eye.

5.6.4 Prototype ALT

No obvious twisting effect was observed during test A, meaning the bottom profile of the ALT design is much stiffer than all the other prototype designs. It produced a perfectly rectangular force-displacement curve, seen in Figure 5-15 a), even including the chipping effect at the beginning due to the asymmetry. There was however no peak in the force at the initial cycles, which is unexpected. The force stabilizes at a value of 18-22 kN, which corresponds to the slip load of 19,4 kN calculated. This indicates that the value of 0,2 for the friction coefficient is close to the real value. The slip force is assumed to be around 20 kN, as this was the mean value of the values observed during the test, and was used for calculating the preload used for the test B, C and D.

Some, but not much preload was lost for test A.

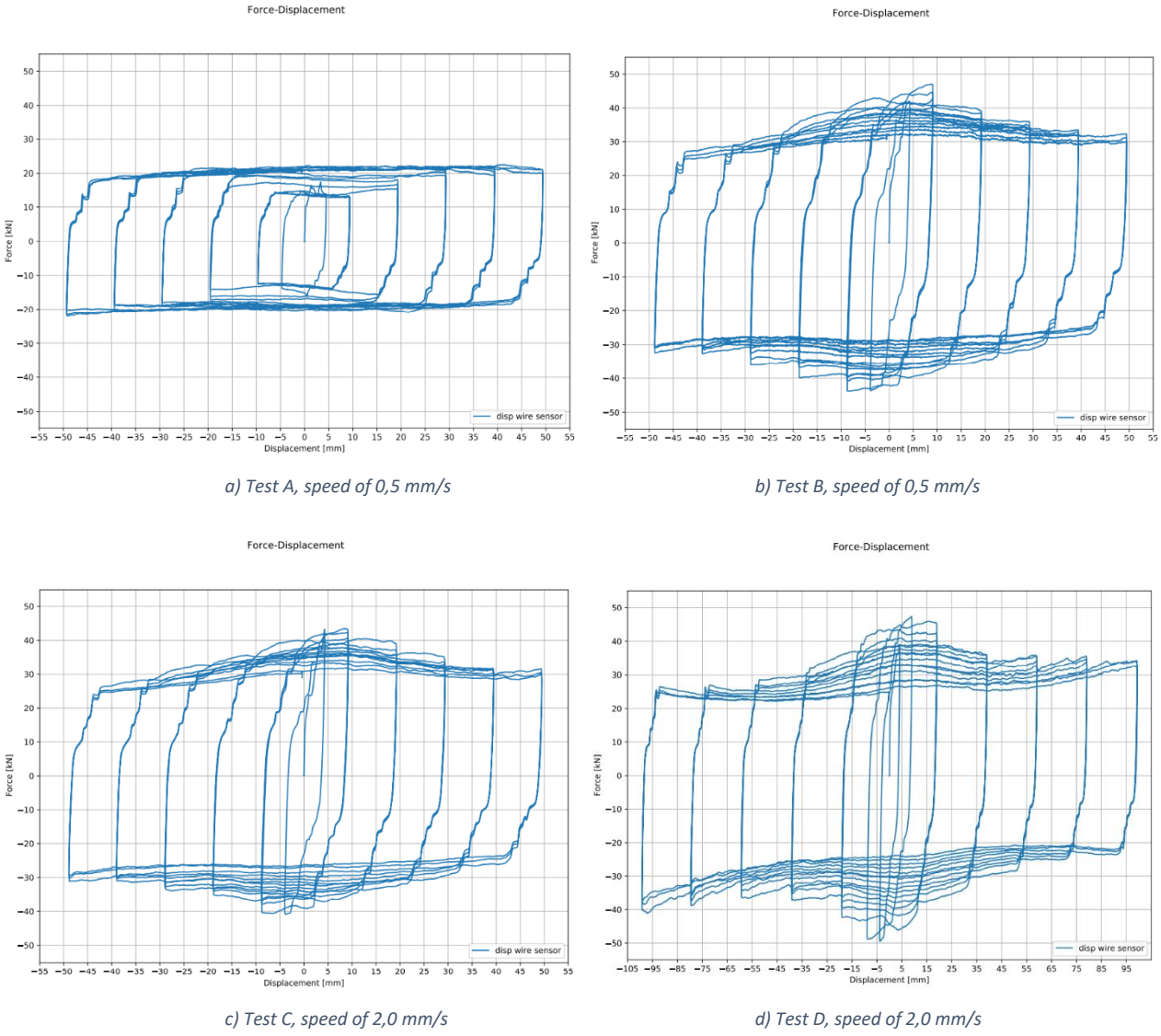

a) Test A, speed of 0,5 mm/s

b) Test B, speed of 0,5 mm/s

c) Test C, speed of 2,0 mm/s

d) Test D, speed of 2,0 mm/s

Figure 5-15: Force-displacement curves for prototype ALT for the cyclic tests using aluminum shim layers.

The peaks in the initial cycles were present for tests B, C and D, seen in Figure 5-15 b), c) and d). The chipping effect was present on all these tests as well. The force in test B and C, and also for the cycles up to 50 mm displacement in test D, was slightly reduced for every cycle. The force was about 25 kN at the end of 50 mm cycles for all three tests, reduced from a value of 40 kN at the initial cycles. As well as this being an indication of preload being lost, this also corresponds to the steel connections using aluminum or brass (which has simular properties as aluminum) shim layers studied in chapter 2.5. More

rectangular and stable results could have been obtained using a harder material for the shim layers. It was found that some preload was lost at the end for all three tests.

For tests C and D there was some twisting observed when the direction of movement changed. The twisting did however not continue during the movement in one direction as in tests performed on previous prototypes. This indicates that only the initial twist due to the bending moment of the bottom profile is present, as the bending moment would be stable at one value since the slip load was almost stable for one length of displacement. Twisting due to the eccentricities was more likely to cause continuous twisting in previous tests of STD and STD-R, which was not here observed, since these forces continuously attempts to rotate (twist) the friction plate of the bottom profile.

The effect of twisting only happening at the change of direction described above was easily observed because of the high speed. If the effect was present also in test B and test A of prototype STD-1H as well is uncertain, as the slow speed did not make it obvious when not looking for it. The theory described above was not necessarily correct, but was an hypothesis of how the system worked. More tests on other prototypes would have to be done to see if this was the case.

For the cycles after 50 mm, the force in test D starts to increase with an increasing displacement. The bolts were at this point pushing against the elongated holes as in previous cases. More twist is however not observed, so this was likely due to the initial twist. The initial twist caused the bolts to move at a slight angle in the elongated holes, so that upon reaching a higher displacement the bolts would reach the edges of the holes. The bolts were of course in contact with the sides of the holes earlier as well, but at this point the bolts were not simply sliding along the edges but pushing against them with some force. The force starts at the slip load of 25 kN observed for the previous cycles, then slowly increases to 35-40 kN, the force being higher when the upper profile was moving down than up. This was seen in Figure 5-15 d).

After test D finished the friction connection was noticeably warmer felt from the outside of the outer plates. The temperature was not measured but could be described as comfortably warm on chilly hands. The sudden increase of the temperature was likely due to the increase in speed and duration of the test. How or if this effected the friction connection was uncertain.

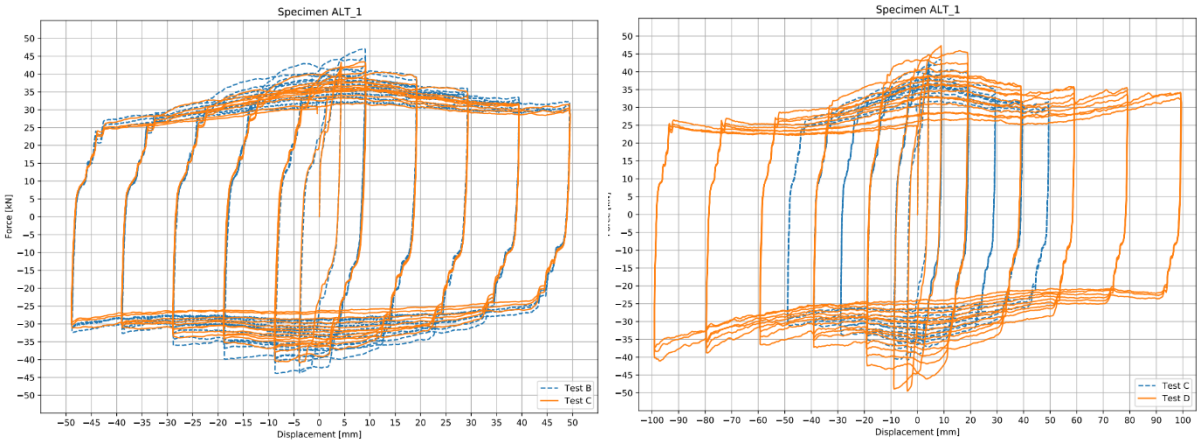

a) Test B and C *b) Test C and D*

Figure 5-16: Comparison of force-displacements curves for tests on prototype ALT for the cyclic tests using aluminum shim layers.

Figure 5-16 demonstrates how the test B, C and D created the same results during cycles of up to 50 mm. This shows that the connection was predictable and that the speed of the protocol did not have an effect on the results.

5.7 Comparison to the analytical and numerical investigation

The forces applied to the systems were a very important difference in the two investigations. The vertical forces in Hatletveit (2020), presented in chapter 3, were used to describe many of the effects in the system. Particularly, the reinforced prototype STD-R made much more sense to use in the case of Hatletveit (2020), as it resisted the vertical forces. In only using the horizontal force applied, this reinforcement served no purpose. The experimental testing did however show that the reinforcement had a negative effect on the connection due to the horizontal forces, meaning it would probably have a negative effect on the connection in total and was not the best solution to choose for resisting the vertical forces.

Both investigations found large stresses in the top bend of the bottom profile, even though Hatletveit (2020) found larger stresses in other bends, assumably due to the vertical forces. The twisting effect the bending moment caused in the friction connection was however not discovered in the analysis. As seen in the displacements presented in chapter 3, the rotation of the U-shape of the bottom profile is discovered, however, the related twisting effect was not. Nor was the effect the bolt arrangements had on the twist. It should also be noted that the preload used in the analysis was smaller than the preload used in all experimental tests, so the loads and deformations should be expected to be lower.

In total, the ALT prototype showed the best results in both investigations. Having this as a result in two different investigations, strengthens the ALT as the better solution for the connection.

6 Summary of all tests

The table on the next page gives an overview of all the tests performed, including specimens, preloads, protocols, and results. The “Test” column refers to the subchapters of chapter 4.5 which describes the tests in detail.

Test	Proto -type	Specimen	Test notation	Preload (% of P_{min})	Protocol type	Displacement protocol	Speed [mm/s]	Shim layer	Notes results
4.5.1	STD	STD_test	-	100%	Monotonic compression	100 mm	4	-	Slip load at 60 kN? Large deformation. Scraping.
4.5.2		STD_1	A	0%	Cyclic	1 x 50 mm 1 x 100 mm	0,5		Movement OK.
			B						Movement and sensors OK.
4.5.3			A	30%		1 x 5 mm 3 x 10 mm 3 x 20 mm 3 x 30 mm			Preload lost. Scraping in beginning. Somewhat rectangular fd-curve. Load decreases.
			B			1 x 5 mm 3 x 10 mm 3 x 20 mm 3 x 30 mm 3 x 40 mm 3 x 50 mm			Preload intact. Load increases.
			C						Some preload lost. Similar to A.
4.5.4		STD_2	A	30%				Aluminum	No scraping washers. Too high bending moment. Preload intact
	STD -1H	STD-1H_1	A	30%					Rect. Fd-curve. Working well.
			B	56%					High bending moment. Stopped.
	STD-R	STD-R_1	A	30%					U-shape of bottom profile acting as a rigid body. Most twisting observed. Stopped early.
	ALT	ALT_1	A	30%					Perfectly rectangular fd-curve.
			B	45%					Nice shape. As expected for aluminum shim layers.
			C				2		Identical to test B. Speed does not have an effect.
			D			1 x 5 mm 1 x 10 mm 3 x 20 mm 3 x 40 mm 3 x 60 mm 3 x 80 mm 3 x 100 mm			Identical to test B and C up to cycles of 50 mm. Load increases slowly with increasing displacements for later cycles. Temperature increase.

Table 6-1: Overview of tests performed and their results.

7 Conclusion

The initial configuration of the friction connection suffered from scraping of the steel material along the outside of the elongated holes, as the washers were acting as a friction surface together with the outside of the elongated holes. This was solved by a new configuration using an additional outside steel plate and two aluminum shim layers. The initial configuration should therefore not be used for the connection.

The preload in all cases tested needed to be much lower than the minimum value specified by the standard. Bolts with a lower capacity in tension and/or with a smaller diameter should therefore be used for the friction connection. Also, the amount of preload lost for each test was unpredictable. Following the standard might have bettered this.

All prototypes suffered from the bending moment produced in the bottom profile due to the applied force resulting in a twisting effect of the plate in the bottom profile in the friction connection. The twisting deformation was an extension of the deformations in the rightmost plate in the U-shape of the bottom profile caused by this bending moment. In this way, the twisting was directly related to the bending moment in the bottom profile. The ALT prototype had a different design of the bottom profile, but this moment worked in a similar way, only the “plate” experiencing the deformation could be seen as being very small.

The arrangement of the bolts in the friction connection being arranged asymmetrically about the z-axis worsened the effect of the twist. The problem of large twisting was the bolts pushing against the sides of the elongated holes, such that the force measured was a combination of this effect and the slip friction load. For this reason, prototypes STD and STD-R should not be used. Also, the reinforcement in STD-R was designed to withstand the vertical forces, only considered in Hatletveit (2020). In the experimental test the effect of twisting was worsened by the reinforcement, making the U-shape of the bottom profile move as one rigid body.

Prototype STD-1H should also not be used, as the bending moment due to the force applied to the friction connection resulted in too much deformation when the needed preload to reach the wanted slip friction load of 30 kN was applied.

Both investigations agreed on prototype ALT being the best designed solution of the connector. The ALT prototype suffered much less bending moment due to its design of the bottom profile and had a favorable arrangement of the bolts in the friction connection. A preload value of 36,1 kN used for this prototype came close to obtaining the wanted slip friction load of 30 kN.

A hypothesis was that the initial bending moment caused directly from the force applied to the friction connection caused the initial twisting of the specimen as it changed direction, while the asymmetrical arrangement of the bolts caused the continuation of the twist during the whole movement of the specimen. To be sure of this theory, it would have to be tested further, as it first became obvious with the last test using a higher speed. In any case, an asymmetrical arrangement of the bolts about the z-axis should not be used for the connection, as the continued twisting produces unwanted effects.

8 Further Work

Suggestions on modifications to be used for future testing of the friction dampers are given here.

8.1 Bolts

The capacity of bolts in friction connection must be reduced to be in accordance with the standards as presented in chapter 2.3. It is specified that the preload value needs to be a minimum of 70% of the bolt's capacity in tension. Bolts exposed to a preload value of 70-100% of their capacity in tension should therefore be used. This is an attempt at solving or bettering the problem of losing an unpredictable amount of preload during testing.

Assuming the preload of 36,1 kN used in the last test on the ALT prototype which came the closest to having a slip friction load of the wanted value of 30 kN, bolts M10 8.8 are suggested giving a utilization of:

$$\frac{P}{f_{ub}A_s} = \frac{36{,}1\ kN}{800\ N/mm^2 * 58\ mm^2} = 78\%$$

Where,

$A_s = 58\ mm^2$ for M10 bolts

Other bolts can also be used, and it is possible to change the number of bolts by adjusting the arrangement of the bolts in the design. The bolts should however not be arranged asymmetrically about the z-axis of the profiles. Also, the shear resistance of the bolts needs to be checked before deciding on the bolts and arrangement to use, though this is only relevant in the case when the bolts reach the ends of the elongated holes. Considering the bolts used in the complete system described in chapter 1, other strength related aspects of the bolts need to be considered as well.

8.2 Preload

Sensors to oversee the actual preload in the bolts at all times need to be used to further study what preload should be used, the preloading methods and what preload they actually produce in the connection, and how and how much preload is lost. HBM-KMR-sensors can be used for this.

8.3 Design of steel damper

The ALT prototype or a design modified from this prototype should be used for further testing, as this prototype showed the most promising results in both this thesis and Hatletveit (2020). The two most important aspects of this design that needs to be continued are:

- Not using the U-shape in the bottom profile, as this showed not to be moment resistant enough.
- Arranging the bolts in the friction connection symmetrically about the z-axis of the profiles, as this reduces the twisting effect.

8.4 Temperature

A temperature change was observed in the last test in this thesis. The temperature change in the friction connection and how or if it affects the connection should be studied. A thermo camera or another type of sensor monitoring the temperature in the connection should be used for future testing.

8.5 Protocols

Protocols closer to the standards presented in chapter 2.6 should be used, also choosing the right standard for the case.

A higher speed should be used for the protocols to better simulate an earthquake, as earthquakes only last for a short while. Also, it could be interesting to perform several tests on the same specimen with only a short break in between to see how the connection would perform in a sequence of earthquakes. This can be particularly interesting in the study of the effect of temperature change.

9 List of figures

10 List of tables

11 References

CEN. (2001). *EN 12512*. Timber structures - Test methods - Cyclic testing of joints made with mechanical fasteners. Brussels.

CEN. (2004). *EN 1998-1*. Eurocode 8: Design of structures for earthquake resistance Part 1: General rules, seismic actions and rules for buildings. Brussels: CEN.

CEN. (2005). *EN 1993-1-8*. Eurocode 3: Design of steel structures -Part 1-8: Design of joints. Brussels.

CEN. (2018a). *EN 1090-2*. Execution of steel structures and aluminium structures - Part 2: Technical requirements for steel structures. Brussels.

CEN. (2018b). *EN 15129*. Anti-seismic devices. Brussels.

Elnashai, A. S. & Sarno, L. D. (2008). *Fundamentals of earthquake engineering*. United Kingdom: John Wiley & Sons, Ltd.

Euler, G. D. (2002). *Bolt Preload Calculation*. Available at: http://euler9.tripod.com/fasteners/preload.html (accessed: 30.10.2020).

Giardini, D., Woessner, J., Danciu, L., Cotton, F., Crowley, H., Grünthal, G., Pinho, R., Valensise, G., Akkar, S., Arvidsson, R., et al. (2013). *European Seismic Hazard Maps*. Seismic Hazard Harmonization in Europe (SHARE). Zürich: ETH. Available at: http://www.share-eu.org/sites/default/files/SHARE_Brochure_public.web_.pdf (accessed: 09.12.20).

Golondrino, J. C., MacRae, G. A., Chase, J. G., Rodgers, G. W. & Clifton, C. G. (2012). *Behaviour of Asymmetrical Friction Connections using different shim materials*. NZSEE Conference, New Zealand.

Group, V. (2018). *STRUCTURAL BOLTING ASSEMBLIES*. EN 14399 PRELOADED ASSEMBLIES: Vescovini Group.

Hatletveit, M. R. (2020). *Mechanical assessment of a steel dissipating system for RC buildings retrofitting with CLT panels*. Ås: Norwegian University of Life Sciences.

ISO. (2003). *ISO16670*. Timber structures - Joints made with mechanical fasteners - Quasi-static reversed-cyclic test method. Switzerland: ISO.

Loo, W. Y., Quenneville, P. & Chouw, N. (2014). A new type of symmetric slip-friction connector. *Journal of Constructional Steel Research*, 94: 11-22. doi: 10.1016/j.jcsr.2013.11.005.

NSC2. (2005). *AD 286: Preloaded Bolts: The Net Effect of Applied Tension and Preload*: Barrett Byrd Associates. Available at: https://www.newsteelconstruction.com/wp/ad-286-preloaded-bolts-the-net-effect-of-applied-tension-and-preload/ (accessed: 30.10.2020).

Roberson, P. (2020). *2020 Magna Earthquake Sequence FAQ*. Utah: The University of Utah. Available at: https://quake.utah.edu/special-events/2020-magna-earthquake-sequence-faq#:~:text=An%20earthquake%20sequence%20is%20a,time%20in%20the%20same%20area. (accessed: 09.12.2020).

Schmitz, T. L. & Smith, K. S. (2012). *Mechanical Vibrations*. New York: Springer.

Shabana, A. A., Hill, R. & Hill, L. (2019). *Theory of Vibration*. 3 ed. Mechanical Engineering Series. Chicago, IL, USA: Springer International Publishing AG.

Tardo, C., Boggian, F., Hatletveit, M., Marino, E. M., Margani, G. & Tomasi, R. (2020). *MECHANICAL CHARACTERIZATION OF ENERGY DISSIPATION DEVICES IN RETROFIT SOLUTION OF REINFORCED CONCRETE FRAMES COUPLED WITH SOLID WOOD PANELS. Proceedings of International Conference on Structural Analysis of Historical Constructions SAHC 2020*. Unpublished manuscript.

Appendix

Appendix A

Measurements of the specimens

UPPER PROFILE

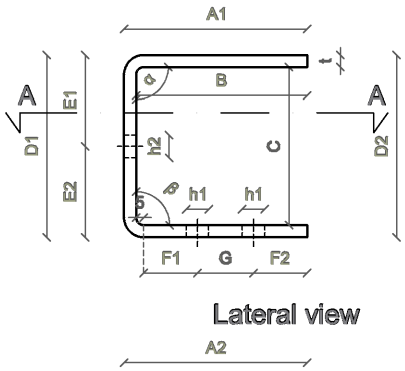

Lateral view

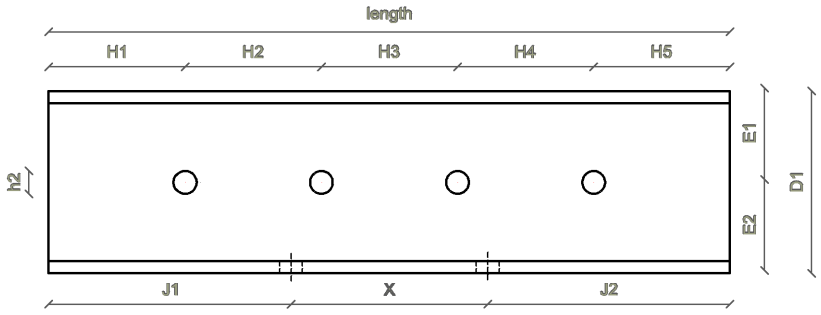

Front view

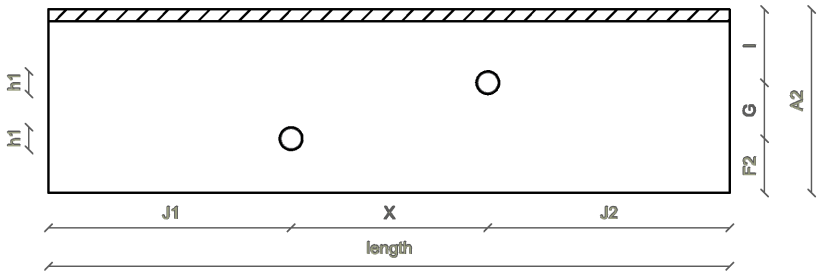

Section A-A

BOTTOM PROFILE

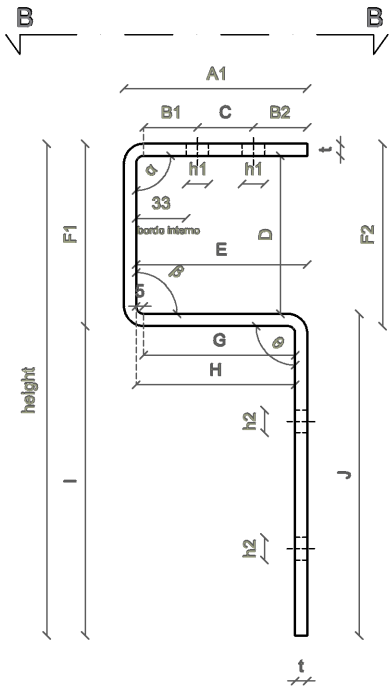

Lateral view

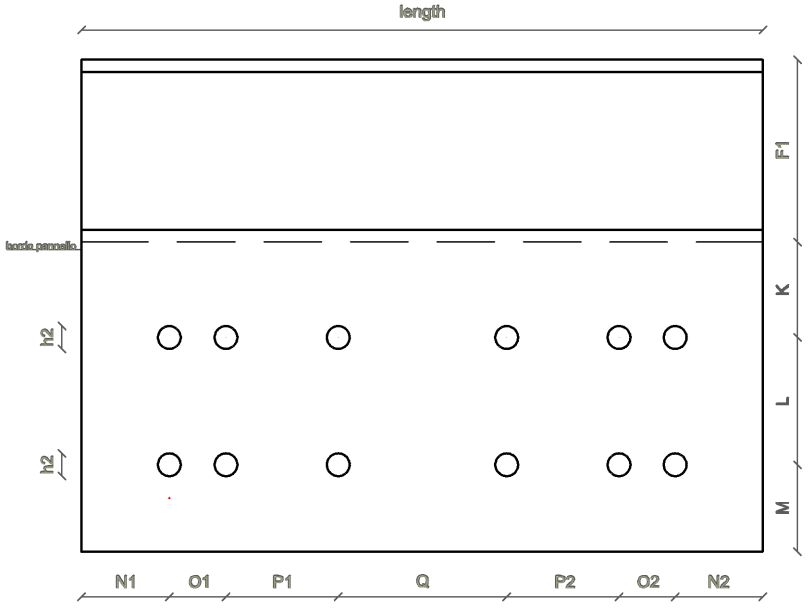

Front view

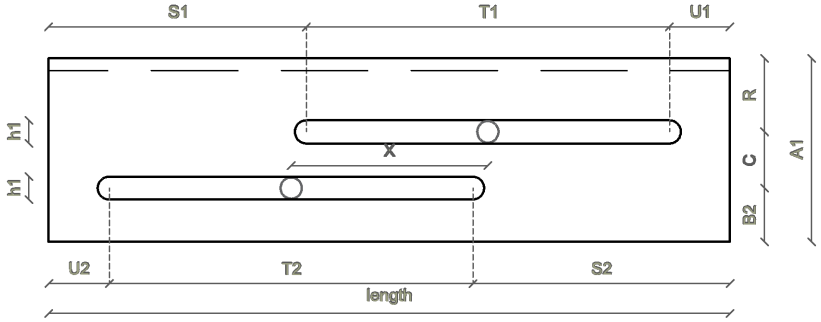

View B-B

Prototype
STD

PRODUCED BY AN AUTODESK STUDENT VERSION

PRODUCED BY AN AUTODESK STUDENT VERSION

UPPER PROFILE

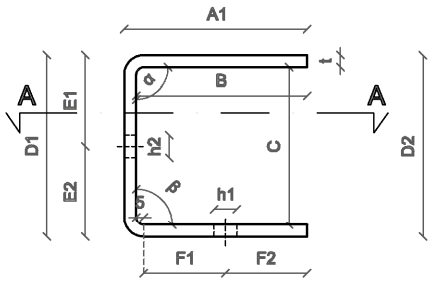

Lateral view

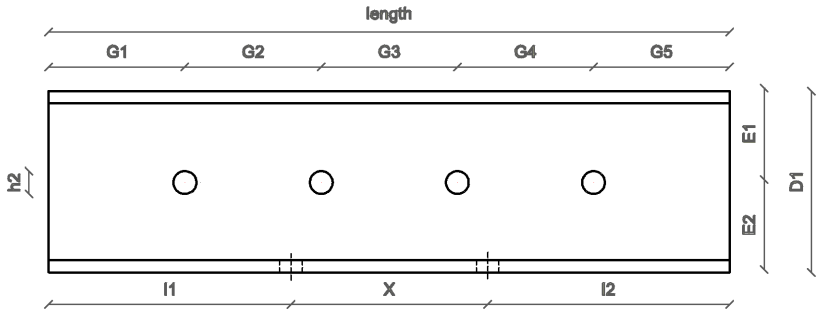

Front view

A2

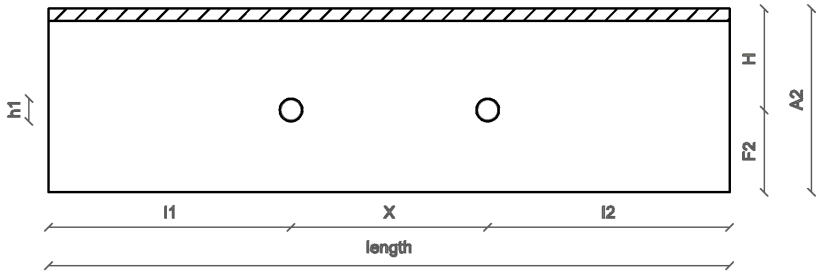

Section A-A

BOTTOM PROFILE

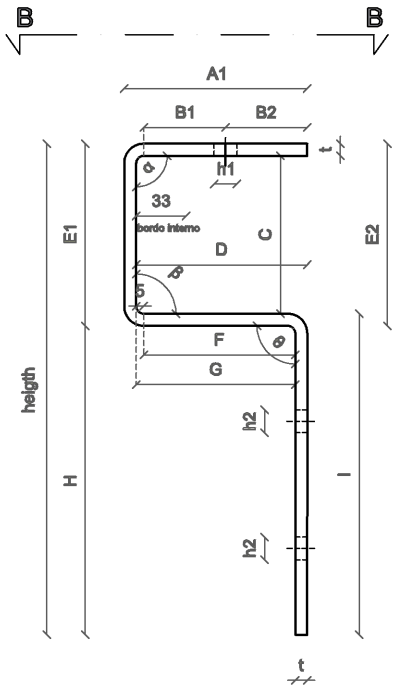

Lateral view

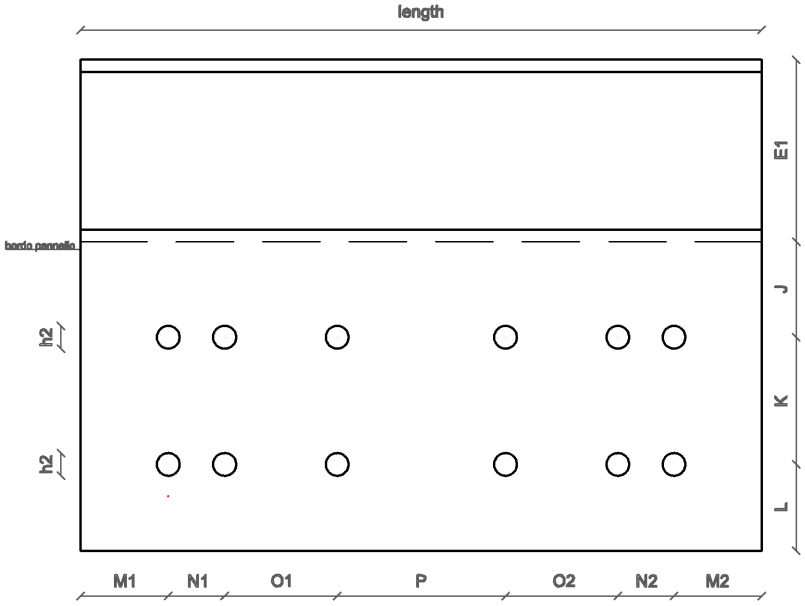

Front view

A2

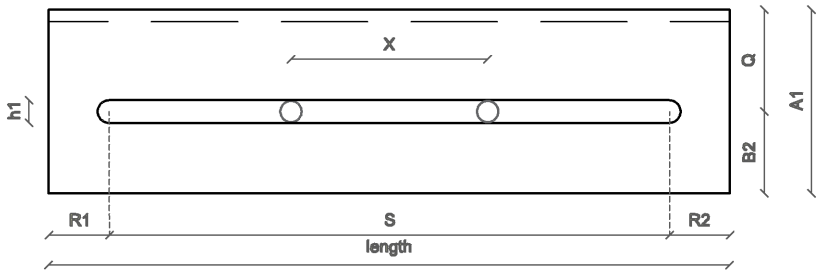

View B-B

Prototype
STD-1H

PRODUCED BY AN AUTODESK STUDENT VERSION

PRODUCED BY AN AUTODESK STUDENT VERSION

PRODUCED BY AN AUTODESK STUDENT VERSION

UPPER PROFILE

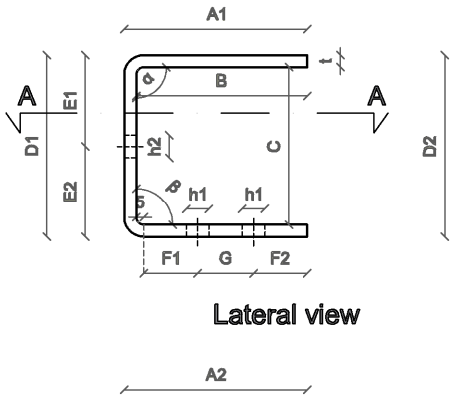

Lateral view

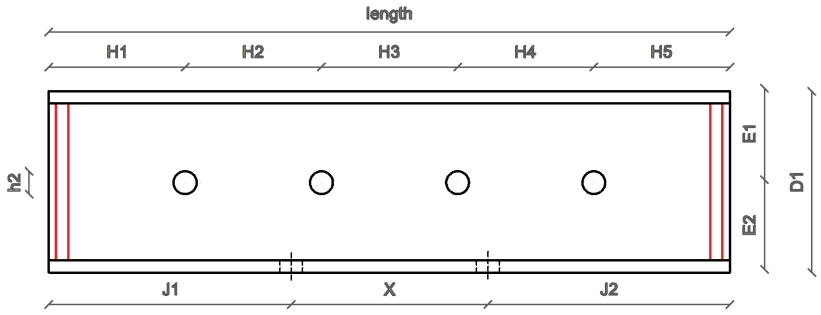

Front view

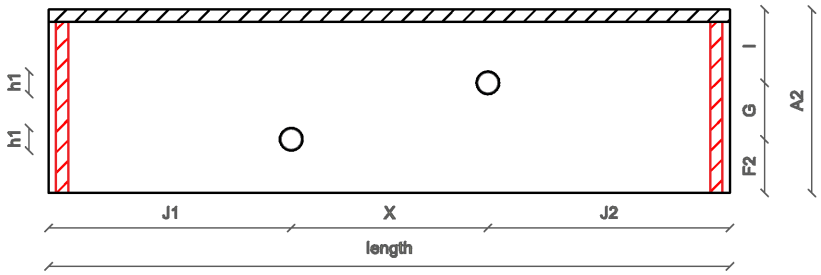

Section A-A

BOTTOM PROFILE

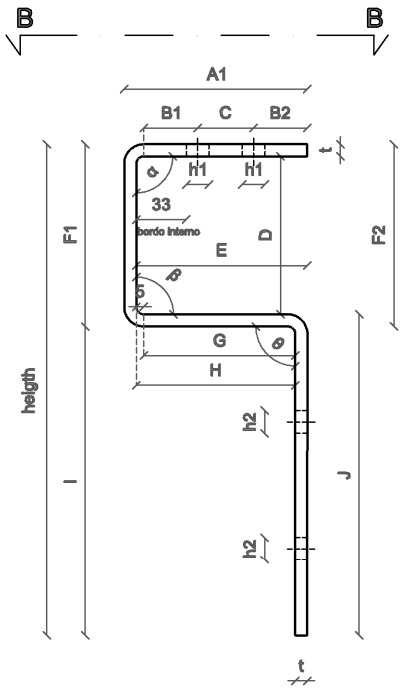

Lateral view

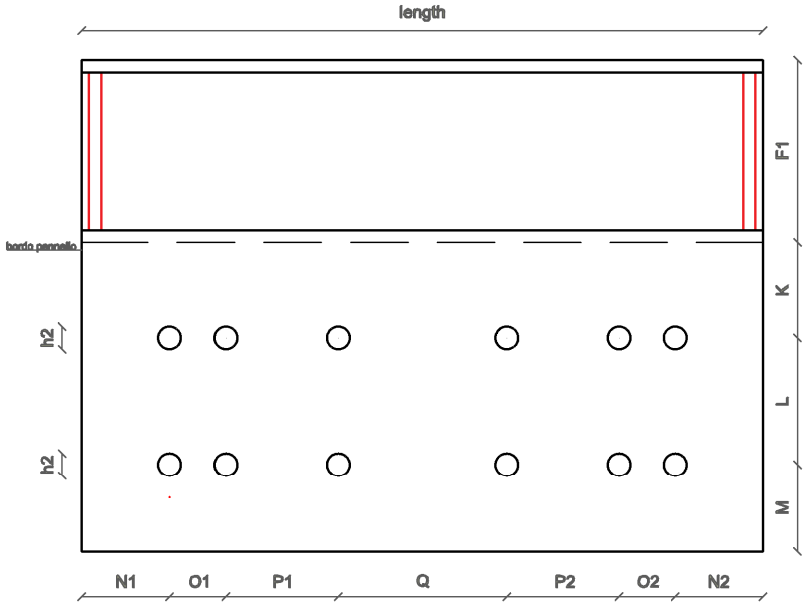

Front view

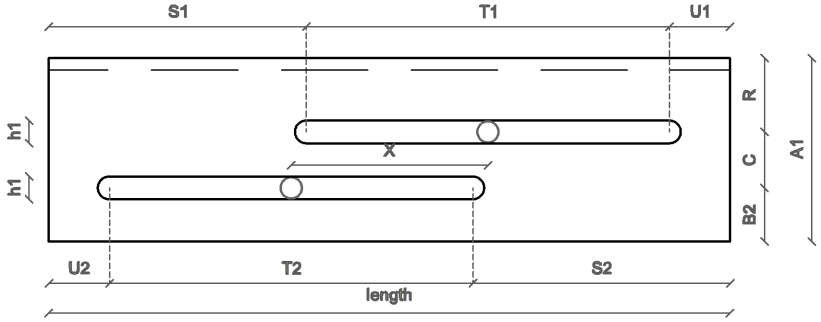

View B-B

Prototype
STD-R

PRODUCED BY AN AUTODESK STUDENT VERSION

PRODUCED BY AN AUTODESK STUDENT VERSION

PRODUCED BY AN AUTODESK STUDENT VERSION

UPPER PROFILE

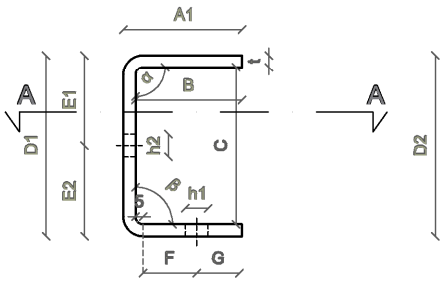

Lateral view

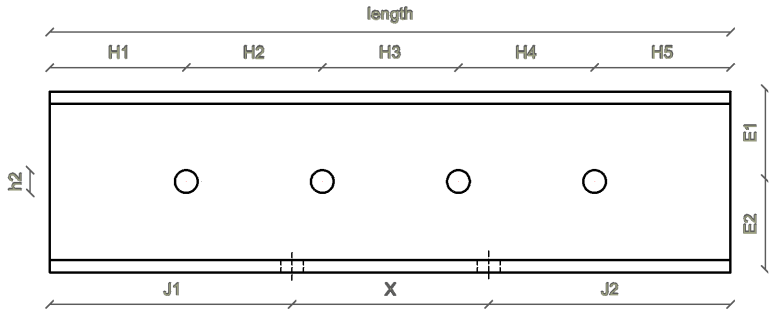

Front view

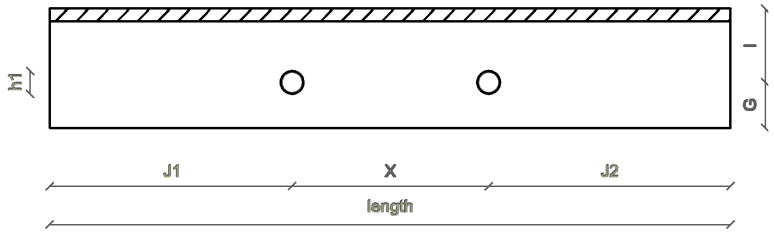

Section A-A

BOTTOM PROFILE

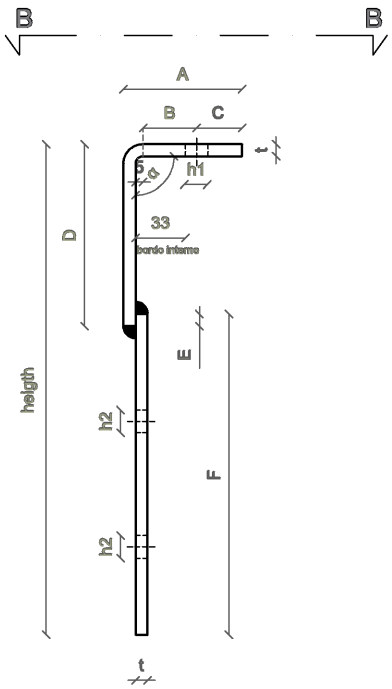

Lateral view

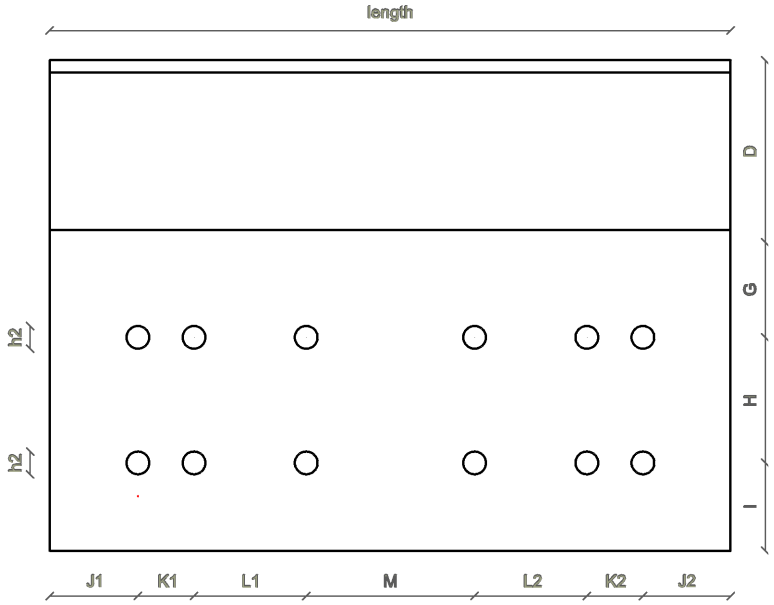

Front view

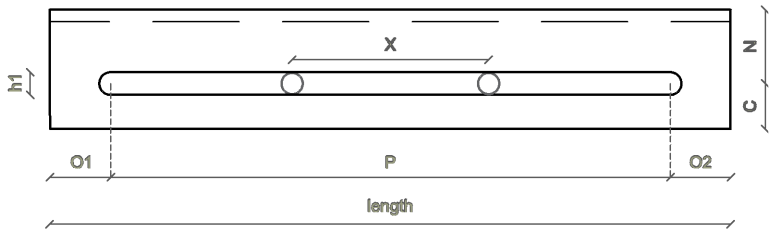

View B-B

Prototype
ALT

PRODUCED BY AN AUTODESK STUDENT VERSION

PRODUCED BY AN AUTODESK STUDENT VERSION

Prototype STD

Prototype STD: upper

Specimen	length	t	h1	h2	α	β	A1	A2	B* (at A1)
Drawing	450	8	15	15	90	90	121	121	113
STD_1	450	8	15	15	90,5	90	119	119	111
STD_2	450	8	15	15	90,5	89,5	119	119	111
STD_3	450	8	15	25	90,5	89,5	118	119	110
STD_test	450	8	15	15	90	90	118,5	119	110,5

Specimen	B* (at A1)	C* (atD1)	C* (at D2)	D1	D2	E1	E2	F1*	F2
Drawing	113	104	104	120	120	60	60	35,5	35,5
STD_1	111	103,5	105	119,5	121	60	60	33,5	35,5
STD_2	111	103	105	119	121	60	60	33,5	35,5
STD_3	111	103	105	119	121	60	60	33,5	35,5
STD_test	111	103	103	119	119	60	60	33,5	35,5

Specimen	G*	H1	H2	H3	H4	H5	I	J1	J2
Drawing	37	90	90	90	90	90	48,5	160	160
STD_1	37	90	90	90	90	90	46,5	160	160
STD_2	37	90	90	90	90	90	46,5	160	160
STD_3	37	90	90	90	90	90	46,5	160	160
STD_test	37	90	90	90	90	90	46,5	160	160

Specimen	X	Comment
Drawing	130	Damaged corners. All have damage at the ends. Some have smaller cut(s) further in. STD_test has one bigger and deeper cut further in.
STD_1	130	
STD_2	130	
STD_3	130	
STD_test	130	

Prototype STD

Prototype STD: bottom

Specimen	length	heigth	t	h1	h2	α	β	θ	A1
Drawing	450	325	8	15	15	90	90	90	121
STD_1	450	324	8	15	15	90	90	90,5	120
STD_2	450	325	8	15	15	89,5	90	90	120
STD_3	450	326	8	15	15	90	90	90	120
STD_test	450	325	8	15	15	89,5	90	89,5	120

Specimen	A2	B1*	B2	C	D* (at F1)	D* (at F2)	E* (at A1)	E* (at A2)	F1
Drawing	121	35,5	35,5	37	104	104	113	113	120
STD_1	116	35,5	35,5	37	104	104	112	108	120
STD_2	116	35,5	35,5	37	105	104,5	112	108	121
STD_3	116	35,5	35,5	37	105	106	112	108	121
STD_test	116	35,5	35,5	37	105	105	112	108	121

Specimen	F2	G*	H*	I*	J	K	L	M	N1
Drawing	120	100	105	205	213	63	84	58	58
STD_1	120	95	100	205	213	63	84	58	58
STD_2	120,5	95	100	205	213	63	84	58	58
STD_3	122	95	100	205	213	63	84	58	58
STD_test	121	95	100	205	213	63	84	58	58

Specimen	N2	O1	O2	P1	P2	Q	R	S1	S2
Drawing	58	37,11	37,11	74,22	74,22	111,33	48,5	170	170
STD_1	58	37,11	37,11	74,22	74,22	111,33	48,5	170	170
STD_2	58	37,11	37,11	74,22	74,22	111,33	48,5	170	170
STD_3	58	37,11	37,11	74,22	74,22	111,33	48,5	170	170
STD_test	58	37,11	37,11	74,22	74,22	111,33	48,5	170	170

Specimen	T1*	T2*	U1	U2	X	Comment
Drawing	240	240	40	40	130	
STD_1	240	240	40	40	130	
STD_2	240	240	40	40	130	
STD_3	240	240	40	40	130	
STD_test	240	240	40	40	130	

Prototype STD-1H

Prototype STD-1H: upper

Specimen	length	t	h1	h2	α	β	A1	A2
Drawing	450	8	15	15	90	90	121	121
STD-1H_1	450	8	15	15	90	89,5	119	119
STD-1H_2	450	8	15	15	90,5	89	119	119
STD-1H_3	450	8	15	15	90	89	120	119
STD-1H_test	450	8	15	15	90	90	119	119

Specimen	B* (at A1)	B* (at A2)	C* (at D1)	C* (at D2)	D1	D2	E1	E2
Drawing	113	113	104	104	120	120	60	60
STD-1H_1	111	111	104	104	120	120	60	60
STD-1H_2	111	111	104	105	120	121	60	60
STD-1H_3	112	111	102	104	118	120	59	59
STD-1H_test	111	111	104	104	120	120	60	60

Specimen	F1*	F2	G1	G2	G3	G4	G5	H
Drawing	54	54	90	90	90	90	90	67
STD-1H_1	52,5	53,5	90	90	90	90	90	65,5
STD-1H_2	52,5	53,5	90	90	90	90	90	65,5
STD-1H_3	52,5	53,5	90	90	90	90	90	65,5
STD-1H_test	52	54	90	90	90	90	90	65

Specimen	I1	I2	X	Comment
Drawing	160	160	130	
STD-1H_1	160	160	130	
STD-1H_2	160	160	130	
STD-1H_3	160	160	130	
STD-1H_test	160	160	130	

Prototype STD-1H

Prototype STD-1H: bottom

Specimen	length	heigth	t	h1	h2	α	β	θ
Drawing	450	325	8	15	15	90	90	90
STD-1H_1	450	326	8	15	15	90	89	90
STD-1H_2	450	326	8	15	15	90,5	90	89,5
STD-1H_3	450	327	8	15	15	91	89	89,5
STD-1H_test	450	327	8	15	15	90	91	89

Specimen	A1	A2	B1*	B2	C* (at E1)	C* (at E2)	D* (at A1)	D* (at A2)
Drawing	121	121	54	54	104	104	113	113
STD-1H_1	120	116	53	54	105	106	112	108
STD-1H_2	120	116	53	54	105	106	112	108
STD-1H_3	120	115	53	54	104	107	112	107
STD-1H_test	120	116	53	54	104	107	112	108

Specimen	E1	E2	F*	G*	H*	I	J	K
Drawing	120	120	100	105	205	213	63	84
STD-1H_1	121	122	95	100	204	212	57	84
STD-1H_2	121	122	95	100	204	212	57	84
STD-1H_3	120	123	94	99	204	212	57	84
STD-1H_test	120	123	95	100	204	212	58	84

Specimen	L	M1	M2	N1	N2	O1	O2	P
Drawing	58	58	58	37,11	37,11	74,22	74,22	111,33
STD-1H_1	58	58	58	37,11	37,11	74,22	74,22	111,33
STD-1H_2	58	58	58	37,11	37,11	74,22	74,22	111,33
STD-1H_3	58	58	58	37,11	37,11	74,22	74,22	111,33
STD-1H_test	58	58	58	37,11	37,11	74,22	74,22	111,33

Specimen	Q	R1	R2	S*	X	Comment
Drawing	67	40	40	370	130	
STD-1H_1	66	40	40	370	130	
STD-1H_2	66	40	40	370	130	
STD-1H_3	66	40	40	370	130	
STD-1H_test	66	40	40	370	130	

Biggest difference in angle, and between E1 and E2. The difference between E1 and E2 can also be seen with a blank eye.

Prototype STD-R

Prototype STD-R: upper

Specimen	length	t	h1	h2	α	β	A1	A2	B* (at A1)
Drawing	450	8	15	15	90	90	121	121	113
STD-R_1	450	8	15	15	90	90	118,5	118,5	110,5
STD-R_2	450	8	15	15	90	89,5	119,5	120	111,5
STD-R_3	450	8	15	15	90,5	90	119	119	111

Specimen	B* (at A2)	C* (at D1)	C* (at D2)	D1	D2	E1	E2	F1*	F2
Drawing	113	104	104	120	120	60	60	35,5	35,5
STD-R_1	110,5	104	104	120	120	60	60	33,5	35,5
STD-R_2	112	102	103	118	119	59	59	34,5	35,5
STD-R_3	111	104	105	120	121	60	60	33,5	35,5

Specimen	G*	H1	H2	H3	H4	H5	I	J1	J2
Drawing	37	90	90	90	90	90	48,5	160	160
STD-R_1	36,5	90	90	90	90	90	46,5	160	160
STD-R_2	37	90	90	90	90	90	47,5	160	160
STD-R_3	37	90	90	90	90	90	46,5	160	160

Specimen	X	Comment
Drawing	130	
STD-R_1	130	
STD-R_2	130	
STD-R_3	130	

Prototype STD-R

Prototype STD-R: bottom

Specimen	length	heigth	t	h1	h2	α	β	θ	A1
Drawing	450	325	8	15	15	90	90	90	121
STD-R_1	450	324	8	15	15	90	90	89	120
STD-R_2	450	324	8	15	15	90	90	89	120
STD-R_3	450	325	8	15	15	90	90	89	120

Specimen	A2	B1*	B2	C	D* (at F1)	D* (at F2)	E* (at A1)	E* (at A2)	F1
Drawing	121	35,5	35,5	37	104	104	113	113	120
STD-R_1	117	34,5	35,5	37	104	104	112	109	120
STD-R_2	116	34,5	35,5	37	104	104	112	108	120
STD-R_3	116	34,5	35,5	37	104	105	112	108	120

Specimen	F2	G*	H*	I*	J	K*	L	M	N1
Drawing	120	100	105	205	213	63	84	58	58
STD-R_1	120	96	101	204	212	62	84	58	58
STD-R_2	120	95	100	204	212	62	84	58	58
STD-R_3	121	95	100	204	212	62	84	58	58

Specimen	N2	O1	O2	P1	P2	Q	R	S1	S2
Drawing	58	37,11	37,11	74,22	74,22	111,33	48,5	170	170
STD-R_1	58	37,11	37,11	74,22	74,22	111,33	47,5	170	170
STD-R_2	58	37,11	37,11	74,22	74,22	111,33	47,5	170	170
STD-R_3	58	37,11	37,11	74,22	74,22	111,33	47,5	170	170

Specimen	T1*	T2*	U1	U2	X	Comment
Drawing	240	240	40	40	130	
STD-R_1	240	240	40	40	130	
STD-R_2	240	240	40	40	130	
STD-R_3	240	240	40	40	130	

Prototype ALT

Prototype ALT: upper

Specimen	length	t	h1	h2	α	β	A1	A2	B* (at A1)
Drawing	450	8	15	15	90	90	78,5	78,5	70,5
ALT_1	450	8	15	15	90,5	89,5	76,5	76,5	68,5
ALT_2	450	8	15	15	90,5	89,5	76	76,5	68
ALT_3	450	8	15	15	90	89,5	76	76,5	68

Specimen	B* (at A2)	C* (at D1)	C* (at D2)	D1	D2	E1	E2	F*	G
Drawing	70,5	104	104	120	120	60	60	35,5	30
ALT_1	68,5	105	106	121	122	60,5	60,5	33,5	30
ALT_2	68,5	105	105	121	121	60,5	60,5	33,5	30
ALT_3	68,5	105	105	121	121	60,5	60,5	33,5	30

Specimen	H1	H2	H3	H4	H5	I	J1	J2	X
Drawing	90	90	90	90	90	48,5	160	160	130
ALT_1	90	90	90	90	90	46,5	160	160	130
ALT_2	90	90	90	90	90	46,5	160	160	130
ALT_3	90	90	90	90	90	46,5	160	160	130

Specimen	Comment
Drawing	
ALT_1	
ALT_2	
ALT_3	

Prototype ALT

Prototype ALT: bottom

Comment: No side A is plane. B and C are in two different planes.

Specimen	length	heigth	t	h1	h2	α min	α max	A	B*
Drawing	450	325	8	15	15	90	90	78,5	35,5
ALT_1	450	324	8	15	15	90	94	76	33
ALT_2	450	323	8	15	15	90	95	76	33
ALT_3	450	323	8	15	15	90	94	76	33,5

Specimen	C	D	E	F	G*	H	I	J1	J2
Drawing	30	120	8	213	63	84	58	58	58
ALT_1	30	119	7	213	64	84	58	58	58
ALT_2	30	119	7	213	64	84	58	58	58
ALT_3	29,5	119	7	213	64	84	58	58	58

Specimen	K1	K2	L1	L2	M	N	O1	O2	P*
Drawing	37,11	37,11	74,22	74,22	111,33	48,5	40	40	370
ALT_1	37,11	37,11	74,22	74,22	111,33	46	40	40	370
ALT_2	37,11	37,11	74,22	74,22	111,33	46	40	40	370
ALT_3	37,11	37,11	74,22	74,22	111,33	46,5	40	40	370

Specimen	X	Comment
Drawing	130	
ALT_1	130	
ALT_2	130	
ALT_3	130	

Appendix B

Guide to use of press and software

Table of Contents

1 Instron

In the timber lab in TF fløy 5 at NMBU, Instron 5800 is installed. Though, updates and adjustments have been installed over the years, meaning that it is not identic to a standard Instron 5800 model. Information found in user manuals from Instron concerning this model can therefore not be assumed to be accurate.

1.1 Safety

The moving press will always continue moving when encountering something it should not unless this is controlled by the user.

The press has a method for setting upper and lower limits for the movement of the beam of the press, as seen in the picture. B moves along with the beam of the press, and when it hits either A or C, it will stop. A and B should be adjusted so that nothing connected to the moving beam should encounter something that it should not.

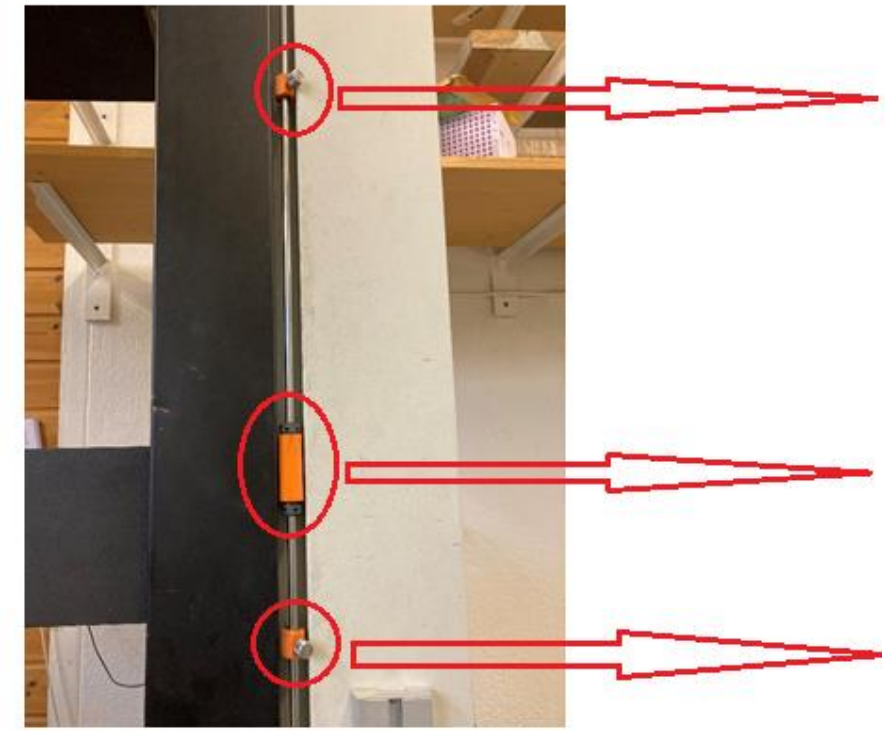

A: Upper limit of the beam of the press.

B: Part moving along with the beam of the press.

C: Lower limit of the beam of the press.

If something goes wrong, the big red button should be pressed, stopping the press right away:

1.2 Restart procedure

When restarting the press, everything must be turned on and off in a specific order due to the system of power supply. The turn-off procedure is as fallows, numbers seen in the figure below.

1. Exit Instron Bluehill and the Instron software, shown as a ribbon on the top of the computer screen.
2. Turn off the computer.
3. Turn off the computer in the back to the right.
4. Turn off the computer in the back to the left.

Two turn back on, due the opposite of above:

4. Turn on computer in the back to the left.
3. Turn on the computer in the back to the right.
2. Turn on the computer.
1. Open the Instron Bluehill software, a shortcut should be on the desktop. (This automatically starts up the Instron software as well.)

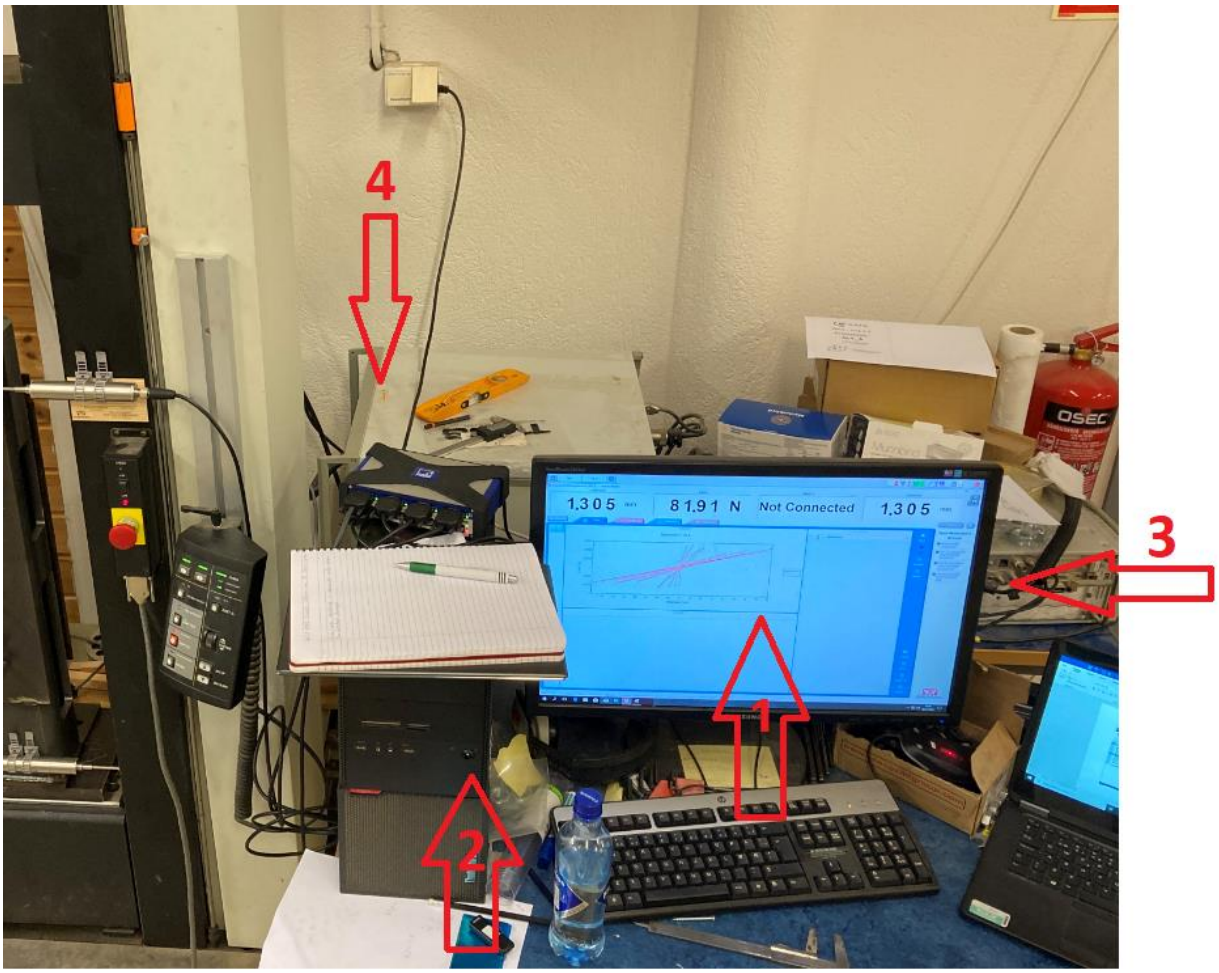

1.3 Speed

The speed can be set using either the extension or load as a base. Using the extension as a base, the maximum speed is 4,2 mm/s. At low speeds, the press has a hard time finding its position, causing it to make loud noise, in addition to the analogue extension output to vary a bit up and down in small intervals. It is not critical, but it gives small wave forms where there should be completely smooth curves in graphs obtained from the data logged.

1.4 Control panel

The control panel is located on the right-hand side of the press.

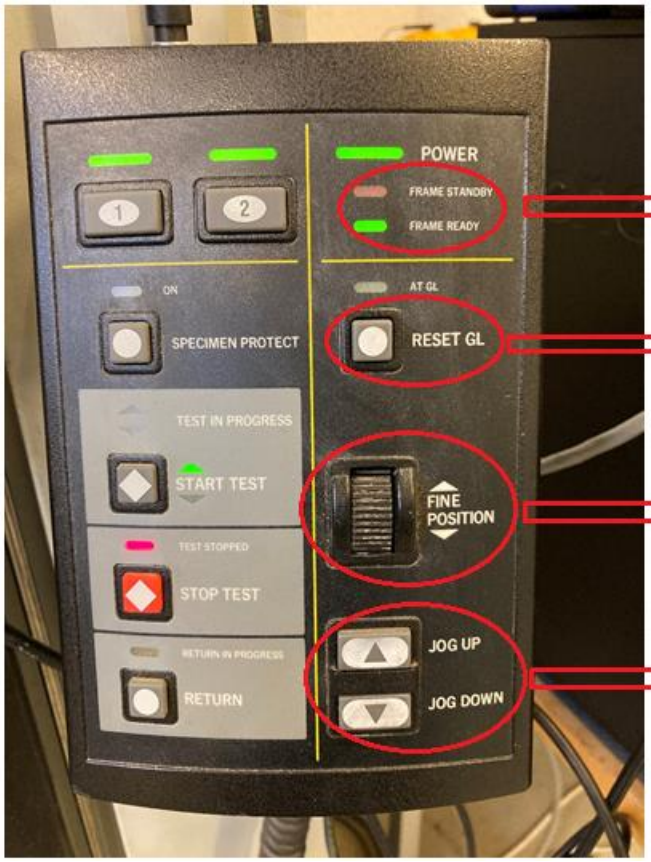

A: Green light means the software on the computer and the press have contact. Red light means they do not have contact.

B: Resets the extension to zero.

C: Fine-tuning of the beam's position. Moves the beam up or dawn with a small extension.

D: Moves the beam of the press up or down.

If the red light in A is on, try first to turn everything on and of (see chapter 1.2). If that does not work, a person responsible for the lab and the press should be contacted. Previously this problem has been solved by changing a fuse.

Note: Everything needs to be turned on and the program started up on the computer for the light i A to be green. See chapter 1.2 for details.

1.5 Load calibration

Load calibration can be used to set the load to zero. The load will not be exactly zero after calibration, but close. The following steps are to be done on the computer connected to the press.

Step 1: Click where shown on the panel in the upper right corner on the computer screen.

Step 2: Go to calibration at the top of the pop-up window, and then click on calibration. (Fine balance can also be used if the adjustment to the load is small.)

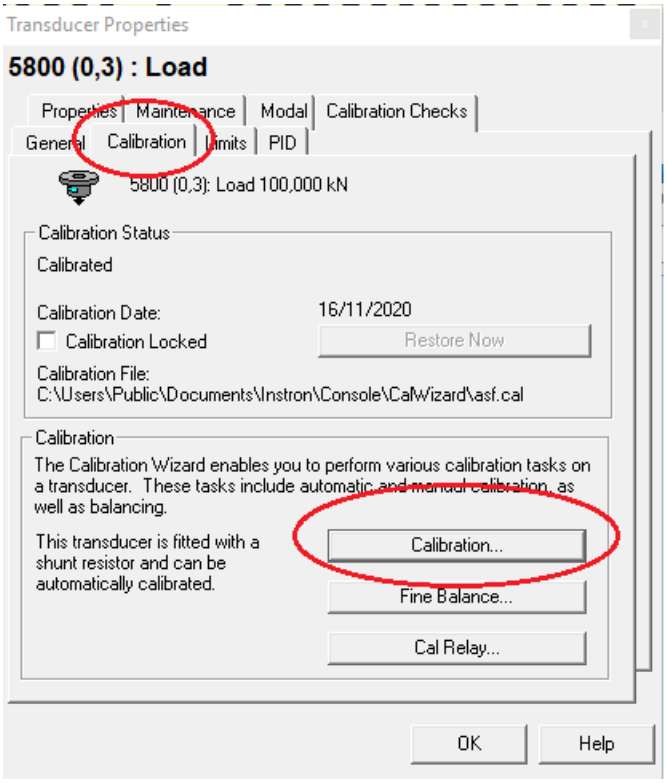

Step 3: Choose balance and click next.

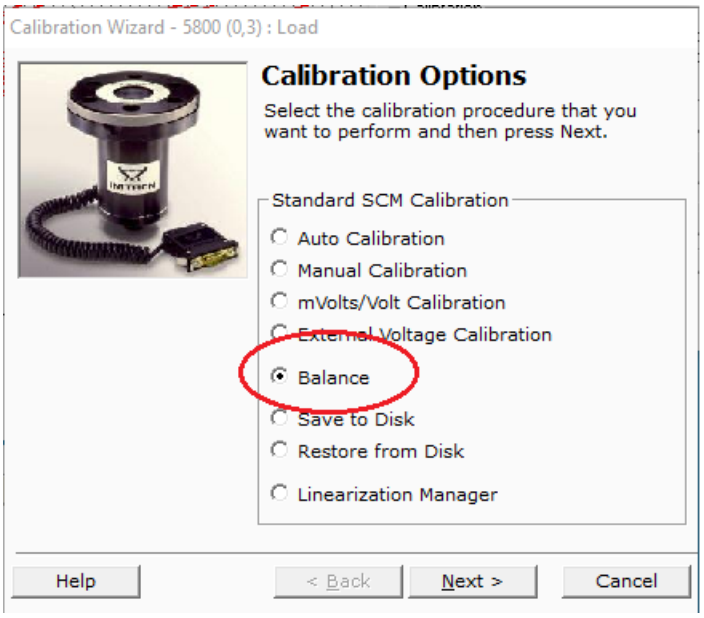

Step 4: The first input should be zero, the second should be the maximum capacity of the load cell. This is normally already there when the window pops up.

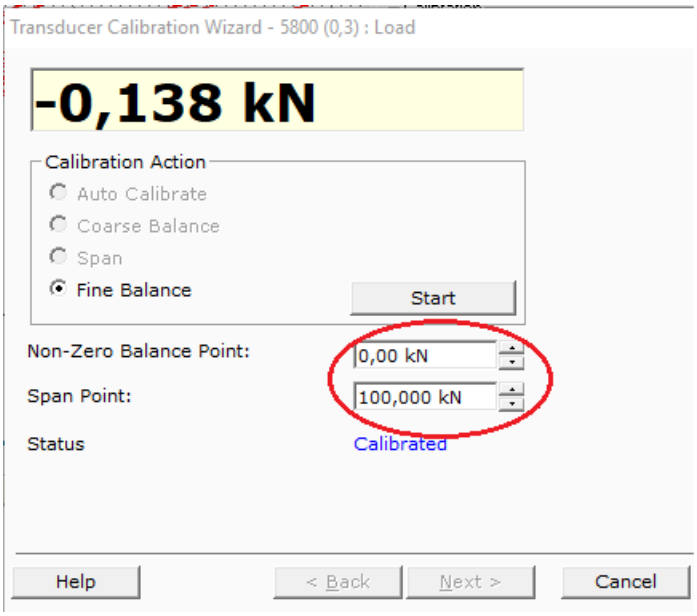

Step 5: Start the calibration.

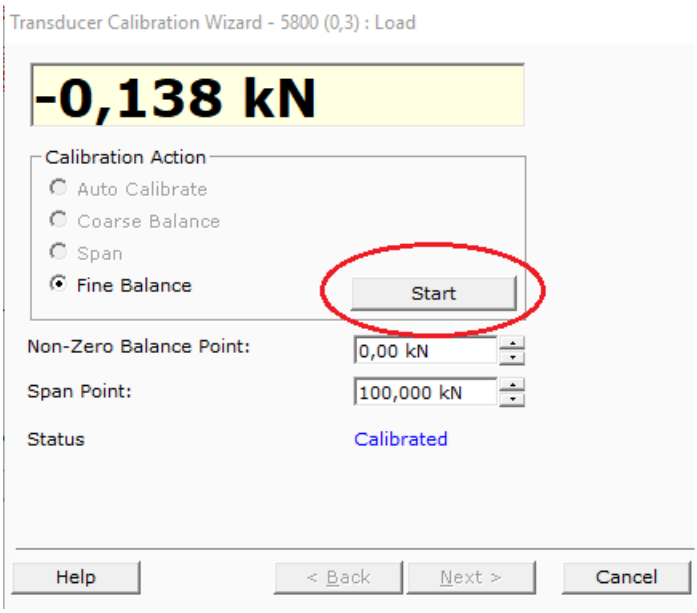

Step 6: Click finish.

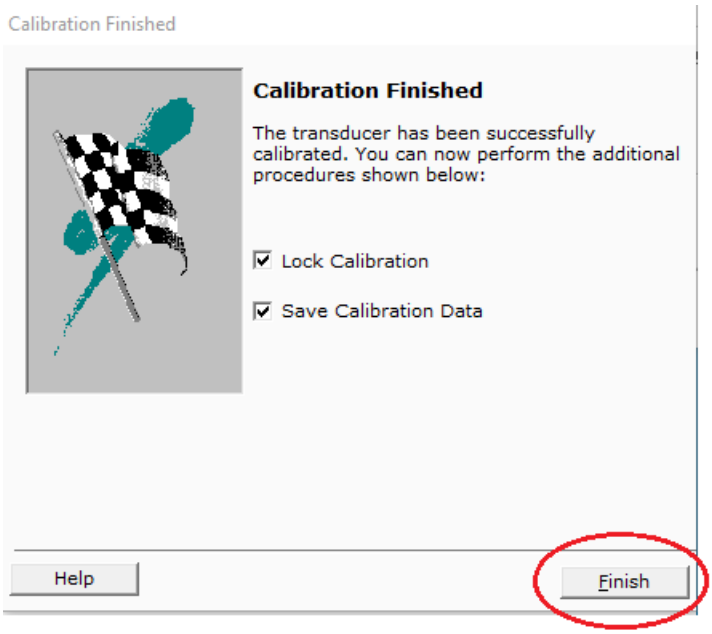

Step 7: Nothing more is needed. Click cancel.

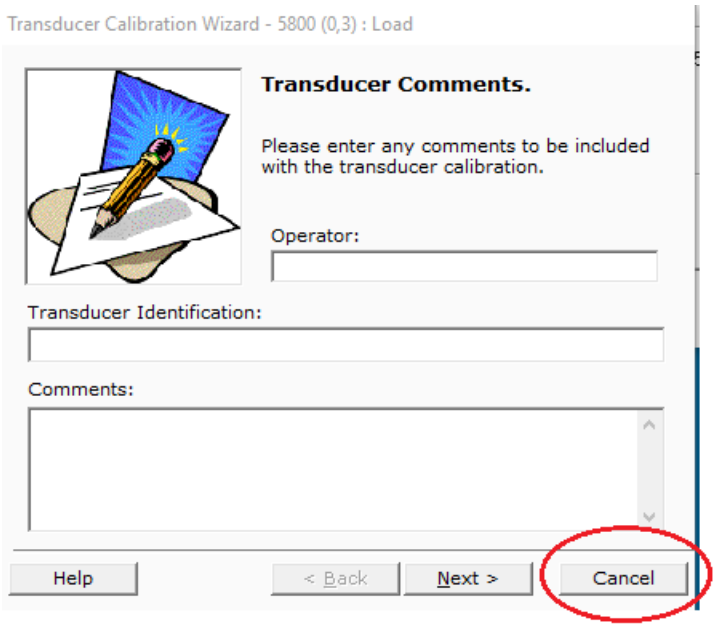

1.6 Analogue output

Instron har a total of five channels for use of analog input and outputs. This chapter concerns how to extract the correct data from Instron.

The picture shows all the connections for extracting the analog output data:

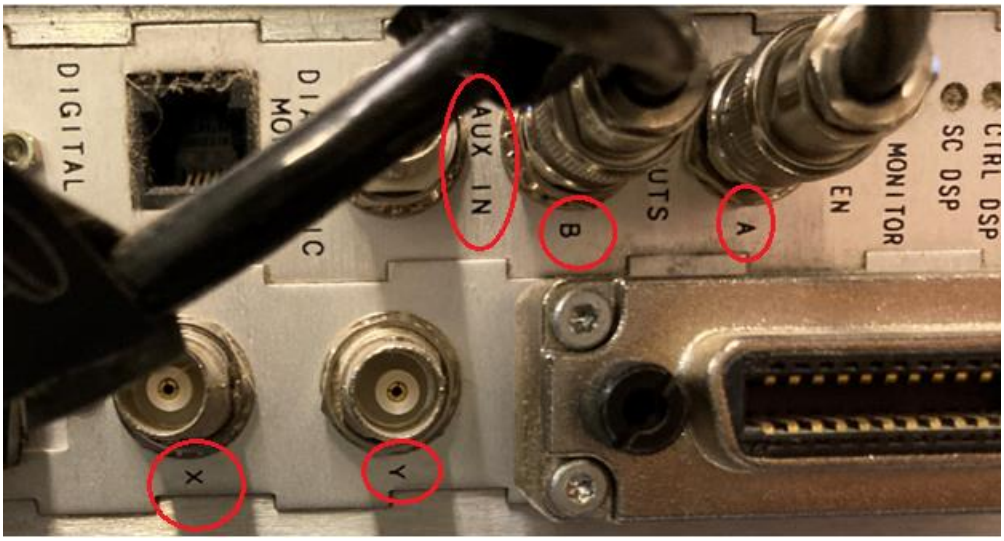

To find information about the analog output channels, click this button on the panel in the upper right corner on the computer screen:

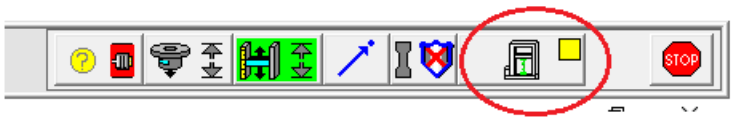

In the window that pops up, go to analog I/O (A):

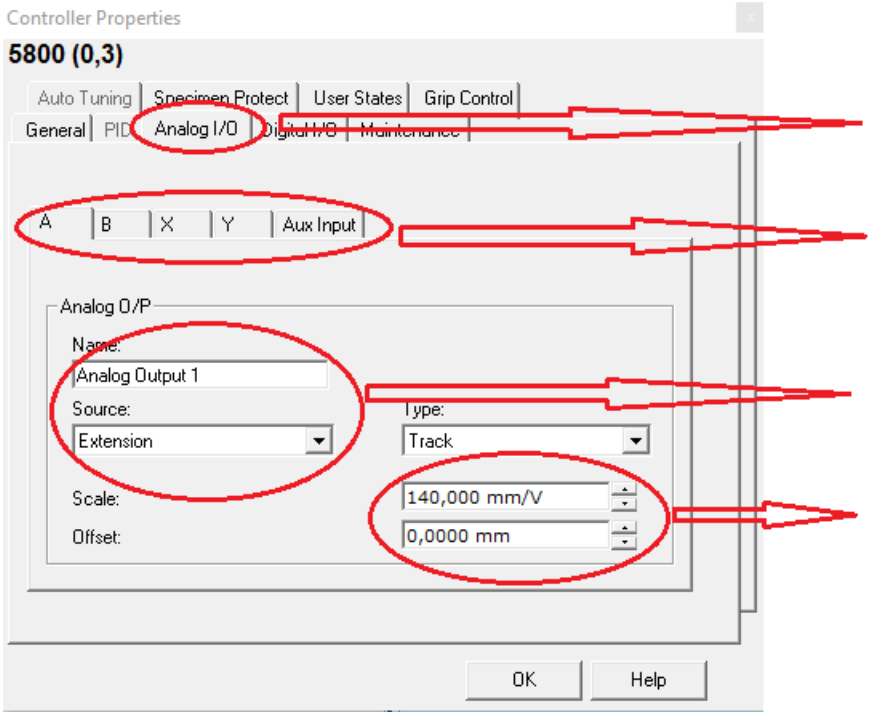

A: Analog I/O is for adjusting the analog input and output channels.

B: All the available channels. Click on one to edit it or see its information.

C: A name can be given to the channel. Choose the source for the channel.

D: Input for the output signals to be correct.

The scale in D should be the sensitivity for the given source. In this case, that is the maximum value of the given source divided by the maximum output in volt. The offset should in most cases be set to zero. It can be used if it is wanted that the output values should be different than that of Instron with a constant “offset” from the value given in Instron.

It can be useful to know where to find information about the maximum extension of the press, load of the load cell, and output in volt.

Here, the maximum extension can be found:

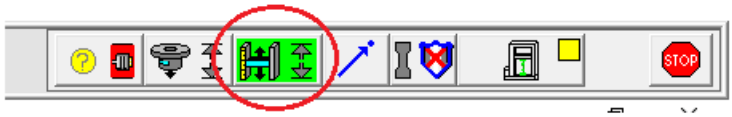

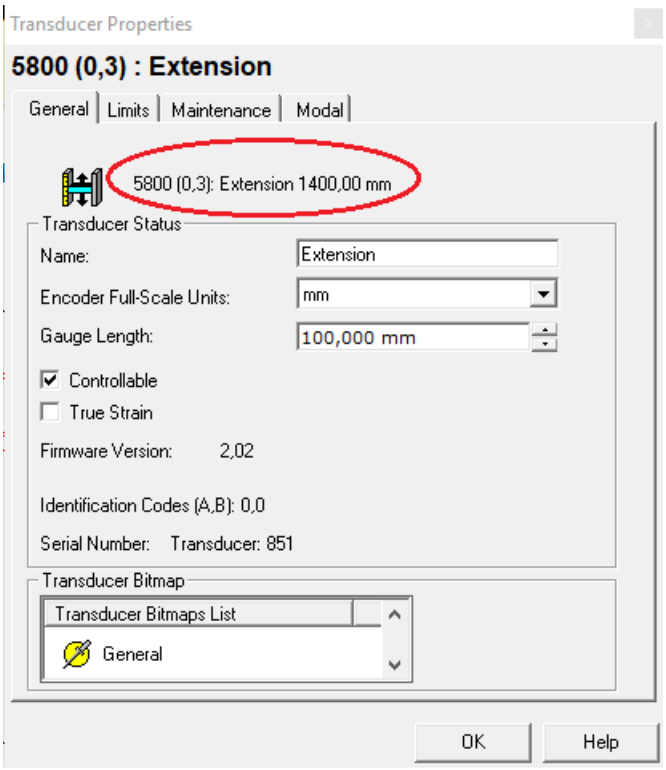

Here, the maximum load can be found:

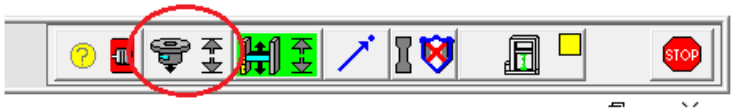

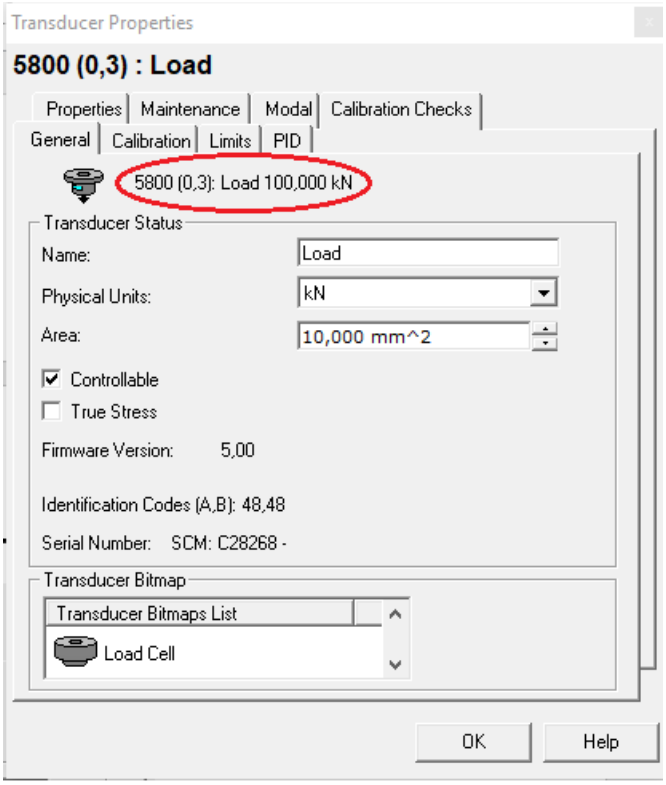

Here, the maximum output in volt can be found:

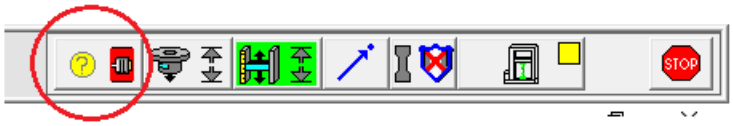

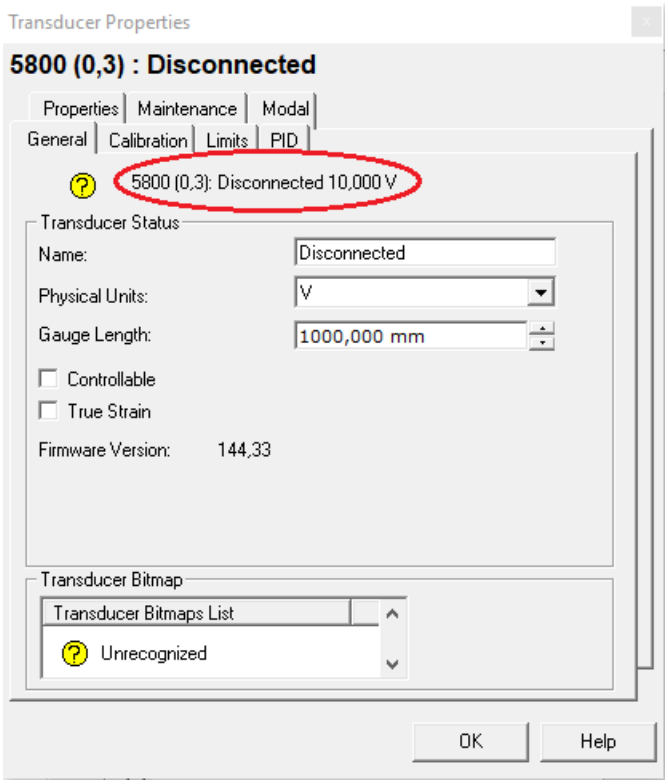
Transducer Properties
5800 (0,3) : Disconnected
Properties
Maintenance
Modal
General
Calibration
Limits
PID
5800 (0,3): Disconnected 10,000 V
Transducer Status
Name:
Disconnected
Physical Units:
V
Gauge Length:
1000,000 mm
Controllable
True Strain
Firmware Version:
144,33
Transducer Bitmap
Transducer Bitmaps List
Unrecognized
OK
Help

2 Instron Bluehill

This guide includes the most important to using the Instron Bluehill software for applying a test procedure (method) and running a test.

2.1 General

When the software is started, this is the start page that pops up:

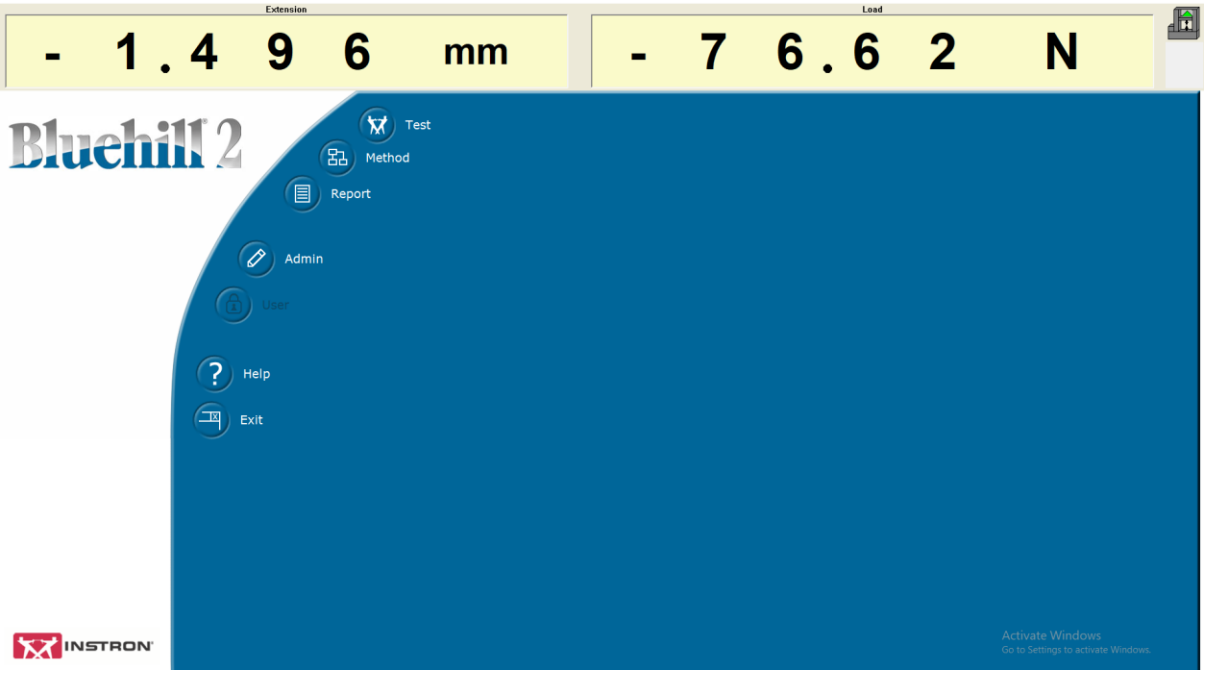

It has six active tabs. All tabs are also directly available when opening the test tab (though a method must already be created to have something to open in the test tab). All tabs, excluding the test tab can be accessed from the method tab. The report tab can easily be accessed when in another tab and does not need to be used form the start page.

In the admin tab, it can be chosen to only let administrators create and edit methods, but such locks do not have to be used.

The help tab is useful for gaining information about how the software works.

The exit tab exits the program.

At the top of the screen in the photo, a live view of the extension of the beam of the press relative to a chosen zero point is shown. Next to it, the live load applied by the press is shown.

2.2 Method tab

Note: Inside a method, all tabs to the left concerning the method are the same for all methods, except for “Test” in the “Control”-tab.

2.2.1 Creating and choosing a method

When clicking on the method tab, a window showing the most resent files that have been opened. Click on a file name and then on “Open” to the far right on the picture to open it. A file can also be opened by clicking on “Browse…” to the far right of the picture and locating the preferred file. A new file can be created by clicking on “New…” to the far right on the picture.

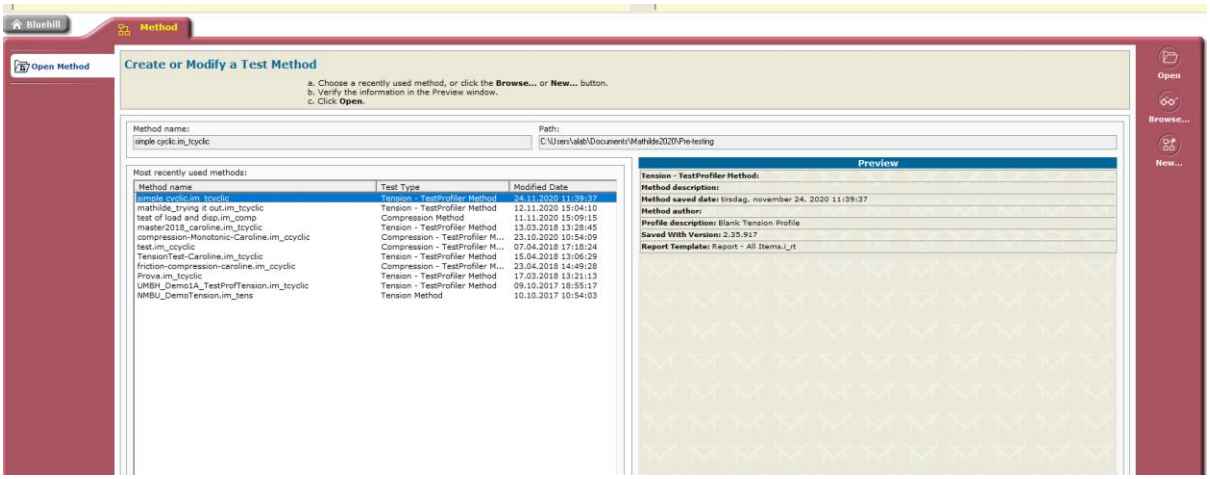

When creating a new method file several options for method types are given. The “Tension Method” is a simple tension method, and the “Compression Method” is a simple compression method. The “Tension – TestProfiler Method” and “Compression – TestProfiler Method” are cyclic test methods.

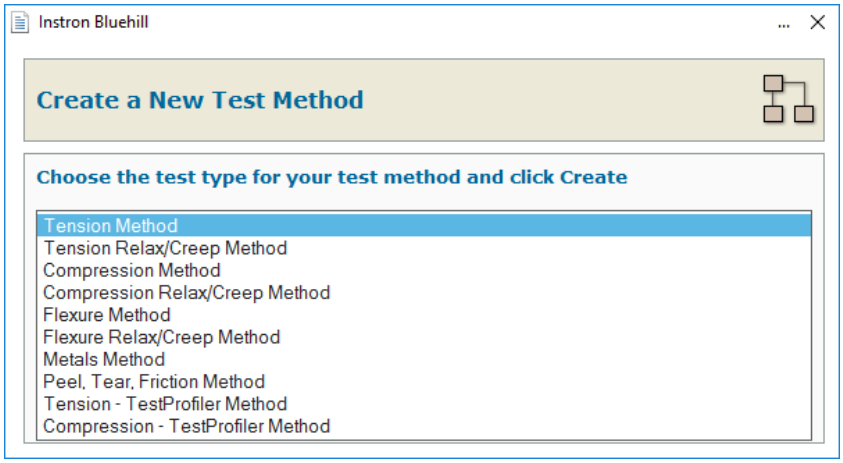

2.2.2 General tab

In the general tab inside a method, the system of units needs to be chosen. By default, “All” is set.

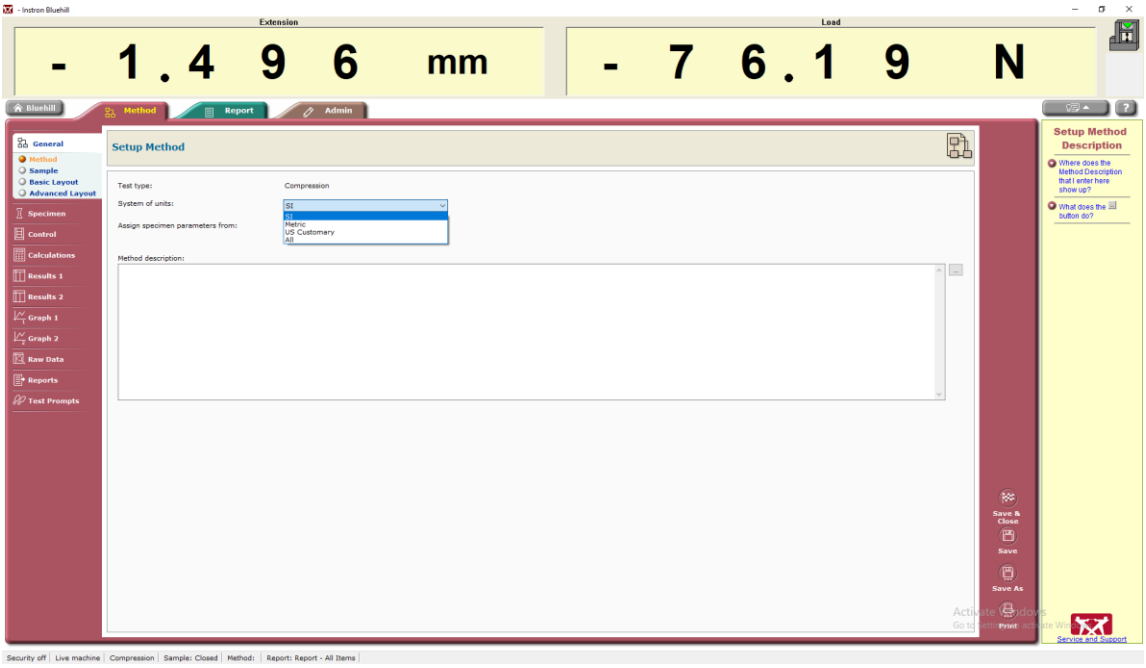

2.2.3 Specimen tab

In the specimen tab, the dimensions of the specimen can be chosen. This is useful if the software is used to directly calculate some properties. Different inputs can also be added here, but no information about doing so will be given here. It is not necessary to edit anything in this tab if only the time, load and extension is needed.

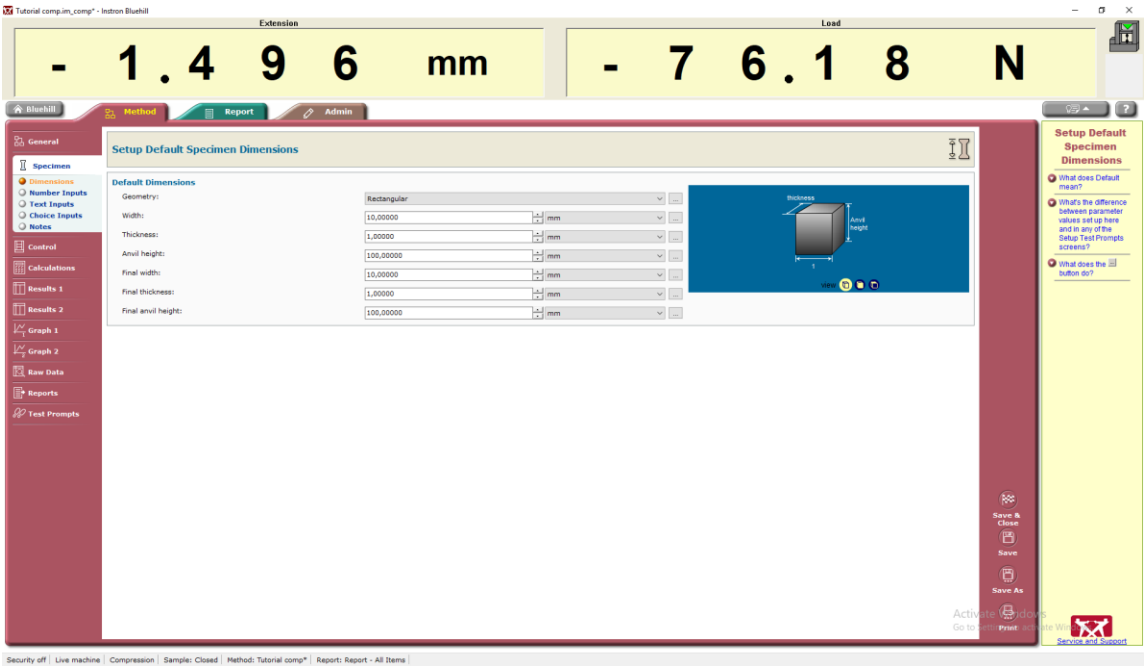

2.2.4 Control tab

“Pre-Test”

“Pre-Test” is typically used in cases where one for example wants to close the gap between the object for applying the load and the specimen, or if the specimen changes qualities early on and needs to be worn out a bit before testing. Detailed information about using a pretest will not be given but can be done here.

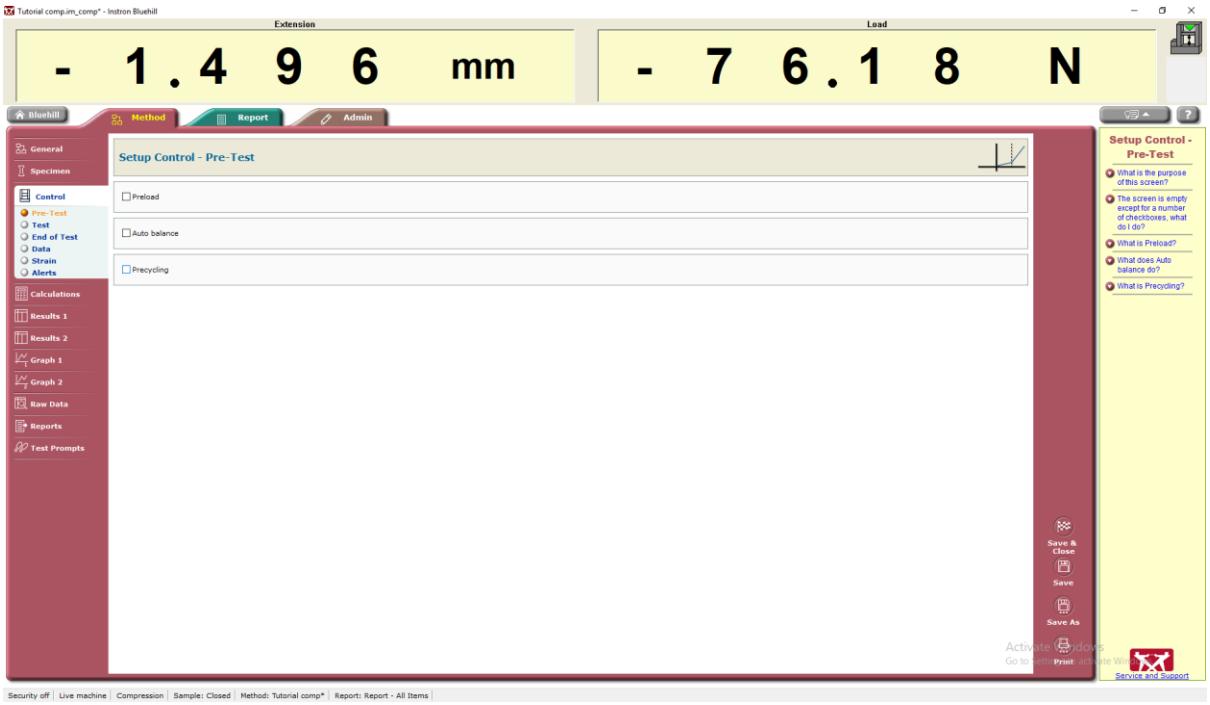

“Test” - Compression/tension method

A compression test is used for showing how to create a procedure for a simple compression test. A tension method is similar.

A simple compression or tension test uses only a speed and one or more “End of Test” criteria to create the procedure.

Which source that should be controlling the test should be chosen from the drop-down menu shown in the picture:

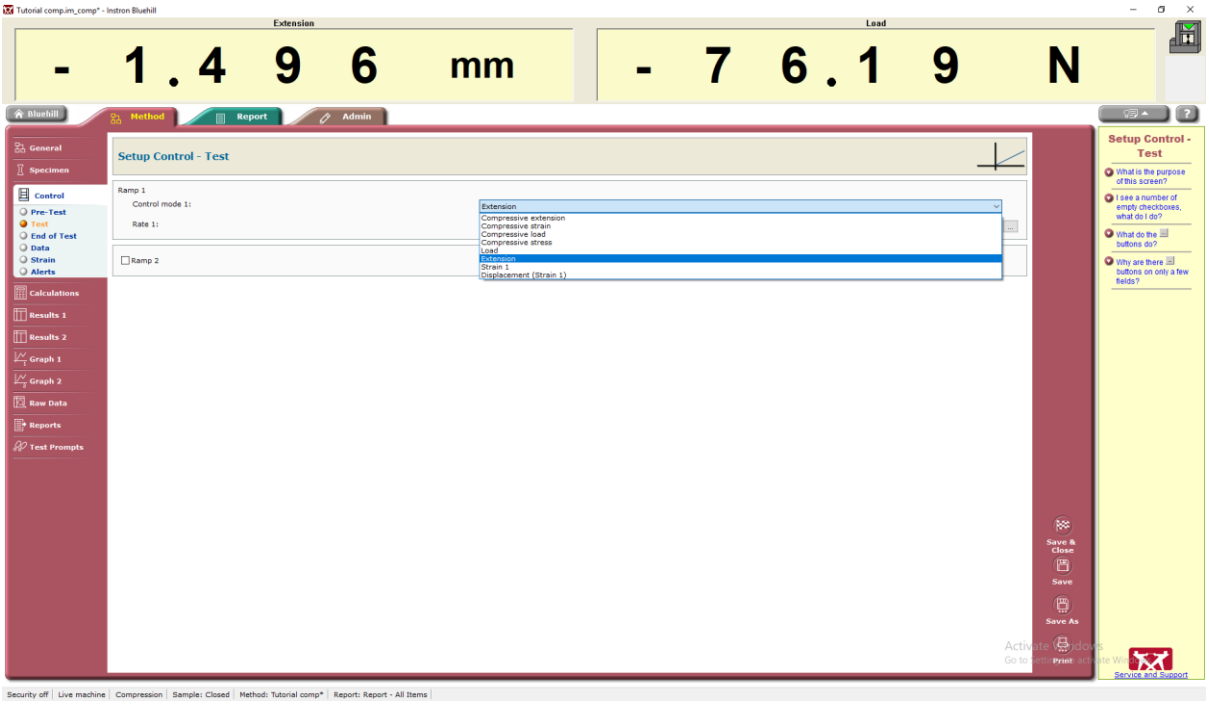

The rate is the same as the speed for the test. The rate must be positive.

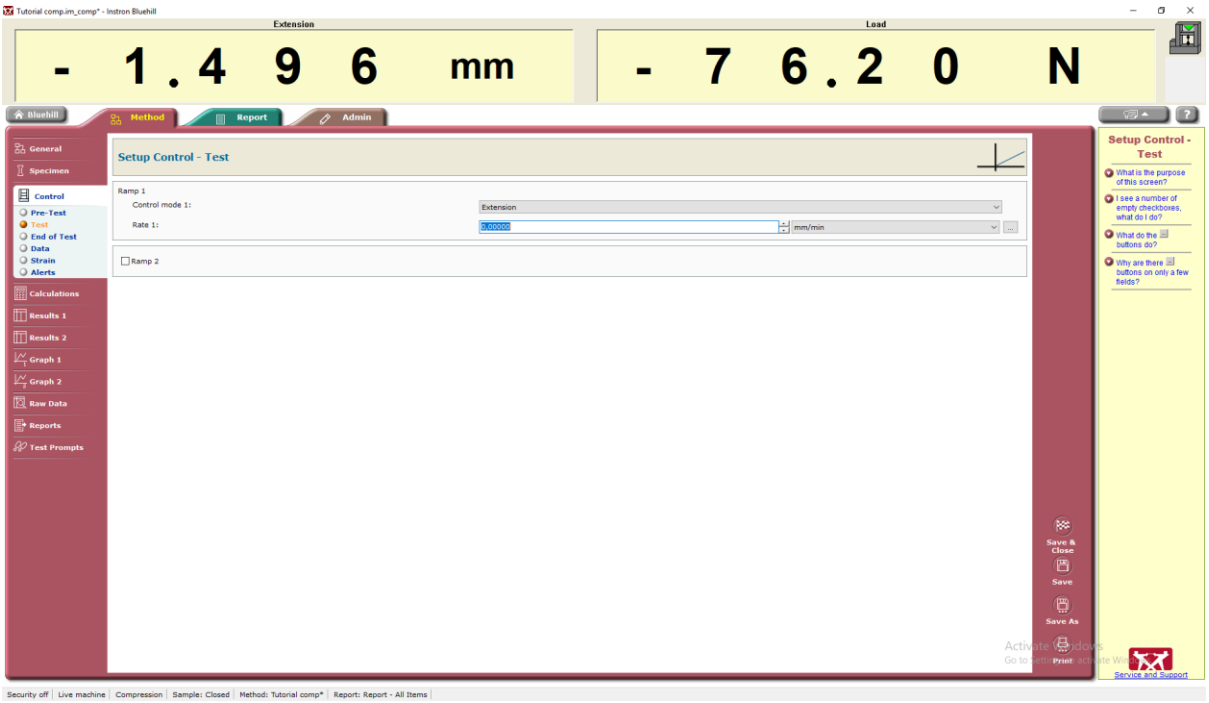

It is possible to change the speed at a given point during the test by choosing to use “Ramp 2”, as shown in the picture:

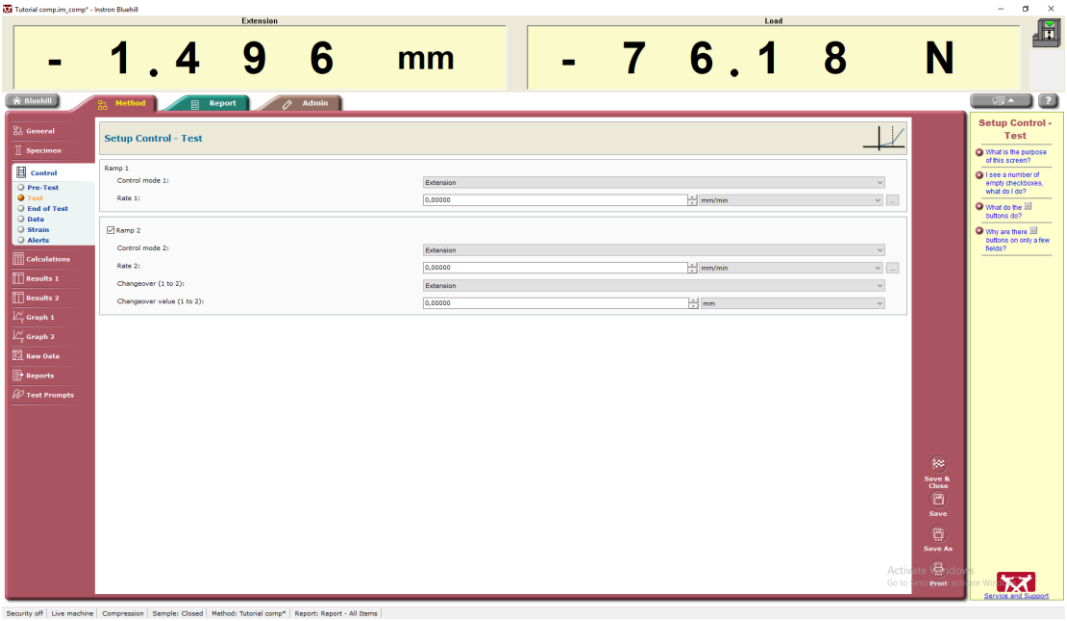

“Test” - Cyclic method (TestProfiler)

The tension – TestProfiler is used here. The compression version is similar. However, the tension version can still go both up and down, so there is really no need to learn to use both.

Click on edit profile to create a cyclic protocol. Note: the method file has to be saved in order to edit the profile.

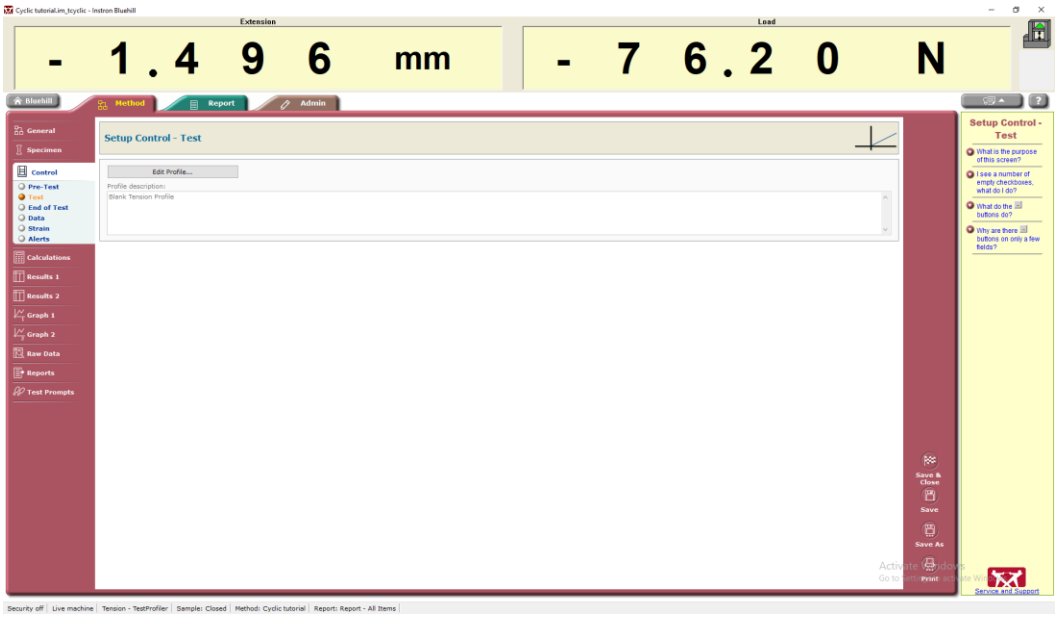

When the window opens, there will at first only be one “block”. A block is used for specifying a certain type of protocol with one type of movement. When one block ends, it will move on to the next. When there are no more blocks, the test will end. Block can be added by going to edit -> append/add block. Append should be used to add the block at the end, add adds the block to the left of the current block. A block can be edited by simply clicking on it and editing the values at the bottom.

A: Choosing the type of movement.

B: Top and bottom position, speed, and number of cycles.

C: Type of movement and chosen name.

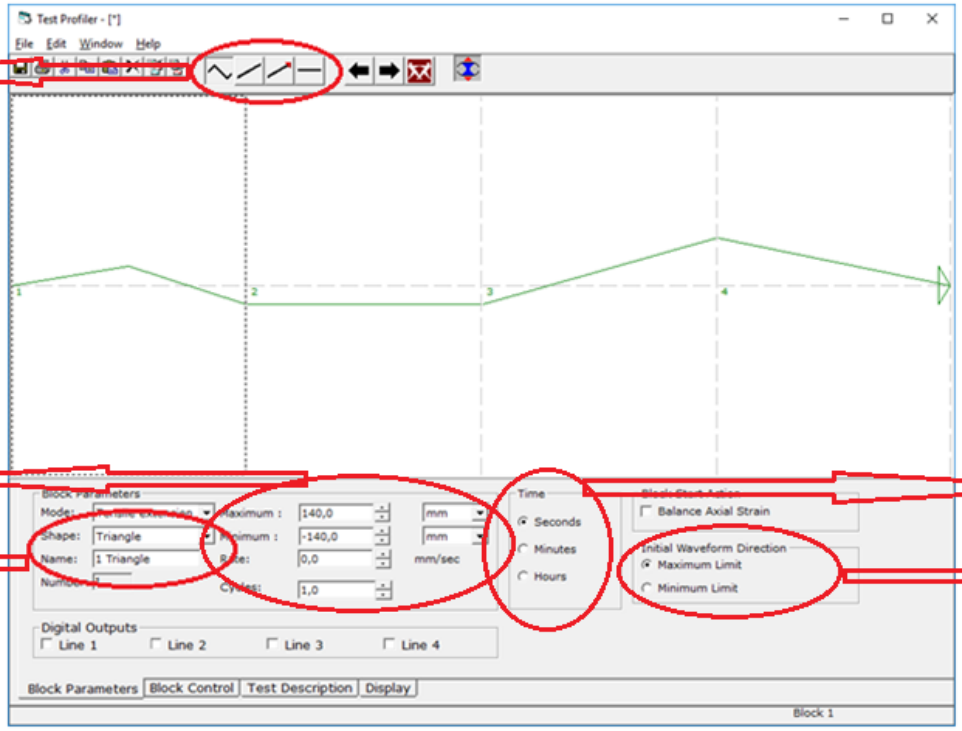

D: Choose what time should be given in.

E: Choose if the press should move to the max or min value first.

A: There are four types of movement that can be chosen. The first here is called “triangle”. It moves up and down between a given maximum and minimum value for a given number of cycles. It starts from where the last block ended (or zero-position if it is the first block), and ends at either the macimum or minimum value for its position.

B: Here, the maximum and minimum values for the position is chosen. The unit the position is given in can be changed to the right. The rate at which the press should move, is the same at the speed. The maximum value i 4,2 mm/s. The unit for setting the rate can be set in D. The number of cycles is also chosen here. It does not need to be a whole number.

C: Here, the type of movemet of the block is specified and can be changed. This is basicly the same as A. If prefered, a name for the block can also be given. By default this is the type of movement the number of the block it is in.

D: The unit time should be given in is chosen here. This effects the units for the rate as well.

E: Here, it can be specified wether the press should move to the maximum or minimum value given first.

The last of the four is called “hold”, which holds the given position for as long as wanted. How long it is to be held, is given by a criterion. By default the criterion is duration, in which a specified duration of time is chosen.

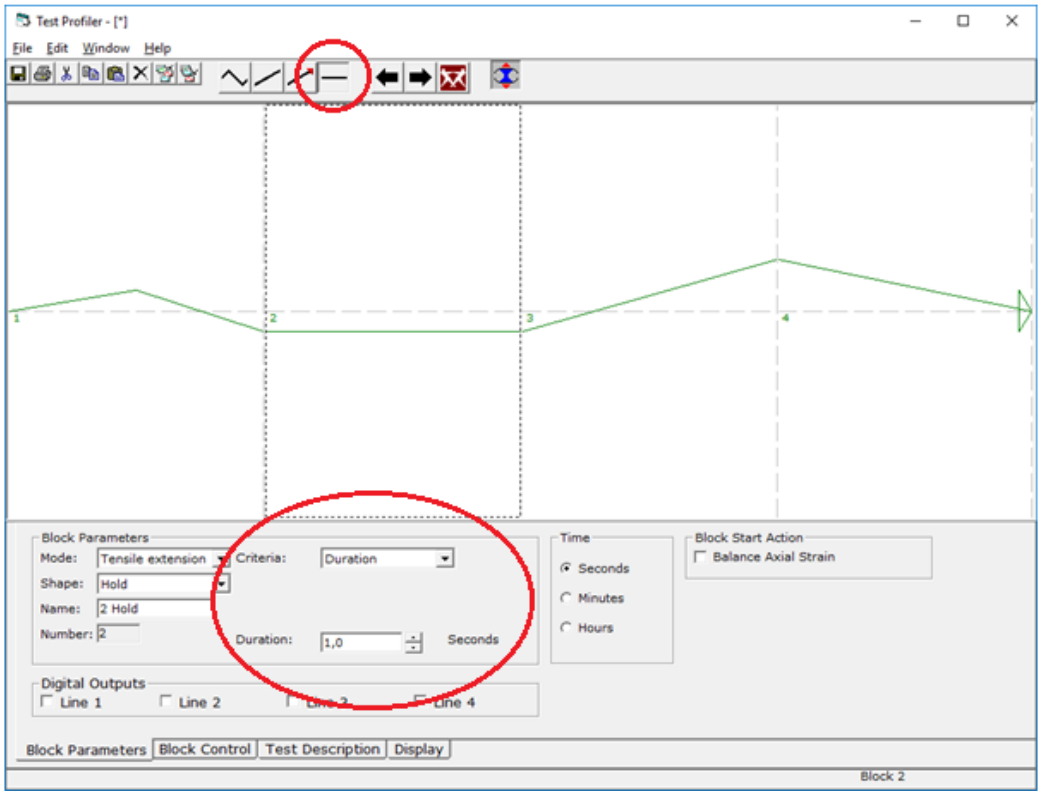

The second of the four is called “relative ramp”. This moves a given distance given by the delta (can be positive or negative depending on the preferred direction of movement) at a given rate.

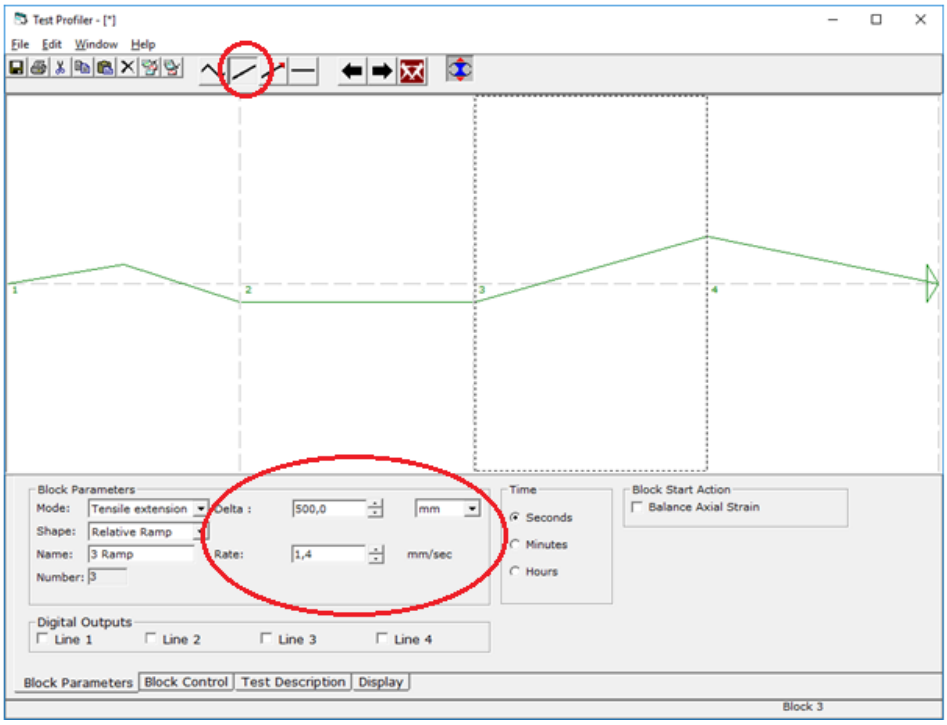

The third of the four is called “absolute ramp”. This moves the press to a specified position at a given rate.

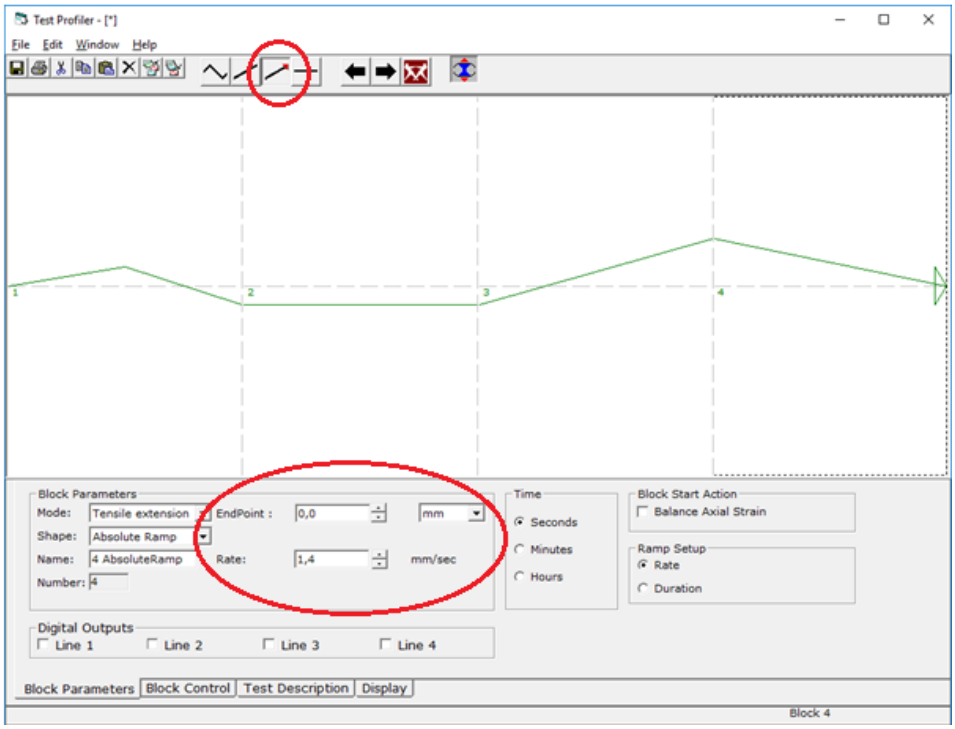

“End of Test”

A least one criterion for ending a test must be given. If this criterion is true, the test will end and the action given for the criterion will play out, even if the protocol has not finished. The default criterion given when creating a method is the rate of load higher than 40%. This means that when the drop of load is high, the test will end. This is useful when testing a specimen to failure.

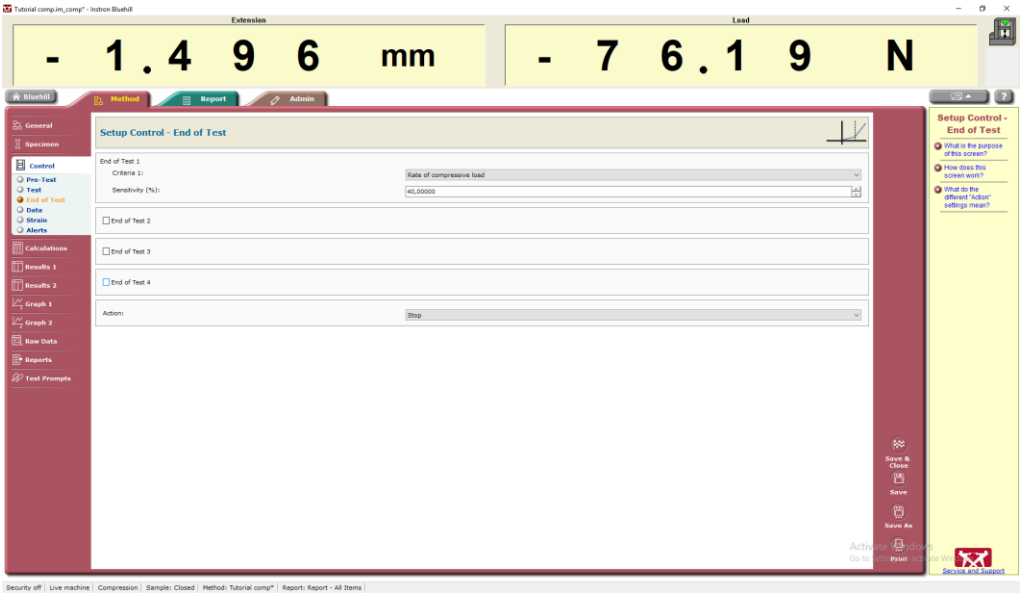

It is possible to change the criterion in the drop-down menu. Load and extension in the drop-down menu are for setting a value in which is not to be exceeded. When the value set is reached, the action given plays out. This is useful when there is a specific extension or load that should not be used. Information about the other choices in the drop-down menu can be found in Instron manuals.

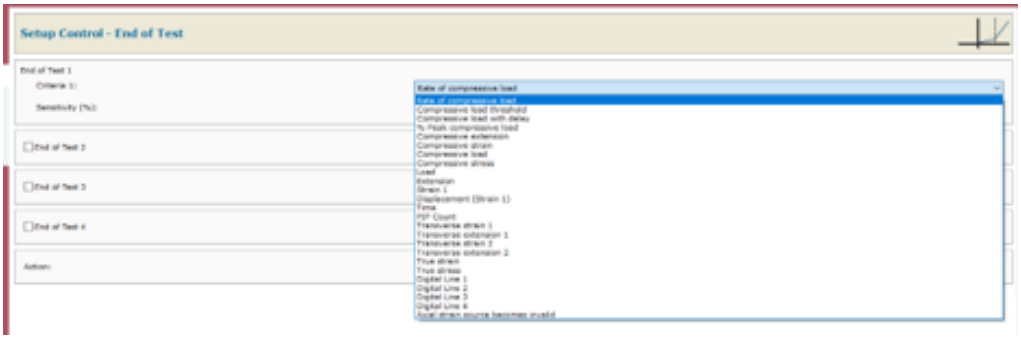

An action to be played out when the criterion/criteria occurs, must be set. The choices are as shown in the drop-down menu.

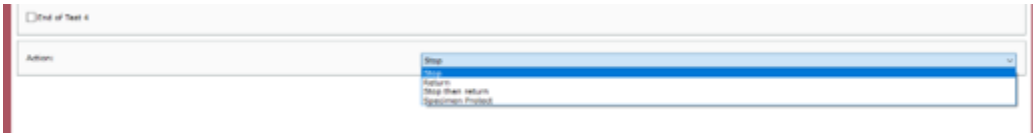

“Data”

The data-tab specifies how often data should be logged by Bluehill. It is by default set to default but can be changed to manual. When set to manual, the criteria shown can be edited. However, the Bluehill software installed in the timer lab in TF fløy 5 at NMBU bugs at this point. If the criteria are edited, the program will stop responding, close, and delete the current file. Therefore, ***the data-tab should never be used.*** The software installed, in general, works poorly for logging of data. It often bugs, stops logging, or does something else unexpected. It is therefore recommended to use some other software to extract the data.

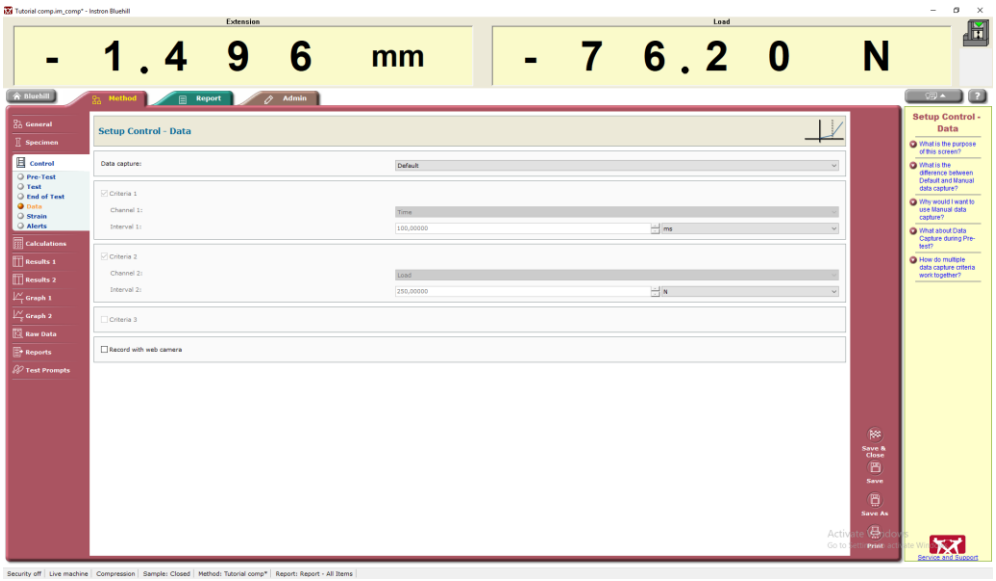

2.2.5 Graph tab

The graph-tab can be used to create graphs from the data obtained. It is possible to create a total of two graphs.

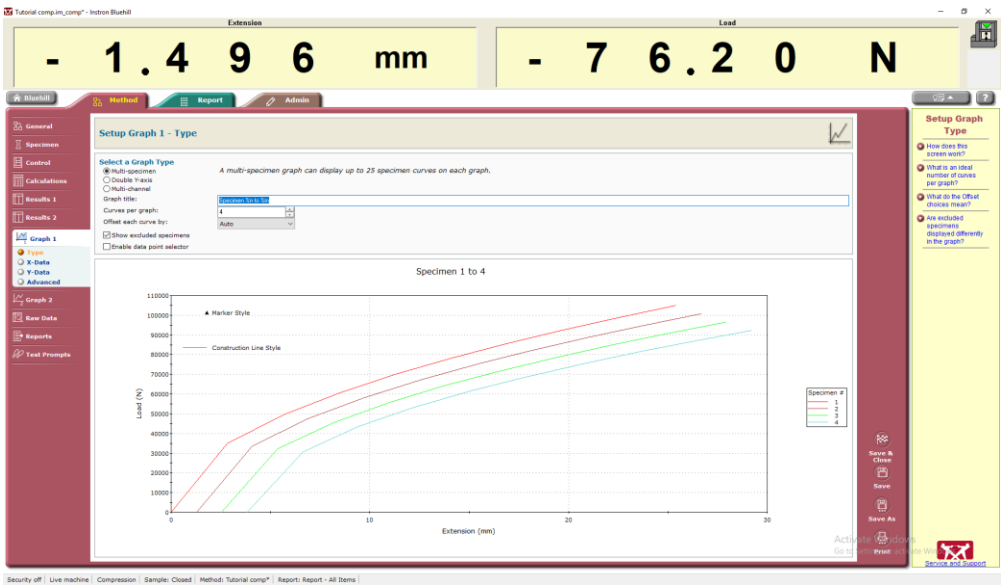

2.2.6 Raw Data tab

In the raw data-tab what data to export can be chosen. By default, the time, extension, and load are exported. The units and how the data would look in an excel file can also be chosen.

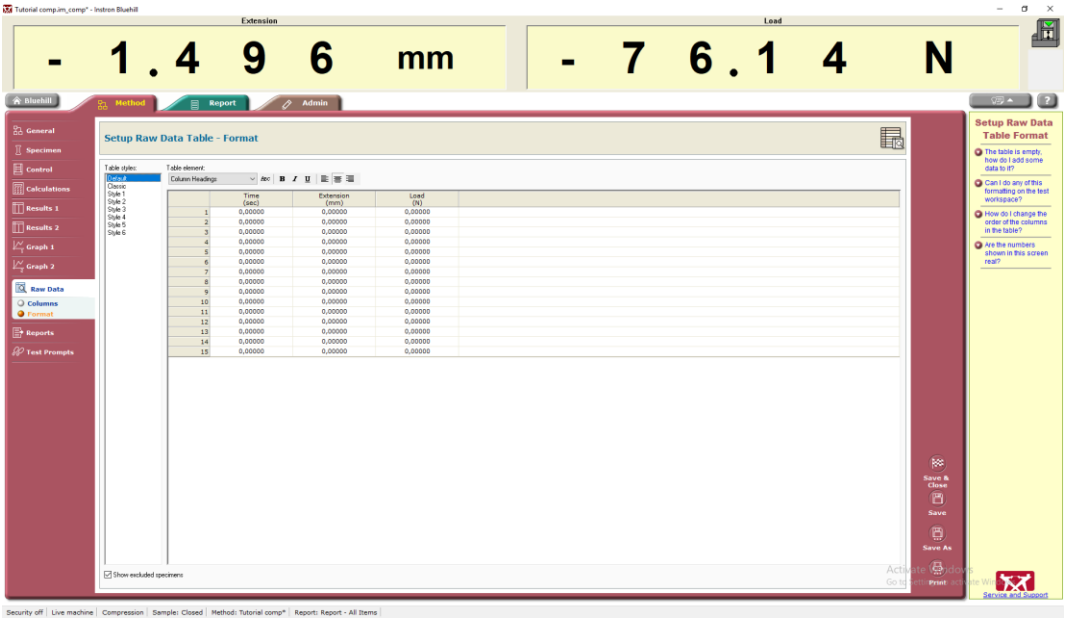

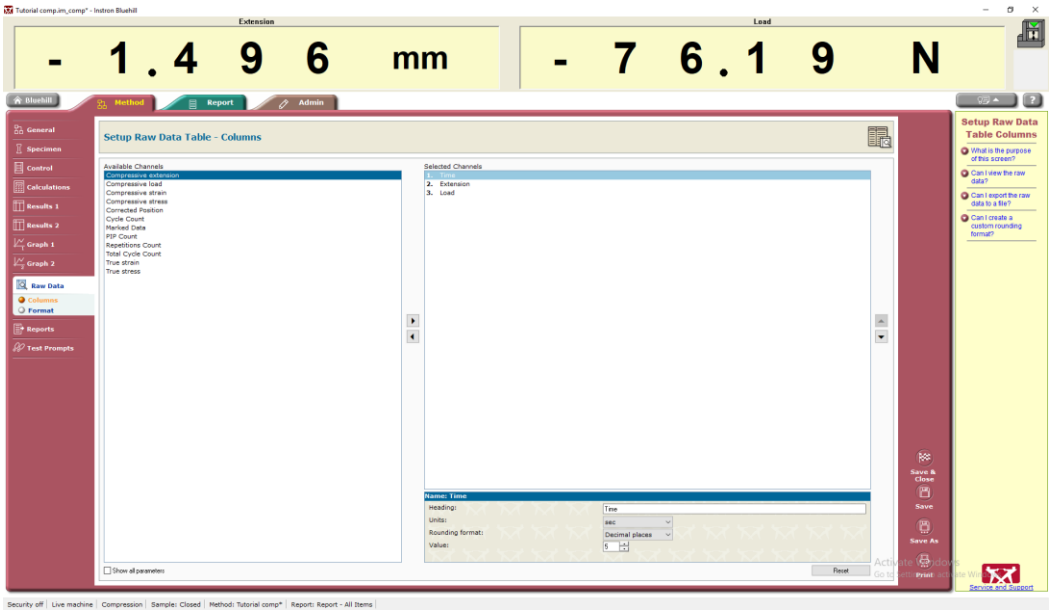

2.2.7 Reports tab

The report-tab is used for editing the format of the report created after running a test, and what this report should include.

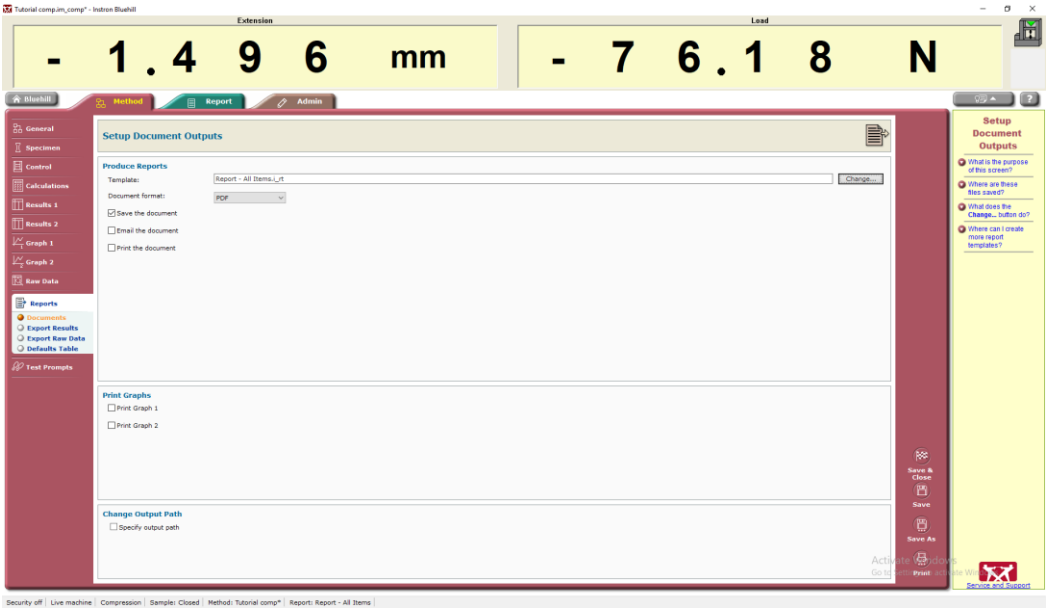

If the results and/or raw data is to be exported, this as to be chosen as shown in the pictures below. The format of the exported results/raw data can be chosen as shown.

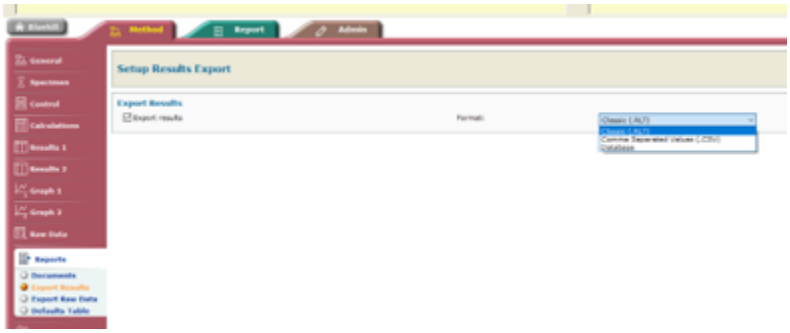

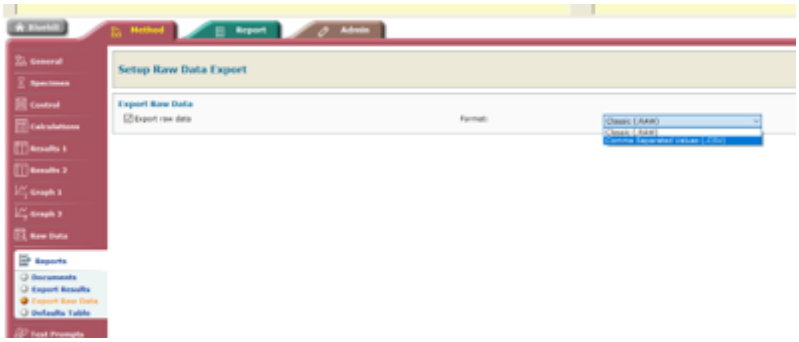

2.3 Test tab

When clicking on the method tab from the main menu, this window opens:

A list of all the methods created is on the left side, sorted by most recently used. Choose the method to use and click next in the top right corner.

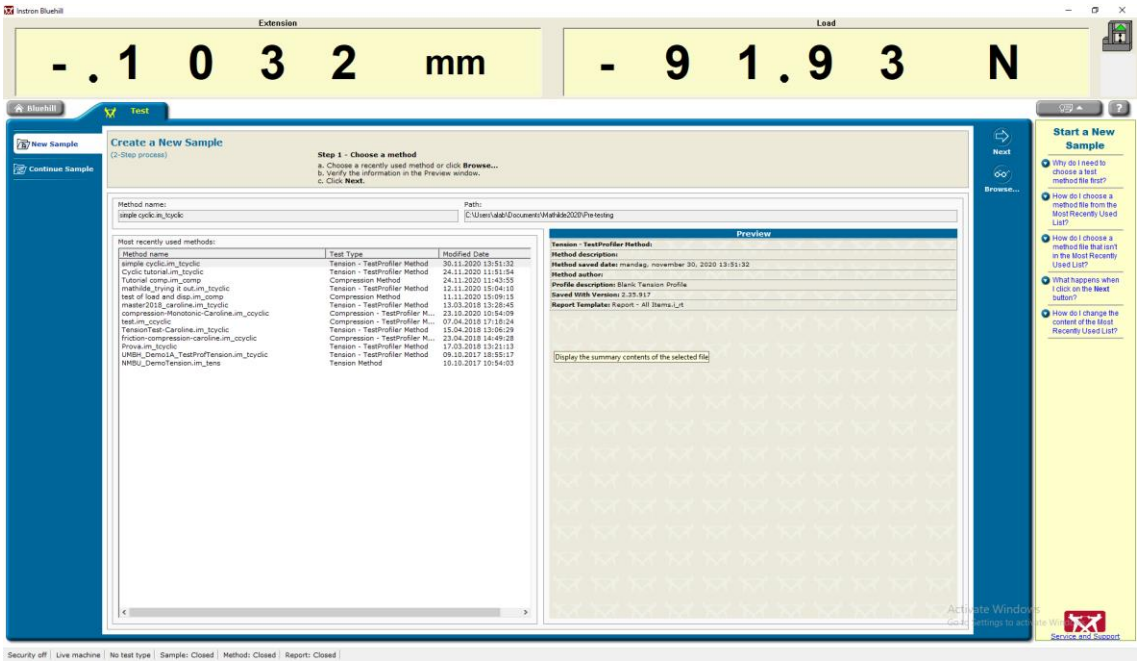

Choose a name and place (Brows.. in top right corner) to save the report created form the test. Click next in the top right corner.

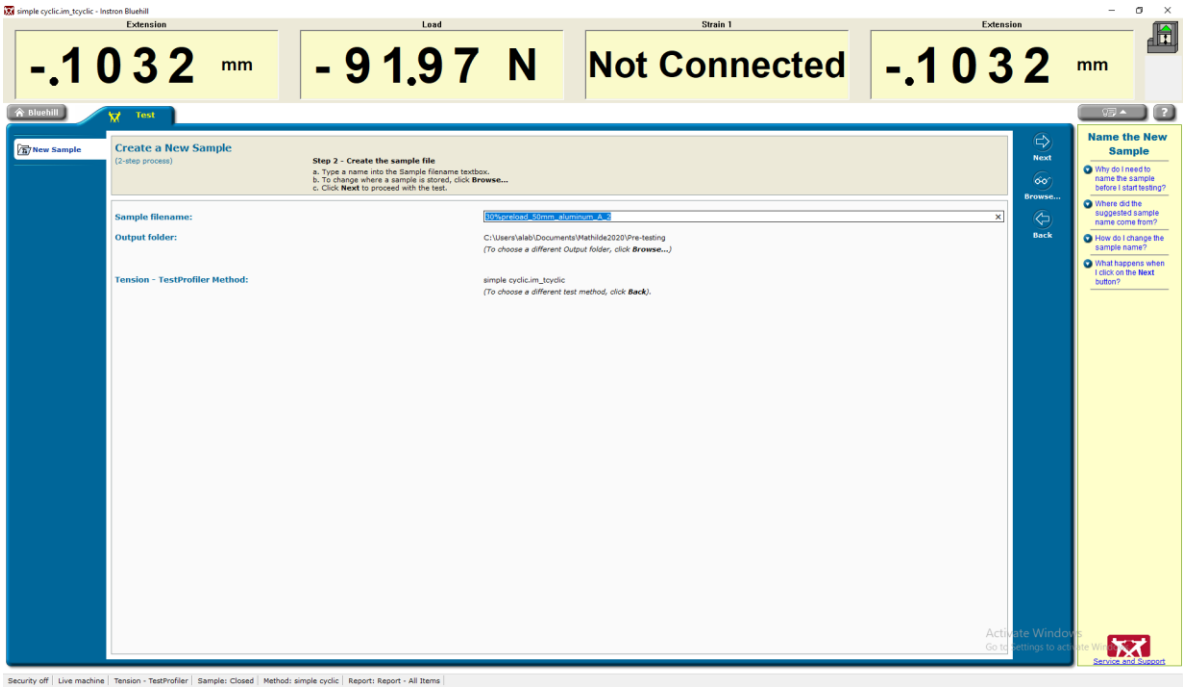

This is the window where the test is performed. Start in the top right corner starts the protocol. Stop stops a test running. Return returns the beam of the press to an extension of zero. Reset resets the measurements taken. Several tests can be run and plotted in the same graph shown in the picture. This graph plots the results during testing. (Data logging with this Instron Bluehill software instlalled does however not work properly, so the curves plotted in this graph does not either.)

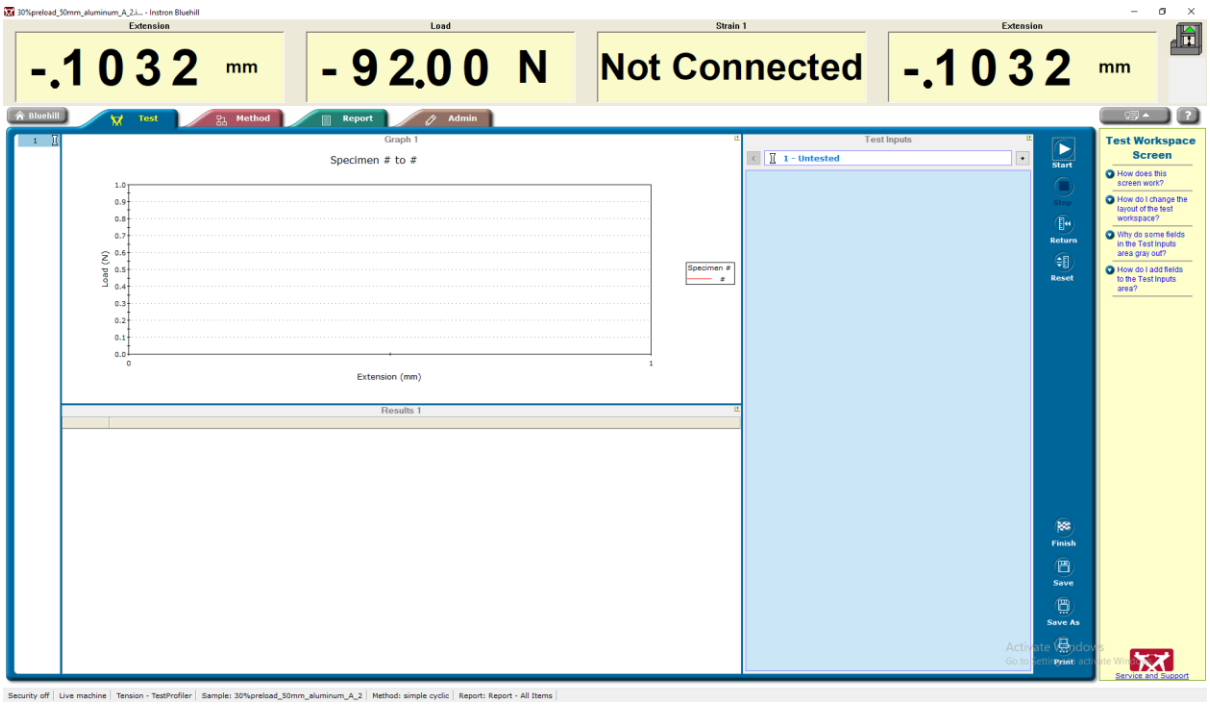

Click finish at the bottom right corner to complete testing and save the report created.

All other tabs can be accessed and edited when the test tab has been opened. The test method can however not be change after an initial test has been completed.

3 Catman

3.1 Connecting the devices

The universal amplifier showed in the picture below is used to read the output from sensors or other sources into the computer. Cables connected to sensors or other sources are connected at the front as shown in the picture below. The green light in the middle at the right means the device is connected to a computer and is OK to be used.

On the back of the universal amplifier, a eternet cable and a power cord is connected. The eternet cable is to be connected to the computer using Catman.

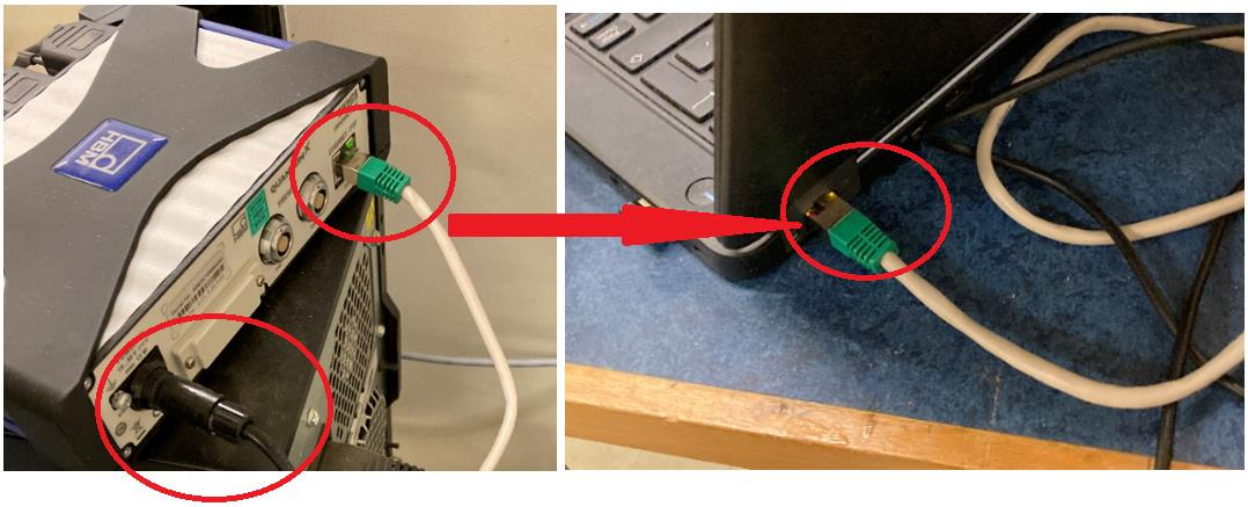

3.2 Starting up

Below, the first window shown below is the fist to pop up when opening Catman. There are four options:

1. Resume my last session
    a. Opens the DAQ project last used
    b. Same universal amplifier as used the last time must be connected

2. Start a new DAQ project
    a. The window in the next picture pops up
3. Load an existing DAQ session
    a. Same universal amplifier as this project was created with must be used
4. Prepare a new DAQ project without connected devices

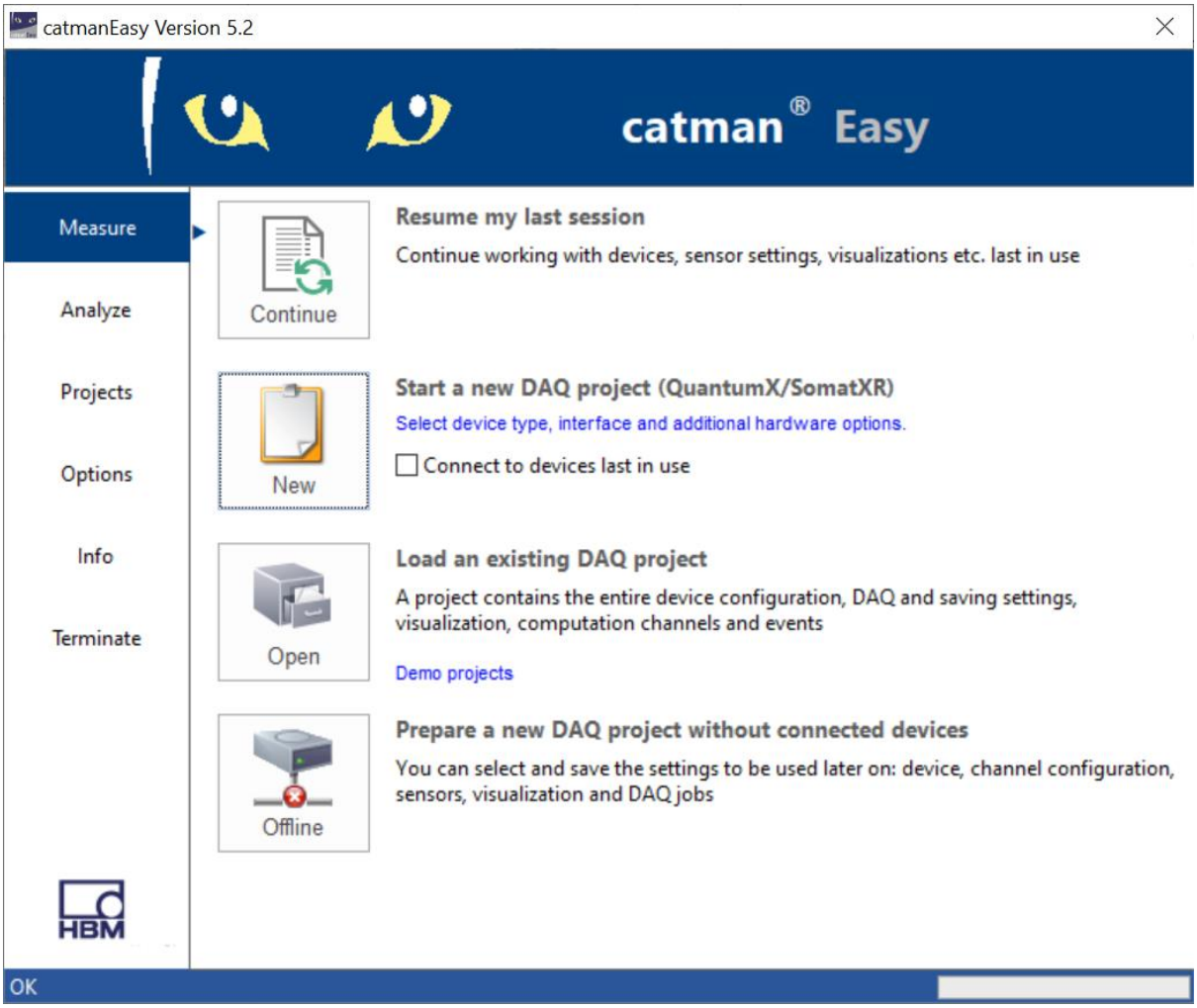

When “start a new DAQ project” is chosen, the window shown below pops up. Here, the devices connected to the computer are displayed. The green light means that the device is connected correctly and is ready to use. Choose the wanted device and click connect.

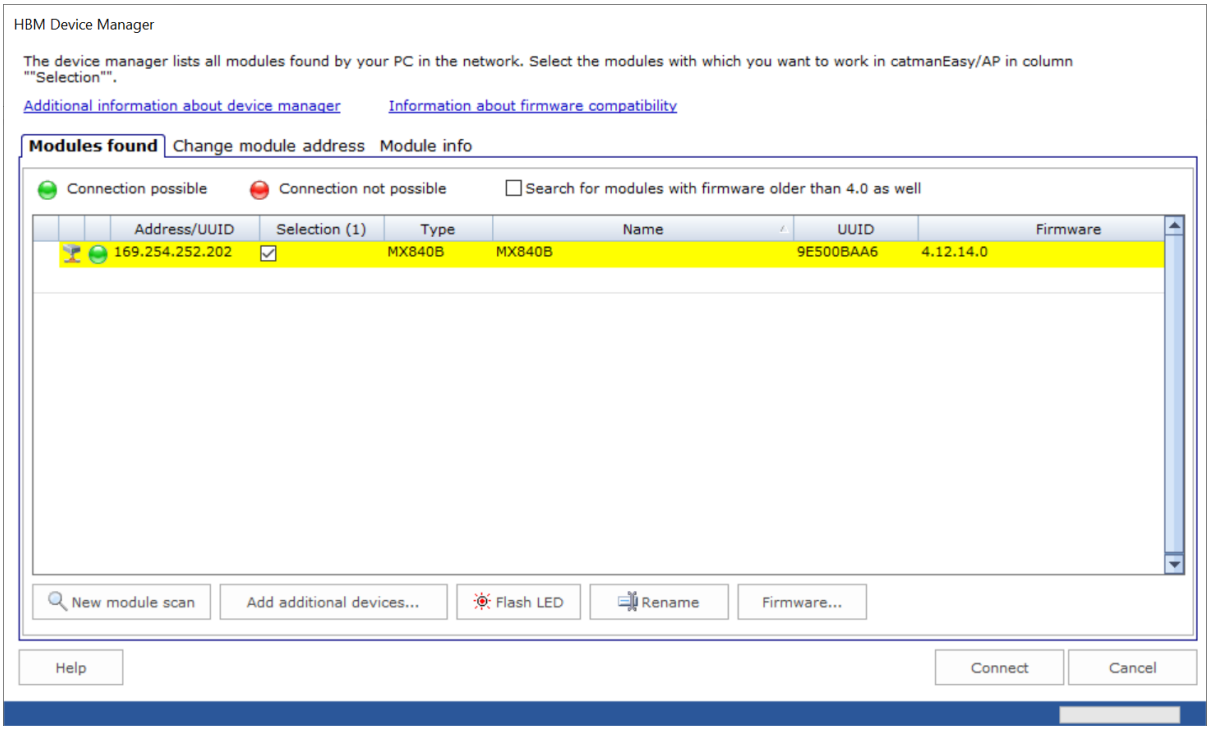

Choose a name and place to save the DAQ project.

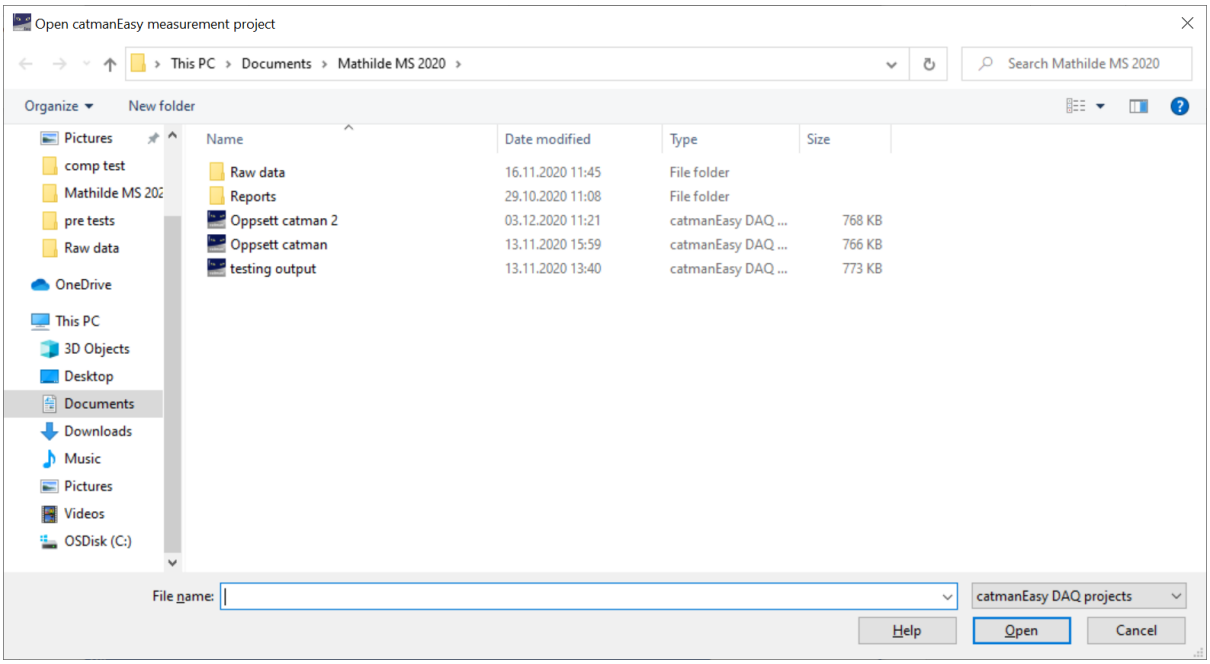

When a project is opened/created, this is the first window showing:

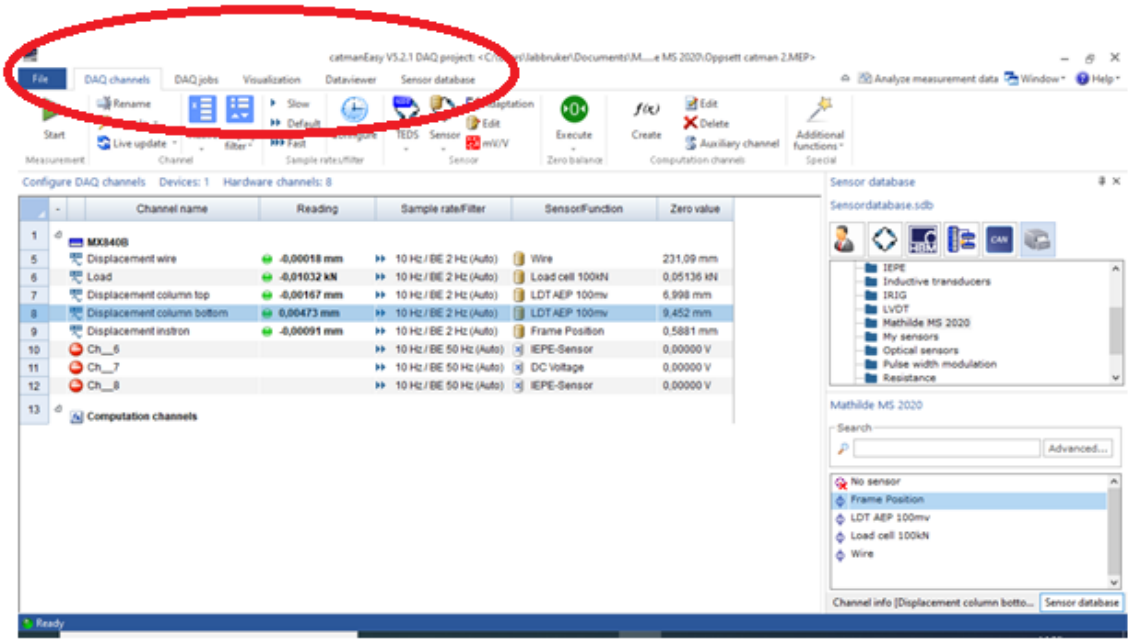

The number of channels match the number of channels that can be connected to the universal amplifier. There are five tabs on top used to set up sensor values and preferences for logging data:

1. DAQ Channels
2. DAQ jobs
3. Visualization
4. Dataviewer
5. Sensor database

3.3 DAQ channel

The number of channels matches the number of channels available in the universal amplifier connected. Additional channels showing a value calculated from the other channels, a formula.

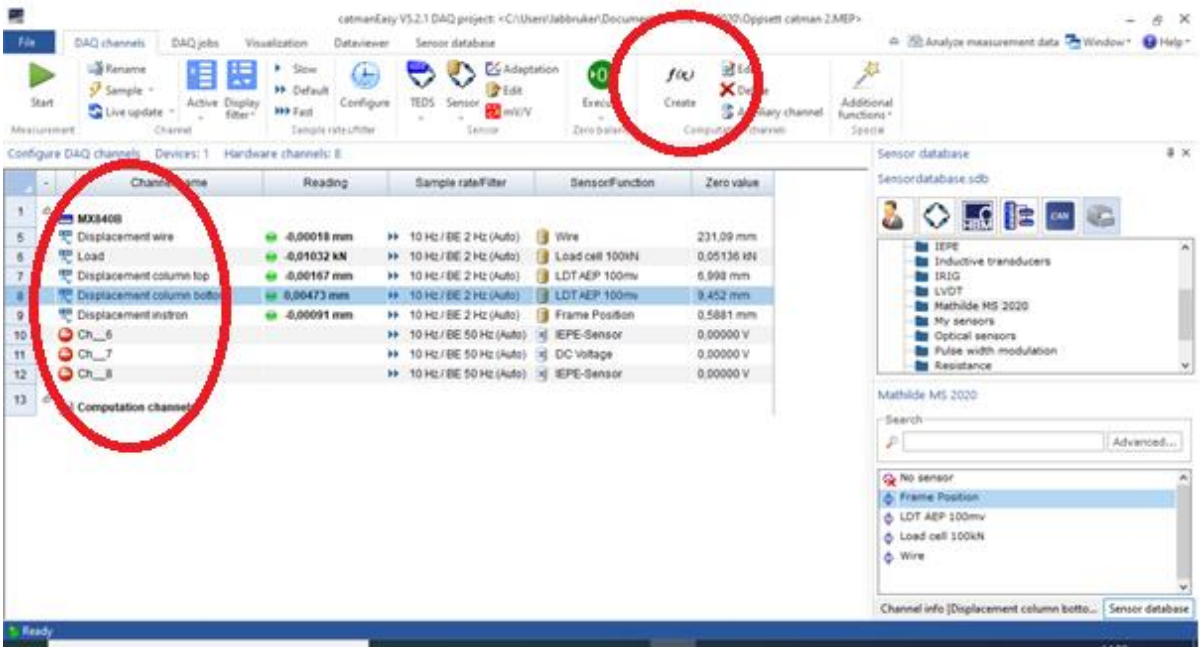

The channels can be activated/deactivated by right clicking in the left most column for the desired channel, as shown in the picture:

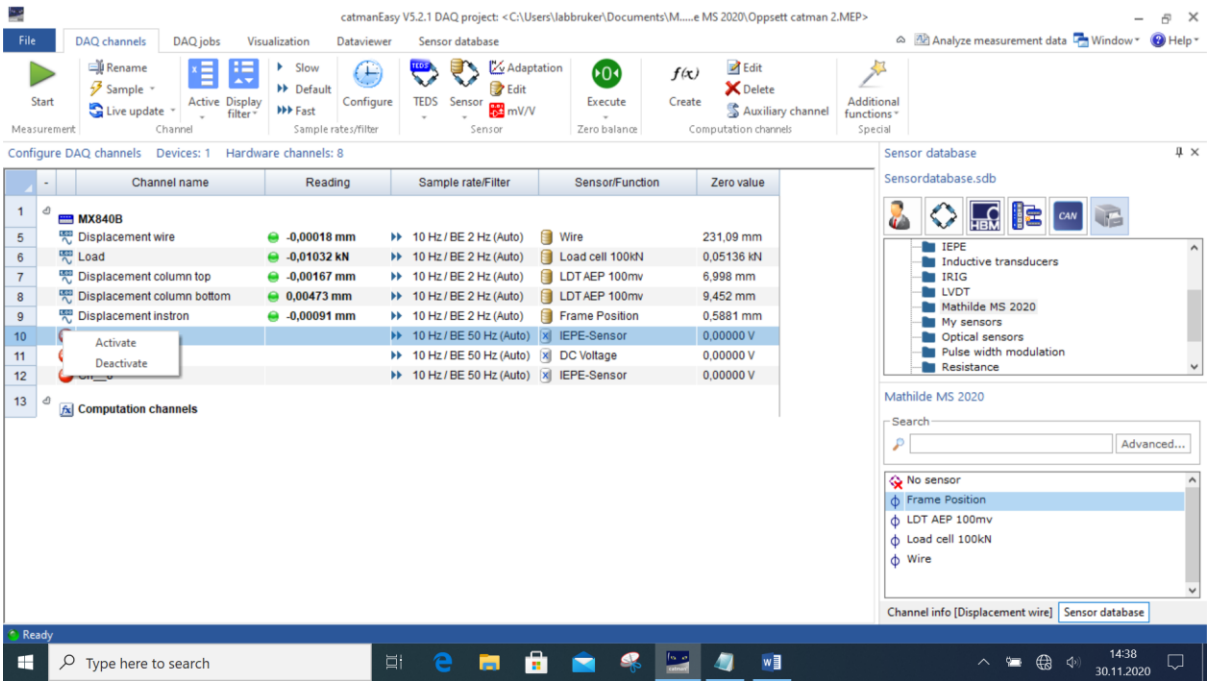

The name of a channel can be changed by double clicking on the channel name. This window pops up, where the name is edited:

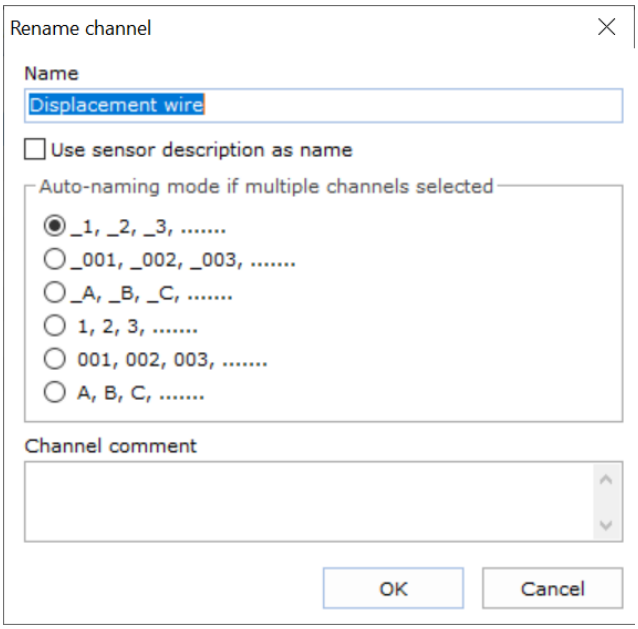

By right clicking in the column “Reading”, the three most useful functions are as in the picture below:

1. Update
    a. Updates the value read into catman for the given sensor.
    b. Can also be done in “sample” in the top left corner in the picture below.
    c. Live update in the top left corner continuously updates the values of all the sensors. This function times out after a while.
2. Zero balance
    a. Sets the value of the sensor to zero.
    b. The rightmost column shows the real value of the sensor where the zero value has been set.
3. Electrical values
    a. Changes between showing the real physical value and the electrical value given by the sensor i volts.

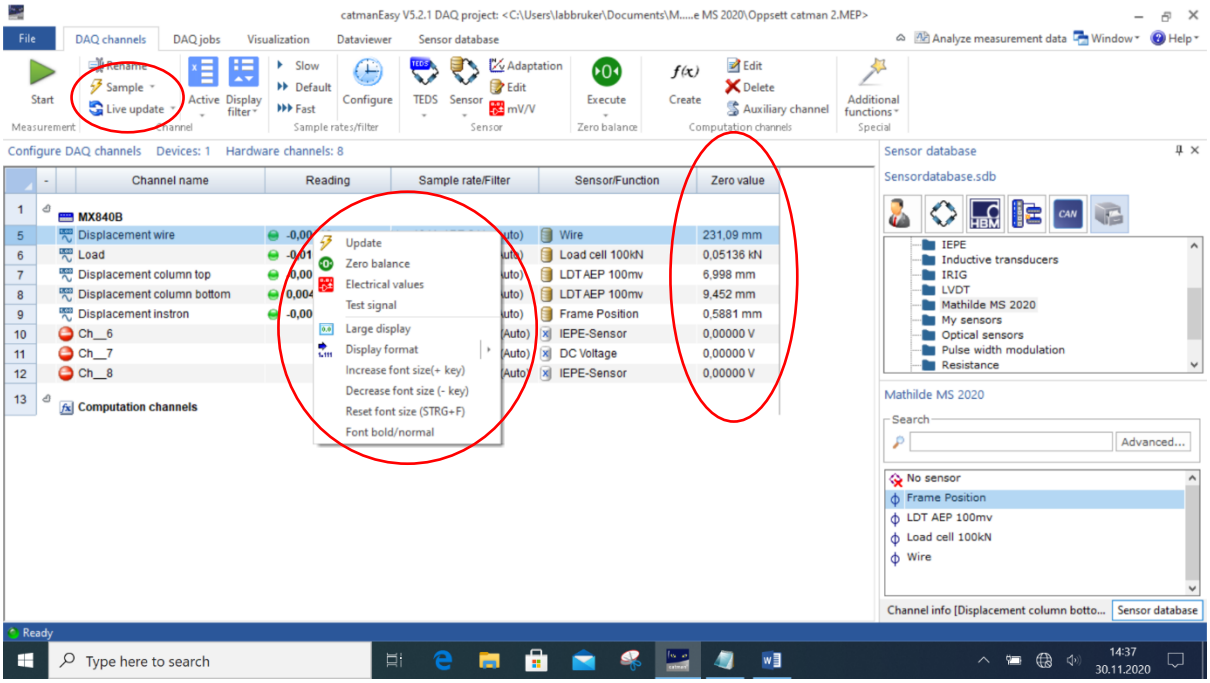

The sensors can be directly edited by right clicking in the column sensor/function. This can also be done in the “sensor database”-tab.

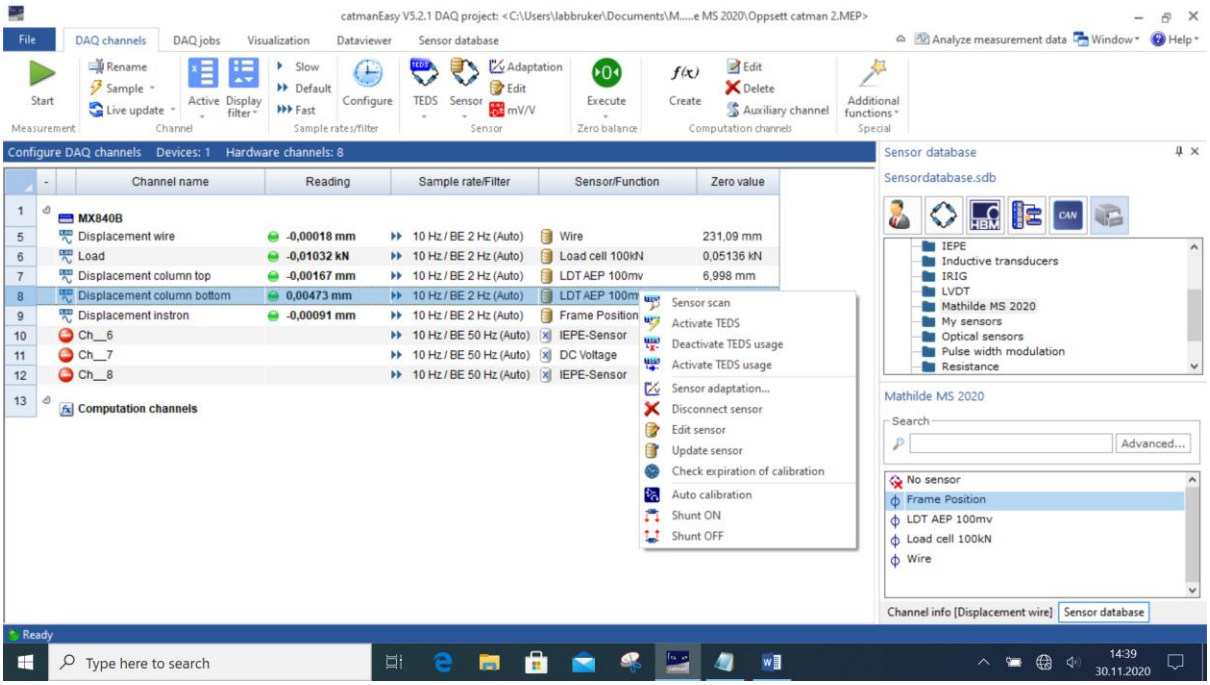

3.4 DAQ jobs

In “general” of the DAQ jobs tab, a criterion for starting and stopping data recording is set. In the rightmost column, how often data is recorded is chosen.

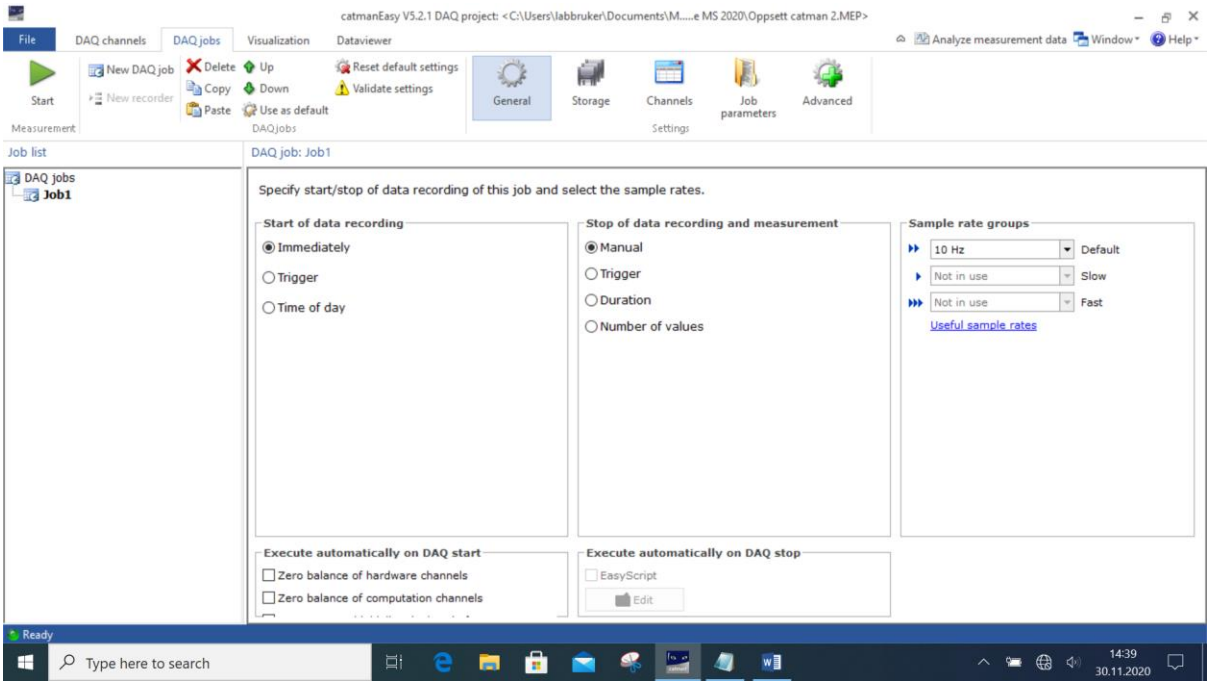

In “storage” information about saving the data file can be set. What data, what type of data file, and the placeholder in files including the name of the file.

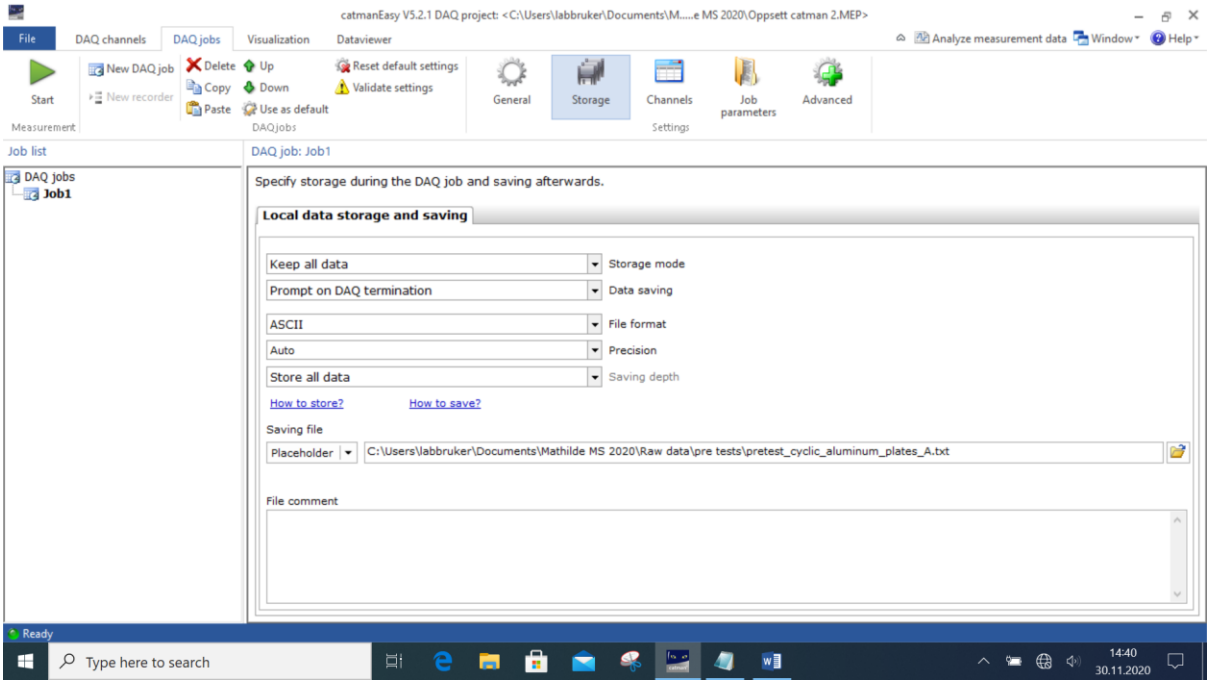

In “channels” channels can be activated/deactivated “active”. Which channels to include in the data file saved can be chosen in “save”.

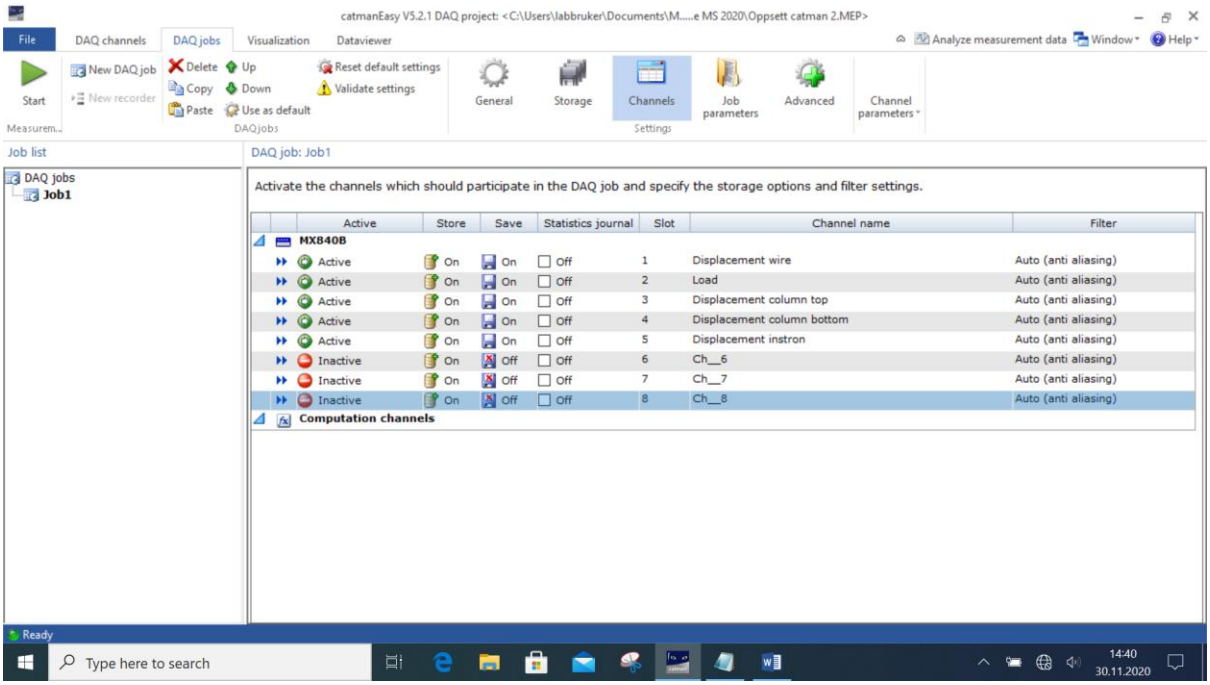

3.5 Visualization

The visualization tab is the only tab showing while a session is active. What is shown here can be chosen. It is also possible to edit during the session. New windows, or “panels”, can be added in “New”.

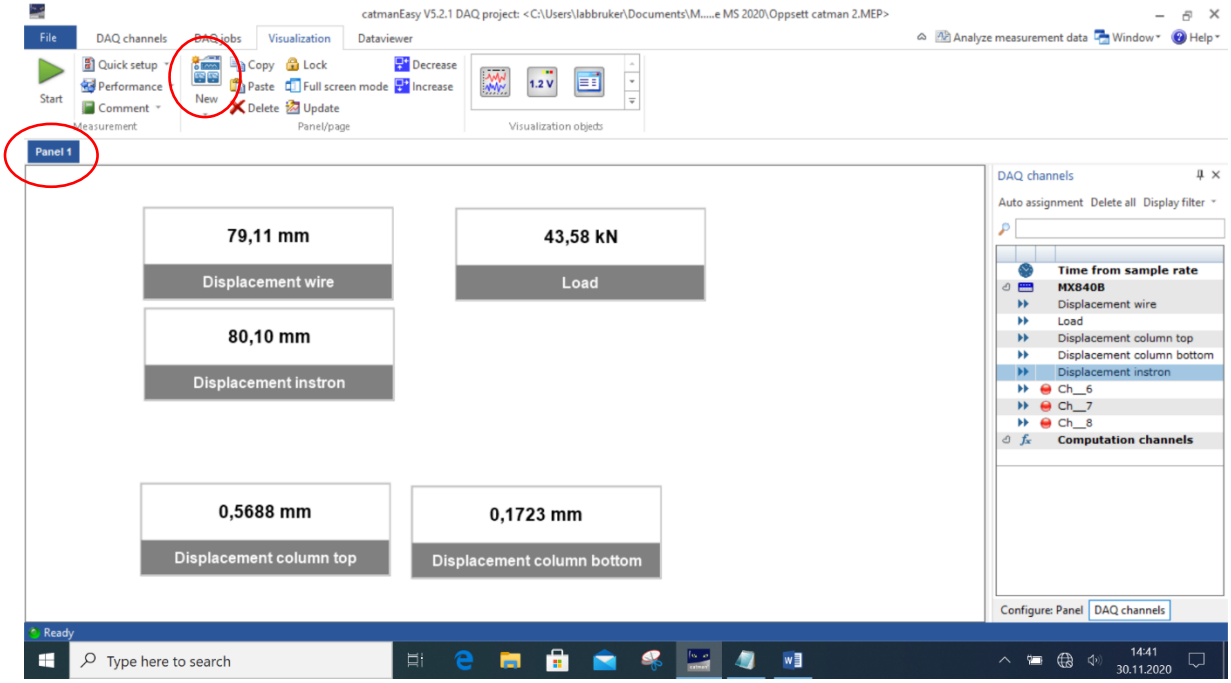

A live view of a channel is added by simply dragging it into the window. The choices on how to view the value can be chosen from the list.

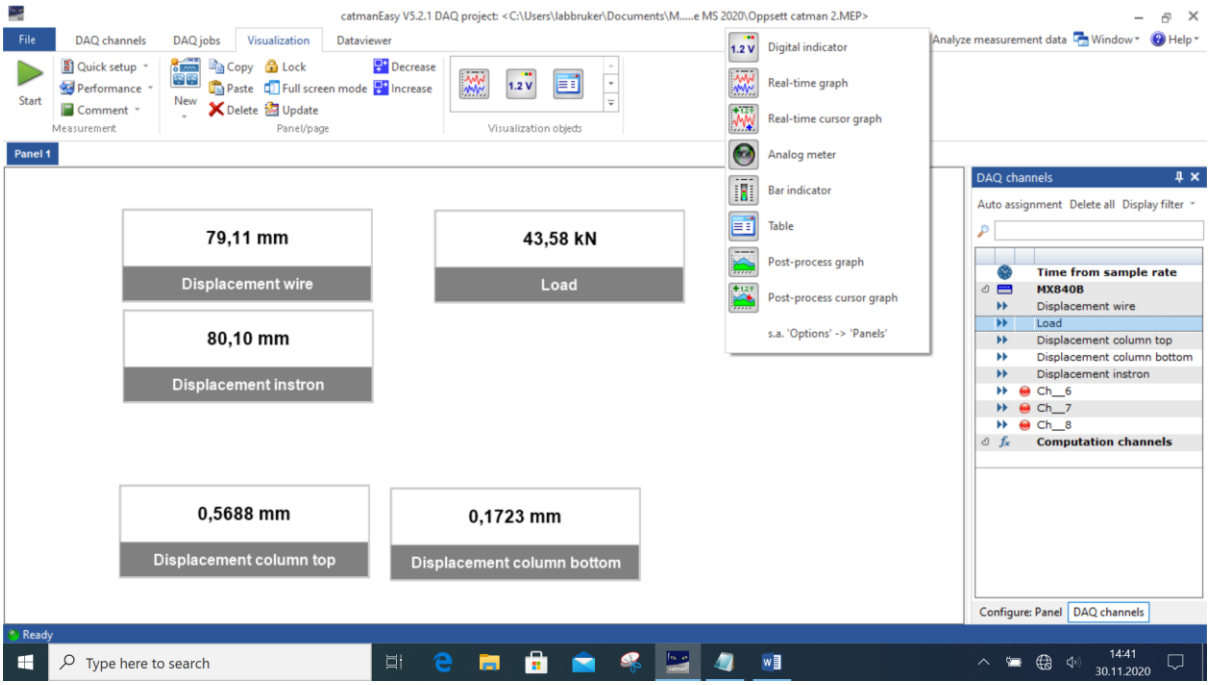

3.6 Dataviewer

In the dataviewer tab, the data from the most recently session is temporarily saved. Channels are added by simply dragging it into the window. The graphs at the bottom can only show the values plotted against time. Useful values such as max/min can quickly be seen in the first window of this tab. It is also possible to export data from one column in addition to the time stap from this tab.

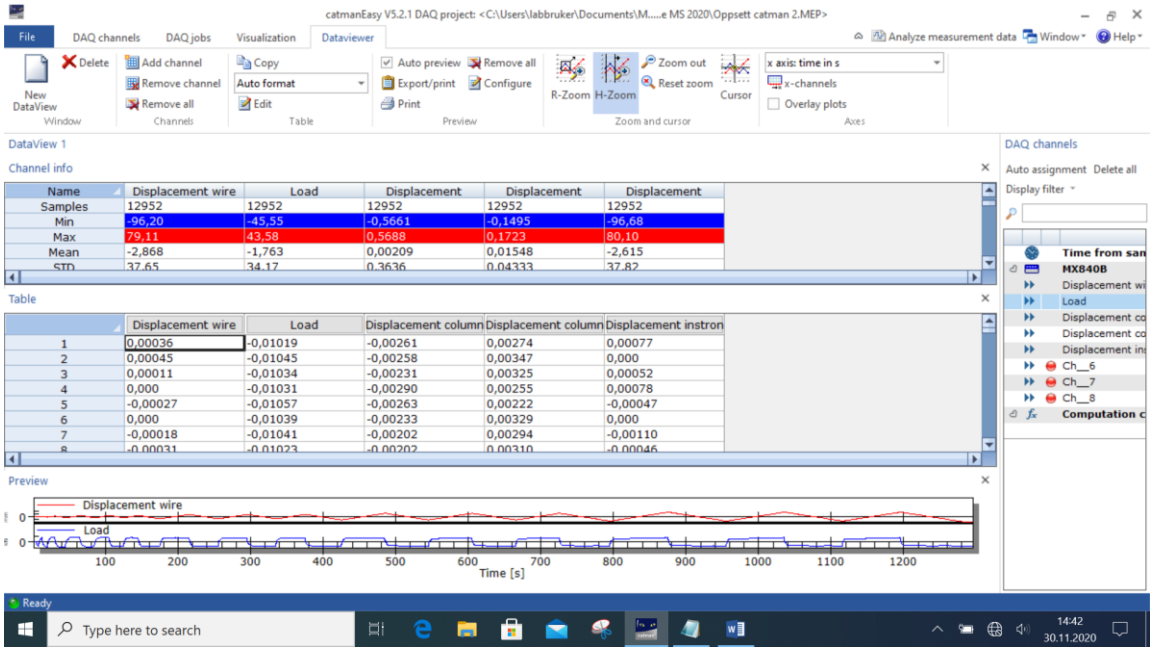

3.7 Sensor database

In the sensor database tab all existing sensors created by the software are placed, in addition to all the ones created and saved by the user.

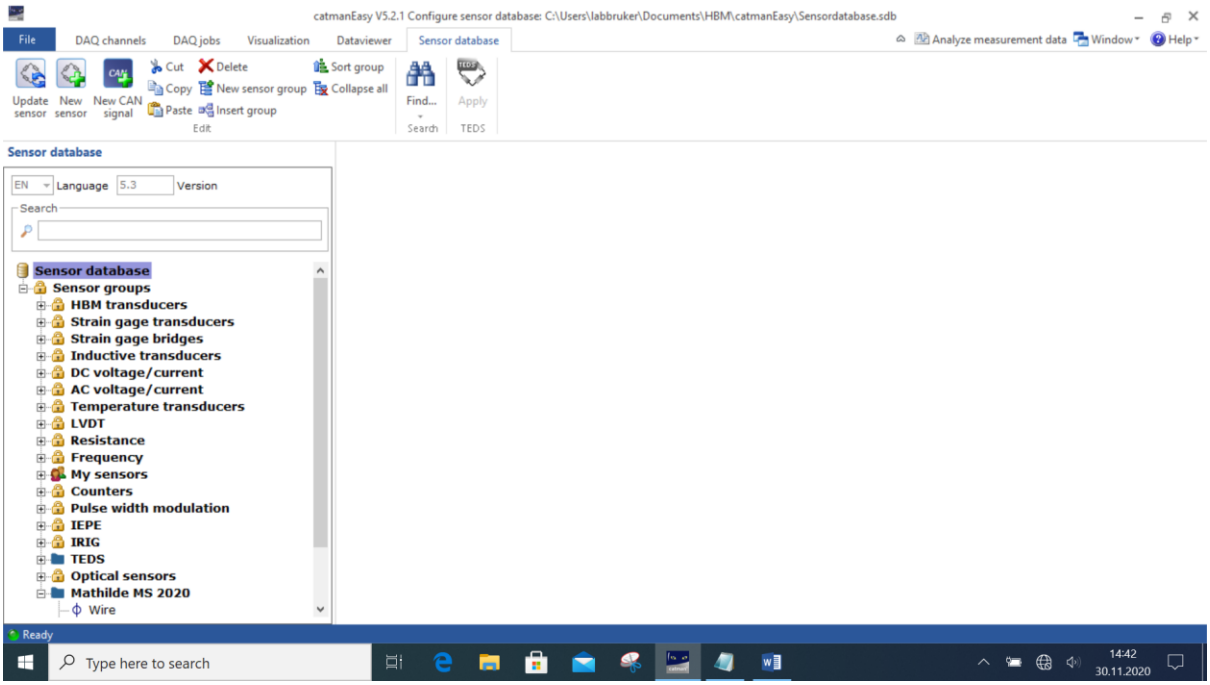

A new sensor or group of sensors (like a folder) can be added either right clicking on the folder where it should be added, or left clicking there and then finding the relevant action in the ribbon above.

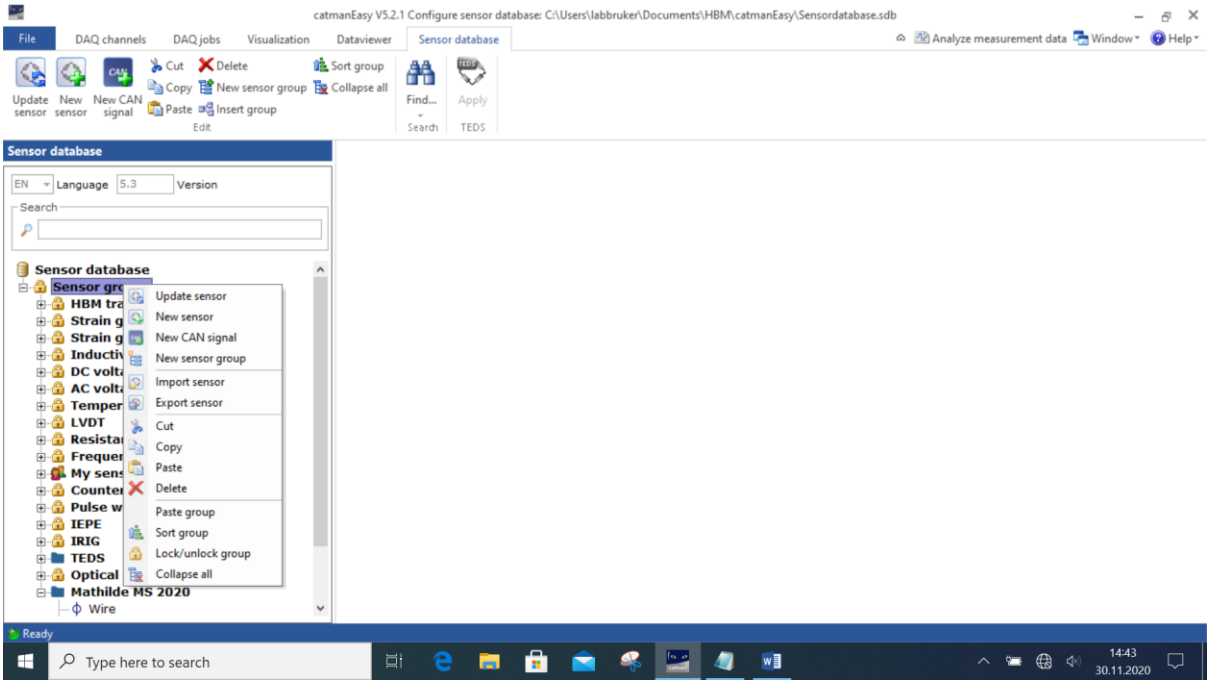

When choosing to create a group, a name is chosen in this pop-up window.

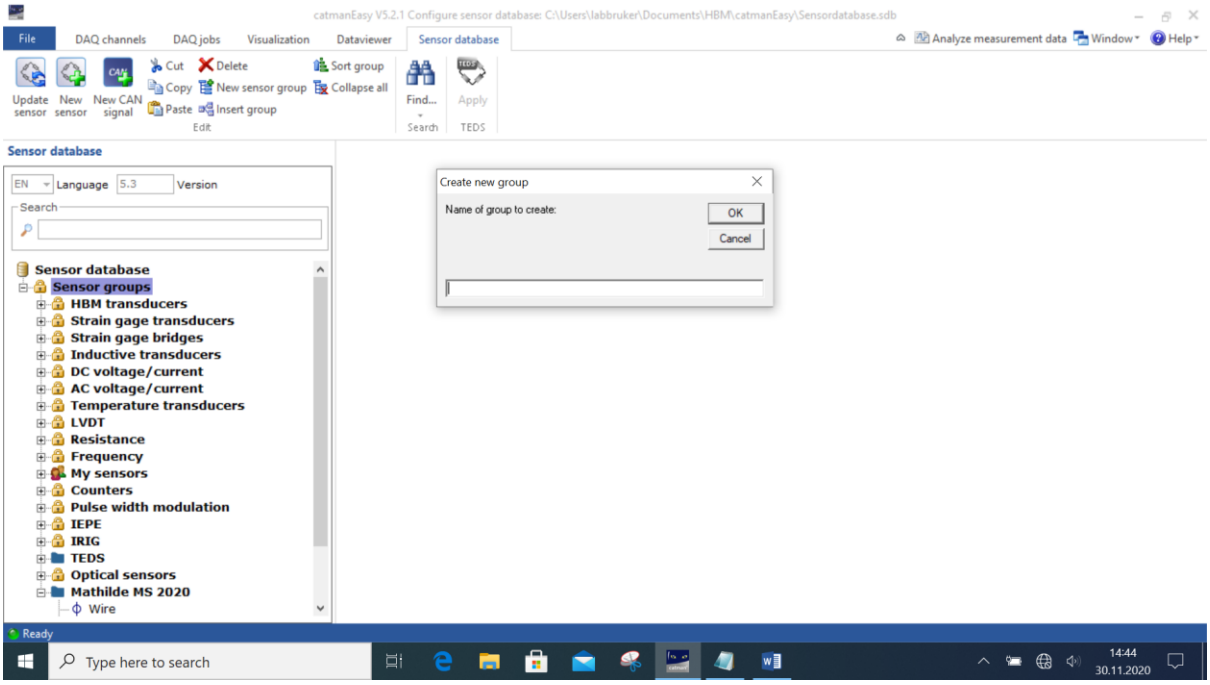

When choosing to create a new sensor, the sensor type must be chosen. Extensive information on this will not be given here. The simplest to choose is the transducer with the same icon as the sensor used as an example in the picture below.

Giving information about how to translate electrical outputs from a sensor can edited on the right by clicking on it. A method for entering the information to translate the electrical value into the corresponding physical value is chosen in the drop-down menu. The simplest is the zero-span or the two-point value. The zero-span shown below uses a zero value for the electrical and physical unit, the sensitivity, and the nominal physical value as input. The two point uses corresponding values at two points of a linear graph relating the two units.

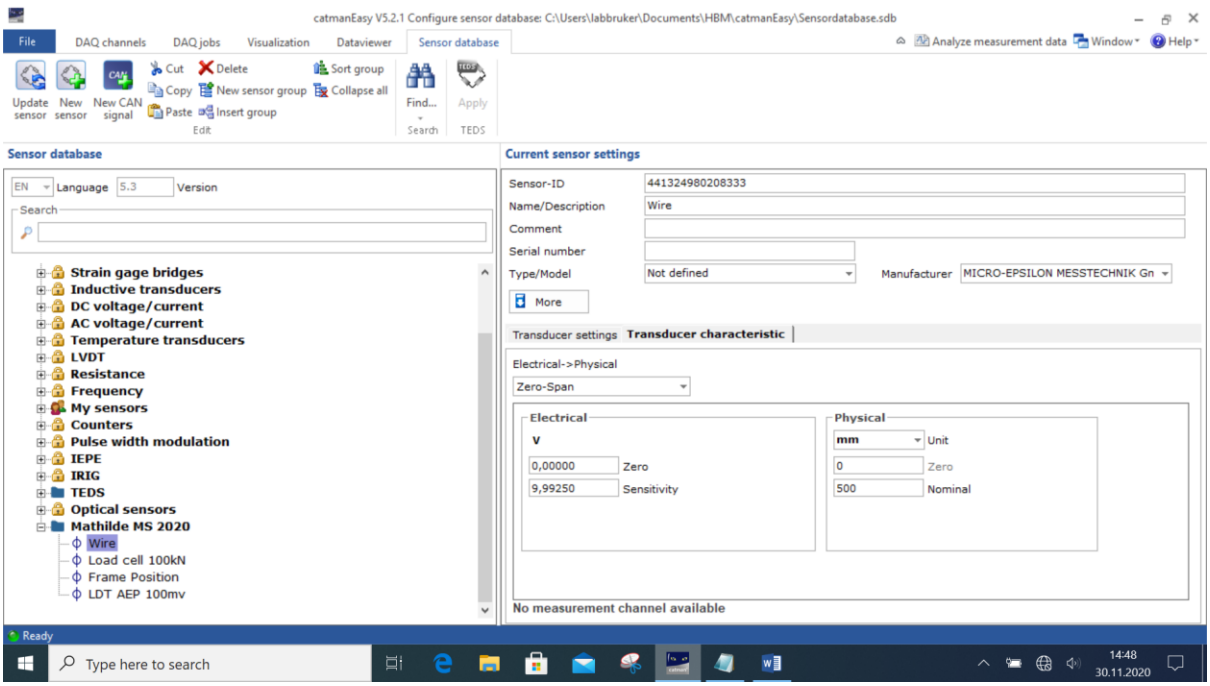

The total supply of voltage for the sensor is added in the second tab in the sensor settings.

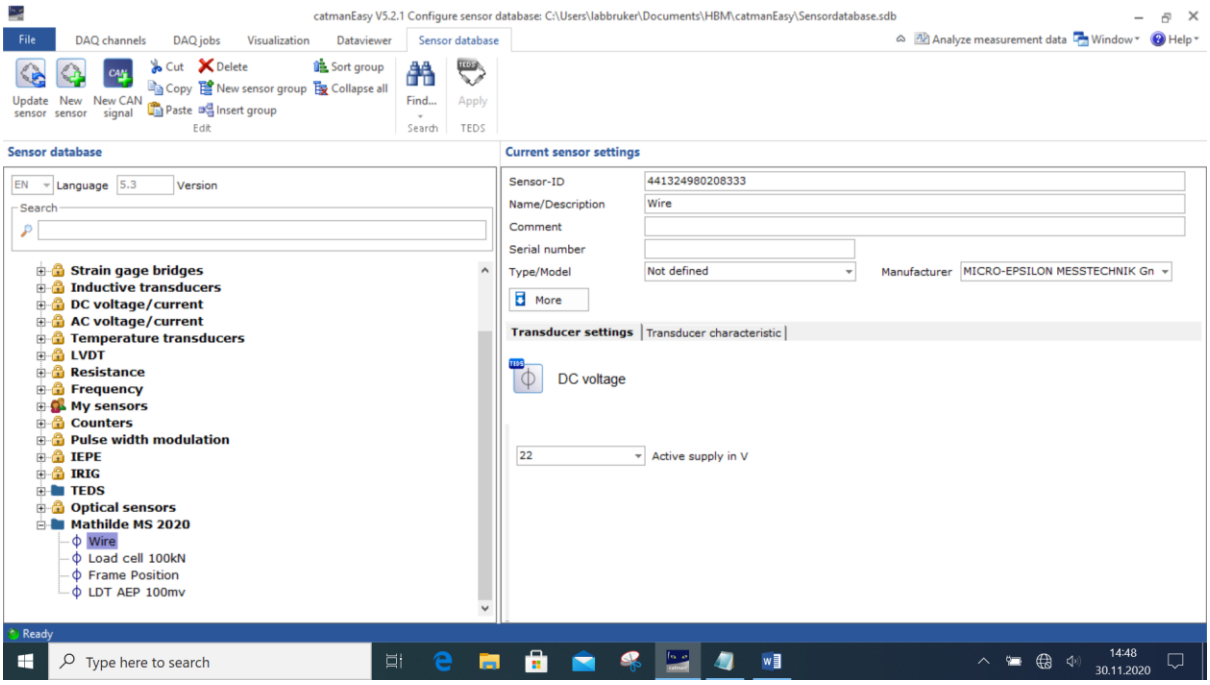

3.8 Starting a session and saving the data

A session is started by clicking on start in the top left corner. Only the visualization tab is shown during the session. The session is stopped by clicking on stop, or if the conditions of a “stop data recording” criterion set in the DAQ jobs tab is satisfied.

When the test has stopped, the window in the picture below pops up. Here, the information given for saving the file set in the DAQ jobs tab is auto filled. The choices can though be changed now as well. Click on save data now when all preferences are satisfied.

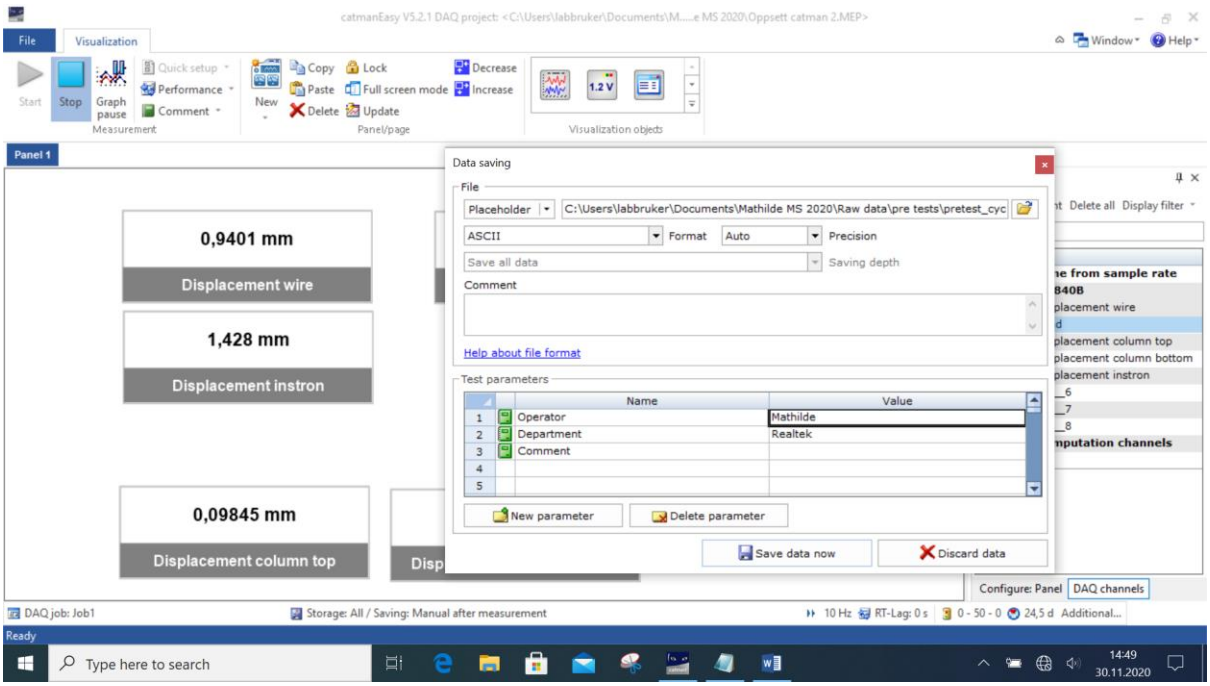

Appendix C

Results extended

STD_TEST-comp

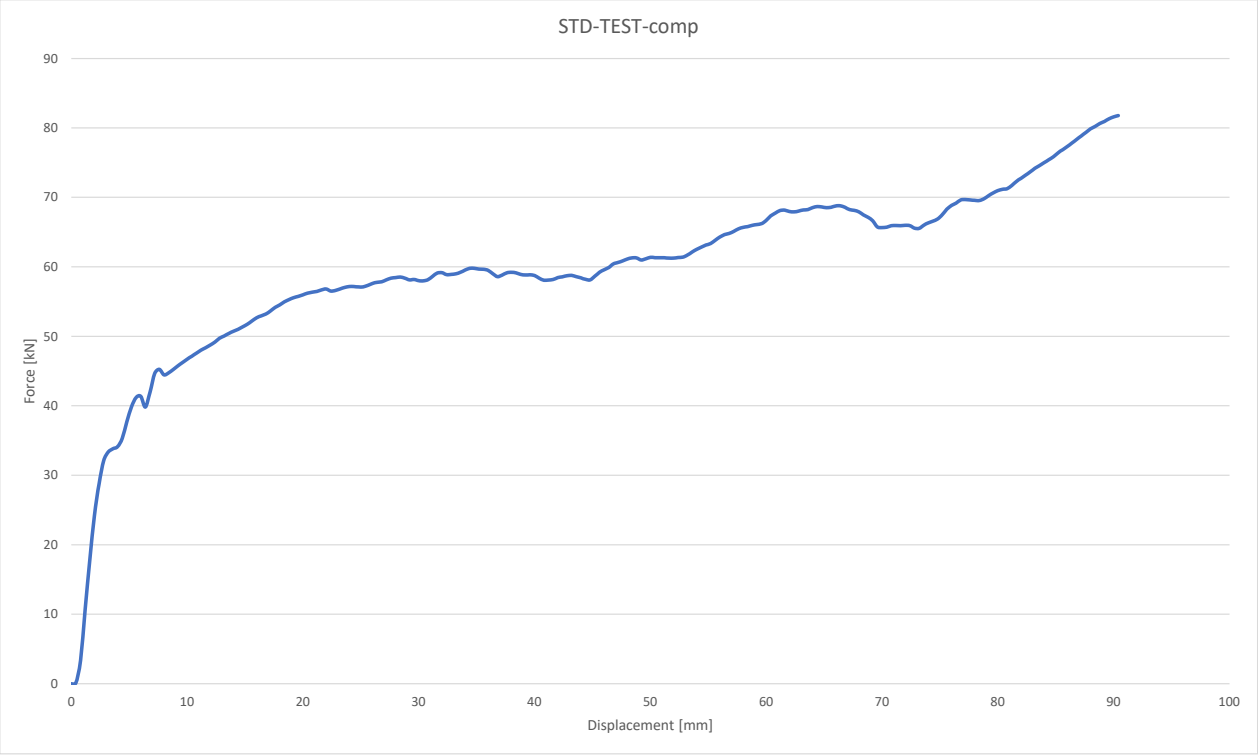

Figure 1: Force displacement curve of STD-TEST-comp

STD_1 Test A-30%

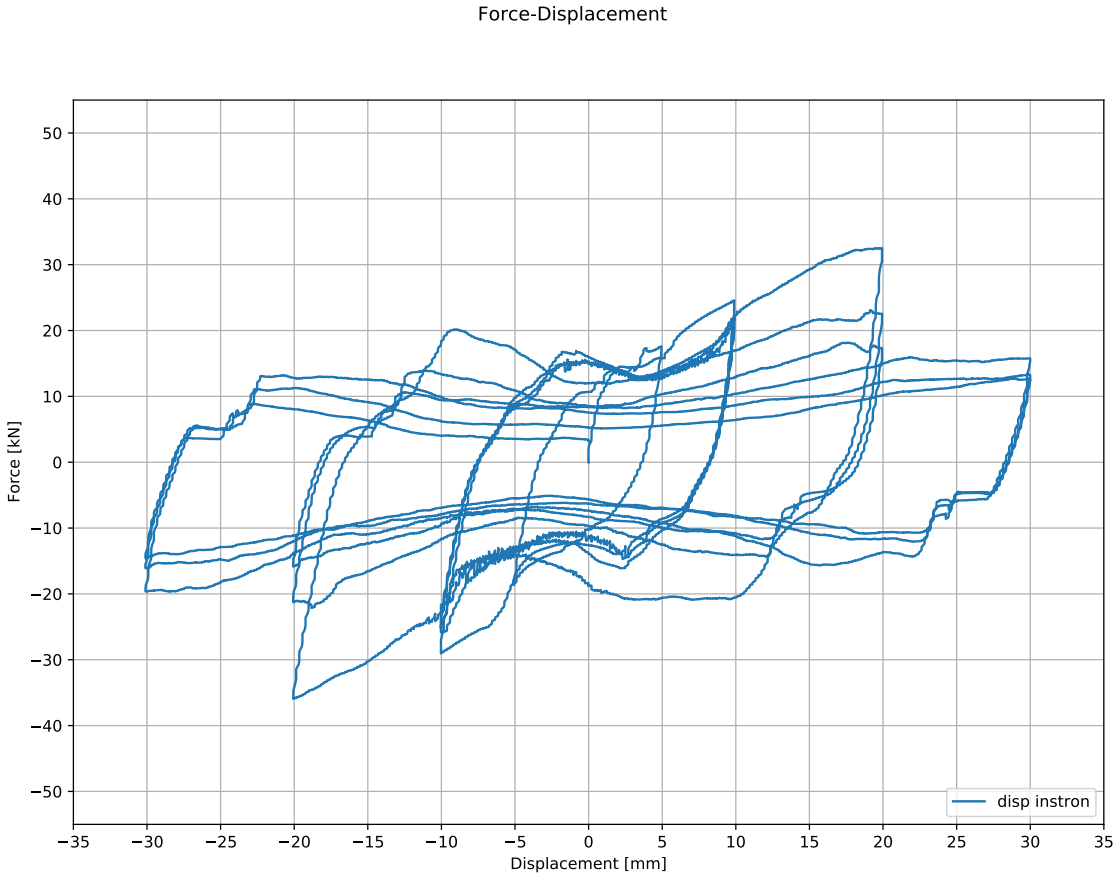

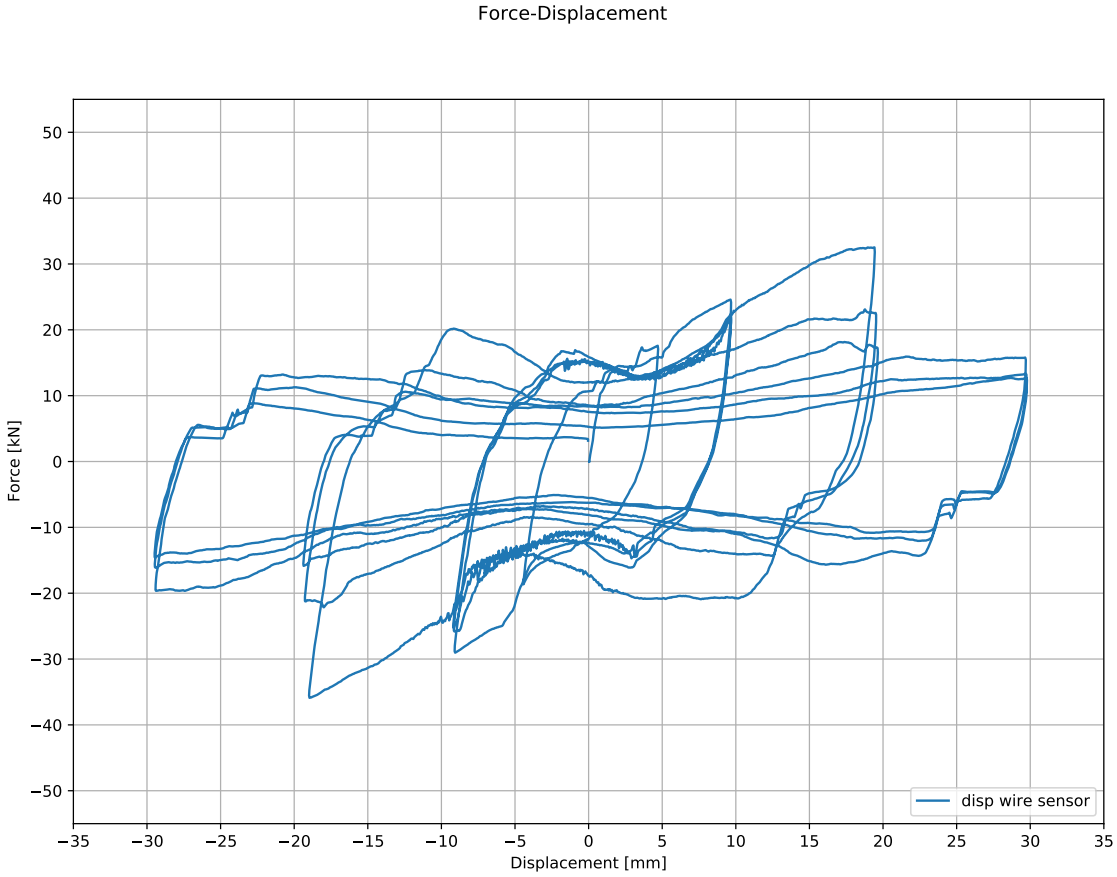

Figure 2: Load displacement graph.

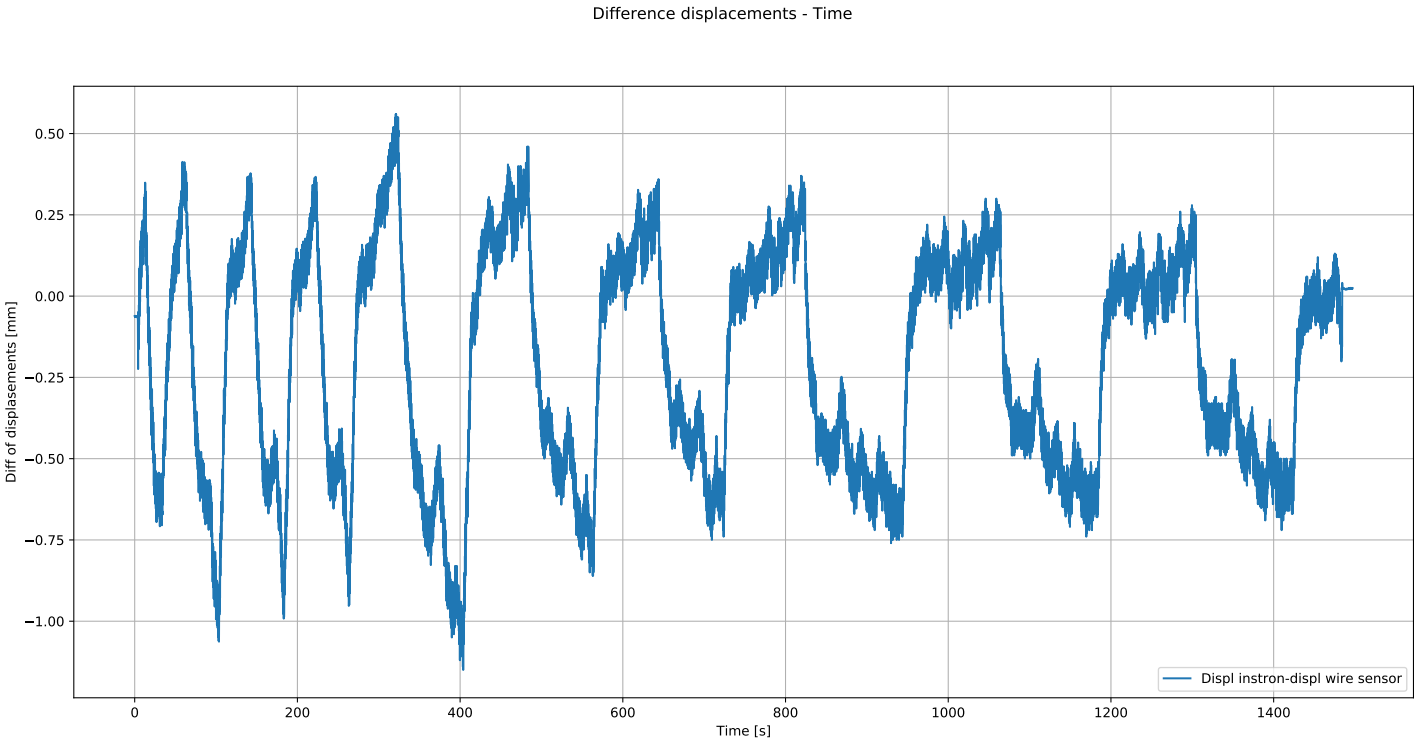

Figure 3: Difference of displacement between instron press and wire sensor.

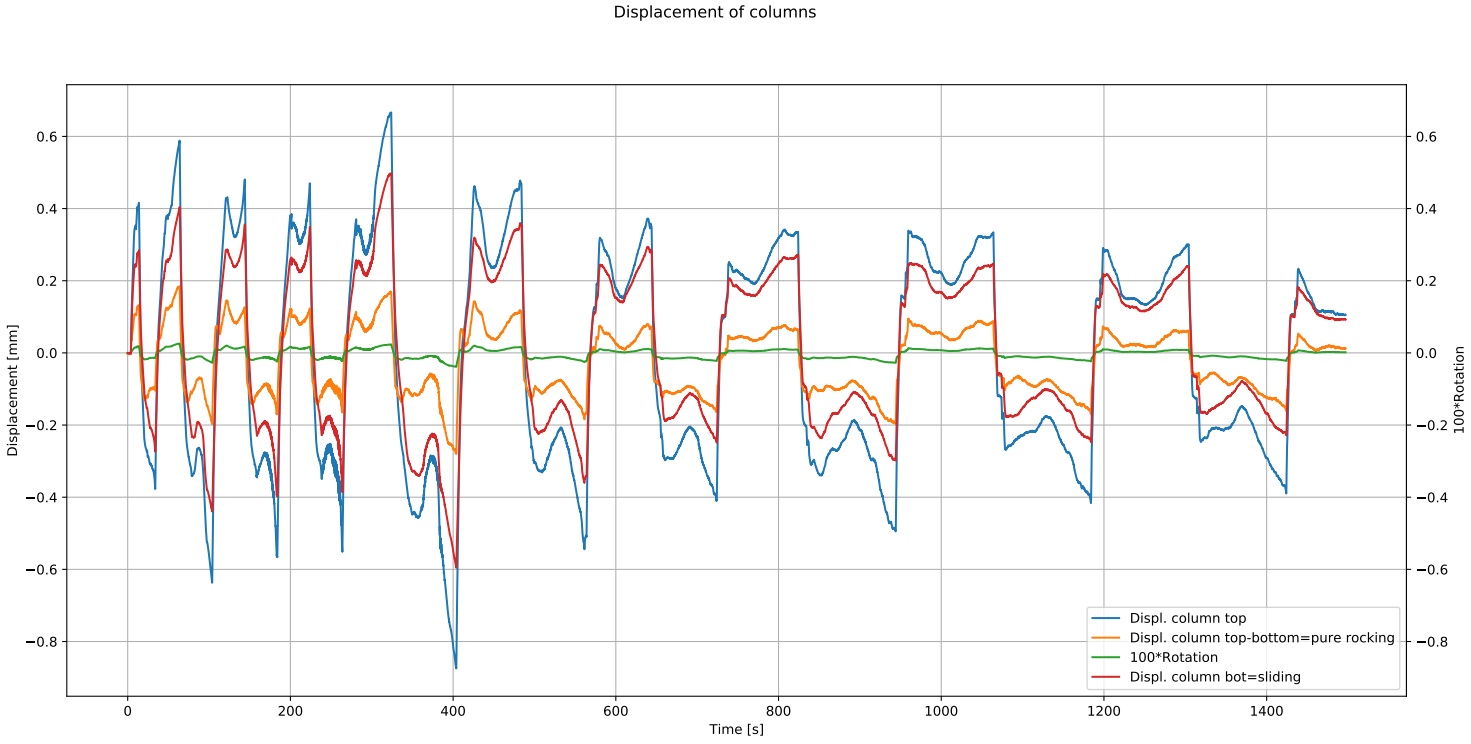

Figure 4: Movements of the column.

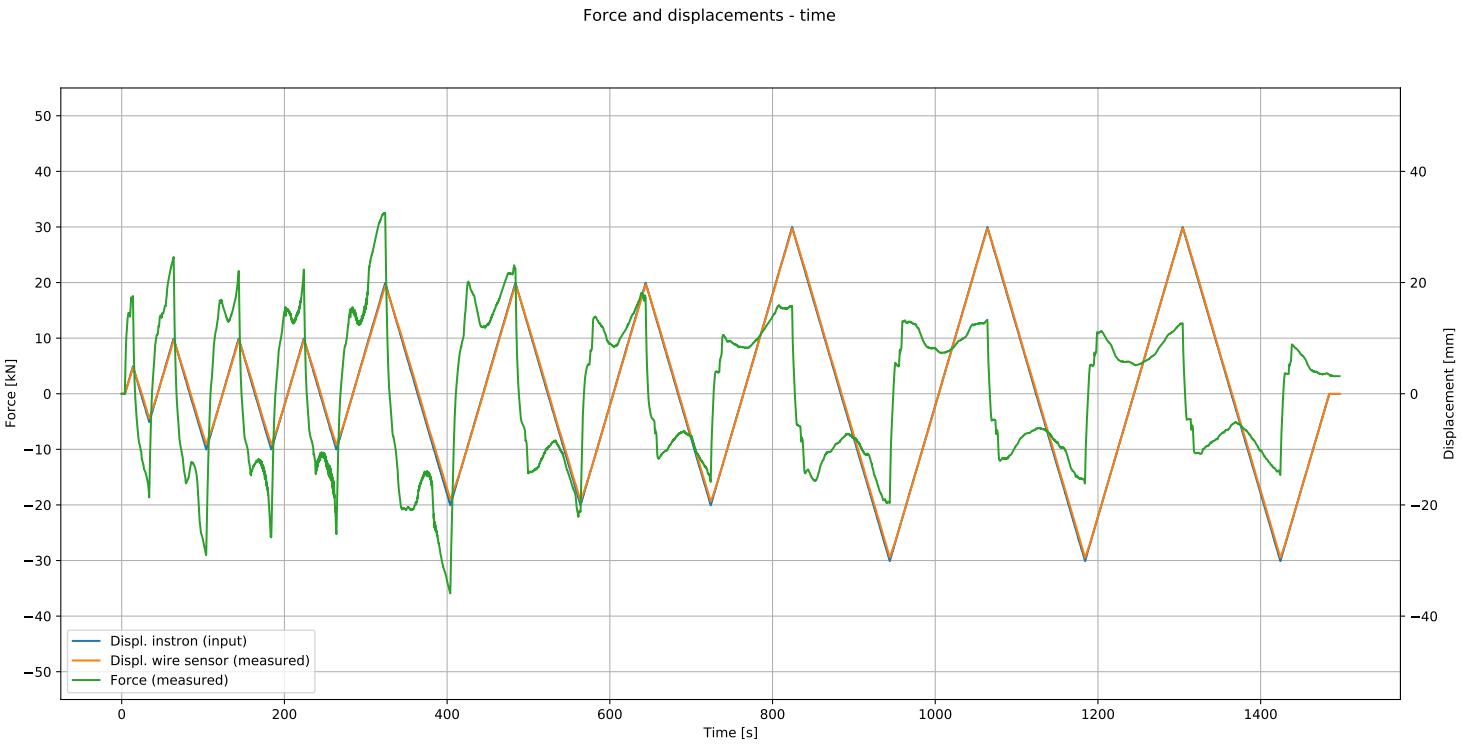

Figure 5: Force and displacement plotted against time.

STD_1 Test B-30%

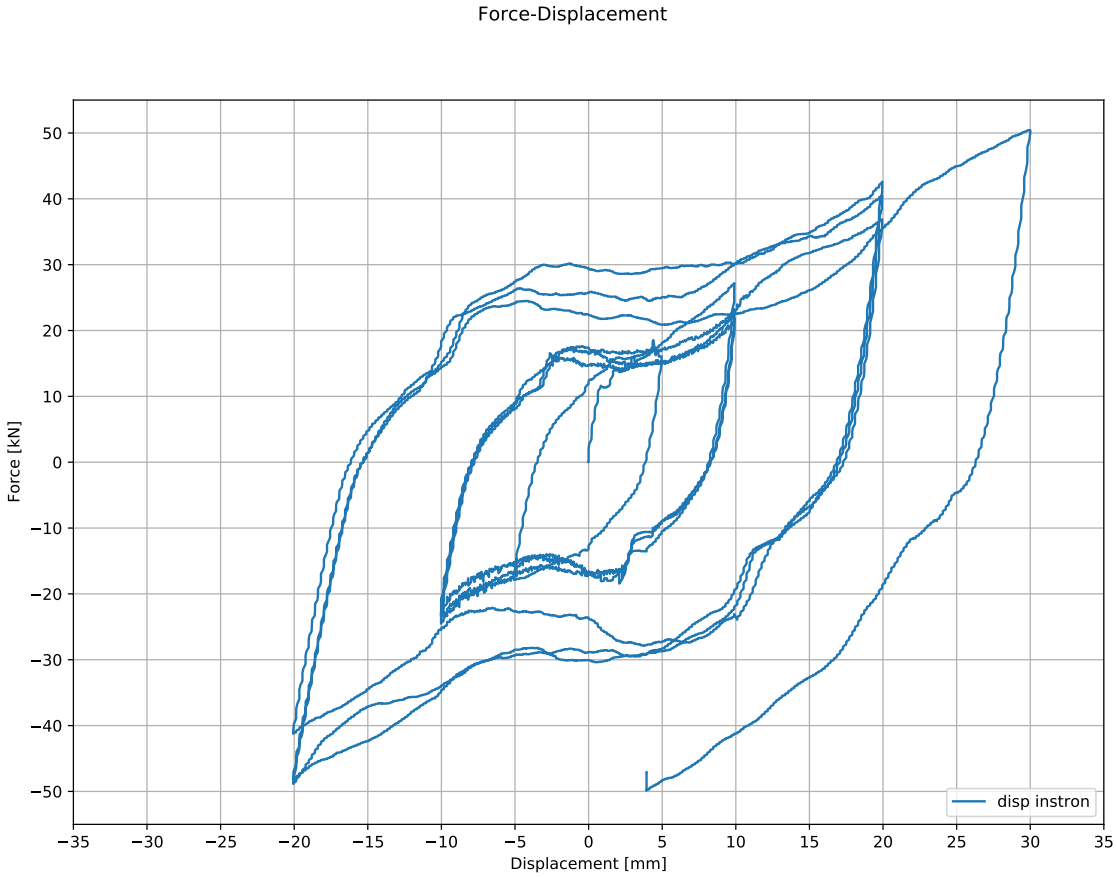

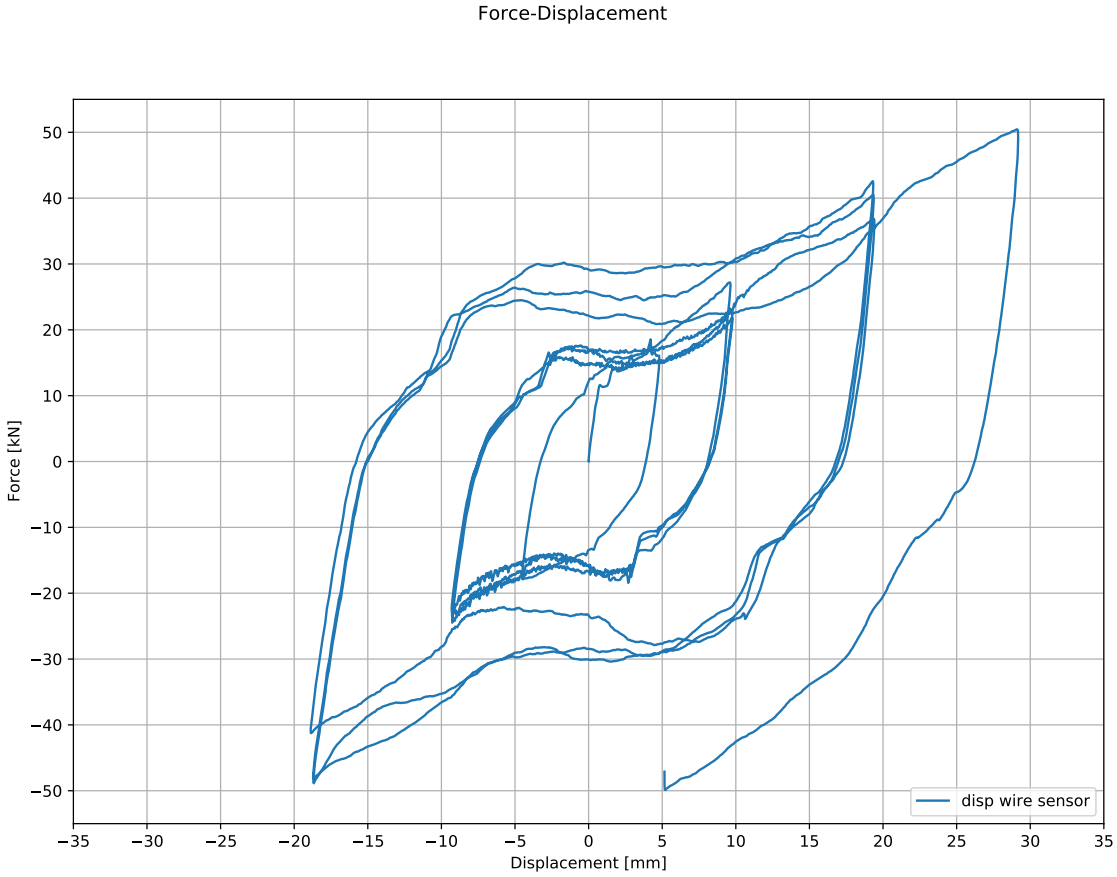

Figure 6: Load displacement graph.

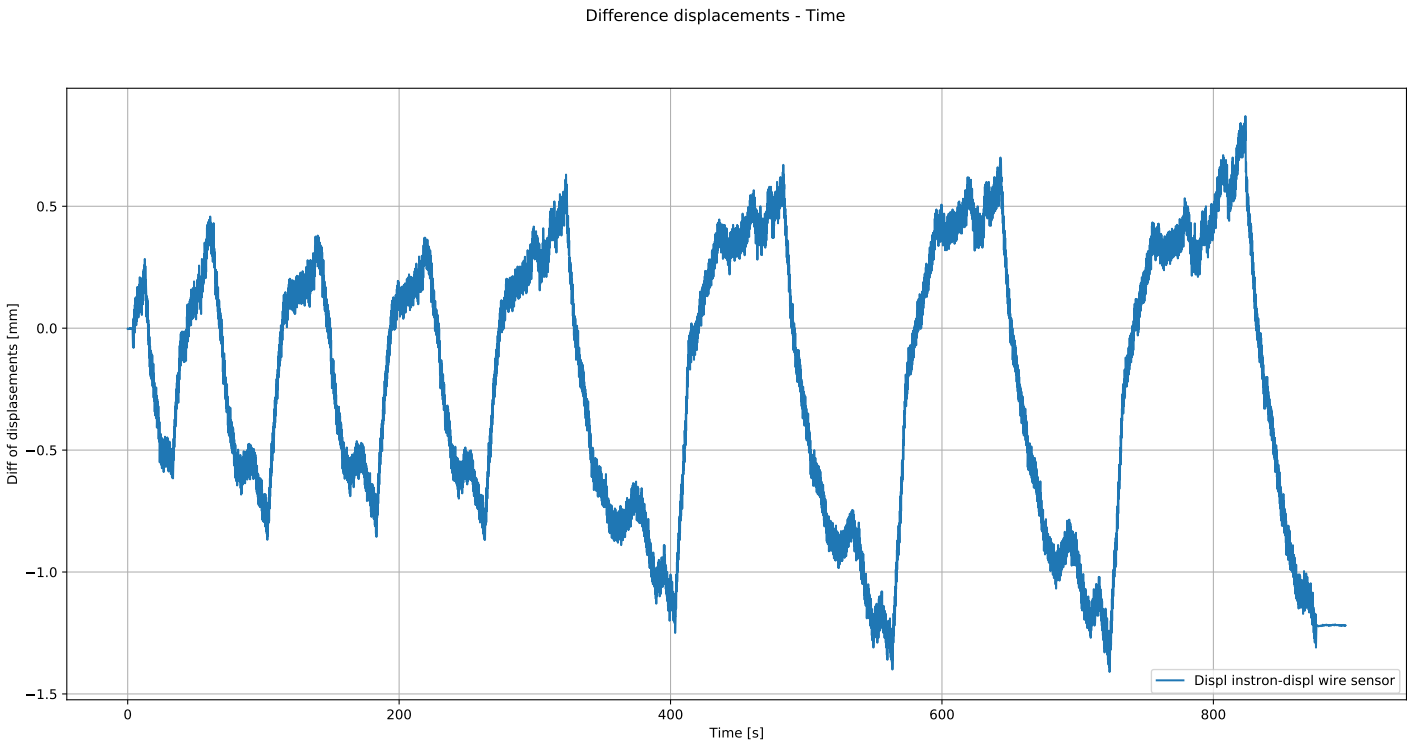

Figure 7: Difference of displacement between instron press and wire sensor.

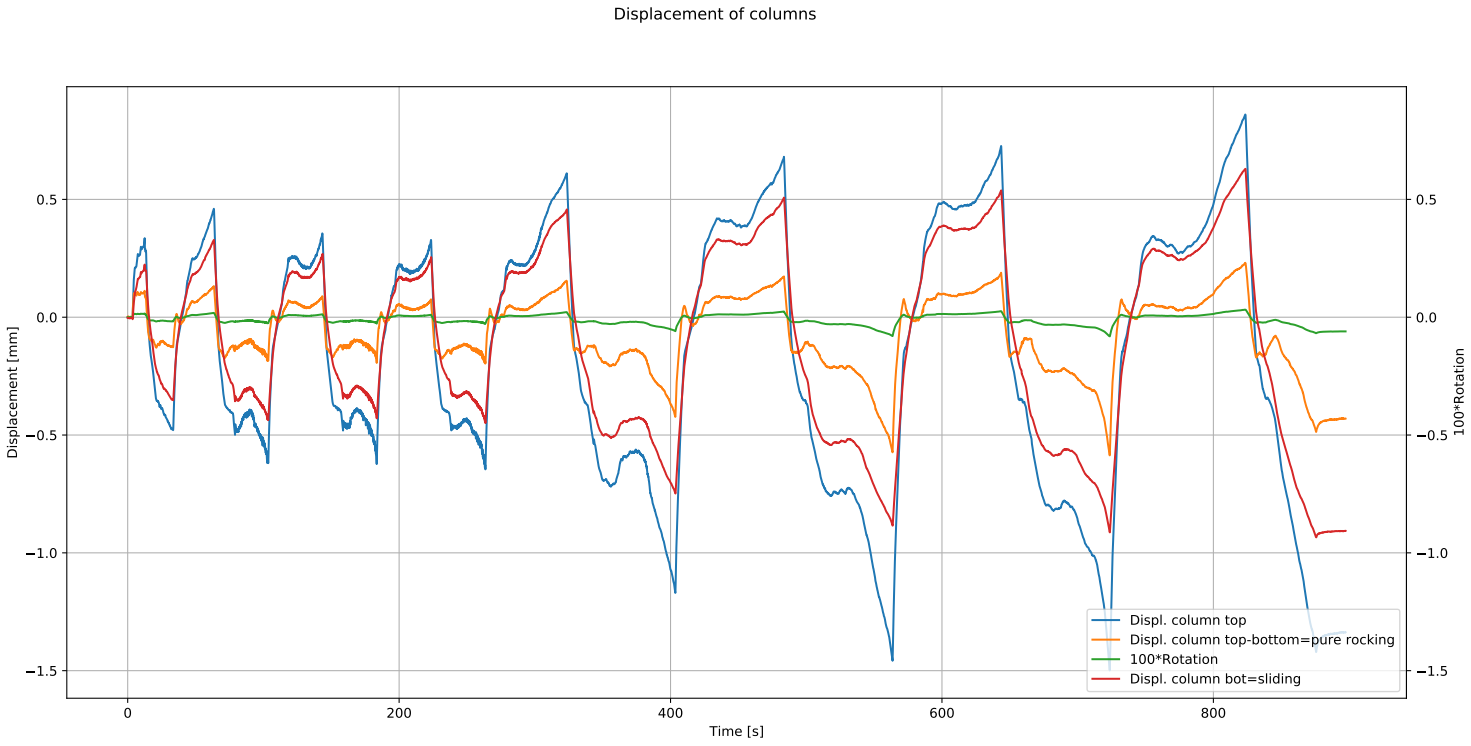

Figure 8: Movements of the column.

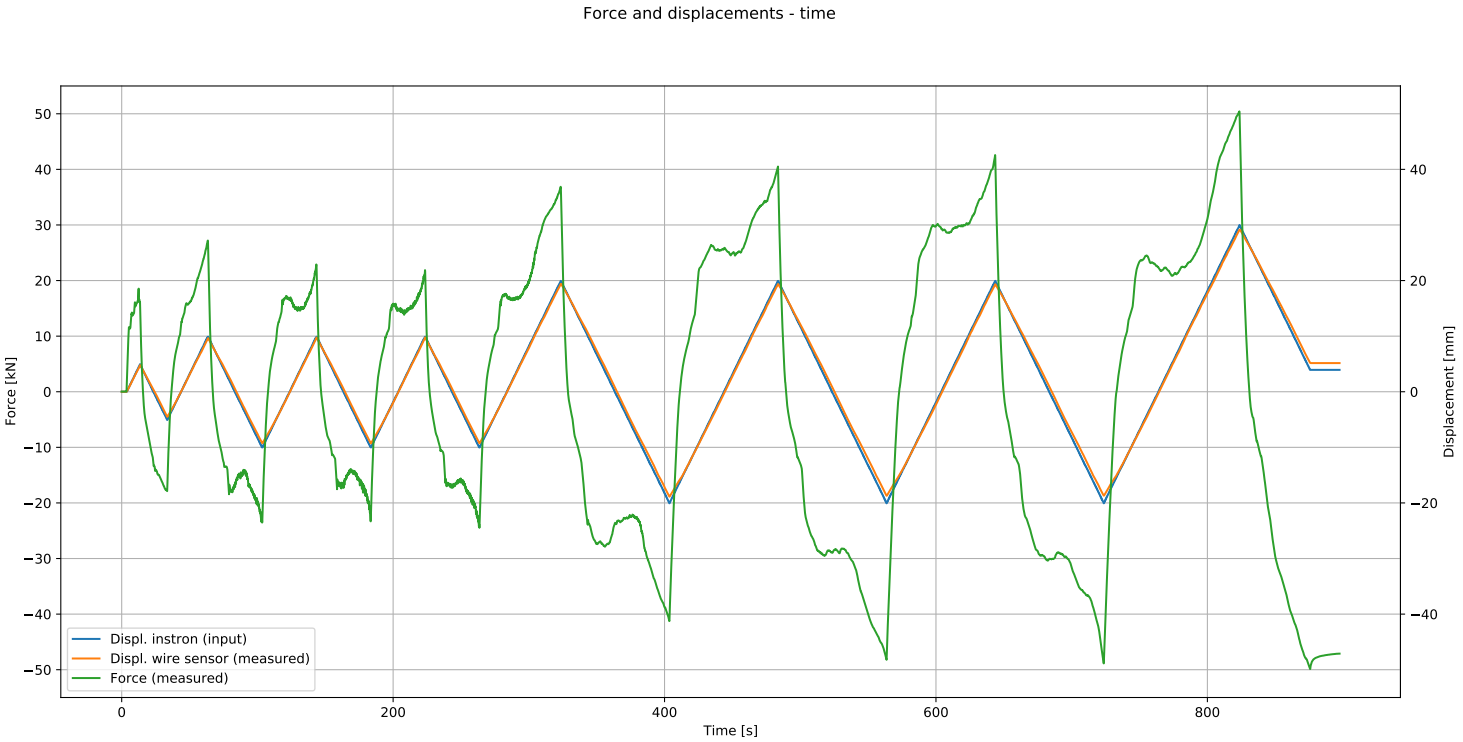

Figure 9: Force and displacement plotted against time.

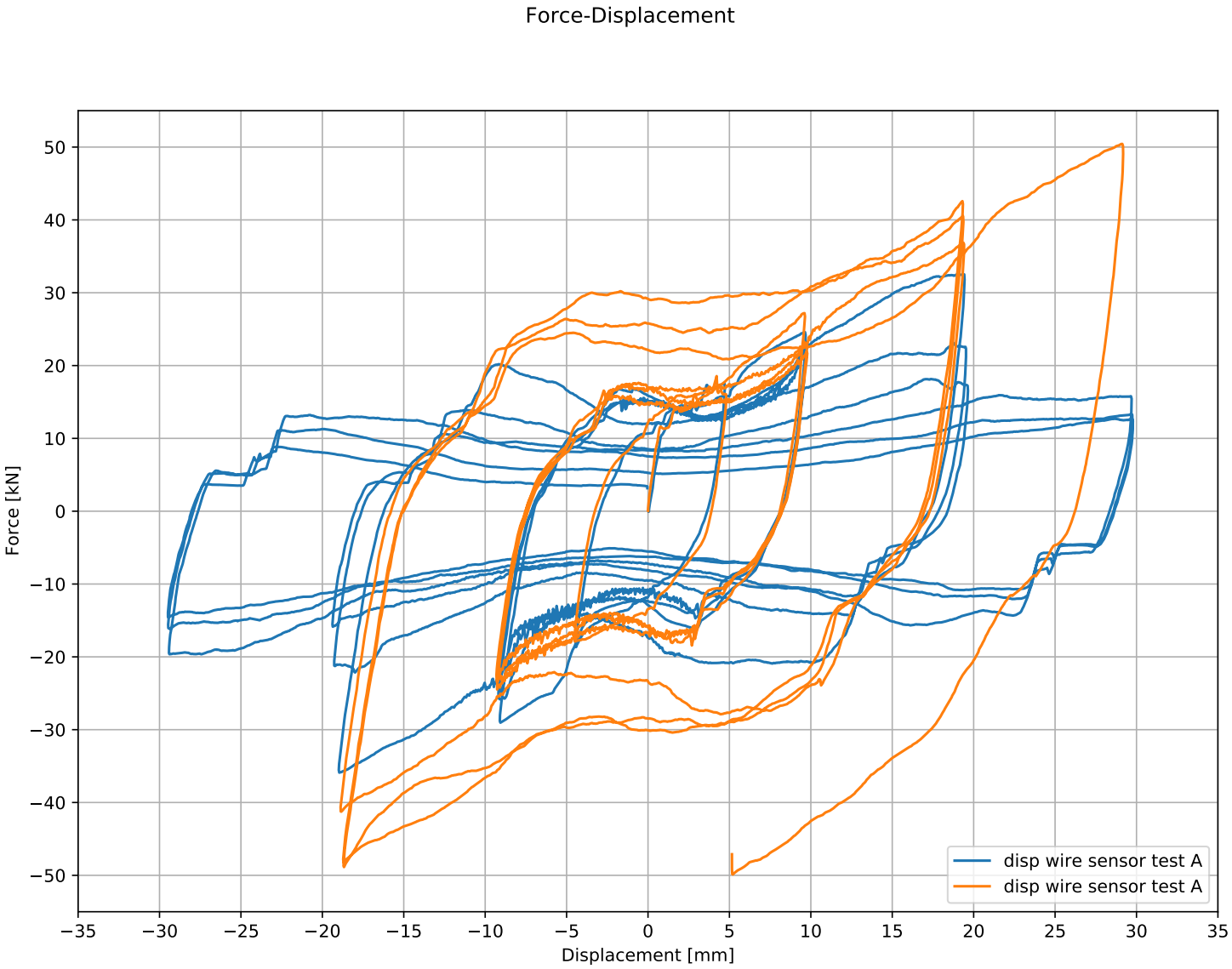

Figure 10: Comparison of test A and B.

STD_1 Test C-30%

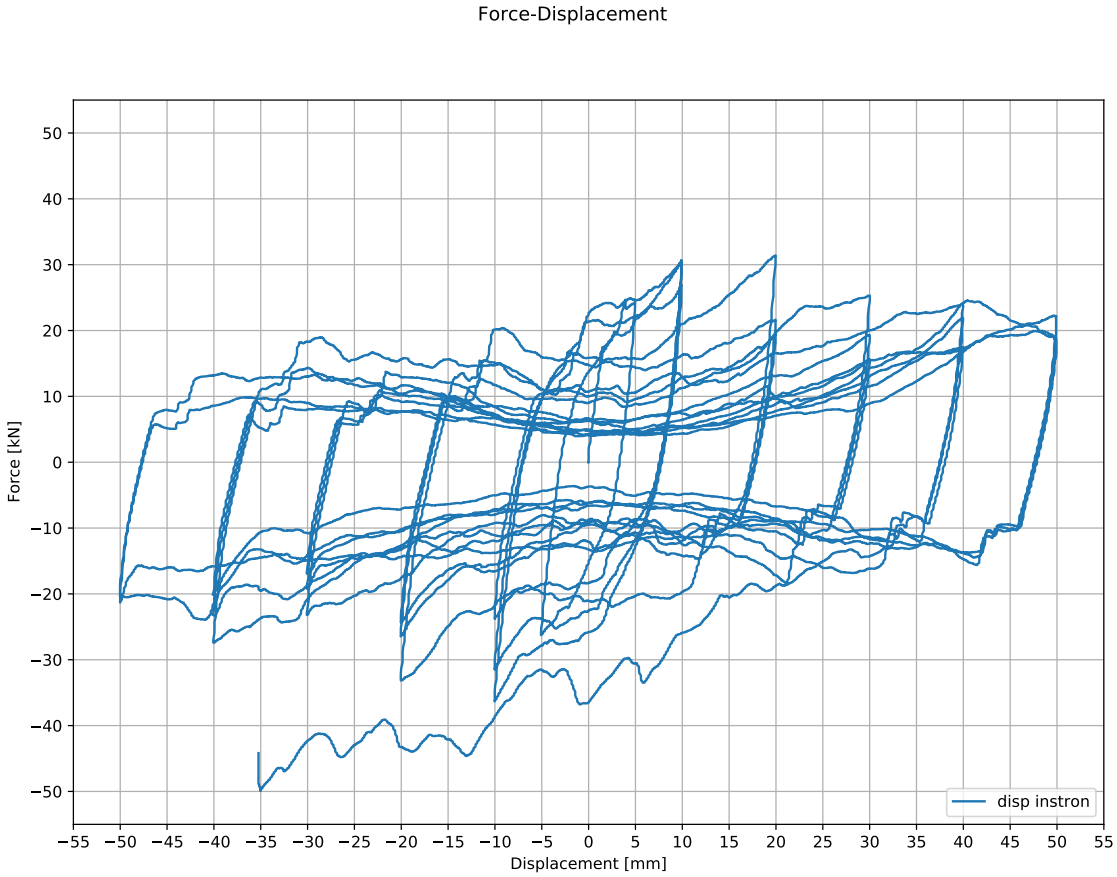

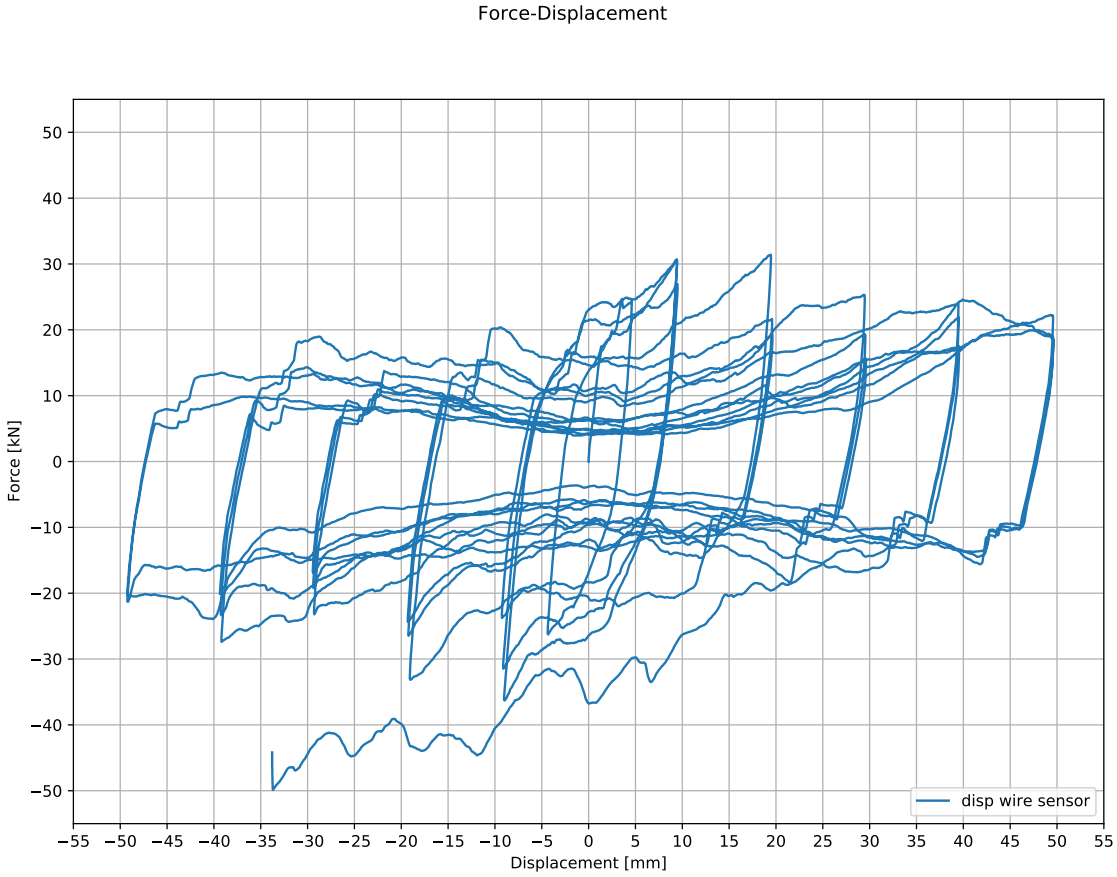

Figure 11: Load displacement graph.

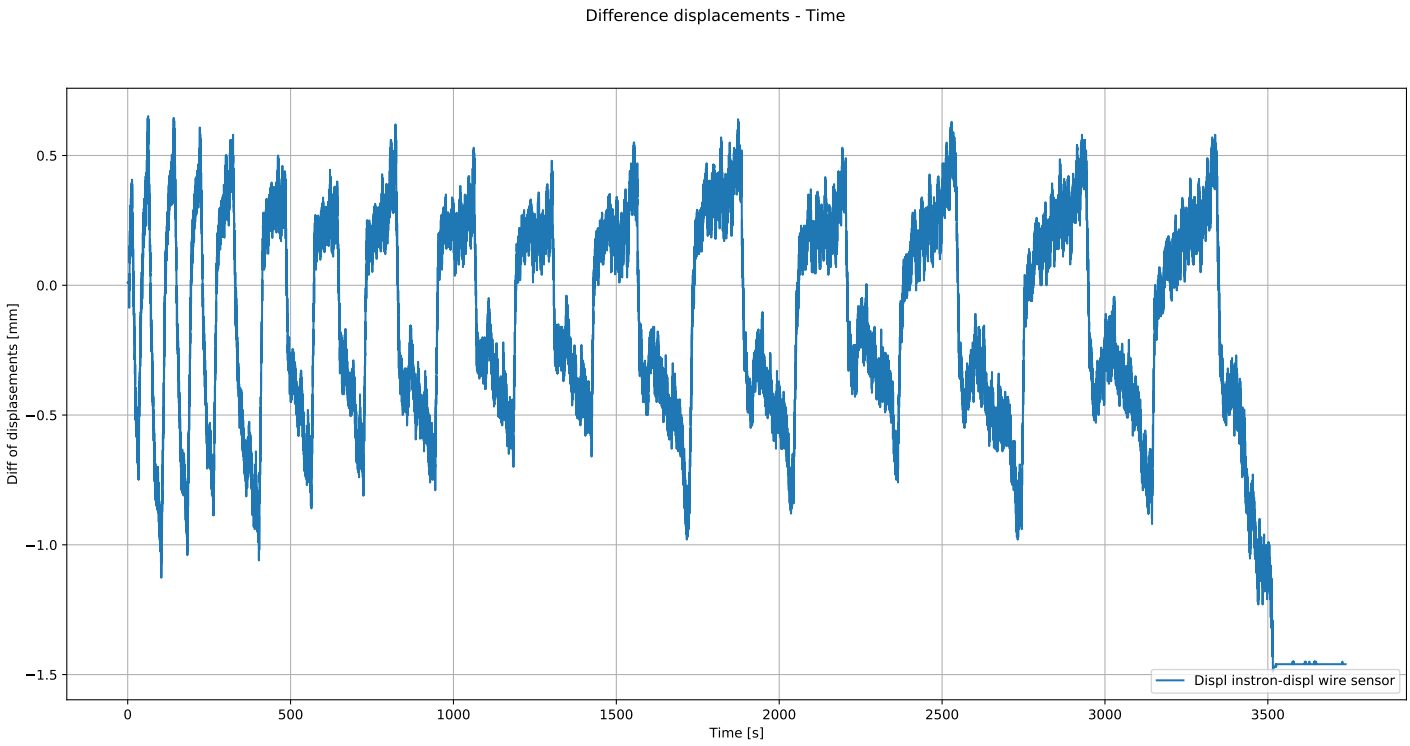

Figure 12: Difference of displacement between instron press and wire sensor.

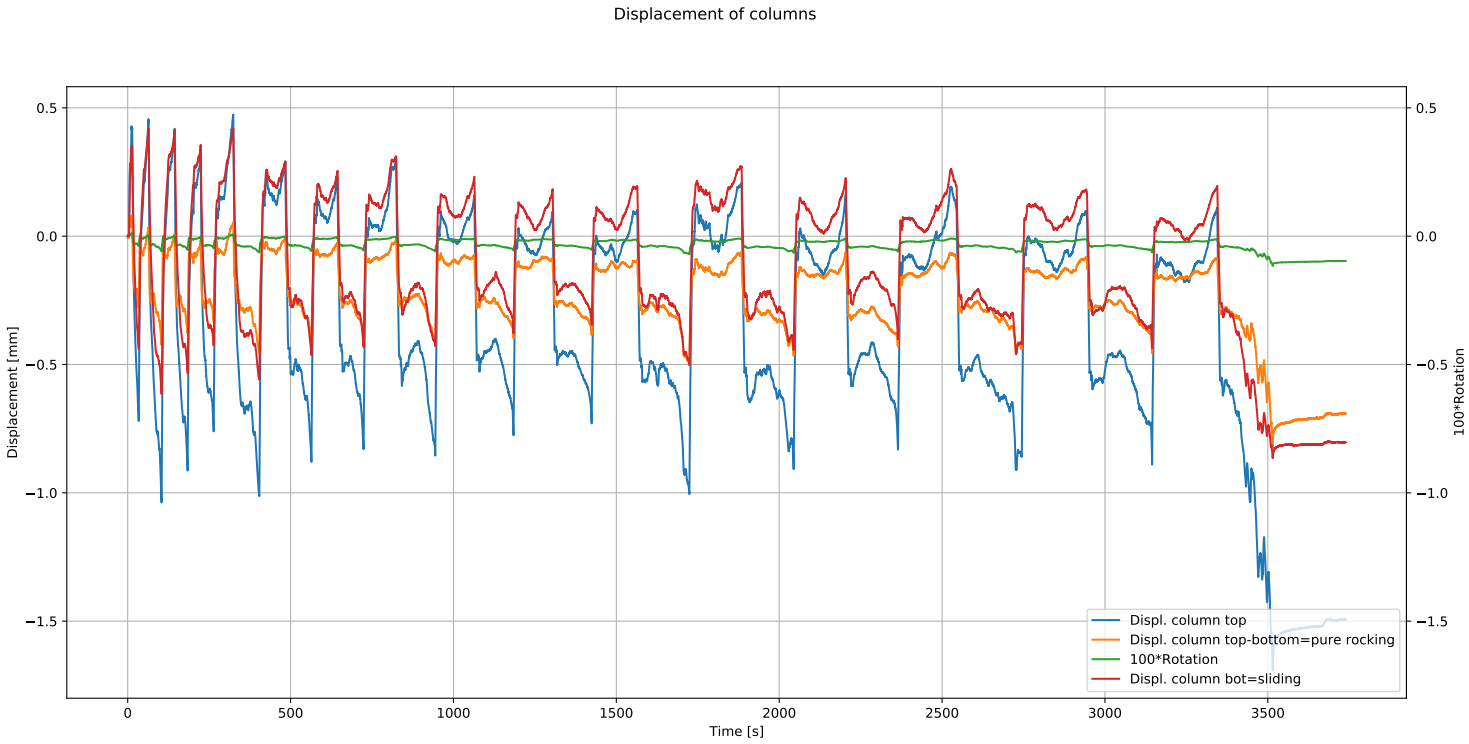

Figure 13: Movements of the column.

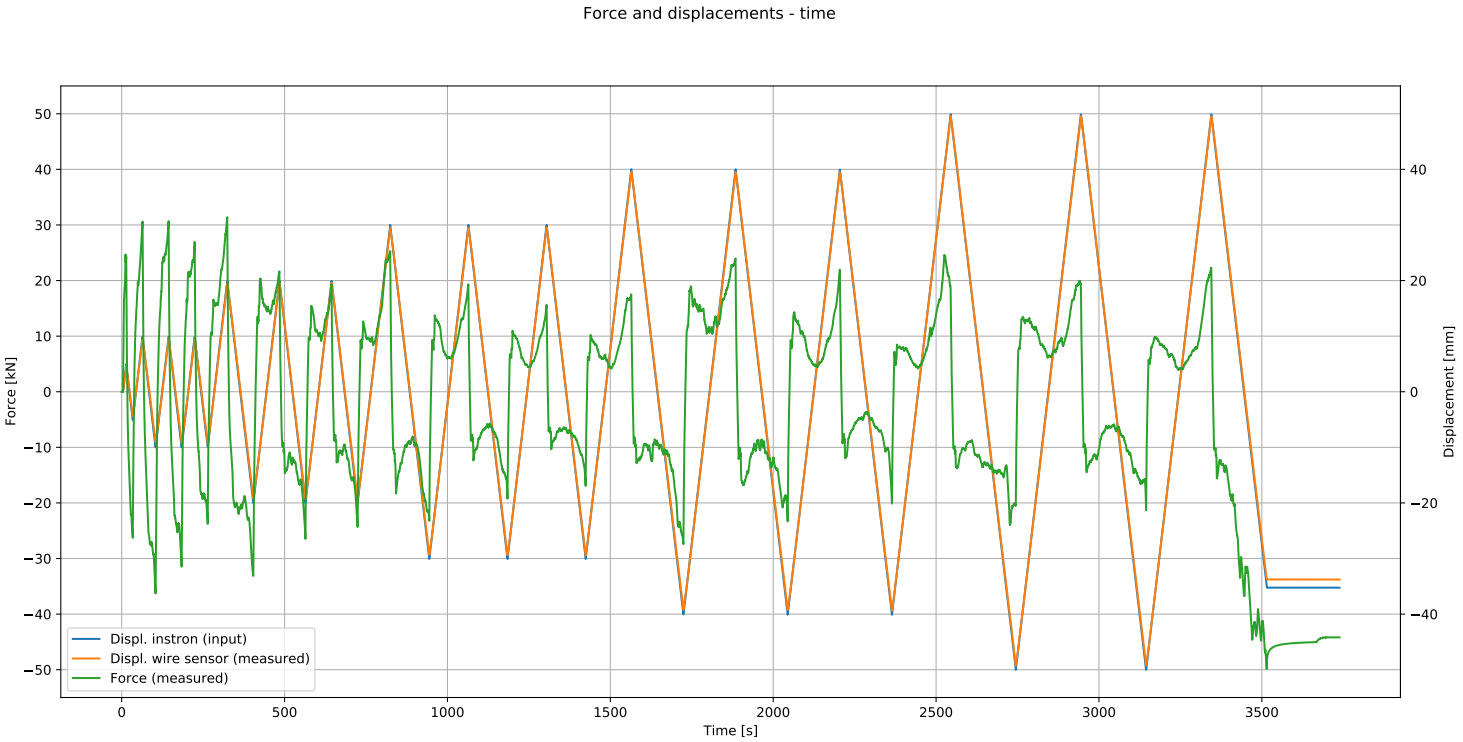

Figure 14: Force and displacement plotted against time.

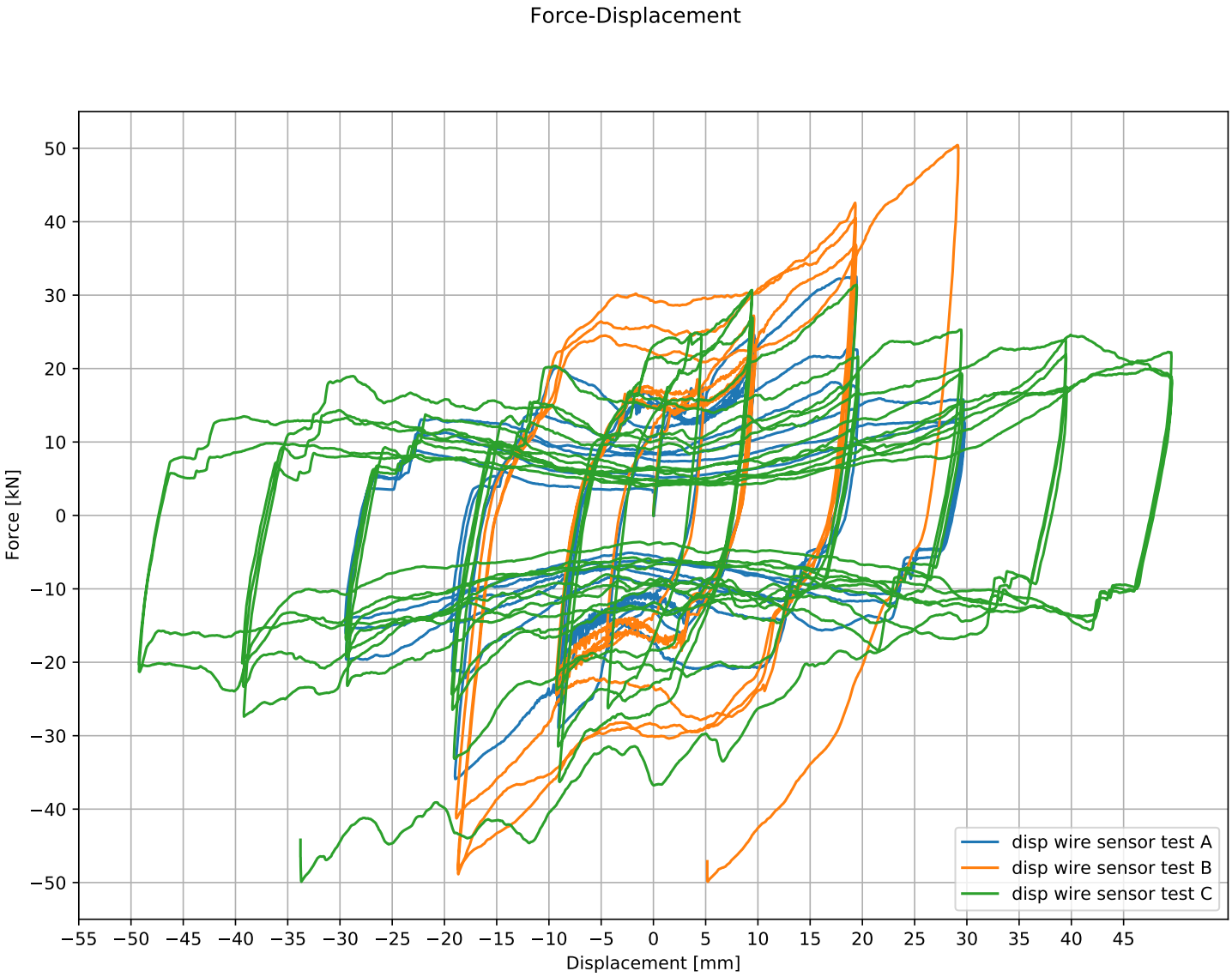

Figure 15: Comparison of test A, B and C.

STD_2 Test A-30%

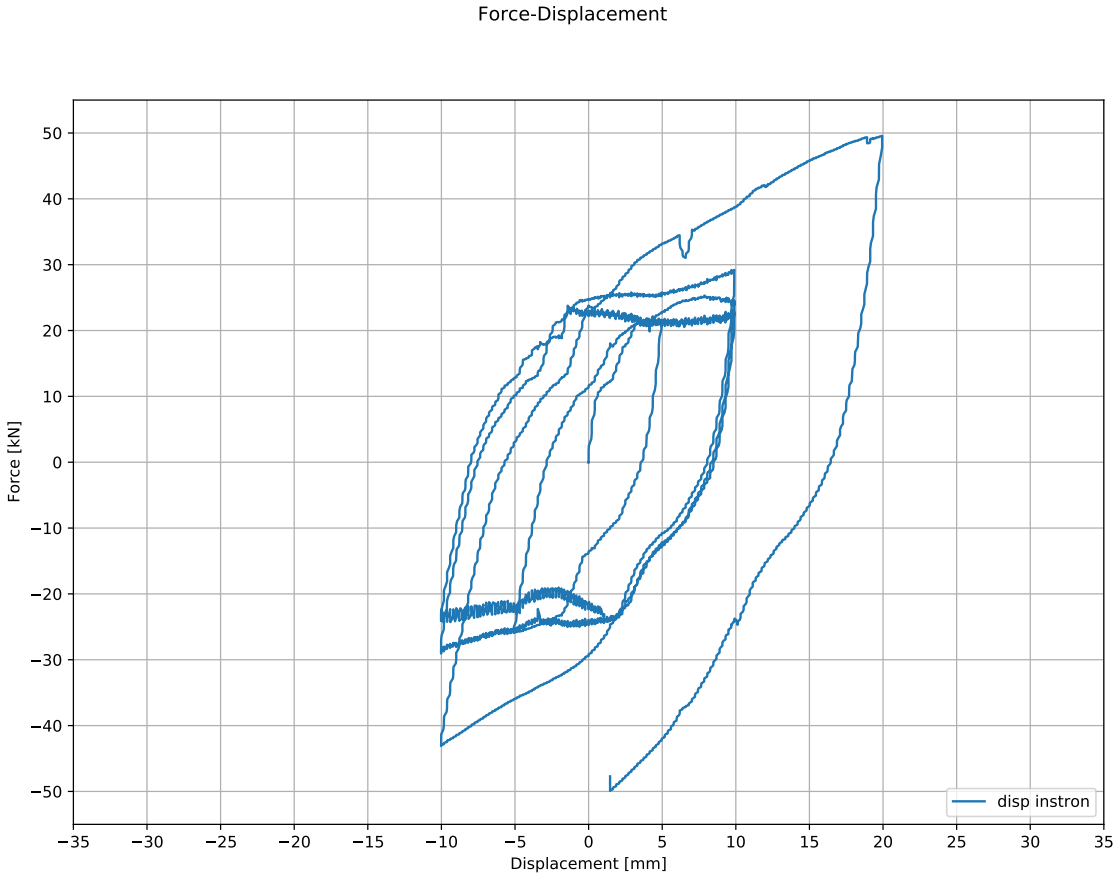

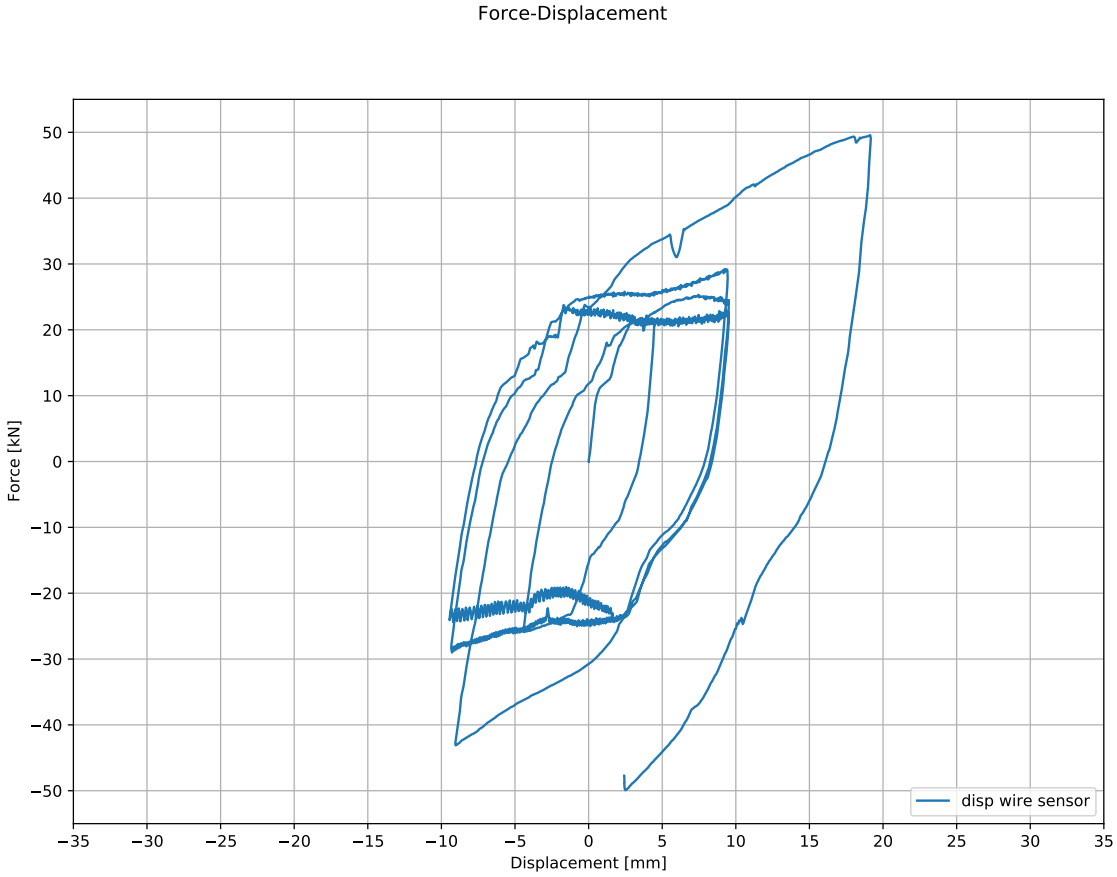

Figure 16: Load displacement graph.

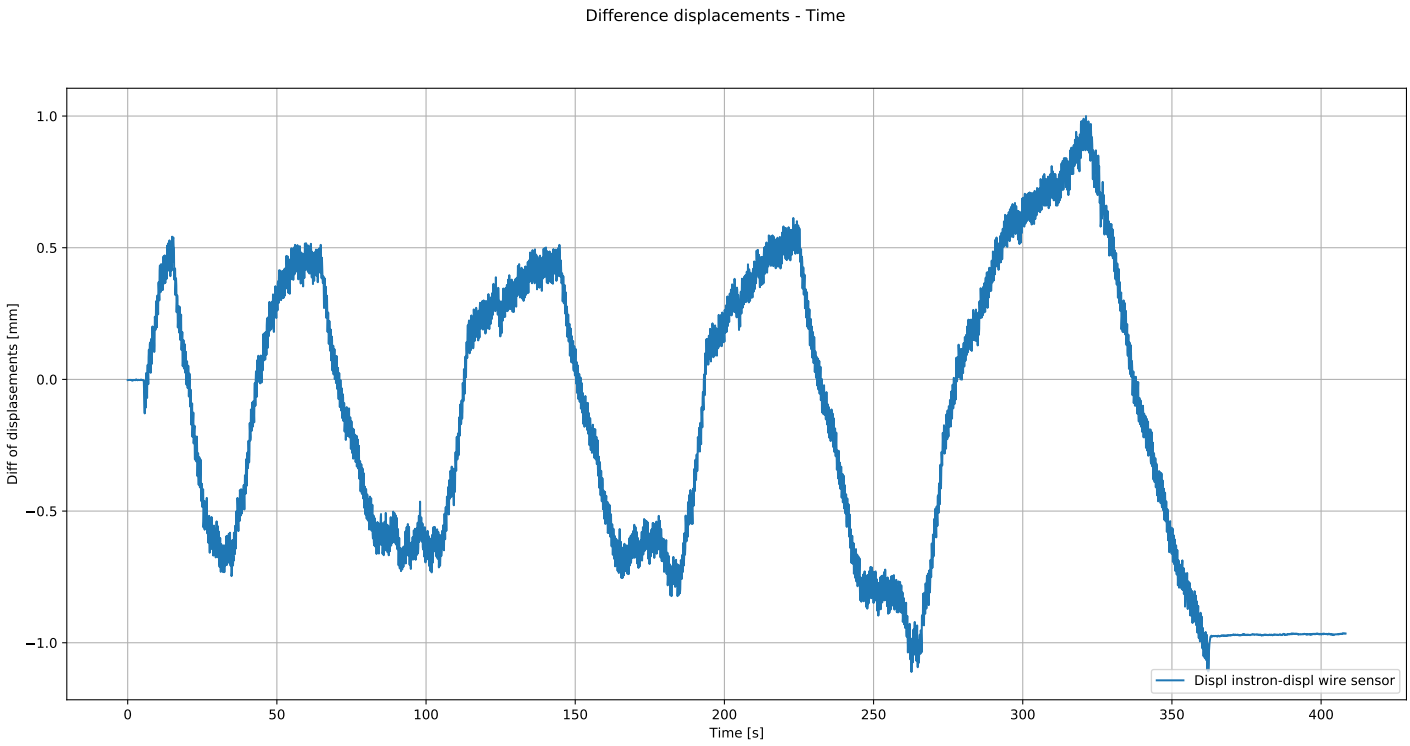

Figure 17: Difference of displacement between instron press and wire sensor.

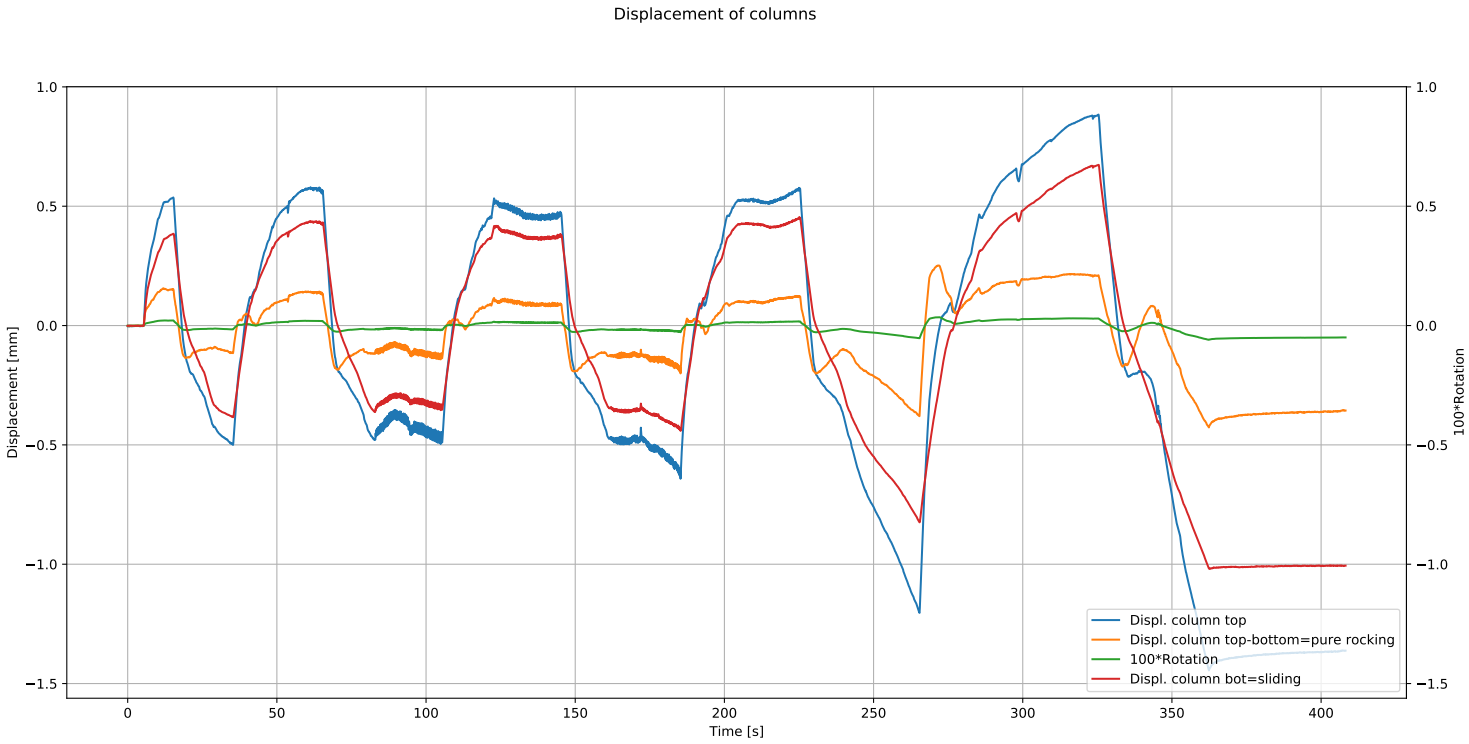

Figure 18: Movements of the column.

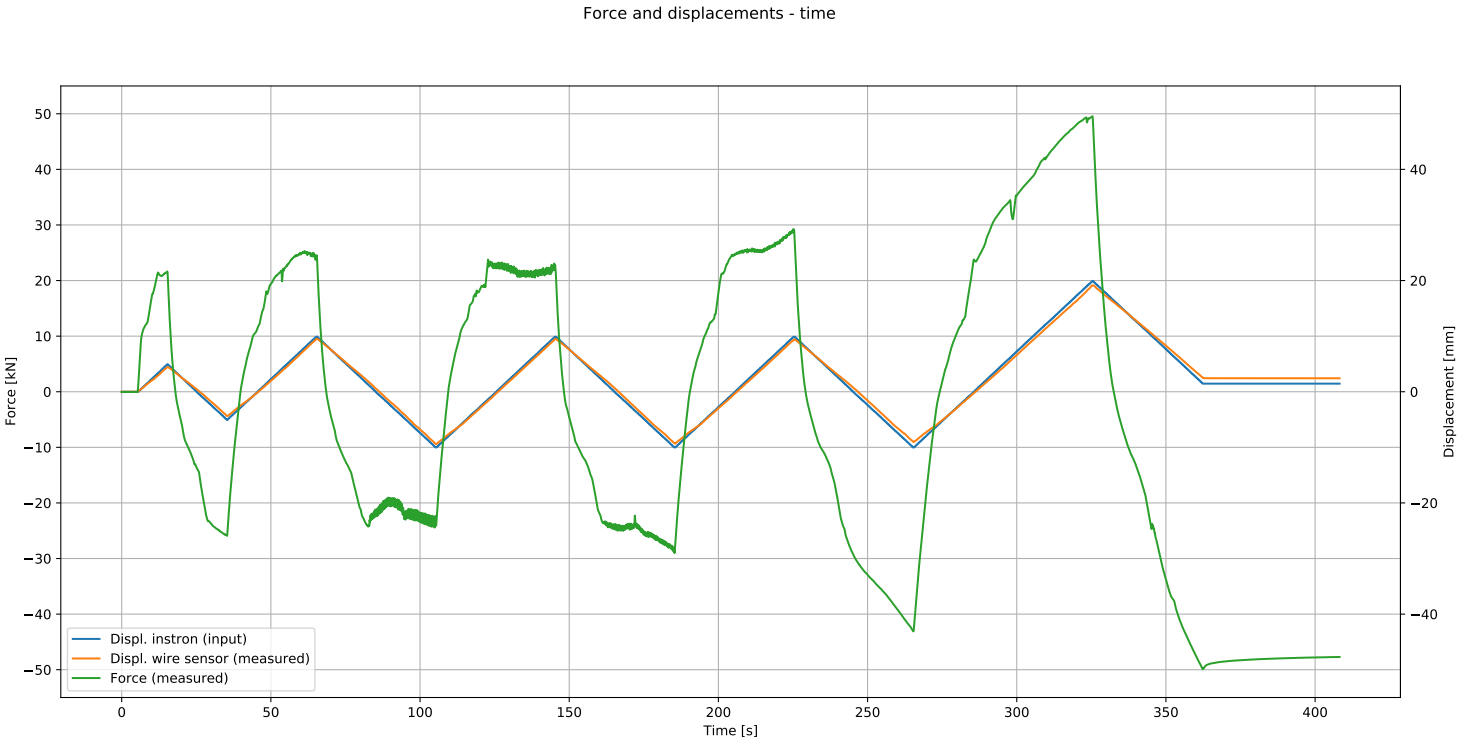

Figure 19: Force and displacement plotted against time.

STD-1H_1 Test A-30%

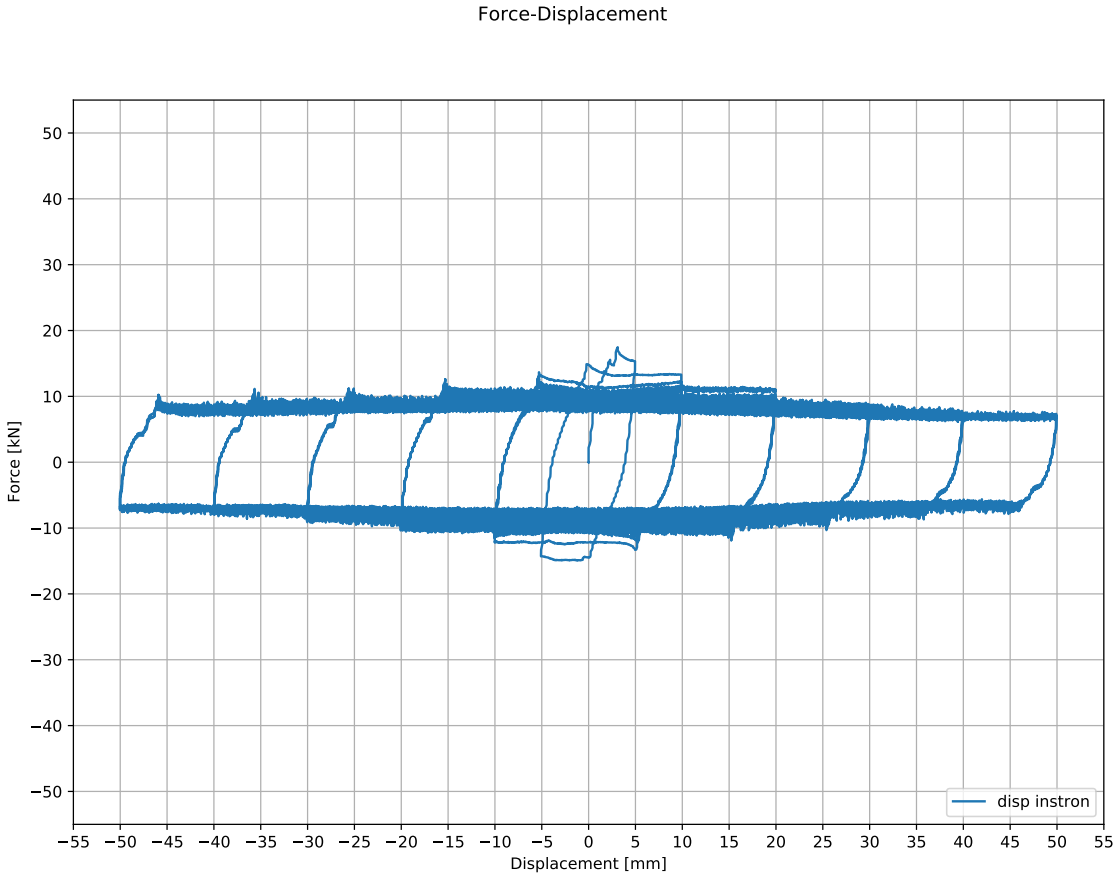

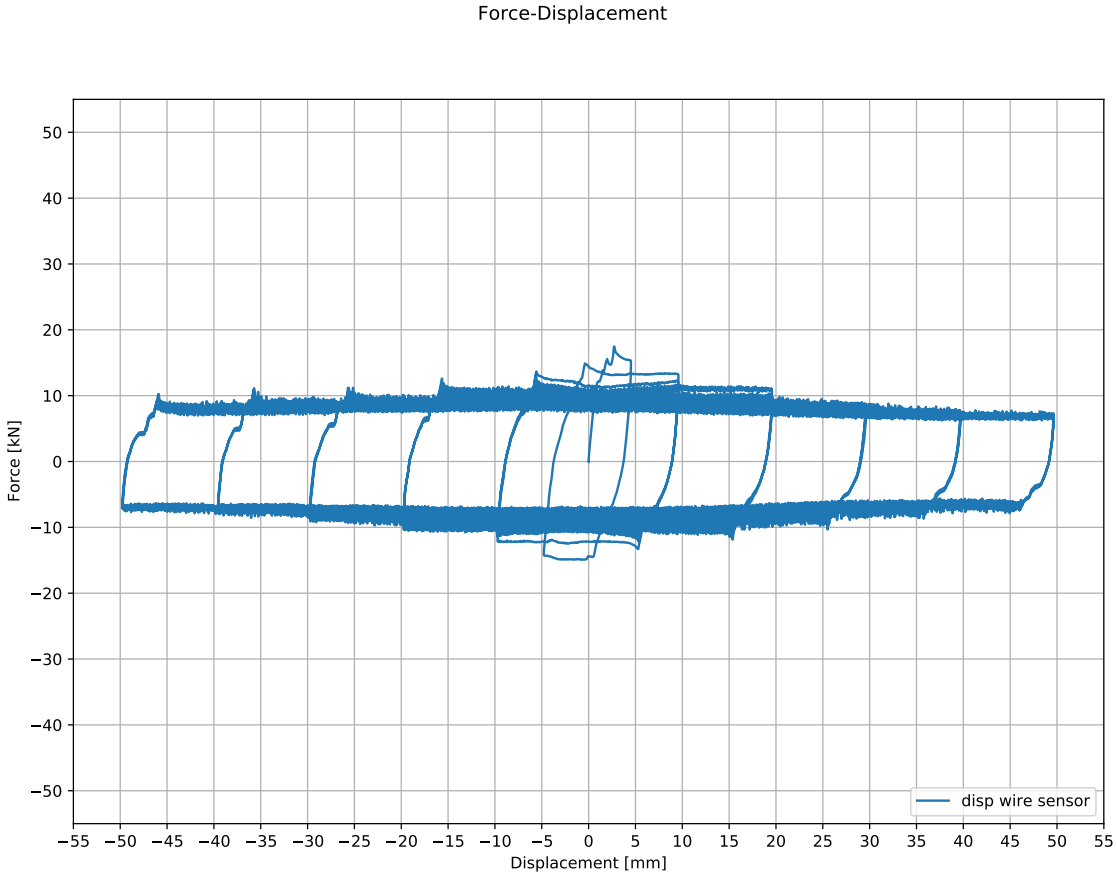

Figure 20: Load displacement graph.

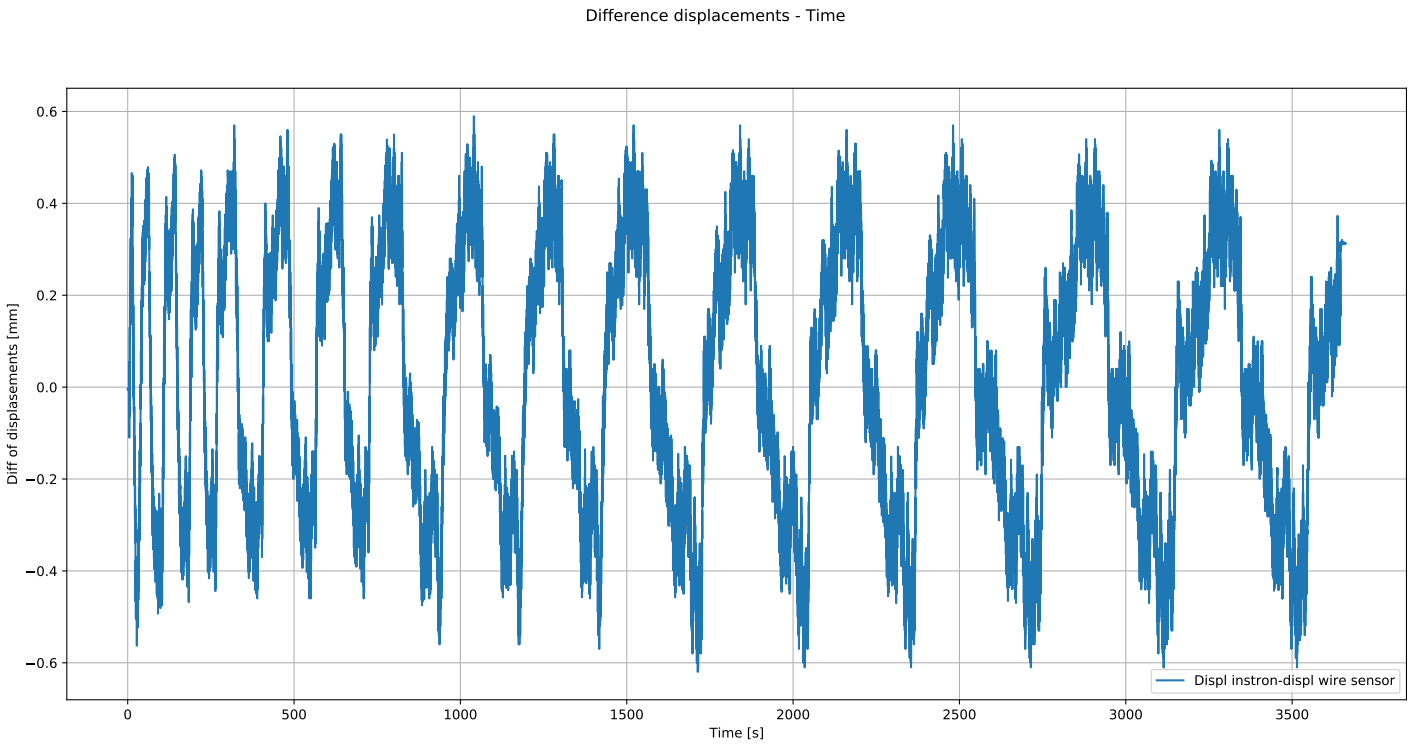

Figure 21: Difference of displacement between instron press and wire sensor.

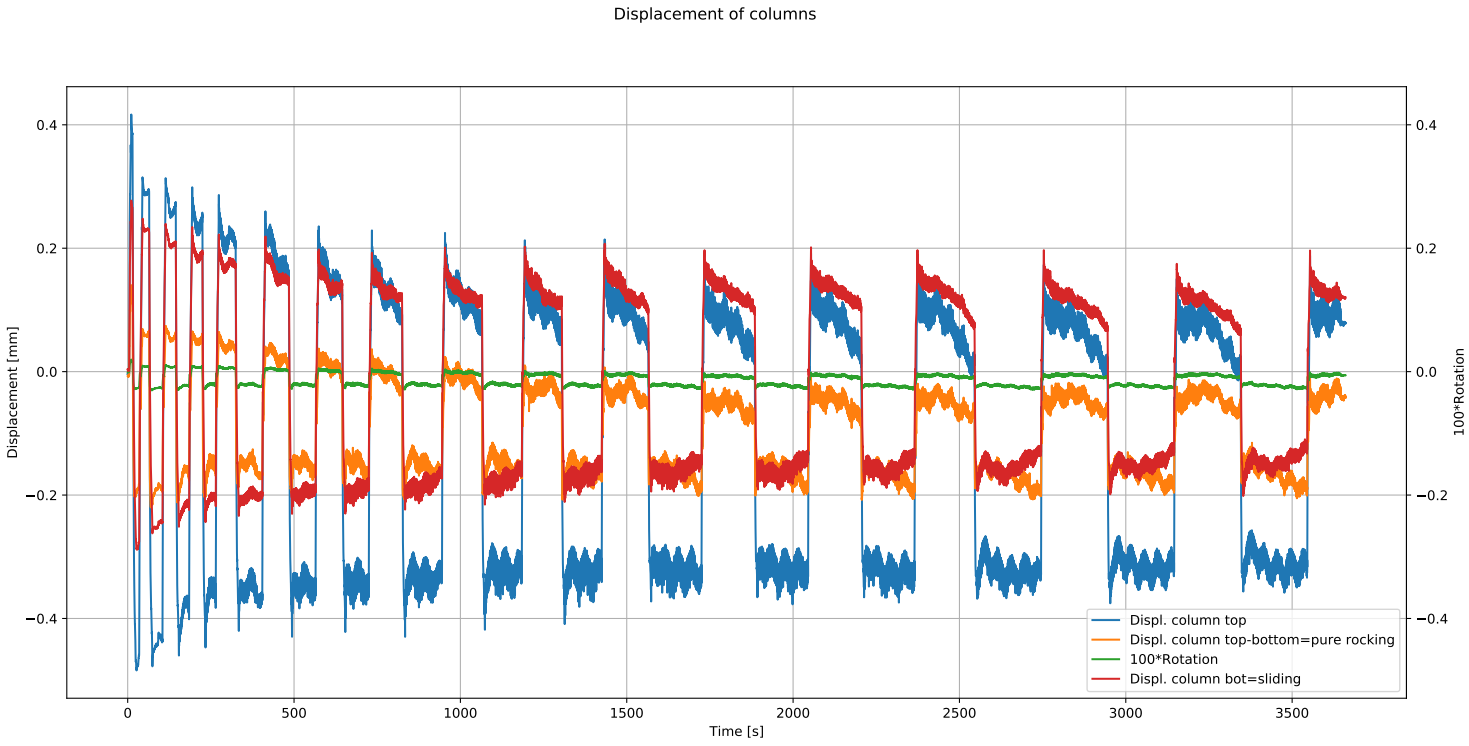

Figure 22: Movements of the column.

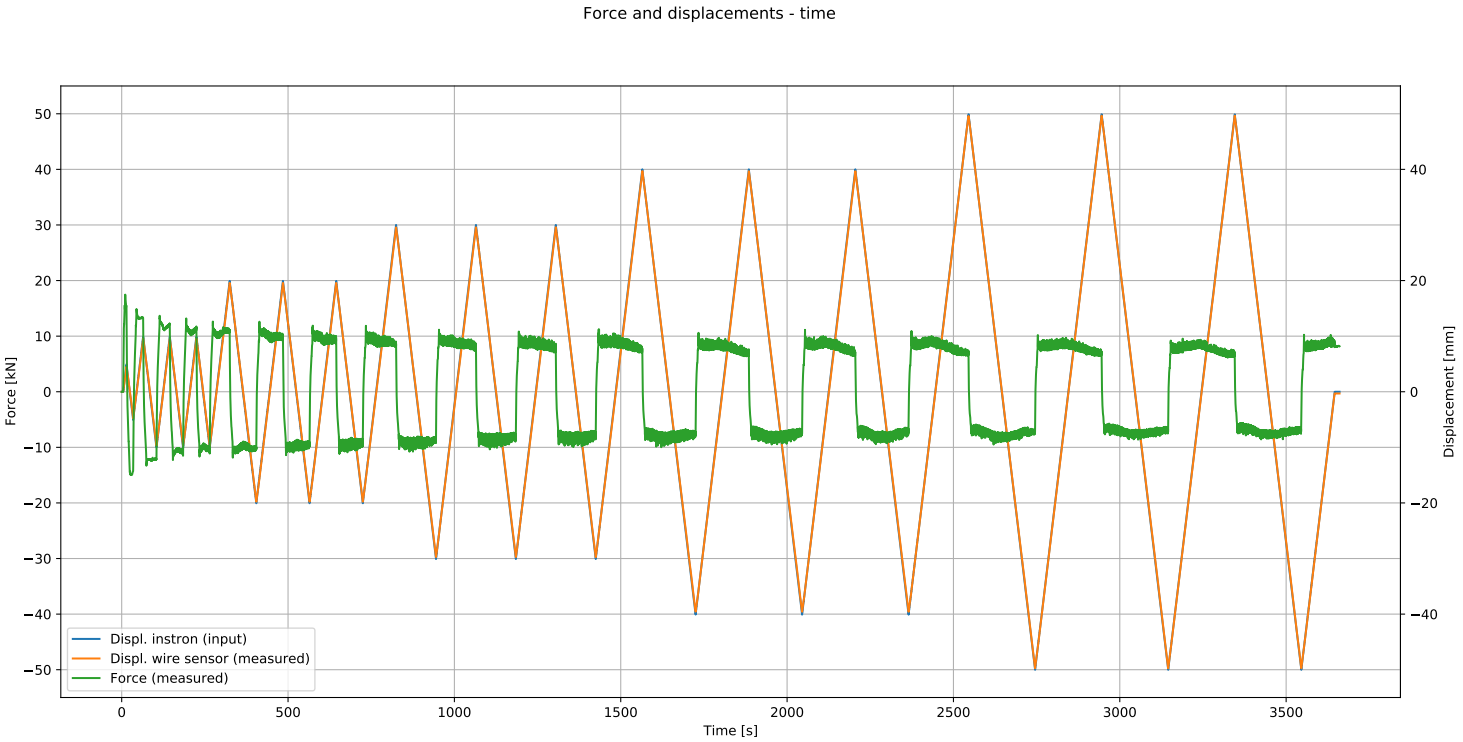

Figure 23: Force and displacement plotted against time.

STD-1H_1 Test B-56%

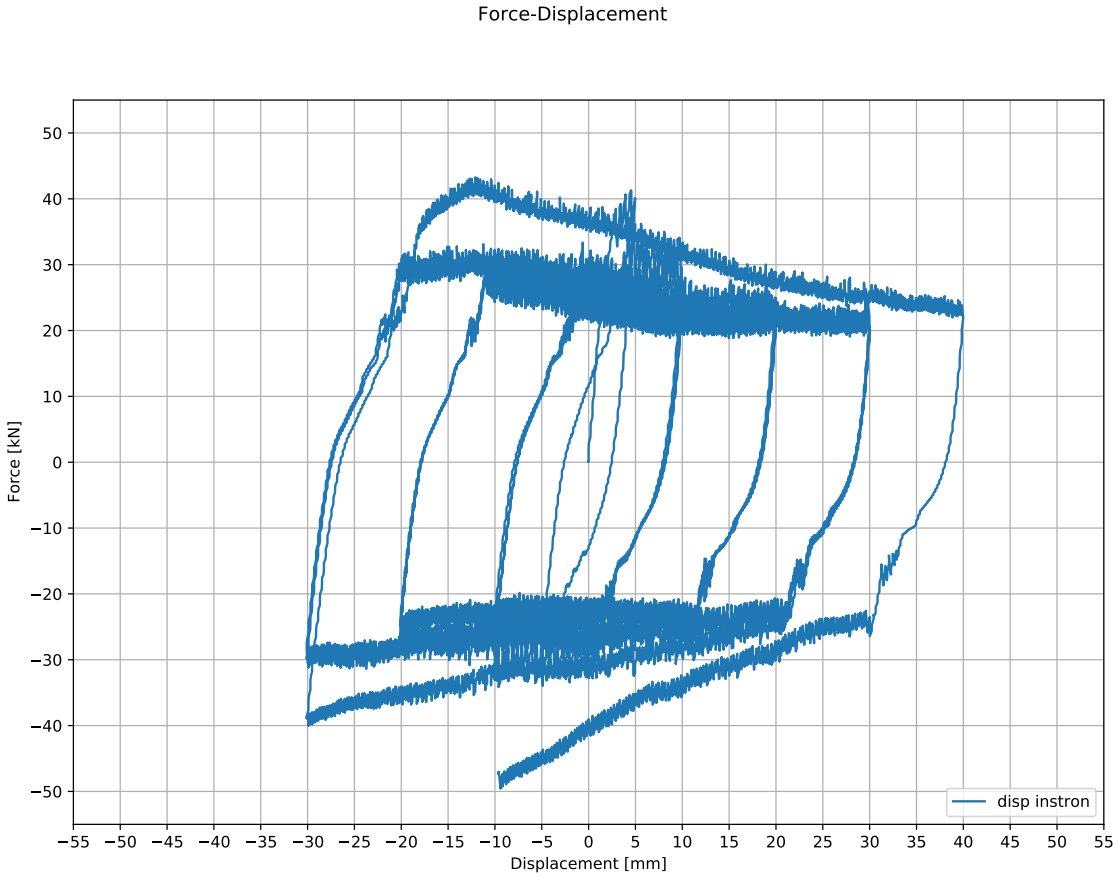

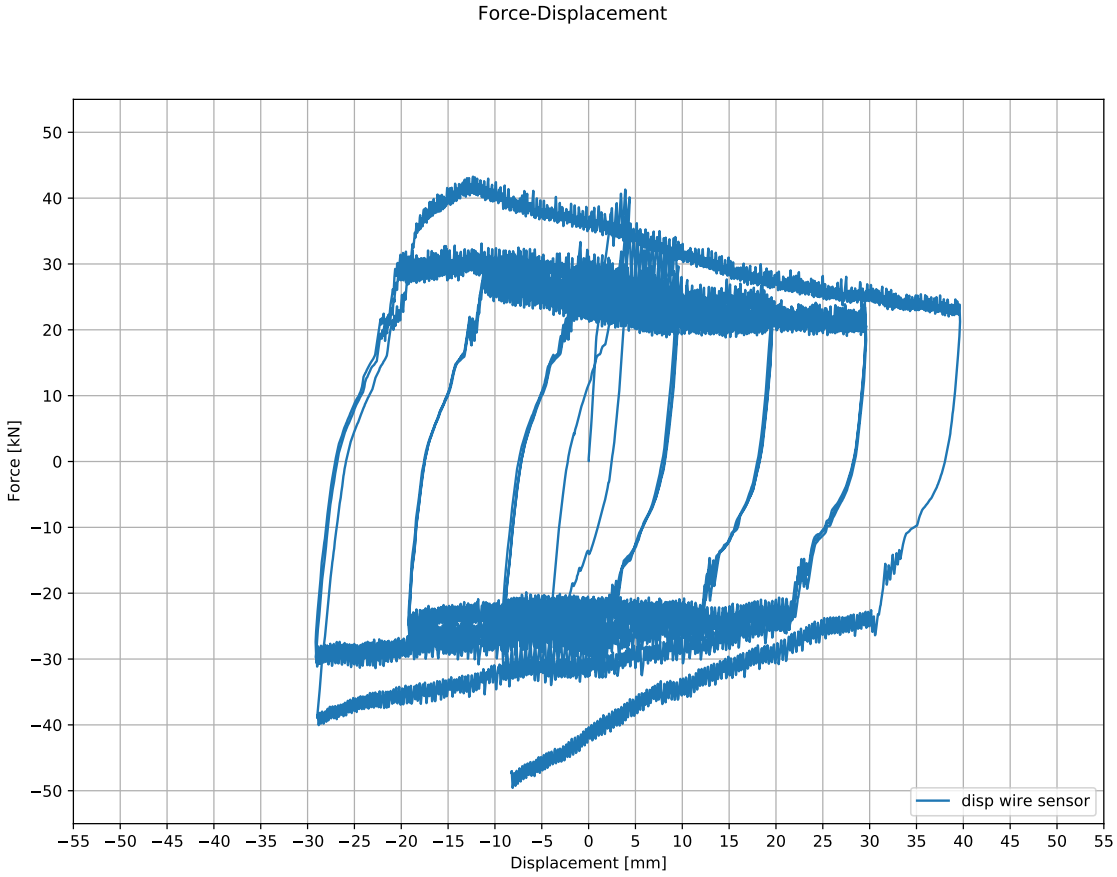

Figure 24: Load displacement graph.

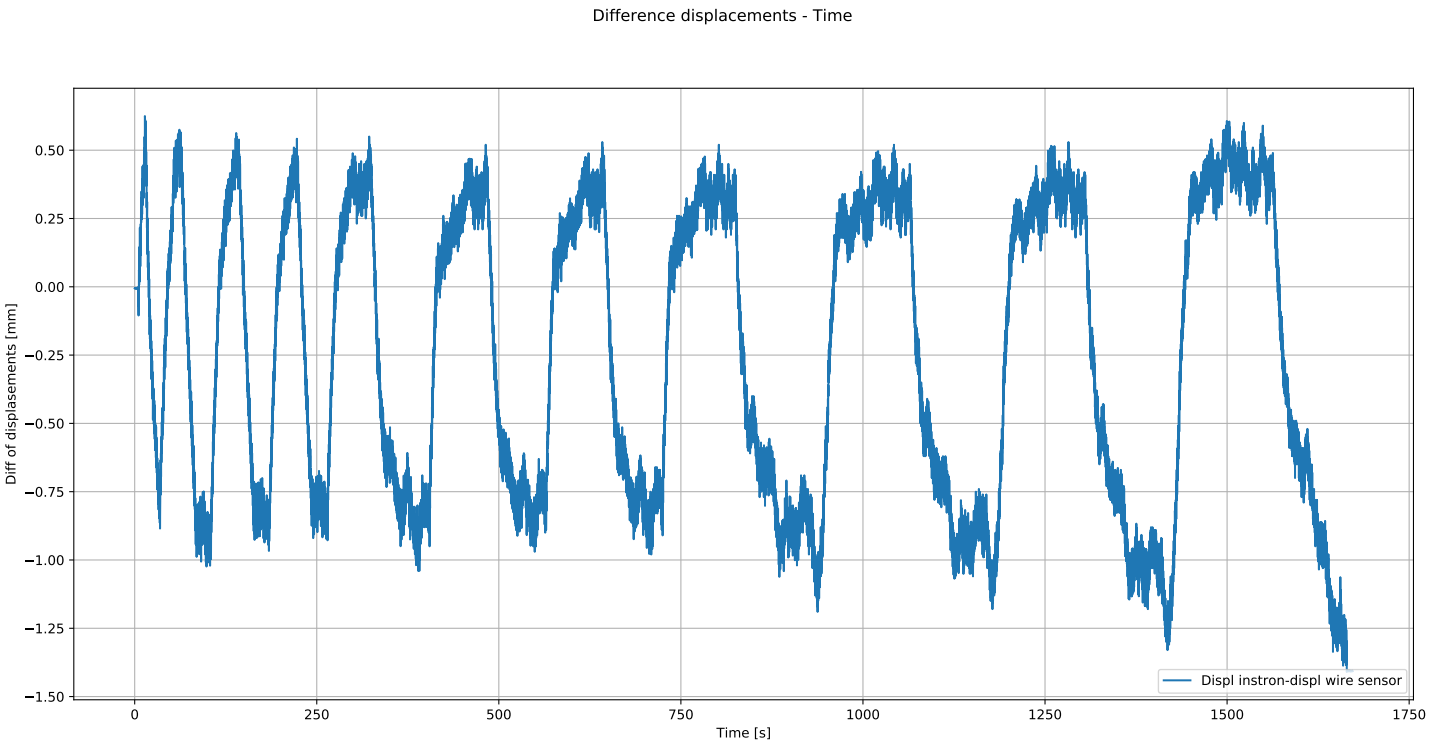

Figure 25: Difference of displacement between instron press and wire sensor.

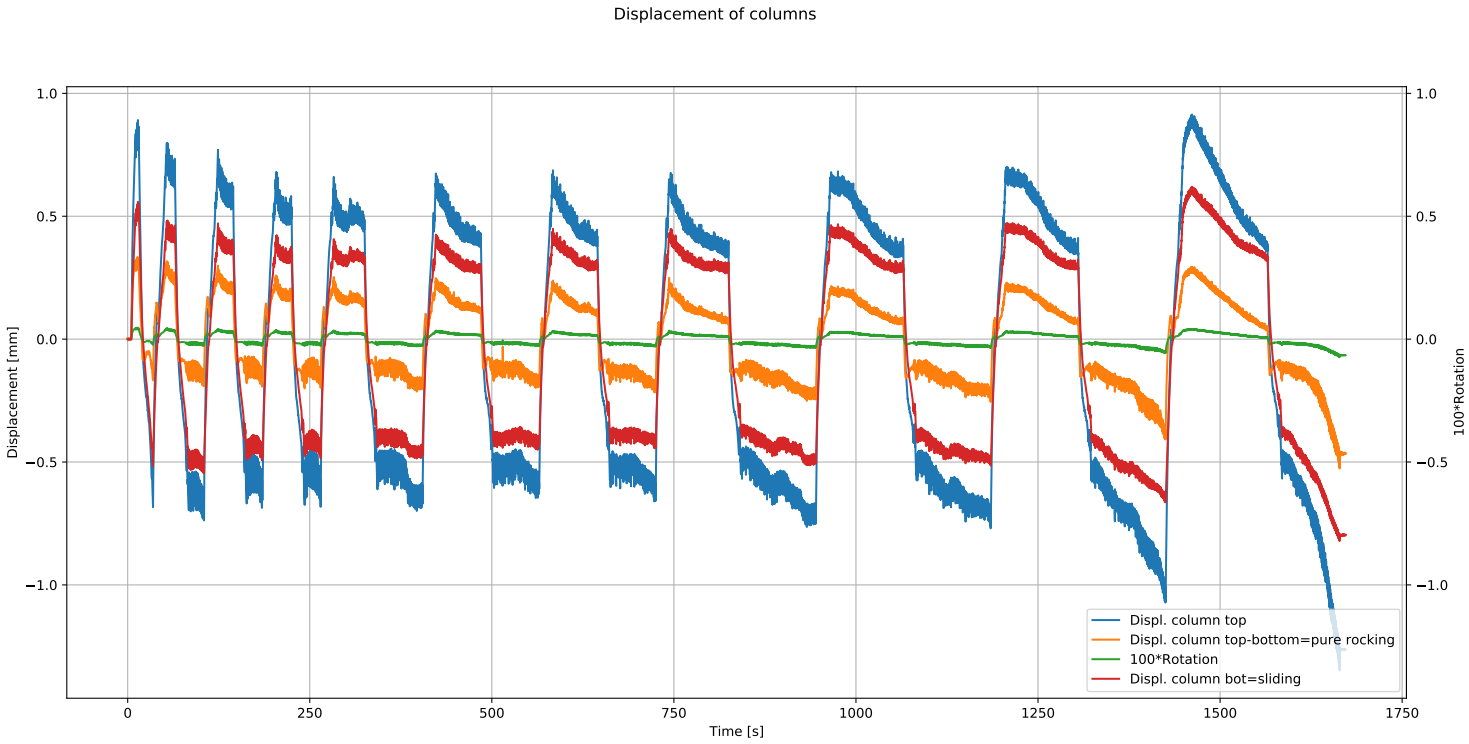

Figure 26: Movements of the column.

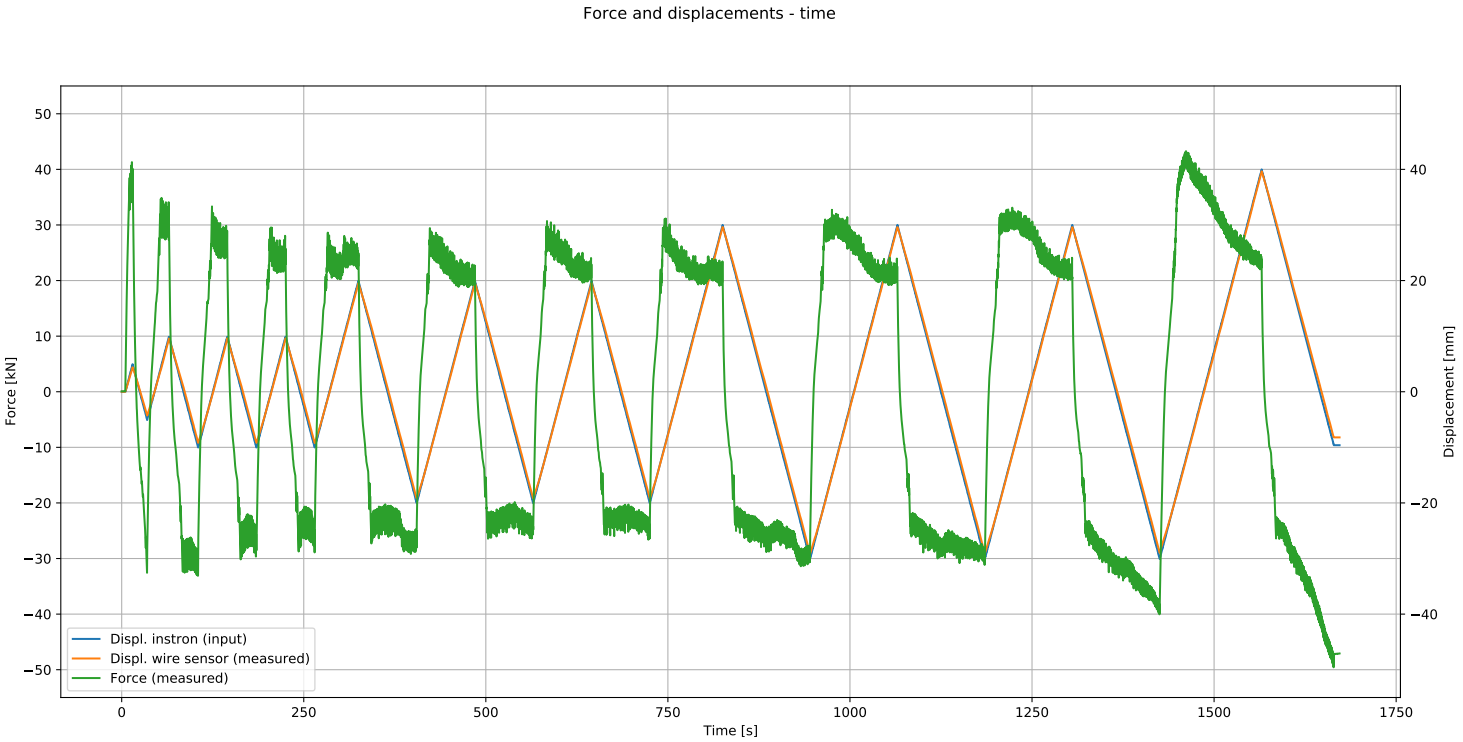

Figure 27: Force and displacement plotted against time.

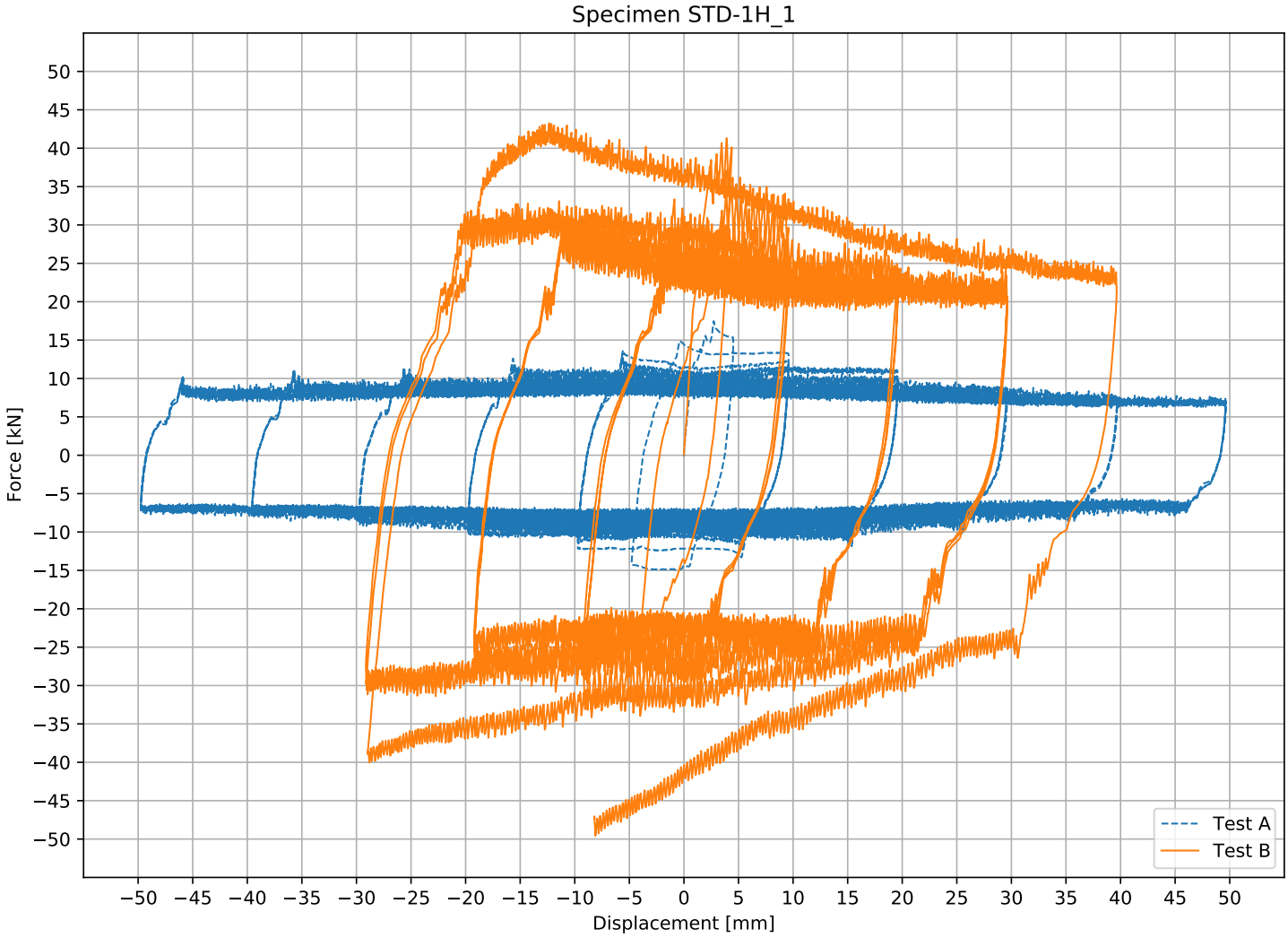

Figure 28: Comparison between test A and B of specimen STD-1H_1, same speed of 0.5mm/s, same excursion of 50mm, different preload: 30% for test A, 56% for test B.

STD-R_1 Test A-30%

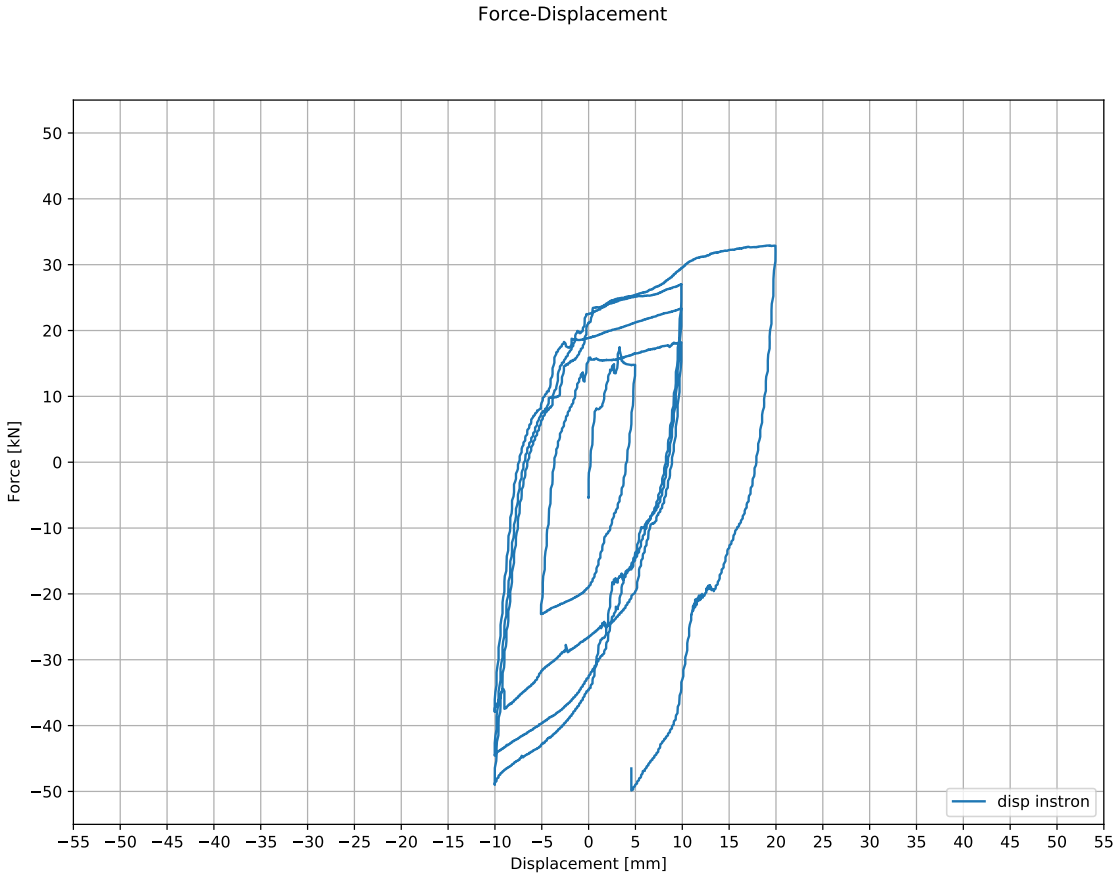

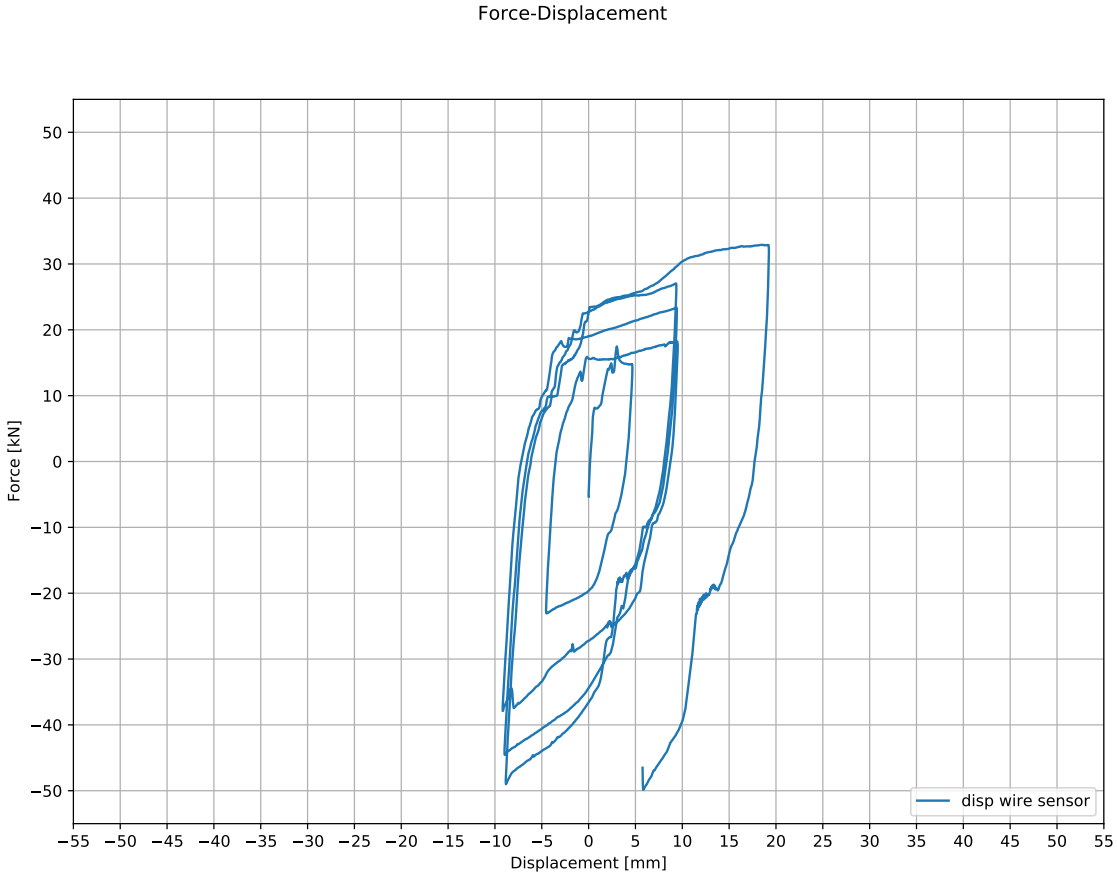

Figure 29: Load displacement graph.

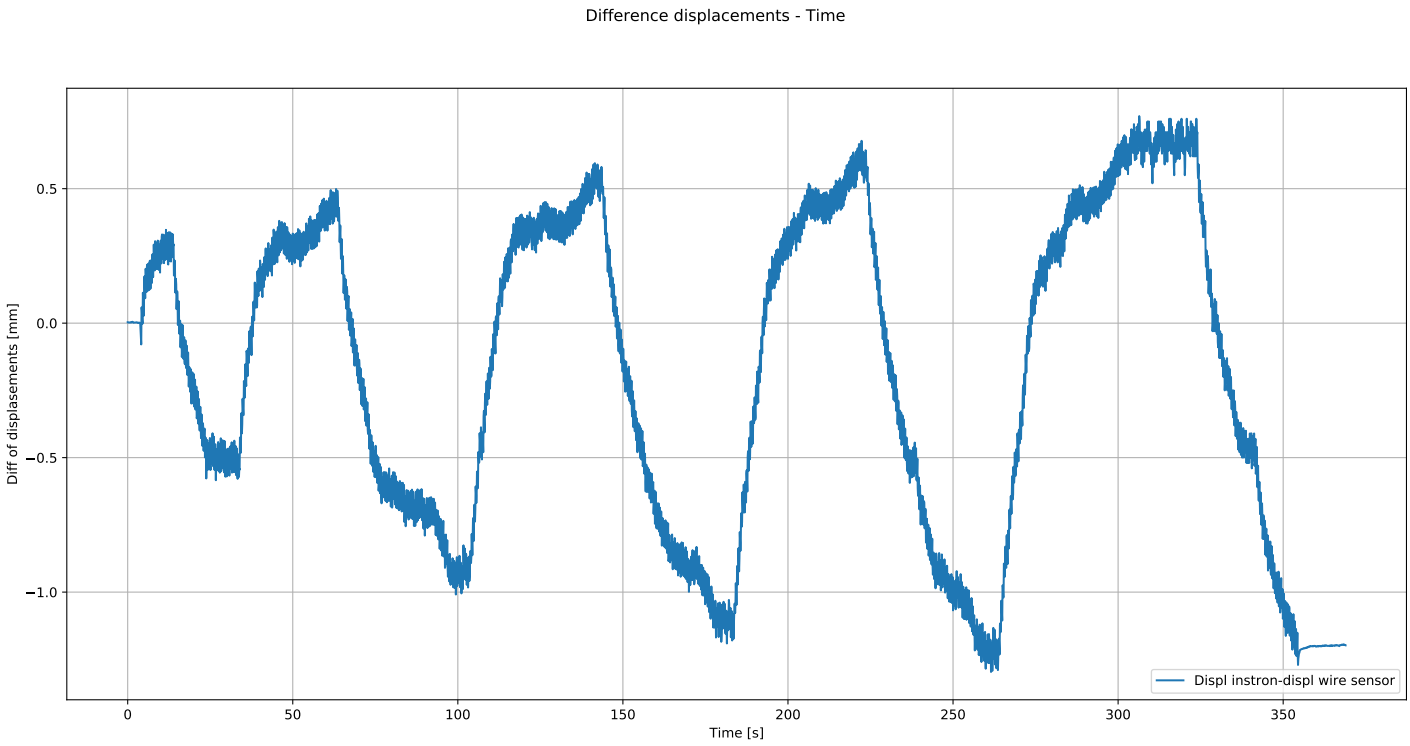

Figure 30: Difference of displacement between instron press and wire sensor.

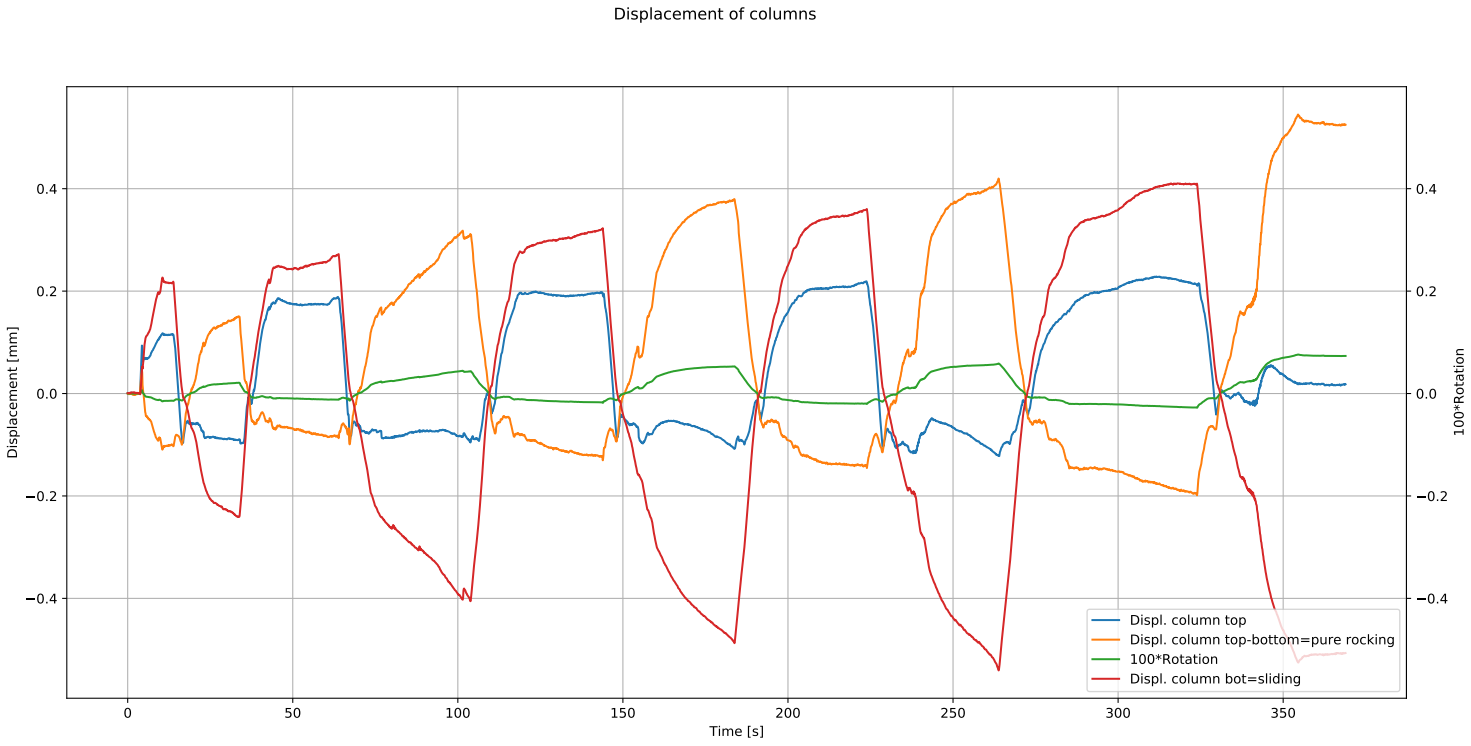

Figure 31: Movements of the column.

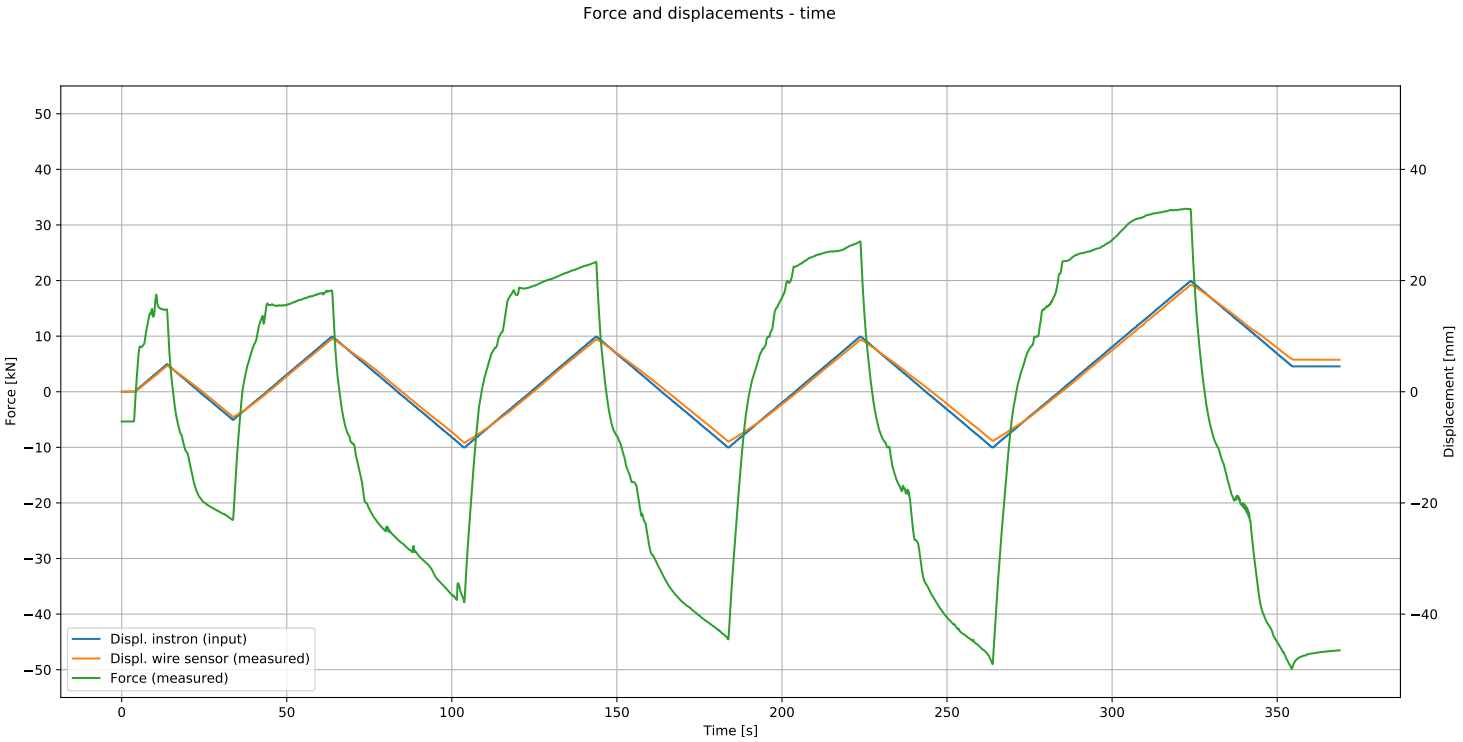

Figure 32: Force and displacement plotted against time.

ALT_1 Test A-30%

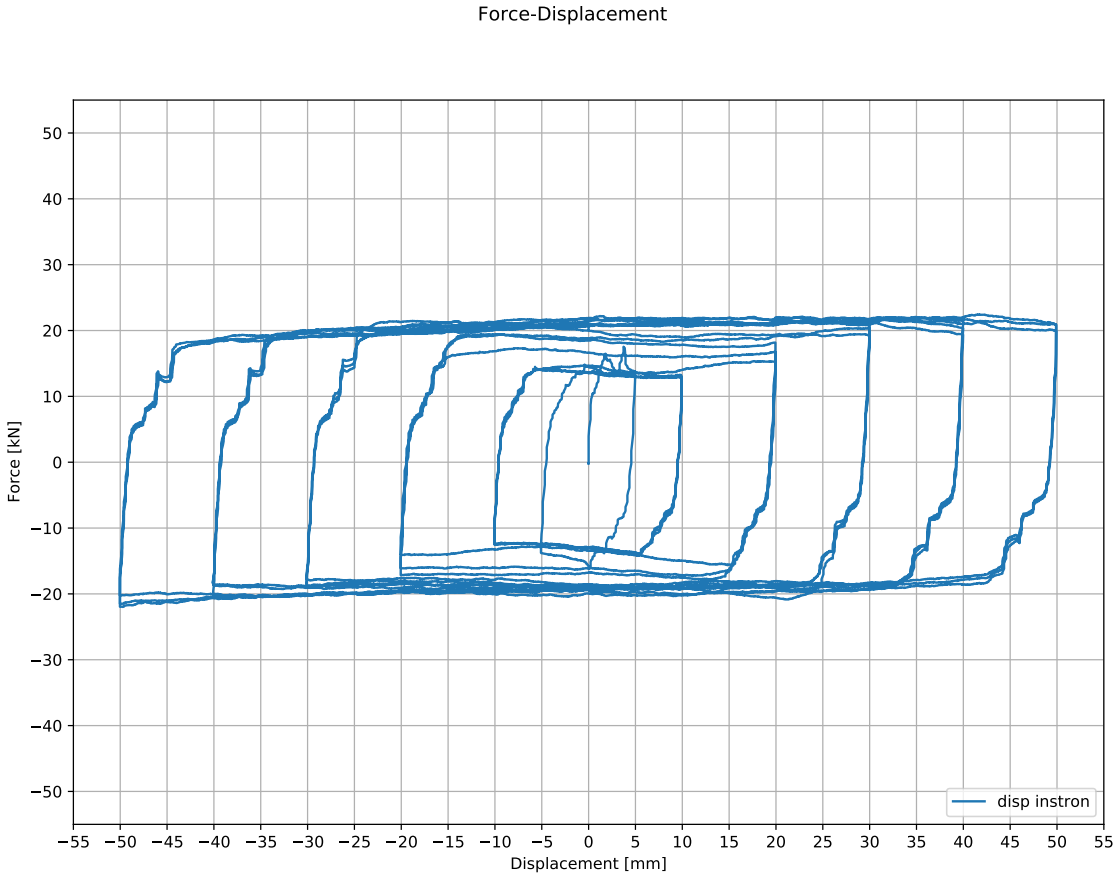

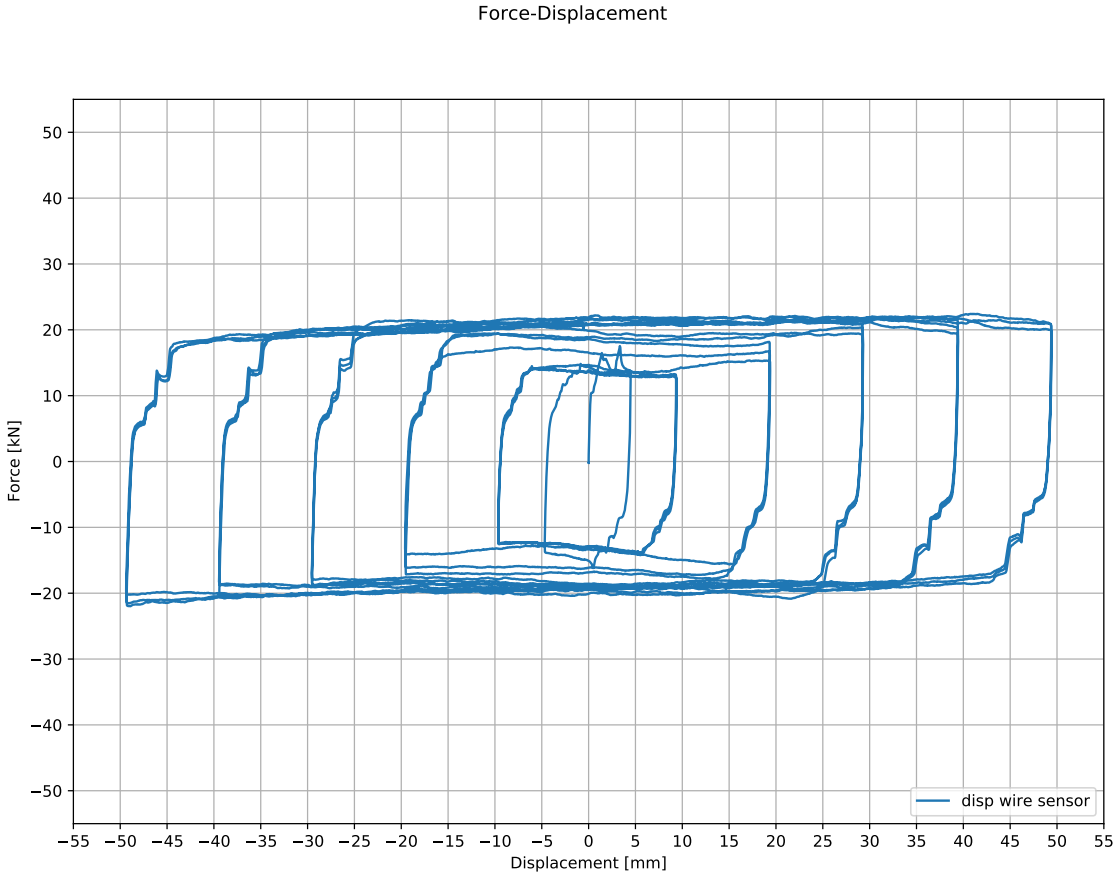

Figure 33: Load displacement graph.

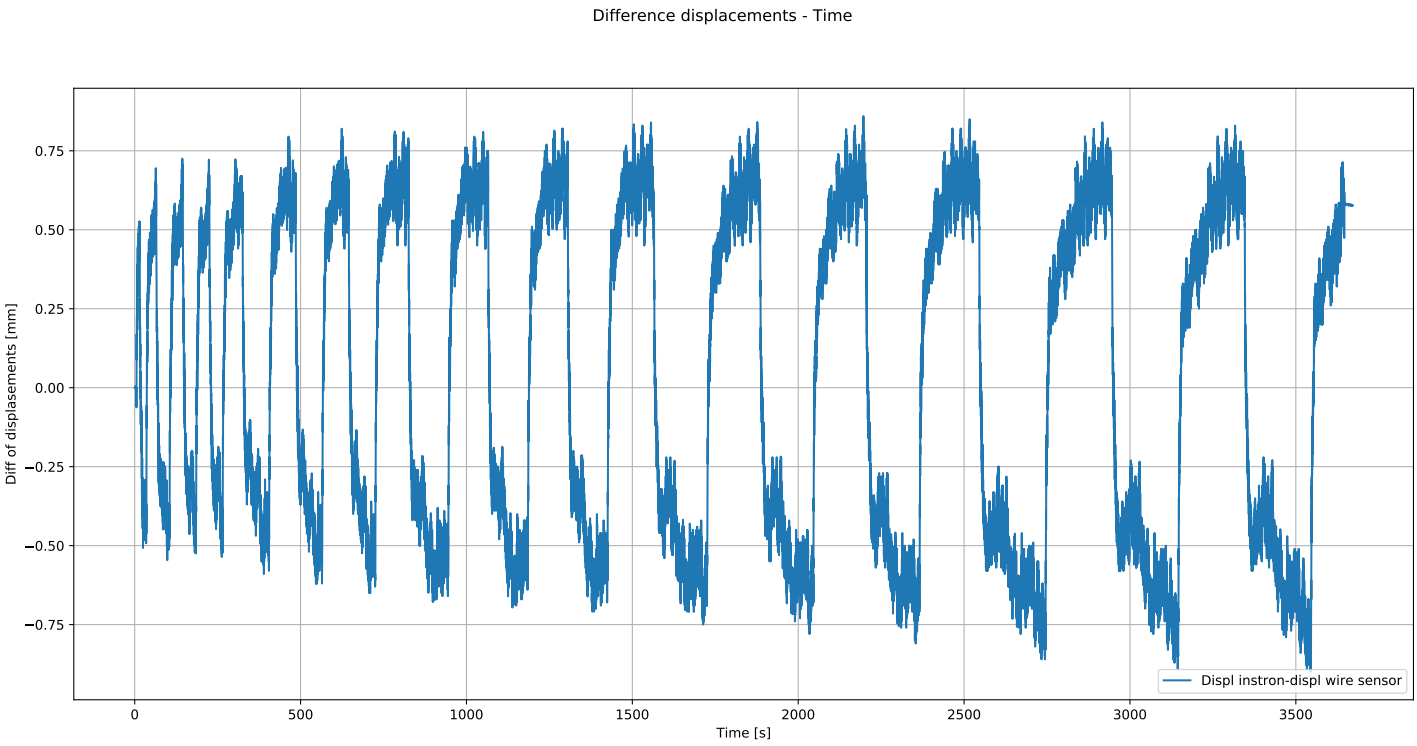

Figure 34: Difference of displacement between instron press and wire sensor.

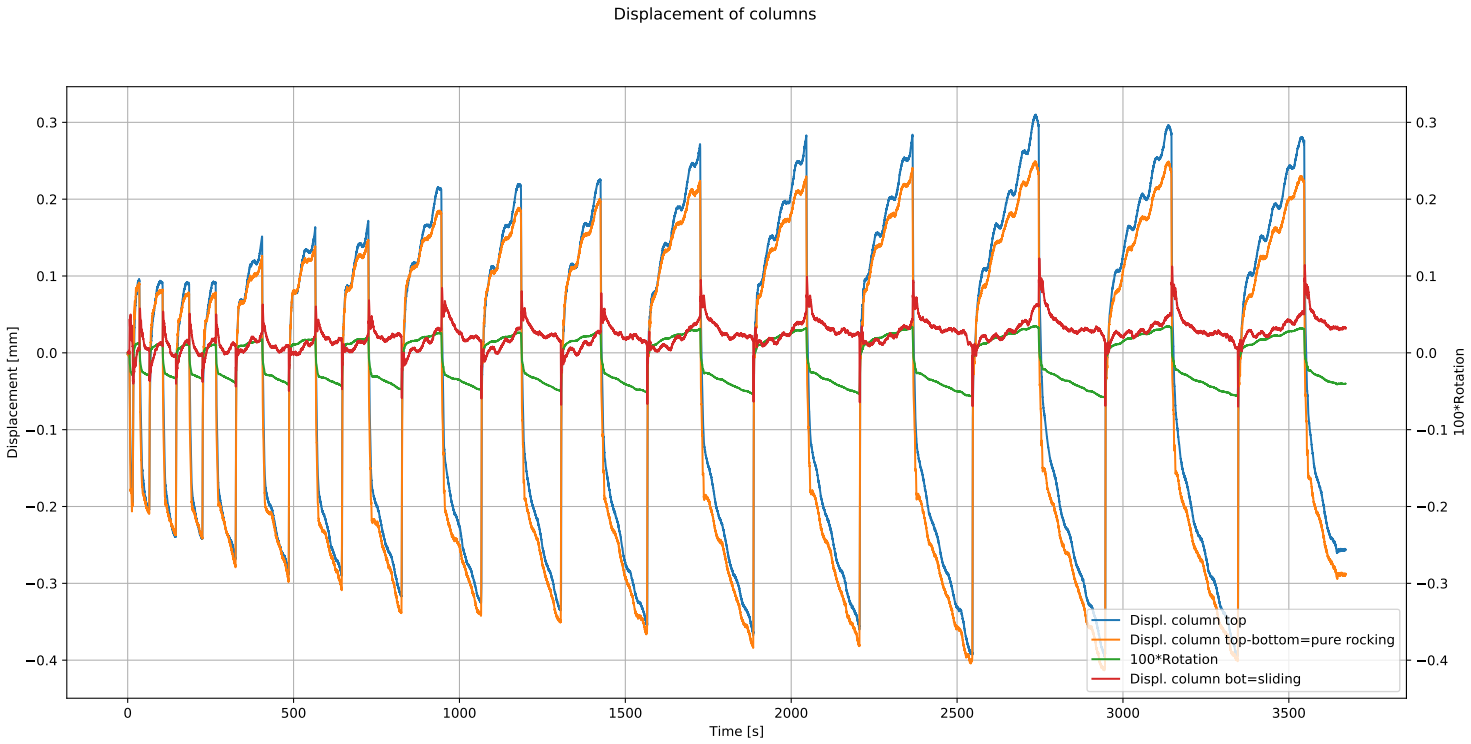

Figure 35: Movements of the column.

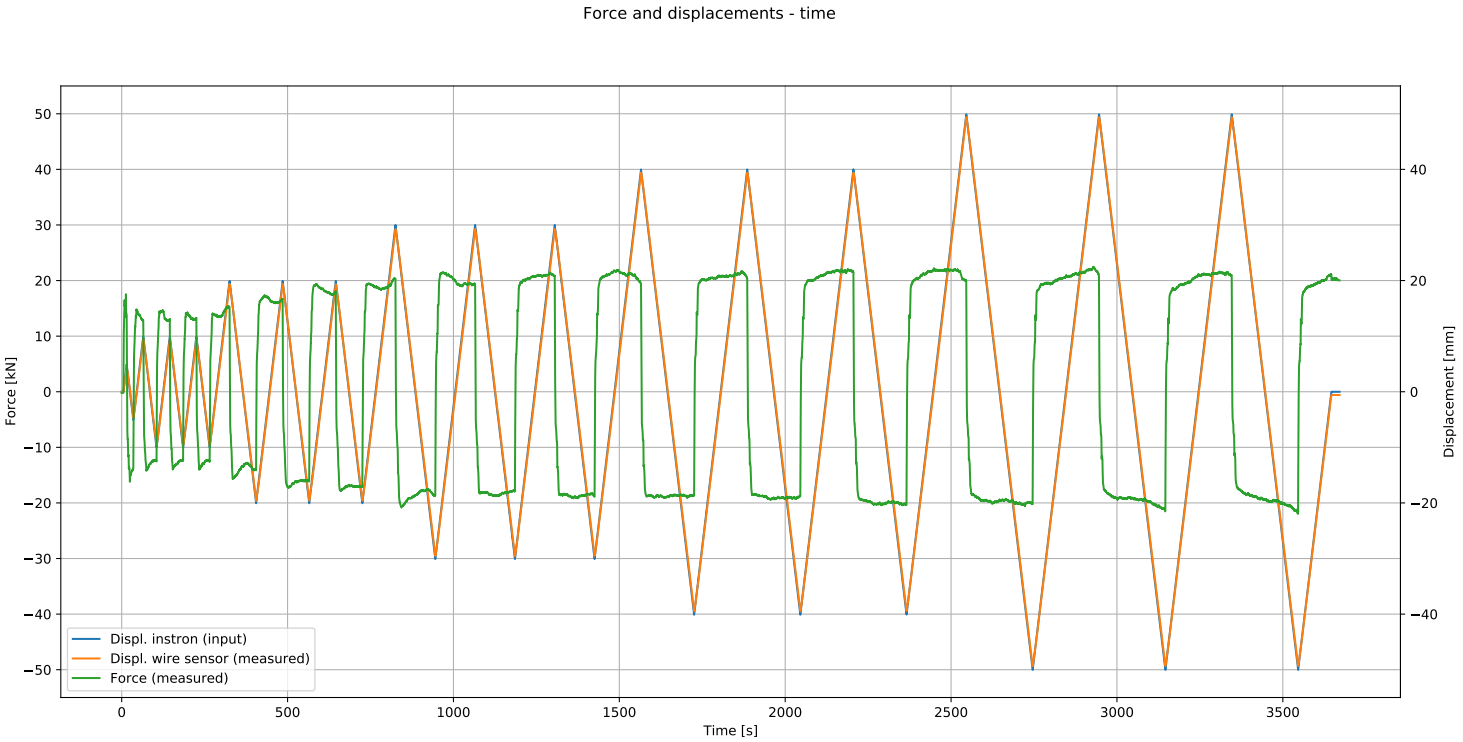

Figure 36: Force and displacement plotted against time.

ALT_1 Test B-45%

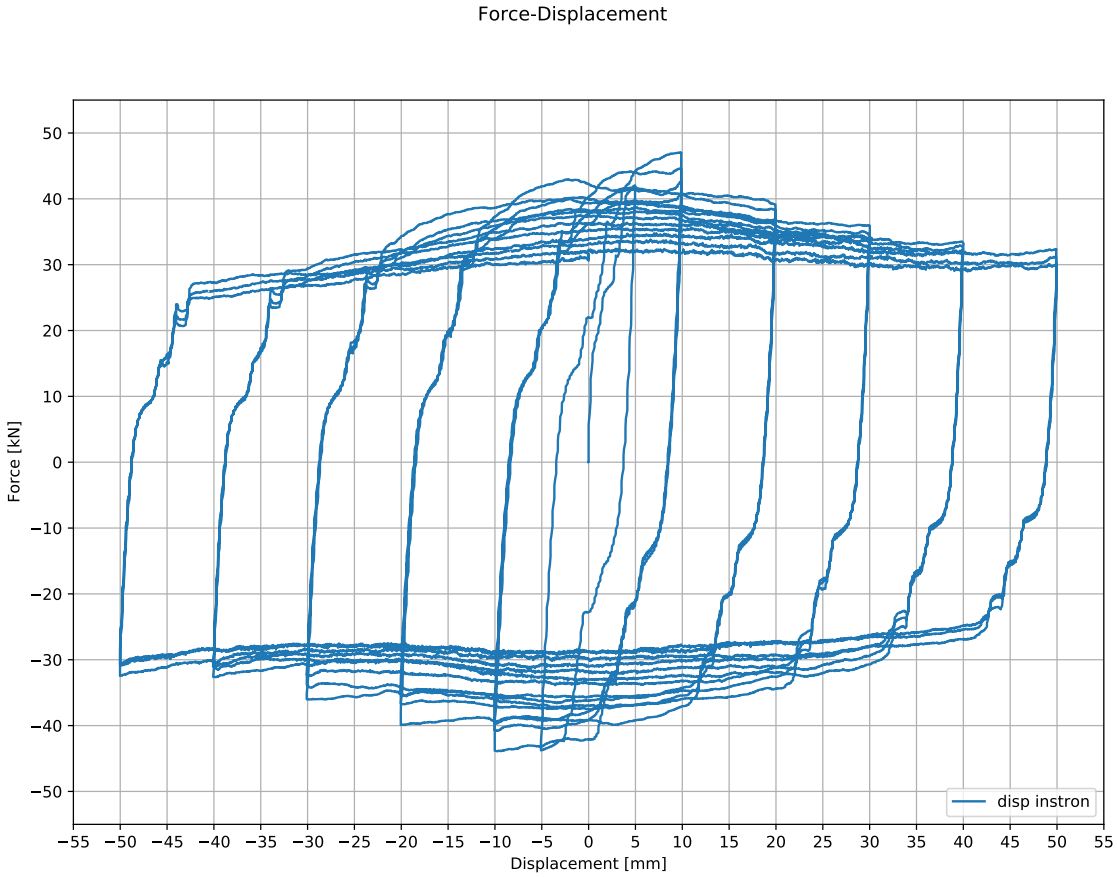

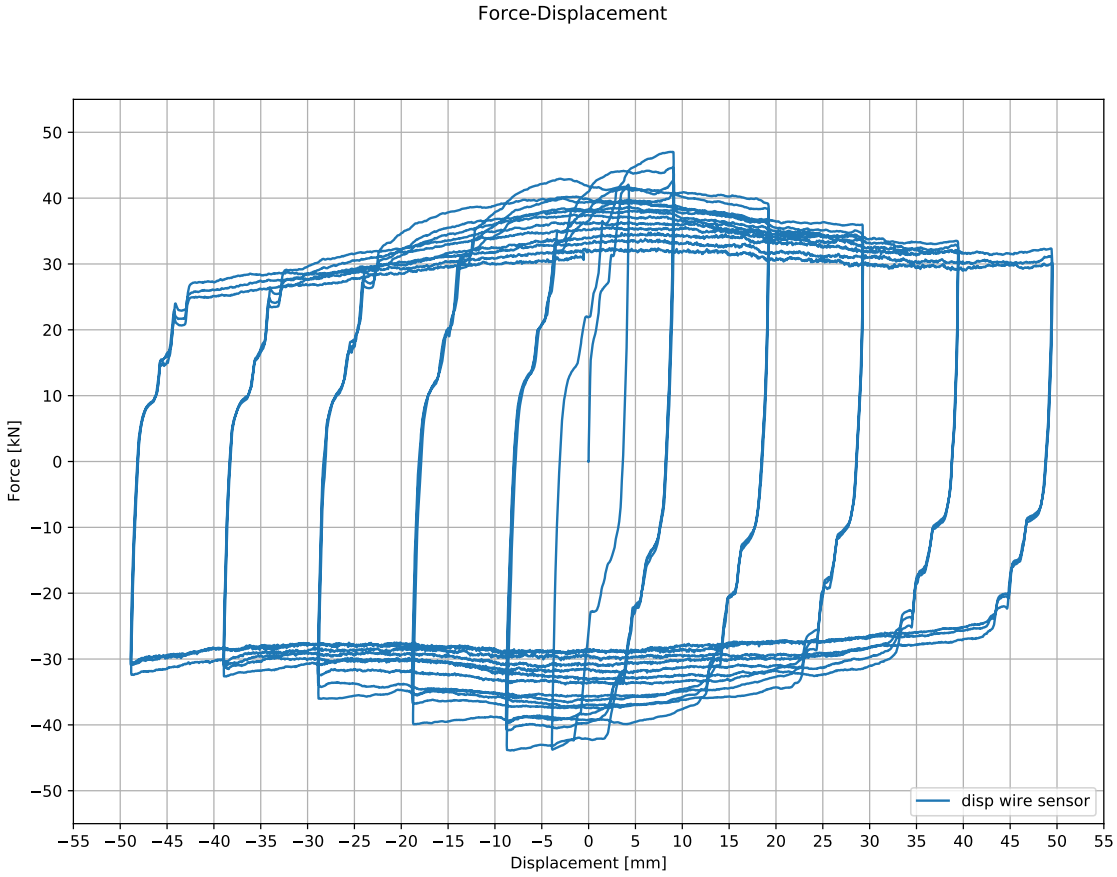

Figure 37: Load displacement graph.

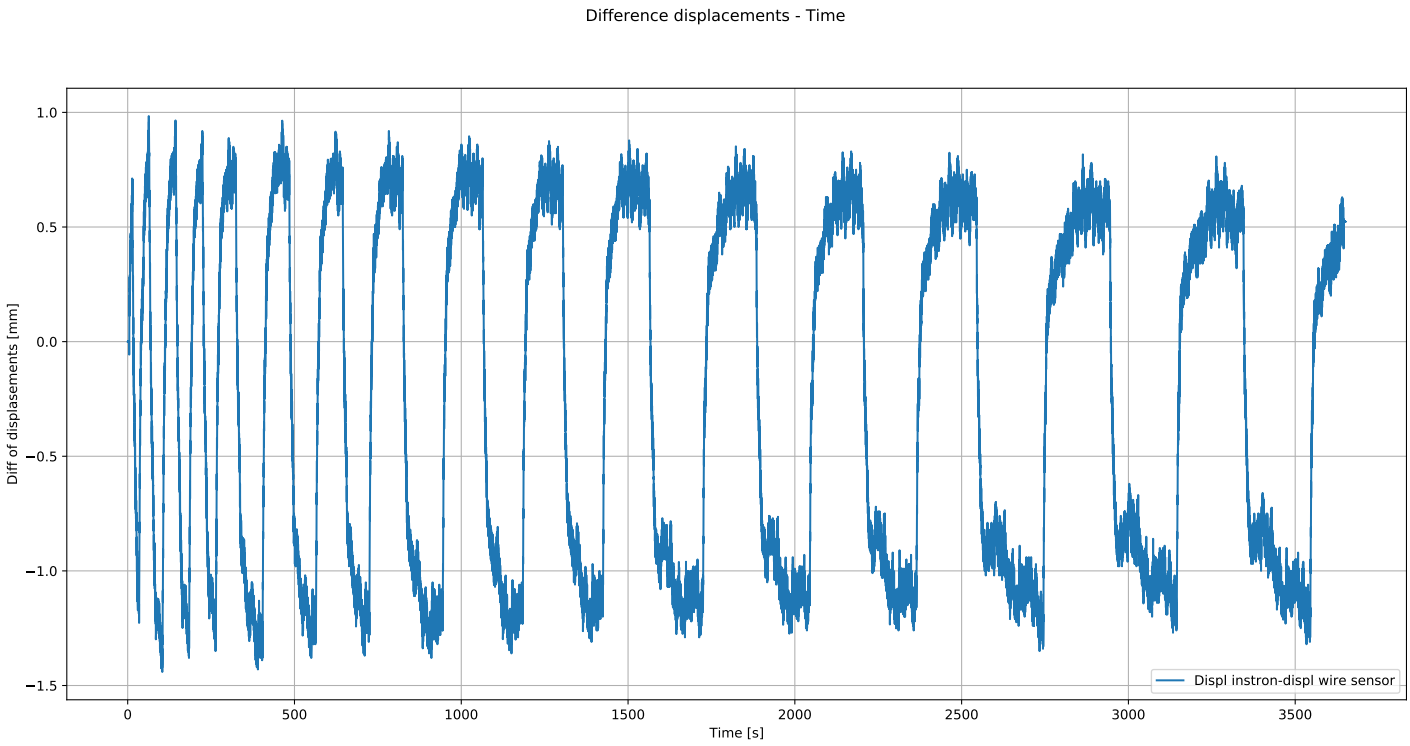

Figure 38: Difference of displacement between instron press and wire sensor.

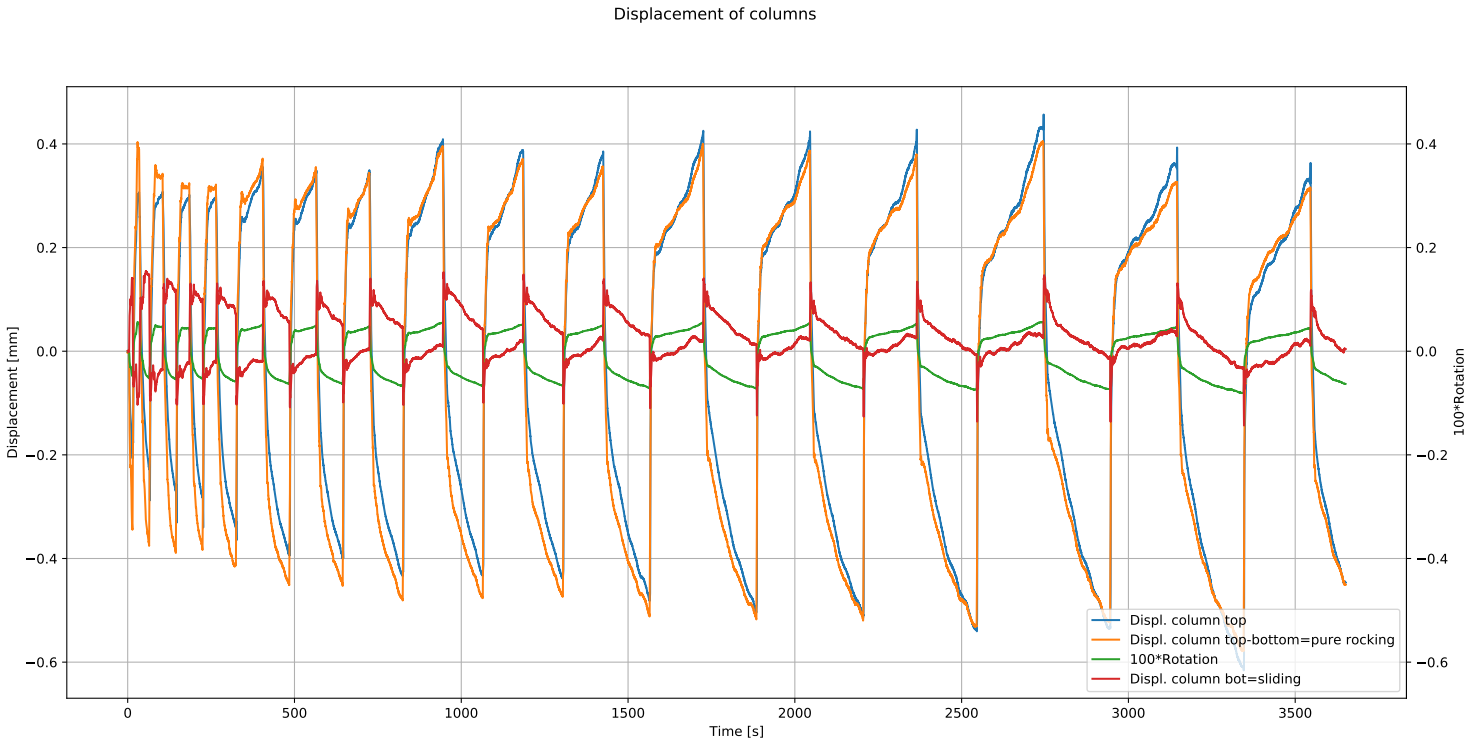

Figure 39: Movements of the column.

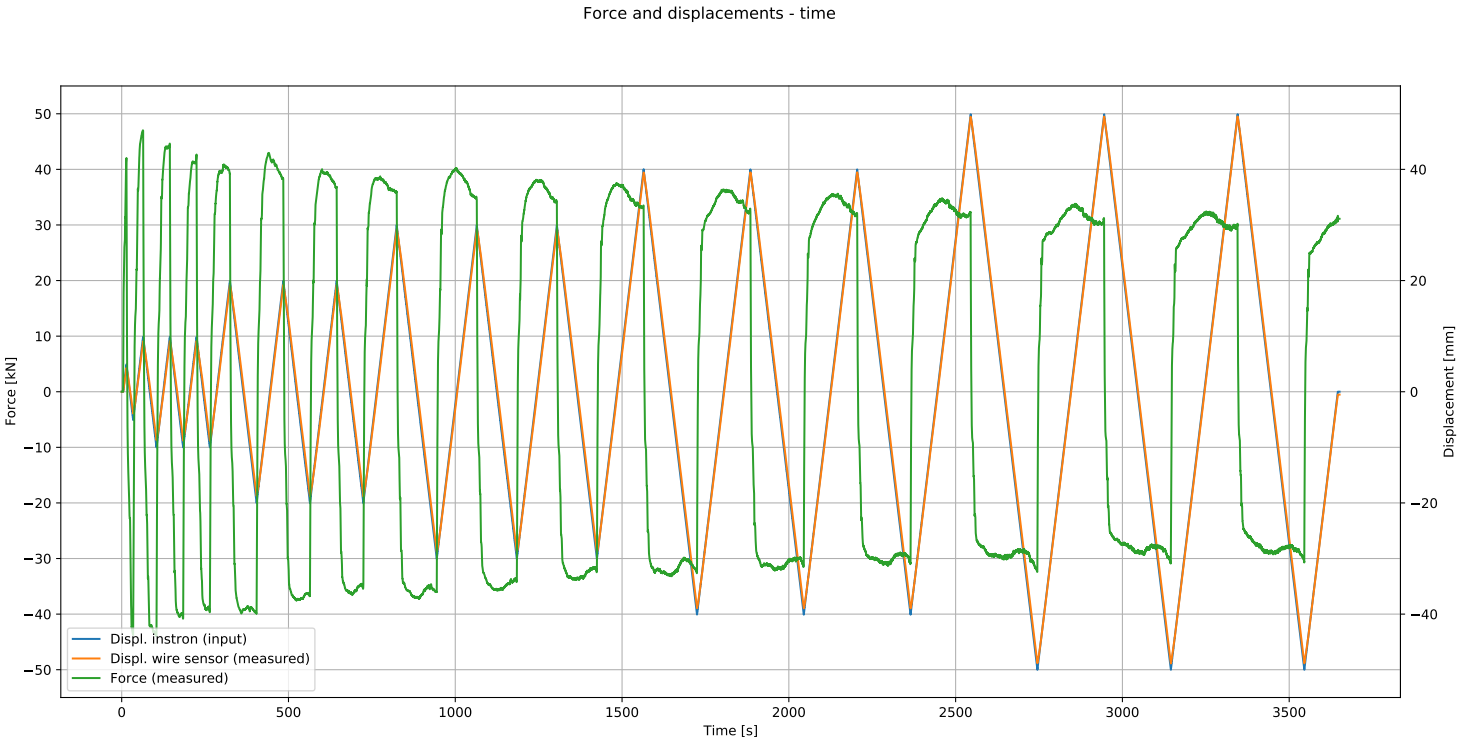

Figure 40: Force and displacement plotted against time.

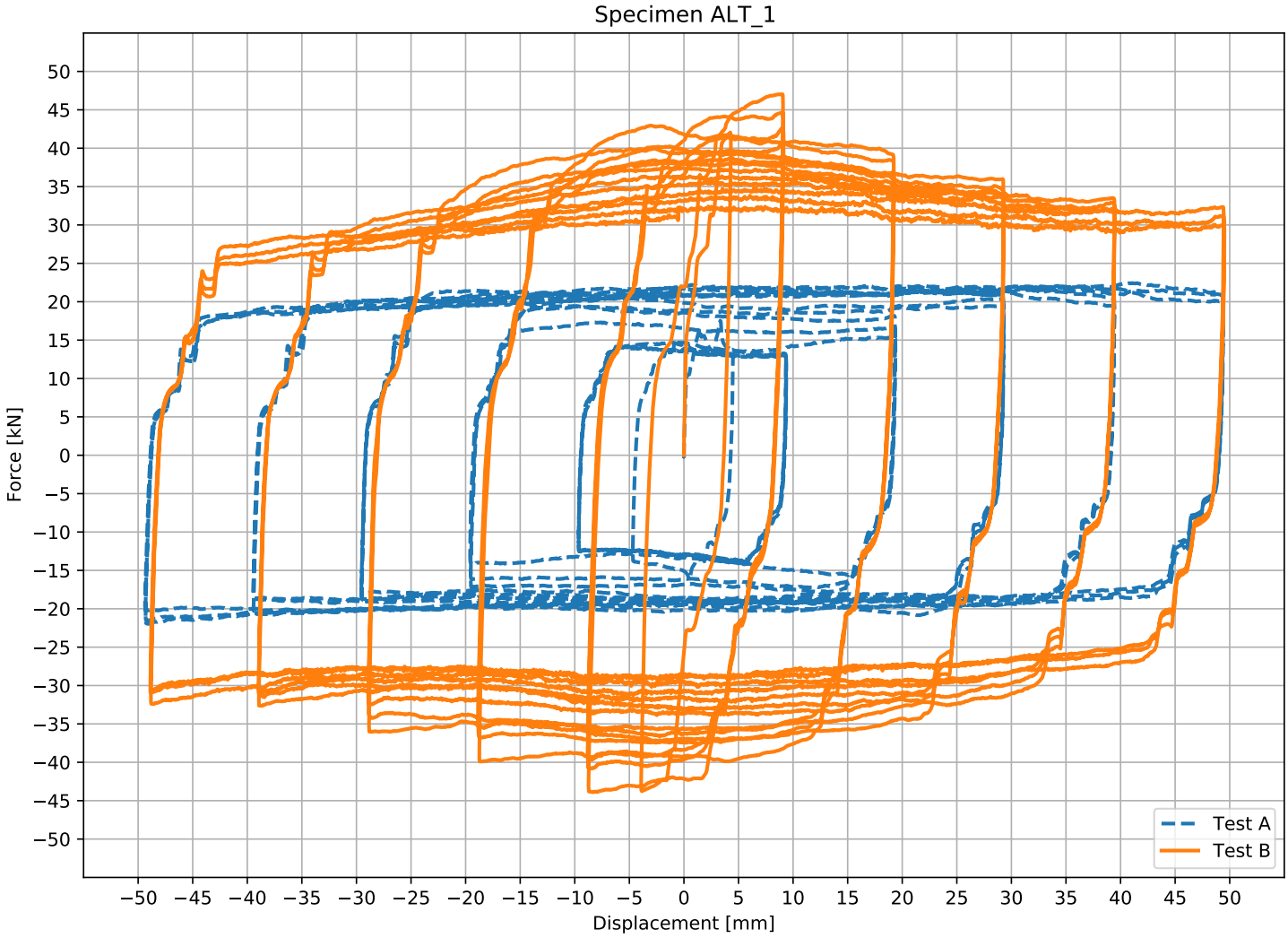

Figure 41: Comparison between test A and B of specimen ALT_1, same speed of 0.5mm/s, same excursion of 50mm, different preload: 30% for test A, 45% for test B.

ALT_1 Test C-45%

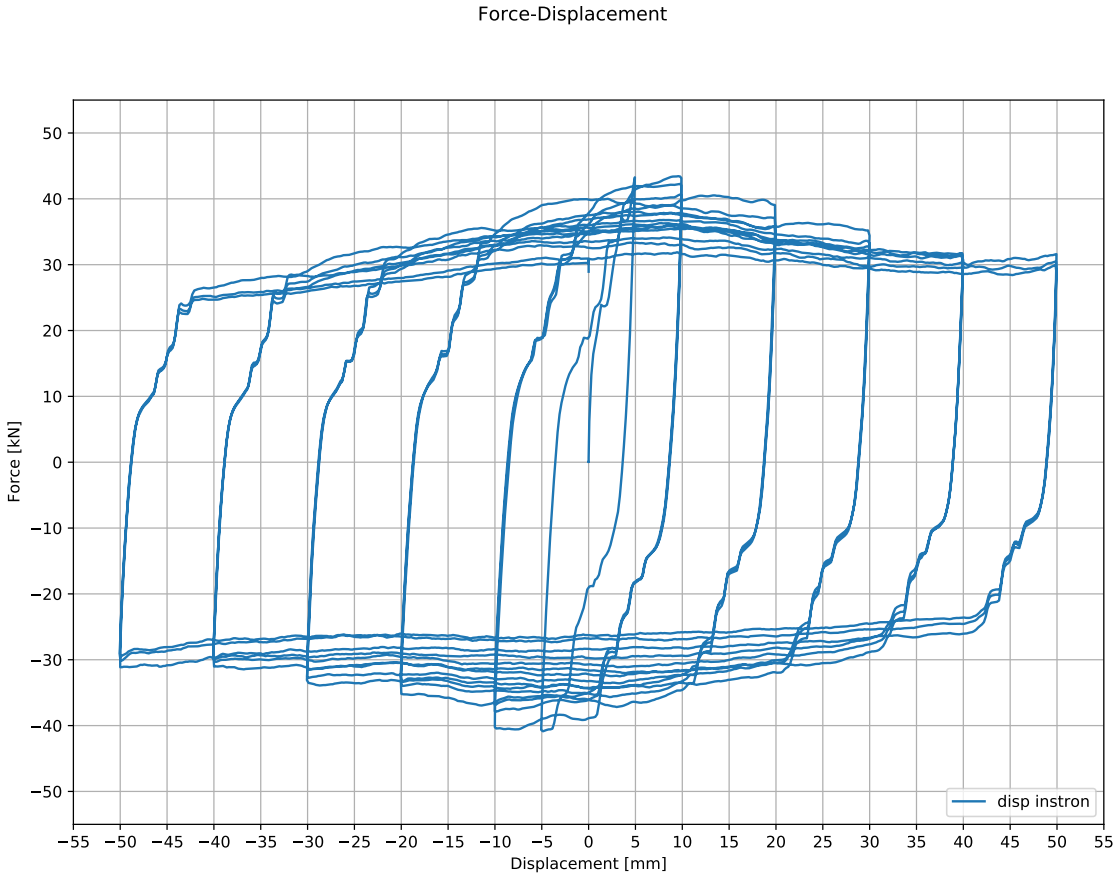

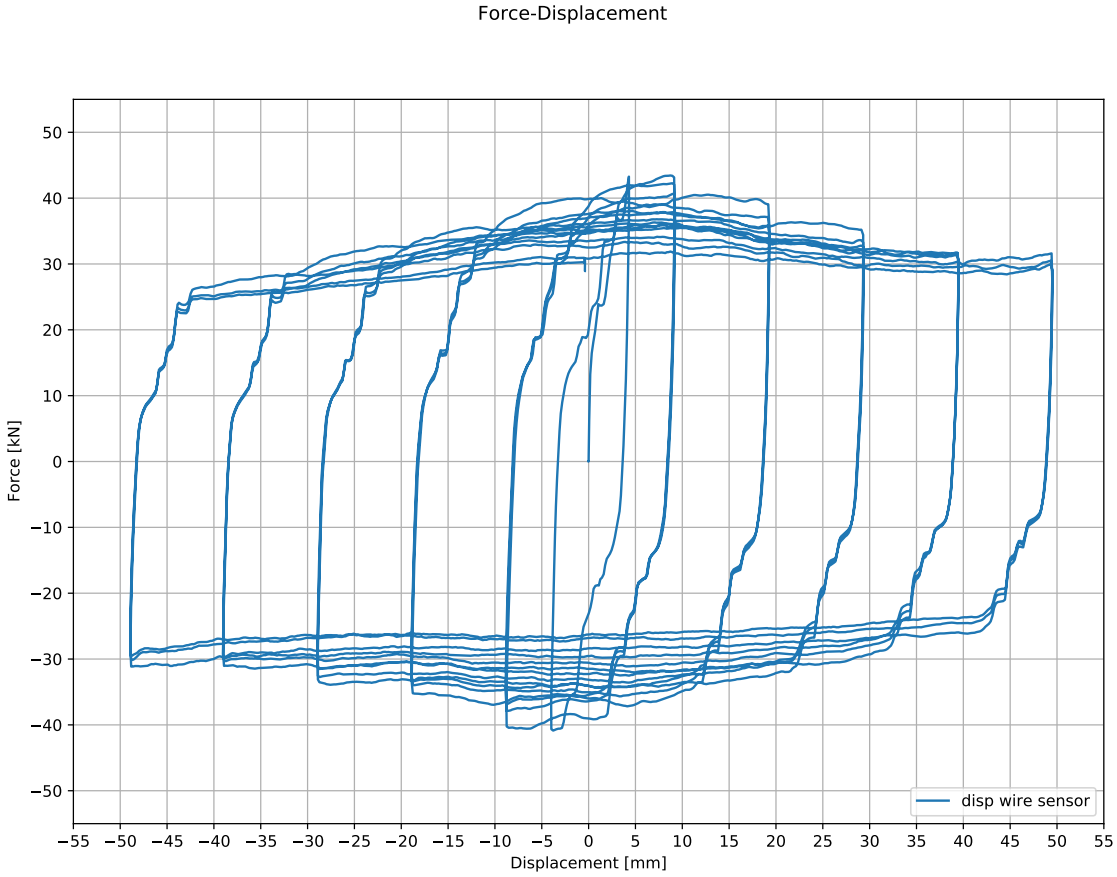

Figure 42: Load displacement graph.

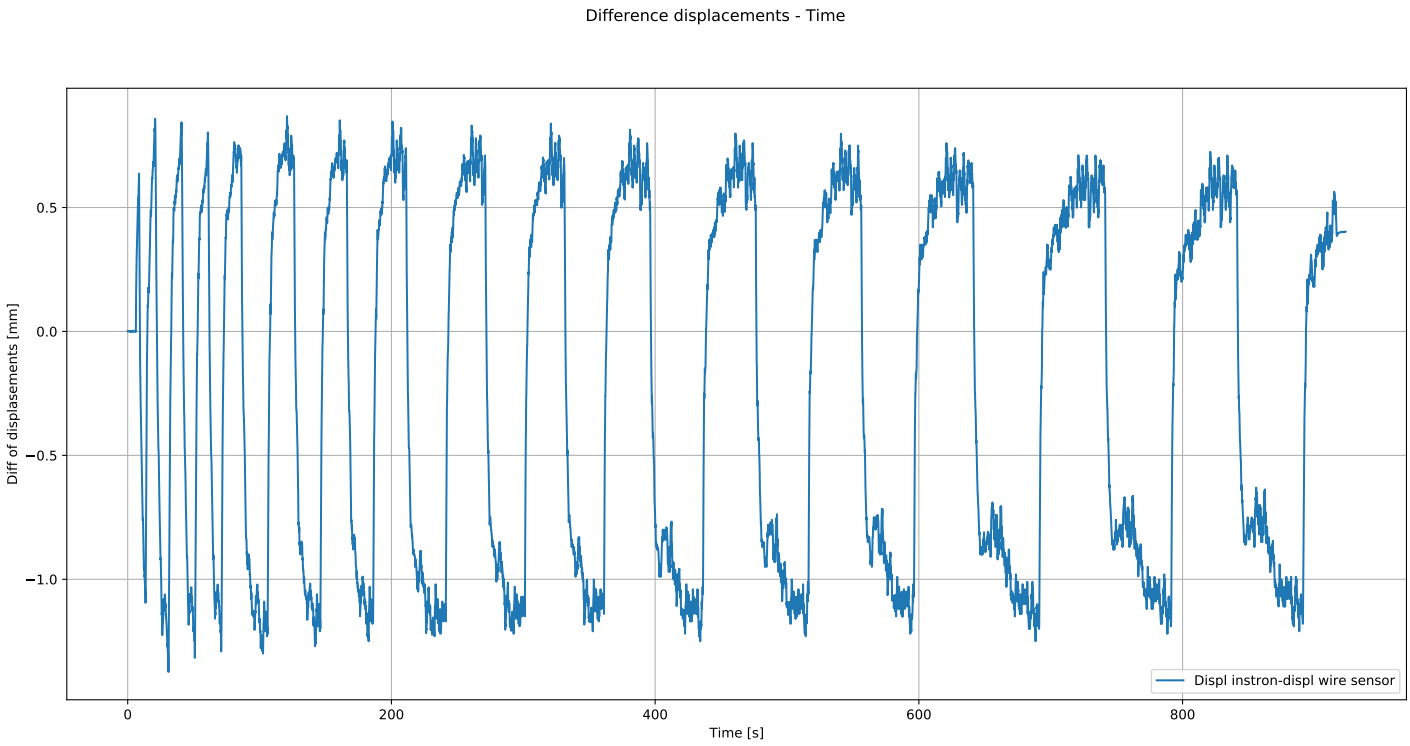

Figure 43: Difference of displacement between instron press and wire sensor.

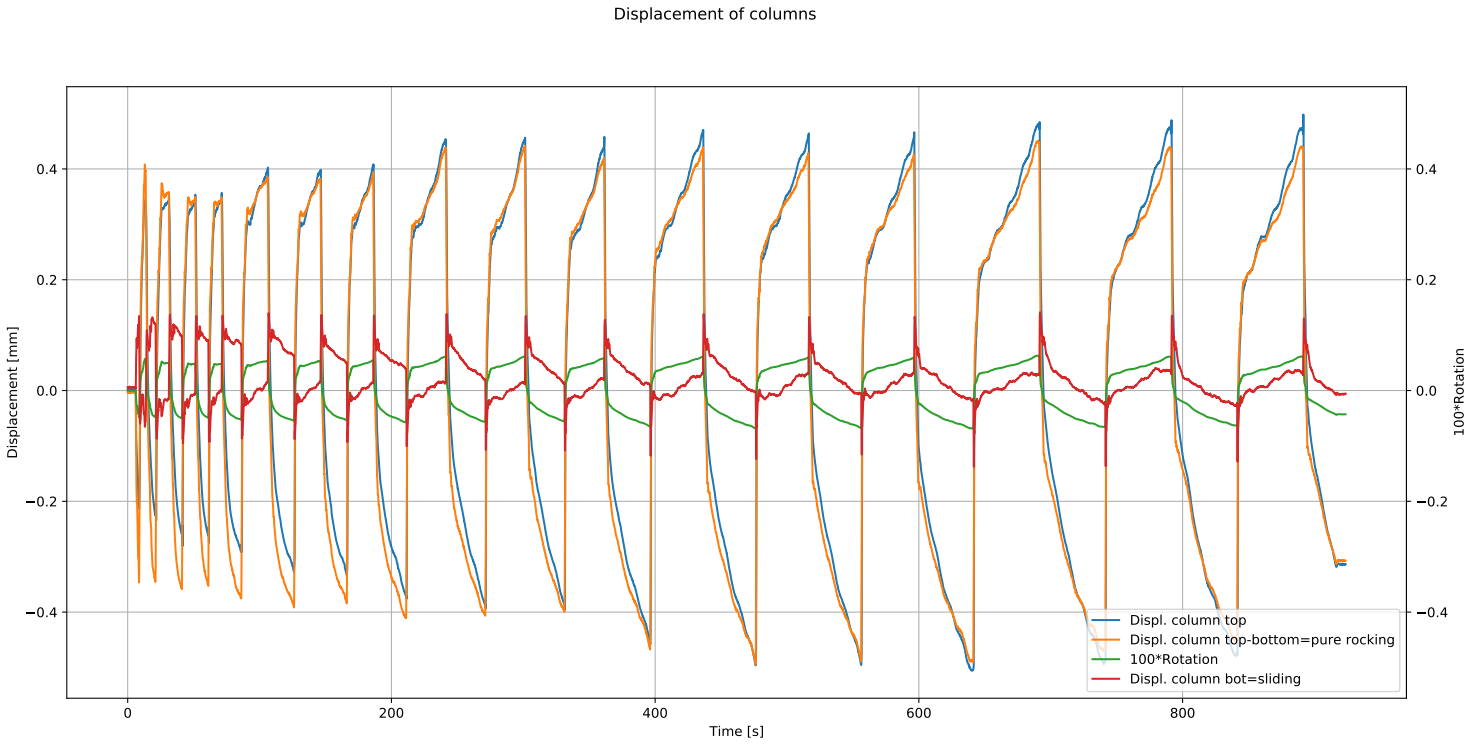

Figure 44: Movements of the column.

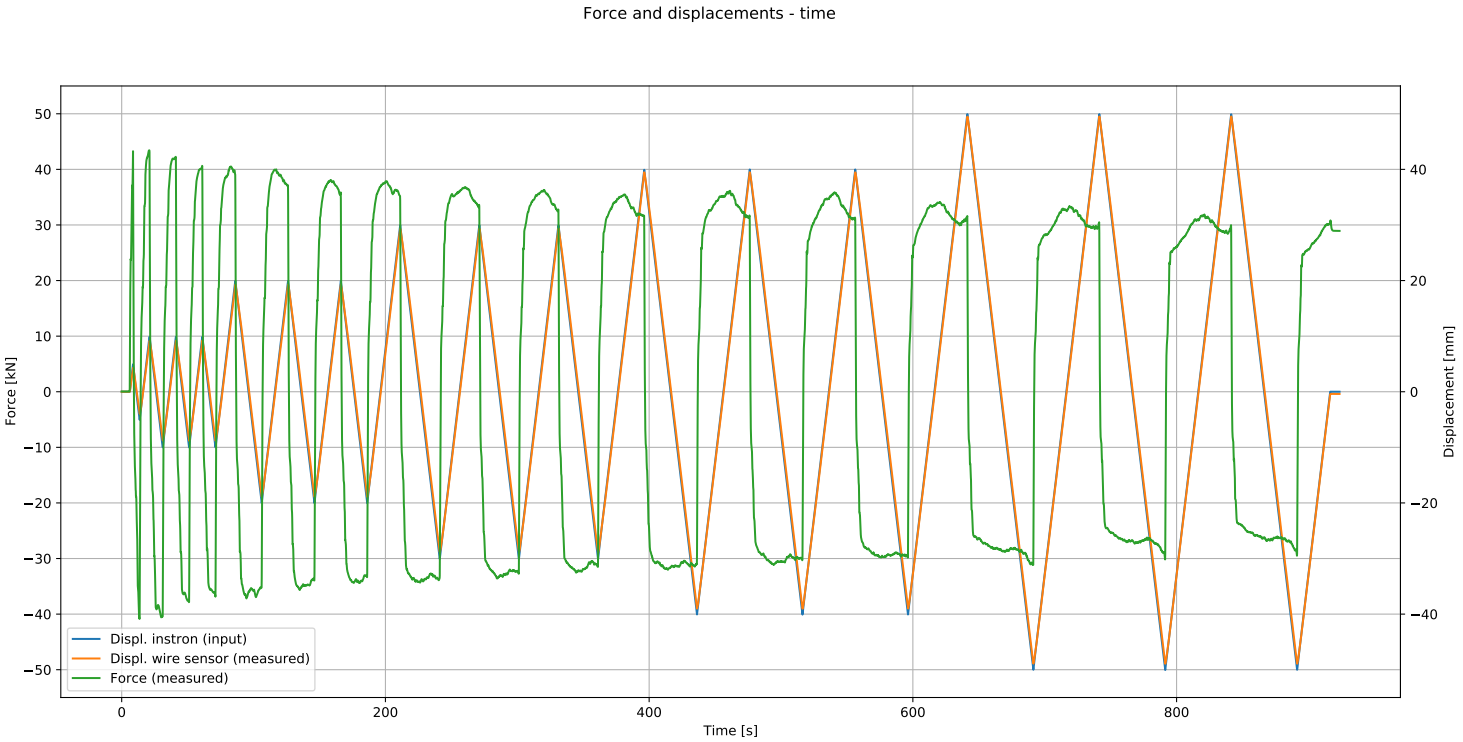

Figure 45: Force and displacement plotted against time.

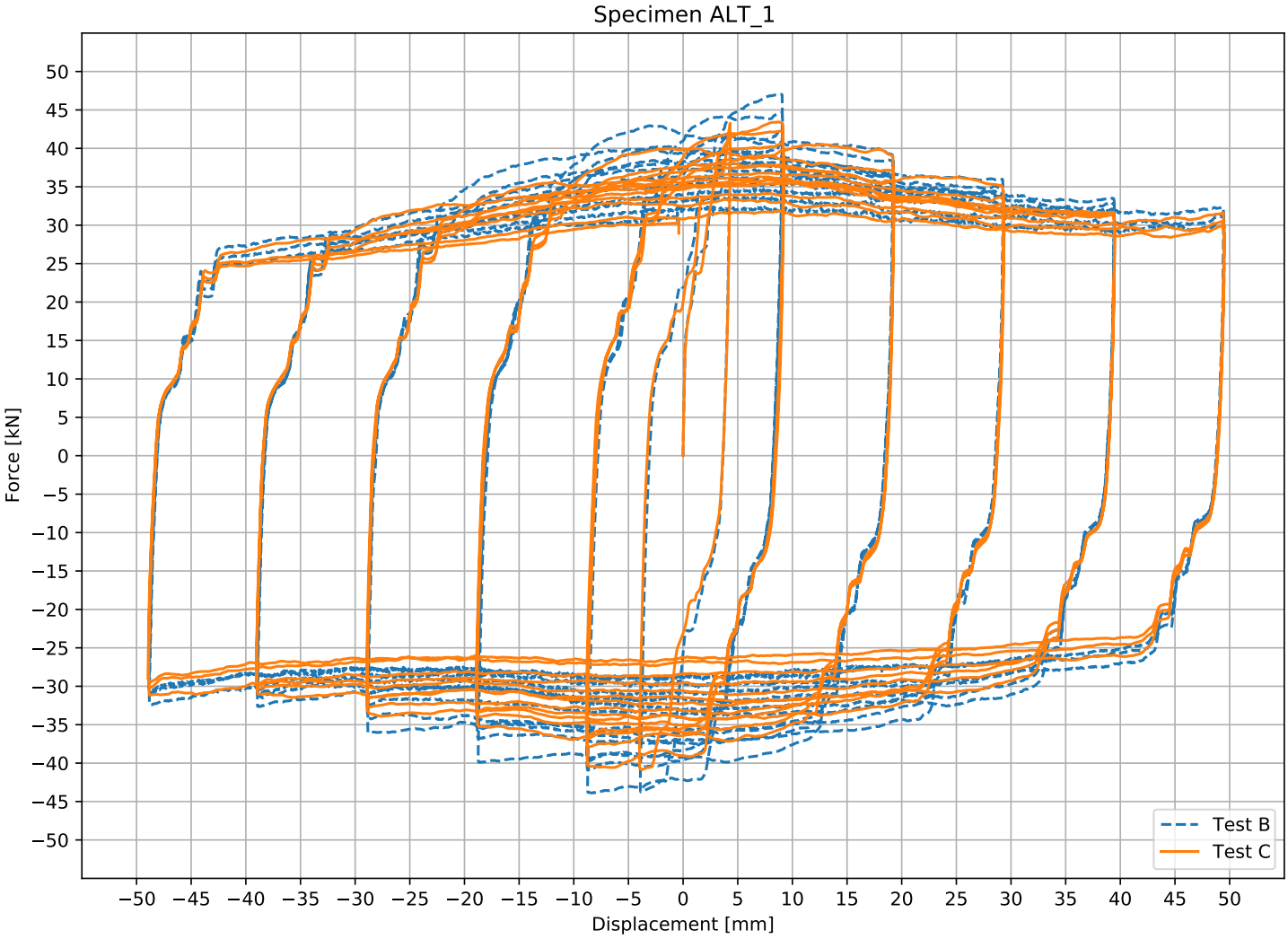

Figure 46: Comparison between test B and C of specimen ALT_1, same preload of 45%, same excursion of 50mm, different speed: test B 0.5mm/s, test C 2mm/s.

ALT_1 Test D-45%

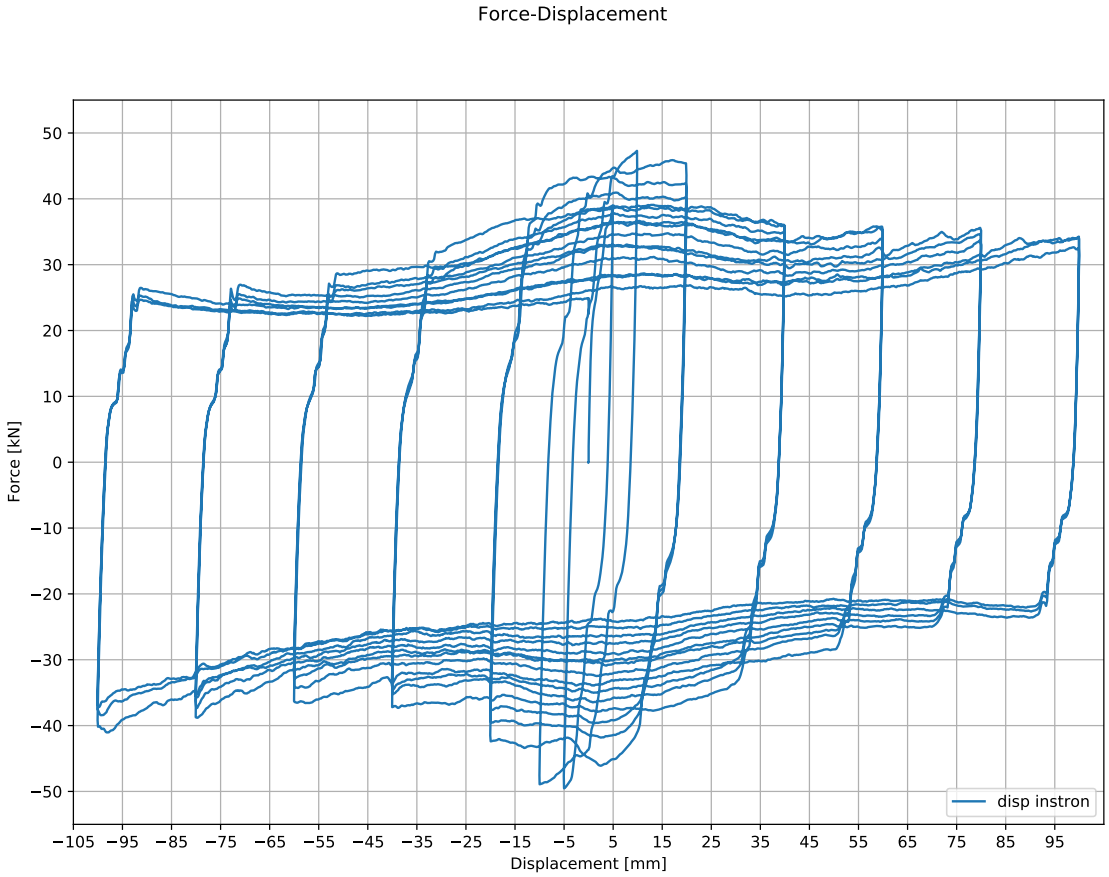

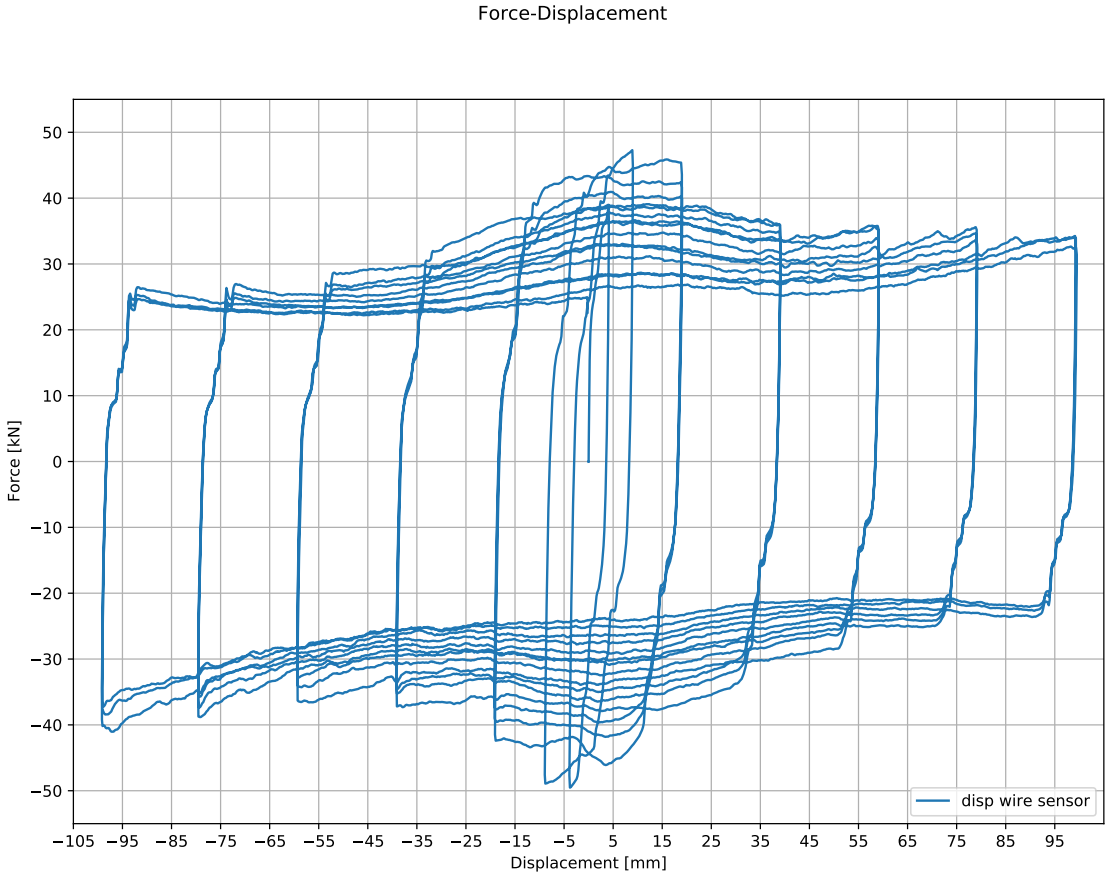

Figure 47: Load displacement graph.

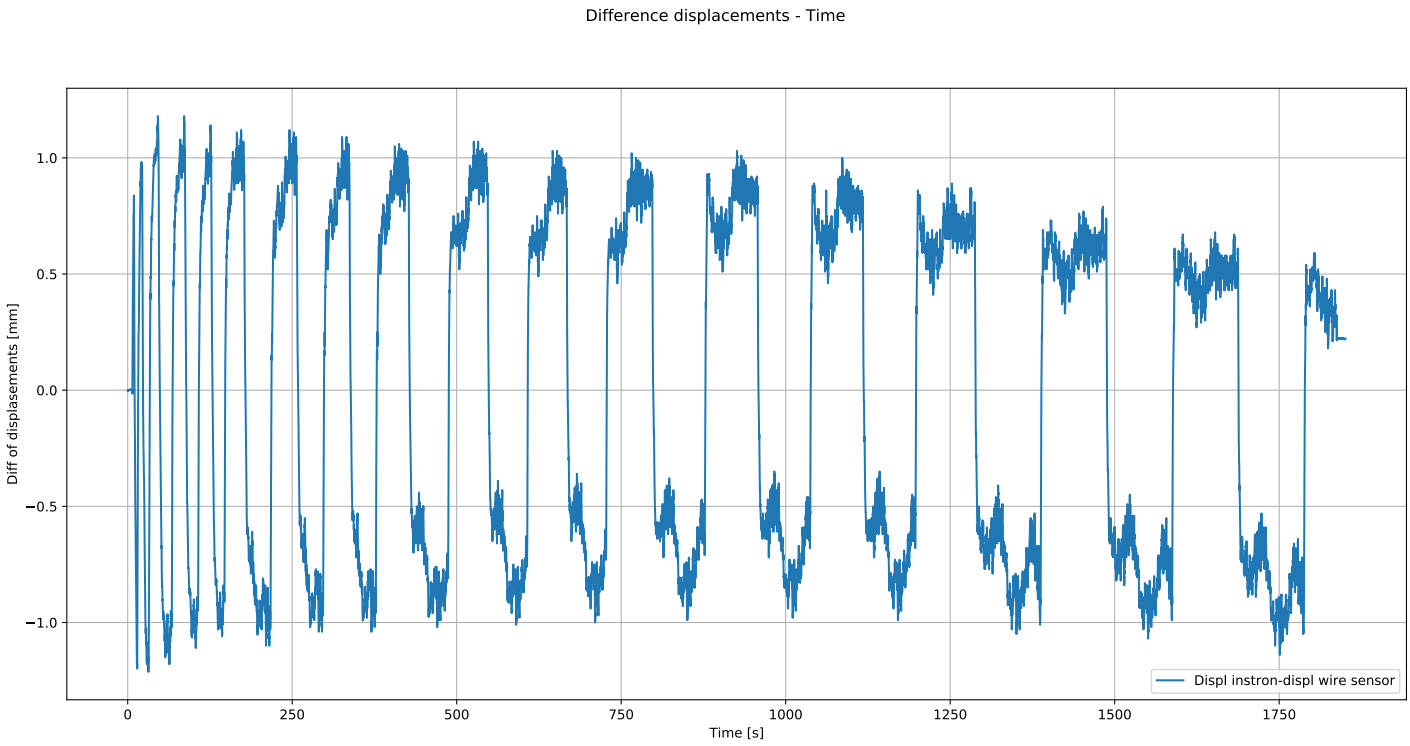

Figure 48: Difference of displacement between instron press and wire sensor.

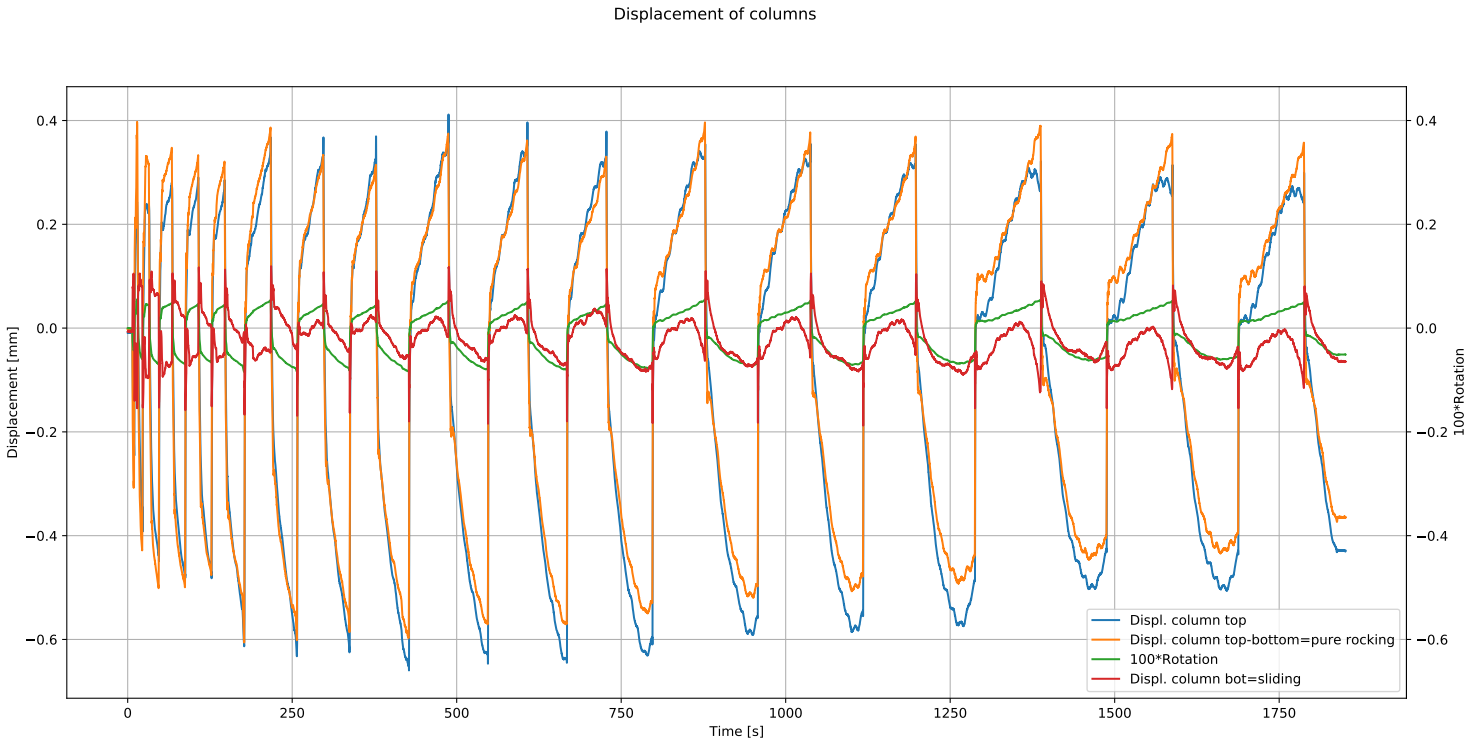

Figure 49: Movements of the column.

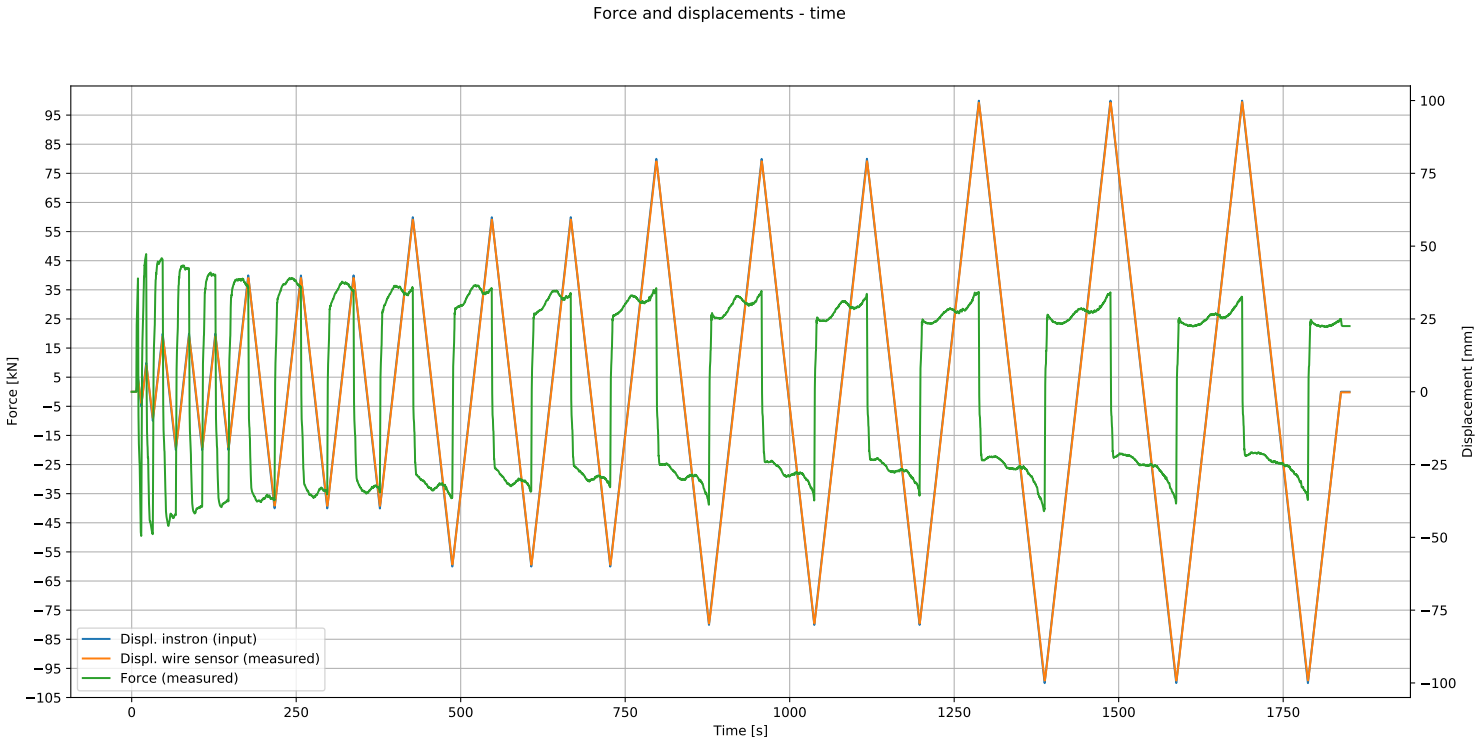

Figure 50: Force and displacement plotted against time.

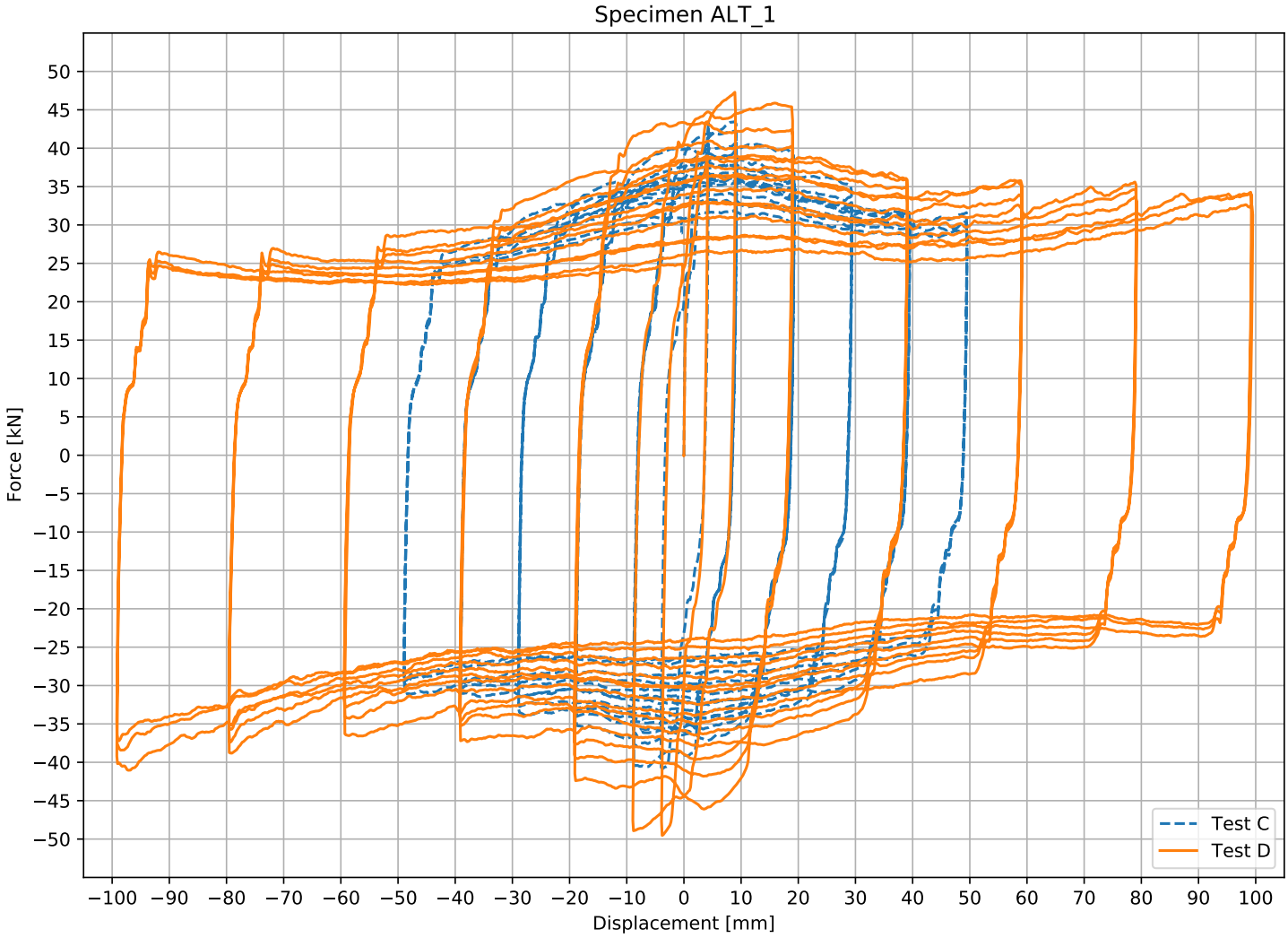

Figure 51: Comparison between test C and D of specimen ALT_1, same preload of 45%, same speed of 2mm/s, different loading protocol with different maximum excursion: test C 50mm and test D 100mm.

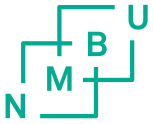

Norges miljø- og biovitenskapelige universitet
Noregs miljø- og biovitskapelege universitet
Norwegian University of Life Sciences

Postboks 5003
NO-1432 Ås
Norway